Stochastic Models of Ion Channels

by Sue Ball

Thesis submitted to the University of Nottingham for the degree of

Doctor of Philosophy, October 2000.

To my wonderful parents Ray and Sylvie who have done so much for me and to my grandmother Lisette who regretfully did not live to see this "book" finished.

Acknowledgements

I would like to thank Frank Ball and Mark Sansom, my supervisors, for all the help, advice, support and motivation that they have provided over many years. I am grateful to Karl Magleby, Robin Milne and Geoff Yeo for useful and motivating discussions on various aspects of ion channel modelling. I would also like to thank the University of Nottingham School of Mathematical Sciences for supporting me during my research and for the facilities provided. In particular, I thank Cliff Litton for his support.

I would like to thank my husband and my parents for all their support and encouragement throughout my years of research and thesis preparation.

This work was supported by the University of Nottingham Research Fund and the Wellcome Trust.

Table of Contents

Abstract

This thesis is concerned with models and inference for single ion channels.

Molecular modelling studies are used as the basis for biologically realistic, large state-space gating models of the nicotinic acetylcholine receptor which enable single-channel kinetic behaviour to be characterized in terms of a small number of free parameters. A model is formulated which incorporates known structural information concerning pentameric subunit composition, interactions between neighbouring subunits and knowledge of the behaviour of agonist binding sites within the receptor-channel proteins. Expressions are derived for various channel properties and results are illustrated using numerical examples. The model is adapted and extended to demonstrate how properties of the calcium ion-activated potassium ion channel may be modelled.

A two-state stochastic model for ion channels which incorporates time interval omission is examined. Two new methods for overcoming a non-identifiability problem induced by time interval omission are introduced and simulation studies are presented in support of these methods. A framework is presented for analysing the asymptotic behaviour of the method-of-moments estimators of the mean lengths of open and closed sojourns. This framework is used to clarify the origin of the non-identifiability and to construct confidence sets for the mean sojourn lengths. A conjecture concerning the number of solutions of the moment estimating equations is proved.

Work reported elsewhere

Ball, F. G., Davies, S. S. and Sansom, M. S. P. (1990) Single-channel data and missed events: analysis of a two-state Markov model. *Proceedings of the Royal Society* B, **242**, 61-67.

Ball, F. G., Davies, S. S. and Sansom, M. S. P. (1993) A sequential allosteric model for receptor-gated ion channels: modelling of single channel properties. *Journal of Physiology*, **467**, 358.

Ball, F. G., Davies, S. S. and Sansom, M.S.P. (1994) Ion channel gating and time interval omission: statistical inference for a two-state Markov model. *Proceedings of the Royal Society* B, **255**, 267-272.

Ball, F. G. and Davies, S. S. (1995) Statistical inference for a two-state Markov model of a single ion channel, incorporating time interval omission. *J. R. Statist. Soc.* B, **57**, 269-287.

Ball, F. G. and Davies, S. S. (1997) Clustering of bursts of openings in Markov and semi-Markov models of single channel gating. *Adv. Appl. Prob.*, **29**, 92-113.

Edeson, R. O., Ball, F. G., Yeo, G. F., Milne, R. K. and Davies, S. S. (1994) Model properties underlying non-identifiability in single channel inference. *Proceedings of the Royal Society* B, **255**, 21-29.

1 Introduction

1.1 Biology of Ion Channels

Each living cell is surrounded by a membrane which separates its interior from its exterior. Ion channels are single, or complexes of, protein molecules which form pores in cell membranes, allowing the cell to communicate with its surroundings (see, for example, Hille (1992), Aidley and Stanfield (1996)). Movement of ions through these pores determines the electrical properties of cells, and thus is ultimately responsible for transmission of information through the nervous system. There are many types of channels and they work in concert, opening and closing to shape the signals and responses of the nervous system. They perform a very wide variety of functions including guiding limbs in their movements, controlling the secretion of digestive enzymes, detecting the sounds that an animal hears and generating the violent electric discharges of the electric eel.

A channel may be regarded as an excitable molecule since it is specifically responsive to a stimulus, such as a membrane potential change or the release of stimulatory molecules, termed agonists, which are recognised by the transmitter receptor. The channel's response, known as gating, is a simple opening or

closing of the pore. When the ion channel is open, it allows particular ions to flow at a very high rate, typically greater than one million ions per second per channel. For voltage-gated channels, this flow of electric currents across the membrane has an immediate effect on membrane potential which can be detected by other voltage-gated channels and they, in turn, become excited. Thus the electric response is regenerative and self-propagating and the signal is thereby carried to a point where a nonelectrical response is generated. Ligand-gated channels also gate ion movements and generate electrical signals, but they do so in response to a specific chemical neurotransmitter, such as the agonist acetylcholine. Hence, transmission of ions through ion channels, whether they are voltage-gated or ligand-gated, is central to signalling within the nervous system.

The regulation of ion channels influences the life and functions of cells in nerve, muscle and other tissues. Ion channels consist of multiple subunits, each with very similar structure but different electrophysiological characteristics and the combination of these subunits into complexes results in a wide variety of properties of ion channels and is reflected in the diversity of diseases (Rose (1998)) resulting from ion channel disorders (channelopathies). Channelopathies may cause an abnormal gain of function (such as epilepsy, myokymia or myotonia) or an abnormal loss of function (such as weakness or numbness) depending on whether loss of channel function leads to excessive membrane

excitability or to membrane inexcitability. An understanding of the process in which ion channels open and close has already provided important insights into the cellular mechanisms underlying several diseases, including cystic fibrosis (in which there is a disorder of the chloride channel) and diabetes. Dominant nocturnal frontal lobe epilepsy is due to mutations in a subunit of the nicotinic acetylcholine receptor (Steinlein (1995)). The neurophysiological abnormalities seen in multiple sclerosis and Guillain-Barré syndrome may be able to be explained by sodium channel dysfunction and, further, the potassium channel blocker 3,4-diaminopyridine can improve leg strength in patients with multiple sclerosis (Bever *et al.* (1996)). Other specific channel modulating drugs are currently under development for migraine, chronic pain and cardiac dysrhythmias. It is hoped that further understanding of ion channel gating will give, not only an increased understanding of disease processes in which neurotransmission is impaired (for example, Parkinson's disease and Alzheimer's disease) but also additional insights into the modes of action of drugs, such as local anaesthetics, which perturb ion channels, and will ultimately result in the rational design of novel drugs acting on the central nervous system.

The electrophysiological technique of patch clamp recording (Neher and Sakmann (1976)) enables the registration of the small (*ca.* 10^{-12} Amp) electrical currents which pass through individual ion channels. An ion channel tends to be closed for much of the time and this corresponds to the situation in which no

current flows across its membrane patch. At apparently random times the channel opens for a short duration of apparently random length, producing a pulse of current which, using the patch clamp recording technique, can be directly observed as it actually happens. Recorded sojourn times in experimentally distinguishable states are used to make inferences about underlying kinetic states, their connectivity, and the chemical rate constants which govern transitions between them. Since the observed behaviour of channels is apparently random, models of ion channel gating mechanisms have been based on a variety of (usually Markov) stochastic process models. Such models are consistent, at least to a first approximation, with current understanding of the physical basis of conformational changes of molecules.

1.2 Mathematical Models of Ion Channels

The gating behaviour of a single ion channel is usually modelled by a continuous time Markov chain with a finite state space (see section 2.1). To a first approximation, most channels in patch clamp experiments show only two conductance levels, namely zero conductance (corresponding to the channel being closed) and 'open' conductance (corresponding to the channel being open). Thus the complete process is unobservable and the state space is partitioned into two classes, termed 'open' and 'closed', and it is possible to observe only which class the process is in. In practice, the sequence of open and closed sojourns of the

channel is reconstructed from the observed single-channel records by using a filter and an associated threshold crossing algorithm (see section 2.2). This results in the loss of very short sojourns in either the open or the closed classes of states, a phenomenon known as time interval omission.

One of the main aims of such single channel modelling is to determine properties of the observable aggregated process from those of the underlying continuous-time Markov chain (see section 2.1). Another of the main aims of modelling is to draw inferences concerning the structure of, and parameter values governing, the underlying continuous time Markov chain from the observed aggregated process (see section 2.3). It is hoped that such modelling will provide insights into the underlying physical processes of channel gating.

Much of the early research into mathematical modelling of ion channels concentrated on the development and analysis of stochastic models (Colquhoun and Hawkes (1982), Fredkin *et al.* (1985), Dabrowski *et al.* (1990), Ball *et al.* (1991), Ball and Rice (1992), etc.) and, with a few exceptions (e.g. Horn and Lange (1983)), problems of statistical inference started to be addressed later (Ball and Sansom (1989), Chung *et al.* (1990), Magleby and Weiss (1990a), Fredkin and Rice (1992a), etc.).

1.3 Main Topics of the Thesis

1.3.1 Models based on the Molecular Structure of Ion Channels

Many recent studies of ion channel gating have employed small state-space Markov models of single-channel behaviour, and have used results derived from the theory of stochastic processes in the development and application of such models. Although major successes have been achieved using this approach, in many cases a problem arises when the experimental data is best described by gating models in which the channel may exist in one of many similar closed states. One solution to this problem is to develop 'traditional' Markov models with suitably large state-spaces. However, this results in models with large numbers of independent parameters, which present considerable difficulties when attempting to obtain parameter estimates from experimental data. Several authors have developed 'alternative' large state-space models which treat channel gating in terms of diffusion-like processes (e.g. Millhauser *et al.* (1988), Sansom *et al.* (1989), Sigg *et al.* (1999)). Although such models benefit from having small numbers of free parameters, it is often difficult to judge their relationship to the underlying structural properties of the ion channels involved.

In parallel with increased understanding of channel gating, the past two decades have seen remarkable developments in the molecular biology of ion channel

proteins, and as a result of such studies, it is now possible to formulate *molecular* models of channel gating. In particular, recent structure determination studies of the nicotinic acetylcholine receptor from the electric ray *Torpedo* have provided a detailed three-dimensional model of the receptor channel (Unwin (1989, 1993, 1995)).

The models which are considered in Chapter 3 of this thesis are an attempt at a synthesis of these two classes of investigations. We have used molecular models as the basis for biologically realistic, large state-space gating models of the nicotinic acetylcholine receptor and the calcium ion-activated potassium ion channel which enable single-channel kinetic behaviour to be characterized in terms of a small number of free parameters. This has resulted in realistic channel models which are sufficiently simple to allow the computation of channel properties.

In Chapter 3, we present, in detail, a model for the nicotinic acetylcholine receptor which incorporates information concerning the structure of the corresponding receptor-channel protein. Our model assumes that the channel consists of 5 subunits arranged in a ring, and that agonists can bind to 2 of these subunits. Each subunit may exist in either a closed or an open conformation, and the channel is open if all 5 subunits are in open conformations. Otherwise, the channel is closed. The model also incorporates interactions between

neighbouring subunits, using ideas from a sequential model for allosteric proteins developed by Koshland *et al.* (1966). Although this model has a large state-space, symmetries can be exploited to considerably reduce the state-space size. Further, the model is defined by a relatively small number of parameters which are directly related to molecular properties of the channel. Under our model, we derive expressions for various channel properties, including equilibrium distributions, open and closed entry process equilibrium distributions and mean lengths of open and closed sojourns and we use numerical algorithms to compute sojourn time probability density functions and correlation functions. We illustrate our results using examples based on parameter values which are chosen by theoretically matching observable properties of our model to those of the model of Jackson (1989), who estimates optimal values for acetylcholine receptor equilibrium constants based on physiological considerations (see also Jackson (1993)).

In Chapter 3, we also describe the formulation of a model for the calcium-activated potassium ion channel based on its underlying molecular structure. Our model is similar to that for the nicotinic acetylcholine receptor, but instead assumes that the channel consists of 4 subunits arranged in a square, and that calcium ions can bind to all 4 of these subunits. Channel openings and closings are modelled in the same manner as in the nicotinic acetylcholine receptor model and this model incorporates two distinct types of interactions between

neighbouring subunits. Firstly, subunits are modelled to open and close at varying rates depending upon the number of neighbouring subunits which are open and, secondly, calcium ion binding and unbinding rates for each subunit are dependent upon whether zero, one or two of the adjacent subunits already have a calcium ion bound. Again this model has a large number of states but symmetries can be exploited to vastly reduce the size of the state-space. This model also has a small number of free parameters which can be interpreted in terms of the molecular channel properties.

1.3.2 Inference for a two-state Ion Channel Model

Making inferences for stochastic models of ion channels is fraught with identifiability problems and these can be classified broadly into three types (see section 2.3.3):

(i) structural non-identifiability (Kienker (1989)) in which two distinct processes can yield probabilistically indistinguishable aggregated processes;

(ii) overparameterised models (Fredkin *et al.* (1985));

(iii) non-identifiability induced by time interval omission.

Chapter 4 is concerned with problem (iii).

INTRODUCTION

Yeo *et al.* (1988) considered the case in which the underlying process has only two states, one open and one closed. Thus successive open and closed sojourn lengths are independent negative exponential random variables, with respective means μ_O and μ_C, say. They studied the problem of estimating (μ_O, μ_C) in the presence of time interval omission and conjectured that the moment estimating equations for (μ_O, μ_C) have either zero, one or two solutions, with two solutions being the usual situation. The distribution of an observed open (or closed) sojourn, incorporating time interval omission, does not admit a simple form, so Yeo *et al.* (1988) considered several approximations. In particular, they considered an approximation in which observed open and closed sojourns are assumed to follow negative exponential distributions with appropriate means. For this approximation, the maximum likelihood and method-of-moments estimators of (μ_O, μ_C) coincide. Clarke *et al.* (1993) used Fréchet-type arguments to derive local asymptotic results, valid under the approximate model, for the two solutions of the moment estimating equations.

A number of authors have proposed methods of overcoming the above identifiability problem. Colquhoun and Sigworth (1983), Blatz and Magleby (1986) and Yeo *et al.* (1988) suggested the use of samples with different minimum detectable sojourns and estimating (μ_O, μ_C) for each sample. Then as the detection limit changes, one estimate of (μ_O, μ_C) remains roughly constant while the other varies significantly, thus permitting the true solution to be

determined. A second computationally highly intensive simulation-based method involving modelling the true effects of the filter was proposed by Magleby and Weiss (1990a). Simulation studies suggest that both these methods will work in practice.

In Chapter 4 two new methods of overcoming the identifiability problem are presented. The first (Ball *et al.* (1990)) is similar to the method of using samples with different detection limits and instead allows the agonist concentration to change between the samples. For agonist-activated channels, the mean length of a closed sojourn is modelled as $a^{-1}\mu_C$, where a is the agonist concentration, which is assumed known. Since the method which uses variation in the detection limit and the method which uses variation in the agonist concentration both involve observing single channel records under different experimental conditions, and many authors fit models using records of reconstructed sojourn times, it is clearly useful to have a method of discriminating between the two solutions on the basis of one such record. The second new method (Ball and Davies (1995), Ball *et al.* (1994)) proposed in Chapter 4 does not require taking samples under different experimental conditions, and instead uses the sample variances of observed open and closed sojourns as a discriminant between the two solutions. Simulation studies are presented and these suggest that both these new methods will work.

Chapter 4 also presents a framework for analysing the asymptotic behaviour of

the method-of-moments estimators under the *exact* model as the numbers of observed open and closed sojourns become large (Ball and Davies (1995)). This framework clarifies the origin of the non-identifiability discussed above and allows us to construct confidence sets for (μ_O, μ_C) corresponding to the two solutions of the moment estimating equations. It also enables an assessment to be made of the accuracy of the simultaneous confidence sets given in Clarke *et al.* (1993), which were based on an approximate model. Further it provides a formal justification of the two methods for overcoming the identifiability problem which involve taking samples under different experimental conditions. We also provide a proof of the conjecture of Yeo *et al.* (1988) concerning the number of solutions of the moment estimating equations.

2 Background

2.1 Markov Models of Ion Channels

A single ion channel gating mechanism is usually modelled by a finite state space, continuous time, Markov chain. Thus, given the successive states visited, the sojourn times in individual states are independent, having exponential distributions with parameters that depend only on the state being visited. Label the states 1, 2,..., n. Let $O = \{1, 2,..., n_O\}$ and $C = \{n_O + 1, n_O + 2,..., n\}$ be the sets of open and closed states respectively. Let n_C be the number of closed states, so that $n_O + n_C = n$. Denote the above Markov chain by $\{X(t); t \geq 0\}$, where $X(t)$ is the state occupied by the channel at time t. The process $\{X(t); t \geq 0\}$ is time homogeneous, irreducible and, within the present context in which there is no external force driving ions through the channel, time reversible (Colquhoun and Hawkes (1983), Läuger (1995)).

For $i \neq j$, let q_{ij} be the transition rate of the channel process $\{X(t); t \geq 0\}$ from state i to state j. Let Q be the $n \times n$ matrix with off-diagonal elements q_{ij} and diagonal elements $q_{ii} = -\sum_{j \neq i} q_{ij}$. It is convenient (see, for example, Ball and Sansom (1987)) to partition the matrix Q into

$$Q = \begin{pmatrix} Q_{OO} & Q_{OC} \\ Q_{CO} & Q_{CC} \end{pmatrix}, \tag{2.1}$$

where, for instance, Q_{OO} is an $n_O \times n_O$ sub-matrix corresponding to transitions that remain within the open states and Q_{OC} is an $n_O \times n_C$ sub-matrix corresponding to transitions from the open states to the closed states. Hereafter in this thesis we do not state the dimensions of sub-matrices of partitioned matrices where such dimensions are apparent from the context. Since the channel process $\{X(t);\ t \geq 0\}$ is irreducible, it will possess an equilibrium distribution, $\pi = (\pi_1, \pi_2, \ldots, \pi_n)^\top$ say, where, throughout this thesis, $^\top$ denotes transpose. Define the transition probability $p_{ij}(t)$ to be

$$p_{ij}(t) = \mathrm{P}(X(t) = j \mid X(0) = i) \qquad (i, j = 1, 2, \ldots, n;\ t \geq 0)$$

and let $P(t)$ be the $n \times n$ matrix whose entries are $p_{ij}(t)$. Throughout this thesis, I denotes an identity matrix whose dimensions are apparent from the context. Note that $P(0) = I$, that $P(t)$ has non-negative entries and row sums equal to one, and that $P(t)$ satisfies the Chapman-Kolmogorov equations $P(s+t) = P(s)P(t)$ for $s, t \geq 0$. Hence, using standard results (e.g. Grimmett and Stirzaker (1982, p149)), we obtain the forward equations

$$P'(t) = P(t)\,Q \qquad (t > 0),$$

where $P'(t)$ denotes the $n \times n$ matrix with entries $p_{ij}'(t)$ and $'$ denotes

differentiation. The forward equations, with $P(0) = I$, have solution

$$P(t) = \exp(Qt) \qquad (t > 0), \tag{2.2}$$

where

$$\exp(Qt) = \sum_{k=0}^{\infty} \frac{Q^k t^k}{k!}$$

is the usual matrix exponential (see, for example, Bellman (1960)).

For $i = 1, 2, \ldots, n$, let $p_i(0)$ be the probability that a channel is in state i at time $t = 0$, and let $\boldsymbol{p}(0)$ be the $1 \times n$ row vector with elements $p_1(0), p_2(0), \ldots, p_n(0)$. Then the expression given by Colquhoun and Hawkes (1977) for $P_O(t)$, the probability that a channel is open at time t, follows immediately from equation (2.2) and is given by

$$P_o(t) = \boldsymbol{p}(0) \exp(Qt)\, \boldsymbol{u}, \tag{2.3}$$

where $\boldsymbol{u}$ is the $n \times 1$ column vector whose first n_O elements are ones, and whose remaining elements are all zero.

Läuger (1995) discusses the important concept of time reversibility in the ion channel context and its equivalence to the assumption that channel gating is not coupled to a source of free energy, such as ion concentration gradients across the membrane. This situation appears to be true for the majority of ion channels,

although there have been a few reports of possible non-reversibility (e.g. Hamill and Sakmann (1981)). The presence of reversibility implies that the stochastic properties of a model are the same whether an ion channel record is read from left to right or from right to left (Kelly (1979)). Moreover, at equilibrium, a reversible cyclic reaction mechanism has no greater tendency to move in one direction around the cycle than in the opposite direction and the mechanism obeys the principle known as microscopic reversibility or detailed balance. This principle is represented by the detailed balance equations

$$\pi_i q_{ij} = \pi_j q_{ji} \qquad (i, j = 1, 2, \ldots, n), \tag{2.4}$$

from which the equilibrium distribution π may be determined.

Let W be the $n \times n$ diagonal matrix with diagonal elements $\pi_1, \pi_2, \ldots, \pi_n$. Then the detailed balance conditions (2.4) imply that

$$W^{1/2} Q W^{-1/2} = (W^{1/2} Q W^{-1/2})^{\top}. \tag{2.5}$$

Hence $W^{1/2}QW^{-1/2}$ is a real symmetric matrix and is therefore diagonalizable with real eigenvalues $\lambda_1, \lambda_2, \ldots, \lambda_n$, say, where one of the eigenvalues is zero and the remaining eigenvalues are all strictly negative, and corresponding orthonormal real right eigenvectors $c_1, c_2, \ldots, c_n$, say. It follows that

$$W^{1/2} Q W^{-1/2} = CDC^{\top},$$

where $D = \text{diag}(\lambda_1, \lambda_2, \ldots, \lambda_n)$ and C is an $n \times n$ orthogonal matrix with columns $\boldsymbol{c}_1, \boldsymbol{c}_2, \ldots, \boldsymbol{c}_n$. Since the matrix $W^{1/2}QW^{-1/2}$ admits the spectral representation

$$W^{1/2}QW^{-1/2} = \sum_{i=1}^{n} \lambda_i (\boldsymbol{c}_i \boldsymbol{c}_i^{\top}),$$

we obtain

$$Q = \sum_{i=1}^{n} \lambda_i E_i, \tag{2.6}$$

where $E_i = W^{-1/2} \boldsymbol{c}_i \boldsymbol{c}_i^{\top} W^{1/2}$. The matrices $E_1, E_2, \ldots, E_n$ satisfy

$$E_i E_j = \begin{cases} E_i & \text{if } i = j \\ 0 & \text{if } i \neq j \end{cases}$$

and

$$E_1 + E_2 + \ldots + E_n = I.$$

Further, if, without loss of generality, $\lambda_1 = 0$, then $E_1 = \mathbf{1}\pi^{\top}$. Application of equation (2.6) to equation (2.3) yields that

$$P_o(t) = \sum_{i=1}^{n} \beta_i e^{\lambda_i t} \qquad (t > 0),$$

where $\beta_i = \boldsymbol{p}(0) E_i \boldsymbol{u}$. In practice, if nothing is known about the process at time

$t = 0$, other than that it is in equilibrium, the equilibrium probability vector π is used as the initial probability vector $\boldsymbol{p}(0)$.

In order to analyse open and closed sojourns, we use the semi-Markov framework of Ball *et al.* (1991, 1993a). Assume that the first open sojourn commences at time $t = 0$ and let $S_0 = 0$. Let $S_1 = \min\{t > 0: X(t) \in C\}$ be the time at which the first closed sojourn starts, $S_2 = \min\{t > S_1: X(t) \in O\}$ be the time at which the second open sojourn starts, $S_3 = \min\{t > S_2: X(t) \in C\}$ be the time at which the second closed sojourn starts, and so on. For $k = 0, 1,...,$ let $J_k = X(S_k)$ be the label of the state occupied by the channel at time S_k. Then $J_0, J_2, J_4,...$ are the open states occupied by the channel at the commencement of successive sojourns in the open class of states and $J_1, J_3, J_5,...$ are the closed states in which the channel commences successive sojourns in the closed class of states. Let $T_0 = 0$ and $T_k = S_k - S_{k-1}$ $(k = 1, 2,...)$. Then $T_1, T_3, T_5,...$ are the lengths of successive sojourns in the open class of states and $T_2, T_4, T_6,...$ are the lengths of successive sojourns in the closed class of states. The process $\{(J_k, T_k)\}$ $(k = 0, 1,...)$ is Markov and is called a semi-Markov sequence.

The probabilistic properties of $\{(J_k, T_k)\}$ are completely determined by its associated semi-Markov kernel, the $n \times n$ matrix function $\boldsymbol{F}(t) = [F_{ij}(t)]$ $(t \geq 0)$, defined elementwise by

$$F_{ij}(t) = \mathrm{P}(T_k \leq t, J_k = j \mid J_{k-1} = i) \qquad (i, j = 1, 2,..., n).$$

Note that some of the rows and columns of $\boldsymbol{F}(t)$ will contain only zeros, reflecting the fact that not all closed (open) states may be reached directly via a transition from the open (closed) class of states. Since the process $\{(J_k, T_k)\}$ $(k = 0, 1,...)$ alternates between open and closed states, we may partition $\boldsymbol{F}(t)$ into

$$\boldsymbol{F}(t) = \begin{pmatrix} 0 & \boldsymbol{F}_{OC}(t) \\ \boldsymbol{F}_{CO}(t) & 0 \end{pmatrix},$$

where $\boldsymbol{F}_{OC}(t)$ is an $n_O \times n_C$ matrix corresponding to open sojourns and $\boldsymbol{F}_{CO}(t)$ is an $n_C \times n_O$ matrix corresponding to closed sojourns. For matrices throughout this thesis, 0 denotes a zero matrix whose dimensions are apparent from the context.

Following a technique used by Colquhoun and Hawkes (1977, 1981) and Fredkin *et al.* (1985), we can define a new process in which no exit from the closed states is possible. Let $\overline{P}(t)$ and $\overline{Q}$ be the transition probability matrix and transition rate matrix, respectively, of this new process. Then we can partition the matrices $\overline{P}(t)$ and $\overline{Q}$ into

$$\overline{P}(t) = \begin{pmatrix} \overline{P}_{OO}(t) & \overline{P}_{OC}(t) \\ 0 & I \end{pmatrix} \quad \text{and} \quad \overline{Q} = \begin{pmatrix} Q_{OO} & Q_{OC} \\ 0 & 0 \end{pmatrix},$$

where I is the $n_C \times n_C$ identity matrix. Then for $i \in O$ and $j \in C$ we have

$$[F_{OC}(t)]_{ij} = [\overline{P}_{OC}(t)]_{ij} \quad \text{and} \quad [f_{OC}(t)]_{ij} = [\overline{P}_{OC}'(t)]_{ij}, \qquad (2.7)$$

where $f(t)$ is the matrix density function corresponding to and partitioned in identical manner to the distribution function $F(t)$. The forward equations can now be written as

$$\overline{P}'(t) = \overline{P}(t)\,\overline{Q} = \begin{pmatrix} \overline{P}_{OO}(t)\,Q_{OO} & \overline{P}_{OO}(t)\,Q_{OC} \\ 0 & 0 \end{pmatrix},$$

from which we have the equation $\overline{P}_{OO}'(t) = \overline{P}_{OO}(t)\,Q_{OO}$ with solution

$$\overline{P}_{OO}(t) = \exp(Q_{OO}t) \tag{2.8}$$

and the equation

$$\overline{P}_{OC}'(t) = \overline{P}_{OO}(t)\,Q_{OC}. \tag{2.9}$$

From equations (2.7), (2.8) and (2.9) we obtain

$$f_{OC}(t) = \exp(Q_{OO}t)\,Q_{OC} \tag{2.10}$$

and hence

$$F_{OC}(t) = \int_0^t \exp(Q_{OO}\,u)\,Q_{OC}\,du = -Q_{OO}^{-1}(I - \exp(Q_{OO}\,t))\,Q_{OC}. \tag{2.11}$$

Similarly we can show that

$$f_{CO}(t) = \exp(Q_{CC}t)\,Q_{CO} \tag{2.12}$$

and hence

$$F_{CO}(t) = -Q_{CC}^{-1}(I - \exp(Q_{CC}t))Q_{CO}. \tag{2.13}$$

Now let $P = F(\infty)$ be the transition matrix of the Markov chain $\{J_k\}$ and partition P into

$$P = \begin{pmatrix} 0 & P_{OC} \\ P_{CO} & 0 \end{pmatrix}.$$

From equations (2.11) and (2.13) we obtain that

$$P_{OC} = F_{OC}(\infty) = -Q_{OO}^{-1}Q_{OC} \tag{2.14}$$

and

$$P_{CO} = F_{CO}(\infty) = -Q_{CC}^{-1}Q_{CO}. \tag{2.15}$$

2.1.1 Equilibrium Behaviour

Since $\{J_k\}$ alternates between open and closed states, it is periodic with period 2 and therefore does not possess an equilibrium distribution. We instead consider the process $\{J_{2k}\}$ ($k = 0, 1,...$), termed the open entry process (Ball *et al.* (1991)), which is a Markov chain recording the state occupied by the channel each time

the class of open states is entered. Entry to the class of open states is usually possible through only a subset of the states in that class and this subset is known as the open gateway states (Ball *et al.* (1991, 1993a)) and denoted O_G. The state space of the open entry process is O_G. Similarly, $\{J_{2k+1}\}$ $(k = 0, 1,...)$ is termed the closed entry process and has as its state space the set of closed gateway states, denoted C_G. Note that $P_O = P_{OC}P_{CO}$ and $P_C = P_{CO}P_{OC}$ are the transition matrices of $\{J_{2k}\}$ and $\{J_{2k+1}\}$, respectively.

Suppose that there are m_O open gateway states and m_C closed gateway states. Without loss of generality we can assume that the open and closed gateway states are labelled 1, 2,..., m_O and $n_O + 1$, $n_O + 2$,..., $n_O + m_C$, respectively. Let $\pi^O = (\pi_1{}^O,\ \pi_2{}^O,...,\ \pi_{m_O}^O)^\top$ be the column vector of open entry probabilities at equilibrium, so that π_i^O is the probability that the class of open states is entered via the ith open state. Note that time reversibility of $\{X(t)\}$ is sufficient to ensure the existence of π^O and the analogously defined closed entry process distribution π^C (see Ball *et al.* (1991, Theorem 3.6)). An expression for π^O can be obtained by considering channel transitions from all closed states to each open state and weighting the corresponding rates according to the fraction of time a channel occupies in each closed state at equilibrium (see Colquhoun and Hawkes (1977)).

Thus

$$\pi_i{}^O \propto \sum_{j \in C} \pi_j q_{ji} \quad (i = 1, 2,..., m_O),$$

which, from the detailed balance conditions (2.4), may be expressed in the form

$$\pi_i^O \propto \pi_i \sum_{j \in C} q_{ij} \quad (i = 1, 2, \ldots, m_O). \tag{2.16}$$

The constant of proportionality in equation (2.16) is chosen so that the equilibrium open entry probabilities sum to one. A similar result holds for the vector π^C of equilibrium closed entry probabilities.

2.1.2 Open and Closed Sojourn Probability Density Functions

To obtain an expression for the unconditional open sojourn time probability density function, $f_O(t)$ say, we calculate a weighted combination of the conditional density functions $[f_{OC}(t)]_{ij}$, where $f_{OC}(t)$ is given by equation (2.10), with weights being the equilibrium open entry probabilities, and we sum over the possible entry states for the succeeding closed sojourn. Let π_O be the $n_O \times 1$ column vector whose first m_O elements are $\pi_1^O, \pi_2^O, \ldots, \pi_{m_O}^O$, and whose remaining elements are all zero. Throughout this thesis **1** (**0**) denotes a column vector of ones (zeros) whose dimension is obvious from the context. Then

$$f_O(t) = (\boldsymbol{\pi_O})^\top f_{OC}(t)\,\mathbf{1} = (\boldsymbol{\pi_O})^\top \exp(Q_{OO}t)\,Q_{OC}\,\mathbf{1} \qquad (t > 0).$$

Note that from the definition of Q, it follows that $Q\mathbf{1} = \mathbf{0}$, which when expanded in partitioned form yields $Q_{OO}\mathbf{1} + Q_{OC}\mathbf{1} = \mathbf{0}$. Using this fact, we can write

$$f_O(t) = -(\pi_O)^{\top} \exp(Q_{OO}t)\, Q_{OO}\mathbf{1} \qquad (t > 0). \tag{2.17}$$

Let W_O be the $n_O \times n_O$ diagonal matrix with diagonal elements $\pi_1, \pi_2, \ldots, \pi_{n_O}$.

Then expansion of the relation (2.5) in partitioned form yields

$$W_O^{1/2} Q_{OO} W_O^{-1/2} = (W_O^{1/2} Q_{OO} W_O^{-1/2})^{\top},$$

and it follows that Q_{OO} possesses a spectral representation similar to that for Q. Let $\omega_1, \omega_2, \ldots, \omega_{n_O}$ be the real (strictly negative) eigenvalues of $W_O^{1/2} Q_{OO} W_O^{-1/2}$ with corresponding real orthonormal right eigenvectors $\boldsymbol{b}_1, \boldsymbol{b}_2, \ldots, \boldsymbol{b}_{n_O}$, and let $E_i^O = W_O^{-1/2} \boldsymbol{b}_i \boldsymbol{b}_i^{\top} W_O^{1/2}$ $(i = 1, 2, \ldots, n_O)$. Then $f_O(t)$ can be expressed in the form

$$f_O(t) = \sum_{i=1}^{n_O} \alpha_i \exp(\omega_i t) \qquad (t > 0), \tag{2.18}$$

where $\alpha_i = -(\pi_O)^{\top} \omega_i E_i^O \mathbf{1}$ $(i = 1, 2, \ldots, n_O)$. Since $\{X(t)\}$ is time reversible, the coefficients α_i $(i = 1, 2, \ldots, n_O)$ are non-negative (see Kijima and Kijima (1987)) so that $f_O(t)$ is a mixture of exponentials. Similar results hold for $f_C(t)$, the unconditional probability density function of closed sojourn times.

2.1.3 Moments

For $k = 0, 1, \ldots$, let $M^{(k)}$ be the $n \times n$ matrix given by

$$M^{(k)} = \int_0^{\infty} t^k f(t)\, \mathrm{d}t.$$

The matrix $M^{(k)}$ contains information regarding the kth moments of open and closed sojourn lengths. Writing

$$M^{(k)} = \begin{pmatrix} 0 & M_{OC}^{(k)} \\ M_{CO}^{(k)} & 0 \end{pmatrix},$$

where, for example, the submatrix $M_{OC}{}^{(k)}$ is the kth moment matrix relating to open sojourn lengths and has dimension $n_O \times n_C$, and using equation (2.10), we have

$$M_{OC}^{(k)} = \int_0^\infty t^k f_{OC}(t)\,\mathrm{d}t = (-1)^{k+1}\, k!\, Q_{OO}^{-(k+1)}\, Q_{OC}\,. \tag{2.19}$$

The analogous result

$$M_{CO}^{(k)} = (-1)^{k+1}\, k!\, Q_{CC}^{-(k+1)}\, Q_{CO} \tag{2.20}$$

holds for the kth moments of closed sojourn lengths.

Now let $\mu_O{}^{(k)}$ be the unconditional kth moment of open sojourns when the channel is in equilibrium. Then

$$\begin{aligned} \mu_O{}^{(k)} &= (\pi_O)^\top M_{OC}^{(k)}\,\mathbf{1} \\ &= (\pi_O)^\top (-1)^{(k+1)}\, k!\, Q_{OO}^{-(k+1)}\, Q_{OC}\,\mathbf{1} \\ &= (\pi_O)^\top (-1)^k\, k!\, Q_{OO}^{-k}\,\mathbf{1}, \end{aligned} \tag{2.21}$$

using the fact that $Q_{OO}\mathbf{1} + Q_{OC}\mathbf{1} = \mathbf{0}$. An equivalent expression exists for $\mu_C^{(k)}$, the unconditional kth moment of closed sojourns when the channel is in equilibrium.

Let $\mu_O = \mu_O^{(1)}$ and $\mu_C = \mu_C^{(1)}$ be the equilibrium mean open and closed sojourn times, respectively. Another equivalent expression for μ_O (Colquhoun and Hawkes (1977)) can be derived as follows. On average the number of channel openings in a unit of time is given by $(\mu_O + \mu_C)^{-1} = \lambda$ say. This is the intensity of the point process describing channel openings and can also be expressed as

$$\lambda = \sum_{i \in C} \pi_i \sum_{j \in O} q_{ij},$$

the rate at which the channel leaves the class of closed states at equilibrium. Since the equilibrium probability that a channel is open is given by $\mu_O / (\mu_O + \mu_C)$, and also by $\pi_1 + \pi_2 + \ldots + \pi_{n_O}$, it follows that

$$\mu_O = (\mu_O + \mu_C) \sum_{i \in O} \pi_i$$

$$= \frac{\sum_{i \in O} \pi_i}{\sum_{i \in C} \sum_{j \in O} \pi_i q_{ij}}$$

$$= \frac{\sum_{i \in O} \pi_i}{\sum_{i \in O} \pi_i \sum_{j \in C} q_{ij}}, \qquad (2.22)$$

using the detailed balance conditions (2.4). A similar expression holds for μ_C. Alternatively an expression for μ_C in terms of μ_O is given by

$$\mu_C = \mu_O((\Sigma_{i\in O}\,\pi_i)^{-1} - 1). \tag{2.23}$$

From equation (2.21) and an equivalent equation for closed sojourns, the variances, σ_O^2 and σ_C^2 say, of open and closed sojourn lengths, respectively, are given by

$$\sigma_O^2 = 2\,\boldsymbol{\pi_O}^{\top} Q_{OO}^{-2}\mathbf{1} - \mu_O^2 \tag{2.24}$$

and

$$\sigma_C^2 = 2\,\boldsymbol{\pi_C}^{\top} Q_{CC}^{-2}\mathbf{1} - \mu_C^2\,. \tag{2.25}$$

where π_C is the $n_C \times 1$ column vector whose first m_C elements are $\pi_1^C,\ \pi_2^C,\ldots,\ \pi_{m_C}^C$, and whose remaining elements are all zero.

2.1.4 Autocorrelation and Cross-Correlation Functions

Several authors have noted that important information concerning the structure of an ion channel gating mechanism is contained in the open and closed sojourn autocorrelation functions (see, for example, Fredkin *et al.* (1985), Colquhoun and Hawkes (1987), Ball and Sansom (1988a and 1988b), Ball and Rice (1989)) and the open-closed and closed-open cross-correlation functions (Ball *et al.* (1988)).

The length of the $(k + 1)$th open sojourn is given by T_{2k+1} $(k = 0, 1,...)$. The covariance of T_1 and T_{2k+1} is

$$\begin{aligned} \mathrm{Cov}(T_1, T_{2k+1}) &= \mathrm{E}[T_1\ T_{2k+1}] - \mathrm{E}[T_1]\,\mathrm{E}[T_{2k+1}] \\ &= \mathrm{E}[T_1\ T_{2k+1}] - \mu_O{}^2. \end{aligned} \tag{2.26}$$

Meanwhile

$$\mathrm{E}[T_1\ T_{2k+1}] = (\pi_O)^{\top}\ M_{OC}^{(1)}\ P_{CO}\ (P_O)^{k-1}\ M_{OC}^{(1)}\ \mathbf{1}\,, \tag{2.27}$$

where π_O weights the expectation according to the probabilities that the first open sojourn starts in the various open states, the first occurrence of $M_{OC}{}^{(1)}$ corresponds to the length T_1 of the first open sojourn, P_{CO} is concerned with transition to the start of the second open sojourn, the product $(P_O)^{k-1}$ contains information regarding transitions to the start of the $(k + 1)$th open sojourn, the second occurrence of $M_{OC}{}^{(1)}$ corresponds to the length T_{2k+1} of the $(k+1)$th open sojourn and the final vector of ones sums over the possible entry states to the succeeding closed sojourn. Substituting expressions (2.14), (2.15) and (2.19) into equation (2.27), we obtain

$$\begin{aligned} \mathrm{E}[T_1\ T_{2k+1}] &= (\pi_O)^{\top}\ (Q_{OO}^{-2}\ Q_{OC})\ (-Q_{CC}^{-1}\ Q_{CO})\ (Q_{OO}^{-1}\ Q_{OC}\ Q_{CC}^{-1}\ Q_{CO})^{k-1} \\ &\quad \times (Q_{OO}^{-2}\ Q_{OC})\,\mathbf{1} \\ &= -\ (\pi_O)^{\top}\ Q_{OO}^{-2}\ (Q_{OC}\ Q_{CC}^{-1}\ Q_{CO}\ Q_{OO}^{-1})^{k}\ (Q_{OO}^{-1}\ Q_{OC})\,\mathbf{1} \\ &= (\pi_O)^{\top}\ Q_{OO}^{-2}\ (Q_{OC}\ Q_{CC}^{-1}\ Q_{CO}\ Q_{OO}^{-1})^{k}\ \mathbf{1}\,, \end{aligned} \tag{2.28}$$

where the final expression is derived using the fact that $Q_{OO}\mathbf{1} + Q_{OC}\mathbf{1} = \mathbf{0}$.

For $k = 1, 2,...,$ let $r_O(k)$ be the open sojourn autocorrelation function which measures the degree of correlation between the ith and the $(i + k)$th channel openings when the channel is in equilibrium, and let $r_C(k)$ be the closed sojourn autocorrelation function. Then since $\{X(t)\}$ is time homogeneous, we can use equations (2.26) and (2.28) to obtain

$$r_O(k) = ((\pi_O)^\top Q_{OO}^{-2} (Q_{OC} Q_{CC}^{-1} Q_{CO} Q_{OO}^{-1})^k \mathbf{1} - \mu_O^2) / \sigma_O^2 \qquad (2.29)$$

(see Fredkin *et al.* (1985)). Similarly,

$$r_C(k) = ((\pi_C)^\top Q_{CC}^{-2} (Q_{CO} Q_{OO}^{-1} Q_{OC} Q_{CC}^{-1})^k \mathbf{1} - \mu_C^2) / \sigma_C^2, \qquad (2.30)$$

In order to obtain a formula for $r_{OC}(k)$ $(k = 1, 2,....,)$, the open-closed cross-correlation function which measures the correlation between the ith open sojourn and the $(i + k)$th closed sojourn, we proceed similarly. The covariance of the first open sojourn T_1 and the $(k + 1)$th closed sojourn T_{2k+2} $(k = 0, 1, 2,....)$ is given by

$$\mathrm{Cov}(T_1, T_{2k+2}) = (\pi_O)^\top M_{OC}^{(1)} (P_C)^k M_{CO}^{(1)} \mathbf{1} - \mu_O \mu_C .$$

Using equations (2.14), (2.15), (2.19) and (2.20) yields

$$r_{OC}(k) = ((\pi_O)^{\top} (Q_{OO}^{-2} Q_{OC}) (Q_{CC}^{-1} Q_{CO} Q_{OO}^{-1} Q_{OC})^k (Q_{CC}^{-2} Q_{CO}) \mathbf{1} - \mu_O \mu_C) / \sqrt{\sigma_O^2 \sigma_C^2}$$

$$= (-(\pi_O)^{\top} Q_{OO}^{-2} (Q_{OC} Q_{CC}^{-1} Q_{CO} Q_{OO}^{-1})^k Q_{OC} Q_{CC}^{-1} \mathbf{1} - \mu_O \mu_C) / \sqrt{\sigma_O^2 \sigma_C^2}, \qquad (2.31)$$

since $Q_{CO}\mathbf{1} + Q_{CC}\mathbf{1} = \mathbf{0}$. It is worth noting that, since the channel process $\{X(t);\ t \geq 0\}$ is time reversible, the closed-open cross-correlation function is identical to the open-closed cross-correlation function, and hence only $r_{OC}(k)$ need be considered (see Ball *et al.* (1988)).

To allow us to derive simpler forms for the autocorrelation and cross-correlation functions, we now show that time reversibility ensures that the matrices P_O and P_C are diagonalizable (Fredkin *et al.* (1985), Ball and Rice (1989)). Using equations (2.14) and (2.15), we can write

$$P_O = Q_{OO}^{-1} Q_{OC} Q_{CC}^{-1} Q_{CO}. \qquad (2.32)$$

Define $\tilde{P}_O$ by

$$\tilde{P}_O = W_O^{1/2} P_O W_O^{-1/2}. \qquad (2.33)$$

Then substitution of (2.32) into (2.33) yields

$$\tilde{P}_O = W_O^{½} Q_{OO}^{-1} W_O^{-½} W_O^{½} Q_{OC} W_C^{-½} W_C^{½} Q_{CC}^{-1} W_C^{-½} W_C^{½} Q_{CO} W_O^{-½}$$

$$= \tilde{Q}_{OO}^{-1} \tilde{Q}_{OC} \tilde{Q}_{CC}^{-1} \tilde{Q}_{CO}, \qquad (2.34)$$

where $\tilde{Q}_{OO}^{-1} = W_O^{½} Q_{OO}^{-1} W_O^{-½}$,

$\tilde{Q}_{OC} = W_O^{½} Q_{OC} W_C^{-½}$,

$\tilde{Q}_{CC}^{-1} = W_C^{½} Q_{CC}^{-1} W_C^{-½}$

and $\tilde{Q}_{CO} = W_C^{½} Q_{CO} W_O^{-½}$.

From equation (2.34) we can write

$$\tilde{Q}_{OO}^{½} \tilde{P}_O \tilde{Q}_{OO}^{-½} = \tilde{Q}_{OO}^{-½} \tilde{Q}_{OC} \tilde{Q}_{CC}^{-½} \tilde{Q}_{CC}^{-½} \tilde{Q}_{CO} \tilde{Q}_{OO}^{-½}. \qquad (2.35)$$

Expansion of equation (2.5) in partitioned form yields that $\tilde{Q}_{OC} = (\tilde{Q}_{CO})^{\top}$, $\tilde{Q}_{OO}^{-1} = (\tilde{Q}_{OO}^{-1})^{\top}$ and $\tilde{Q}_{CC}^{-1} = (\tilde{Q}_{CC}^{-1})^{\top}$, and hence equation (2.35) becomes

$$\tilde{Q}_{OO}^{½} \tilde{P}_O \tilde{Q}_{OO}^{-½} = A^{\top} A, \qquad (2.36)$$

where $A = \tilde{Q}_{CC}^{-½} \tilde{Q}_{CO} \tilde{Q}_{OO}^{-½}$. Now, using equations (2.33) and (2.36), we obtain

$$P_O = (W_O^{½} Q_{OO}^{½})^{-1} A^{\top} A (W_O^{½} Q_{OO}^{½}),$$

demonstrating that P_O is similar to the real symmetric matrix $A^{\top}A$ which is positive semi-definite and hence has real non-negative eigenvalues (see, for

example, Mardia *et al.* (1979), Section A.7). Therefore P_O is diagonalizable with non-negative real eigenvalues (see, for example, Fröberg (1969)). Similarly, it can be shown that P_C is similar to $AA^\top$. Since the eigenvalues of $AA^\top$ are the same as those of $A^\top A$ (see, for example, Mardia *et al.* (1979), Theorem A.6.2), P_C is diagonalizable with the same eigenvalues as P_O.

Since P_O and P_C are diagonalizable, the autocorrelation and cross-correlation functions admit simple forms (Fredkin *et al.* (1985), Ball and Rice (1989)). Suppose that the matrix P_O admits the spectral representation

$$P_O = \sum_{i=1}^{n_O} \kappa_i F_i$$

say, where κ_i ($i = 1, 2, \ldots, n_O$) are the eigenvalues of P_O with corresponding spectral matrices F_i determined in the same way as those of Q and Q_{OO} above. Since P_O is the transition matrix of the open entry process which is an irreducible aperiodic Markov chain on the finite state space O, the Perron-Frobenius Theorem (see, for example, Grimmett and Stirzaker (1982, p134)) tells us that one of the eigenvalues of P_O, κ_1 say, is one and that the remaining eigenvalues $\kappa_2, \kappa_3, \ldots, \kappa_{n_O}$ satisfy $|\kappa_i| < 1$. Hence, for $i = 2, 3, \ldots, n_O$, $0 \le \kappa_i < 1$. Since π_O is the $n_O \times 1$ vector which gives the equilibrium distribution of the open entry process, it follows that $\mathbf{1}(\pi_O)^\top P_O = \mathbf{1}(\pi_O)^\top$, or equivalently that $F_1 = \mathbf{1}(\pi_O)^\top$. Let $M = \min(m_O, m_C)$. Since P_{OC} (P_{CO}) has at most m_O (m_C) non-

zero rows and at most m_C (m_O) non-zero columns, it follows that rank (P_{OC}) ≤ M (rank (P_{CO}) ≤ M). Since $P_O = P_{OC}P_{CO}$, a standard result in linear algebra tells us that the rank of P_O is at most M. Thus at most M of the eigenvalues κ_i ($i = 1, 2,..., n_O$) are non-zero. Thus, from equation (2.27),

$$\mathrm{E}[T_1\ T_{2k+1}] = (\pi_O)^{\top}\, M_{OC}^{(1)}\, P_{CO} \left(\sum_{i=1}^{M} \kappa_i^{k-1}\, F_i \right) M_{OC}^{(1)}\, \mathbf{1}$$

$$= (\pi_O)^{\top}\, M_{OC}^{(1)}\, P_{CO}\, \mathbf{1}\, (\pi_O)^{\top}\, M_{OC}^{(1)}\, \mathbf{1} + (\pi_O)^{\top}\, M_{OC}^{(1)}\, P_{CO} \left(\sum_{i=2}^{M} \kappa_i^{k-1}\, F_i \right) M_{OC}^{(1)}\, \mathbf{1}$$

$$= \mu_O^{\,2} + \sum_{i=2}^{M} \kappa_i^{k-1}\, (\pi_O)^{\top}\, M_{OC}^{(1)}\, P_{CO}\, F_i\, M_{OC}^{(1)}\, \mathbf{1}\,.$$

Hence

$$r_O(k) = \sum_{i=2}^{M} \kappa_i^{k-1}\, \alpha_i \qquad (k = 1, 2,...) \tag{2.37}$$

where

$$\alpha_i = \left((\pi_O)^{\top}\, M_{OC}^{(1)}\, P_{CO}\, F_i\, M_{OC}^{(1)}\, \mathbf{1} \right) / \sigma_O^{\,2} \qquad (i = 2, 3,..., M)\,.$$

Equivalent formulae can be shown to hold for $r_C(k)$ and $r_{OC}(k)$ so that each of $r_O(k)$, $r_C(k)$ and $r_{OC}(k)$ can be written as a sum of M - 1 terms of the form $\alpha_i\ \kappa_i^k$ ($i = 1, 2,..., M$ - 1) where $0 \le \kappa_i \le 1$ and $\alpha_i \ge 0$ (see Fredkin *et al.* (1985) and Ball

and Sansom (1988a)). Ball and Rice (1989) show that, for the autocorrelation functions, the coefficients α_i (not generally the same for each function) are non-negative and hence that these two autocorrelation functions are decreasing, non-negative, and convex. Since P_O and P_C have the same eigenvalues, the geometrically decaying terms κ_i are necessarily the same for each of the autocorrelation and cross-correlation functions (Ball and Rice (1989)).

Correlation functions can give information which aids the process of accepting, rejecting and choosing between different proposed models. Firstly, Markov models which yield negative autocorrelation functions cannot be time reversible and since it seems to be the case that no experimentally observed negative autocorrelations have been reported in the literature (Ball and Rice (1989)), this correlation-based evidence suggests that most channel gating mechanisms are indeed time reversible. Secondly, correlation functions provide information concerning the numbers of open and closed states and the number of transition routes between the open and closed classes of states (Fredkin *et al.* (1985), Colquhoun and Hawkes (1995)). In fact, at least two open states (with the same conductance) and at least two closed states (with the same conductance) are required if correlations are to arise and, moreover, there must be at least two transition routes between the open and closed classes of states (Colquhoun and Hawkes (1987), Ball and Sansom (1988b)). Further, a lower bound for $\min(m_O, m_C)$ can, in principle, be obtained by fitting expressions of the form of

equation (2.37), and an equivalent equation for closed sojourns, to estimated autocorrelation functions for observed open and closed sojourns. Thirdly, a number of authors (e.g. Colquhoun and Sakmann (1985), McManus *et al.* (1985)) have reported that channel openings adjacent to short closings tend to be long. McManus and Magleby (1989) point out that some non-Markov models can be rejected on the basis that they do not predict this type of behaviour. Fourthly, the behaviour of a channel following a jump in agonist concentration or voltage depends on the correlation functions. The time that elapses before the first channel opening occurs is known as the first latency. In the absence of correlations, the lengths of all open and closed sojourns after the first latency have exactly the same distributions as at equilibrium, whereas in the presence of correlations these sojourn lengths do not immediately attain their equilibrium distributions, although this does occur given sufficient time (Colquhoun and Hawkes (1995)).

2.1.5 Clustering

In many experiments (e.g. Sakmann *et al.* (1980)) it has been observed that channel openings, or equivalently points in time when a single channel moves from a closed state to an open state, are grouped together in bursts, and moreover, these bursts of channel openings themselves occur in clusters. Colquhoun and Hawkes (1982) modelled this situation by assuming that the closed states are

further partitioned into short-lived, long-lived and very long-lived closed states, corresponding to gaps between openings *within* a burst, gaps *between* bursts within a cluster of bursts, and gaps *between* clusters of bursts, respectively. They presented general methods of deriving expressions for a large number of observable characteristics of bursts and clusters, such as the total length of a burst and the number of bursts per cluster. Further, Ball and Sansom (1987) derived an expression for a simple descriptive measure which indicates whether or not a given model does indeed display clustering of openings, and Ball and Davies (1997) derived an equivalent expression to determine whether or not a given model displays clustering of bursts of openings.

The approach of both Ball and Sansom (1987) and Ball and Davies (1997) was as follows. Let $\{N(t)\} = \{N(t); t \geq 0\}$ be a point process. Thus $N(0) = 0$ and for $t > 0$, $N(t)$ is the number of points occurring in $(0, t]$. Then the measures

$$\frac{\text{Var}[N(t)]}{\text{E}[N(t)]} \quad (t > 0) \qquad \text{and} \qquad \lim_{t \to \infty} \left(\frac{\text{Var}[N(t)]}{\text{E}[N(t)]} \right) \tag{2.38}$$

contain information concerning the temporal clustering of the point process $\{N(t)\}$. In particular, if the point process is highly clustered, these measures are much greater than one, whereas, if the point process is evenly spaced, their values are much smaller than one. Note that, in the case in which $\{N(t)\}$ is Poisson, $\text{Var}[N(t)] / \text{E}[N(t)]$ has value one.

2.1.5.1 Clustering of Openings

In this section, we give the expressions derived by Ball and Sansom (1987) for the measures (2.38) when $\{N(t)\}$ is the point process describing channel openings. Recall from equation (2.6) that an $n \times n$ transition matrix Q may be written in the form

$$Q = \sum_{i=1}^{n} \lambda_i E_i,$$

where $\lambda_1 = 0$ and $\lambda_2, \lambda_3, \ldots, \lambda_n$, the eigenvalues of Q, are strictly negative and expressions for and properties of the matrices $E_1, E_2, \ldots E_n$ are given in section 2.1. Furthermore, define the $n \times n$ matrix Q^*_{CO} by

$$Q^*_{CO} = \begin{pmatrix} 0 & 0 \\ Q_{CO} & 0 \end{pmatrix}$$

and, for $i = 1, 2, \ldots, n$, let $E^*_i = Q^*_{CO} E_i Q^*_{CO}$. Then Ball and Sansom (1987) show that

$$\mathrm{E}[N(t)] = \boldsymbol{m}(t)^{\top} \boldsymbol{\pi}$$

and

$$\mathrm{Var}[N(t)] = \boldsymbol{h}(t)^{\top} \boldsymbol{\pi} + \boldsymbol{m}(t)^{\top} \boldsymbol{\pi} - (\boldsymbol{m}(t)^{\top} \boldsymbol{\pi})^2,$$

where

$$\boldsymbol{m}(t) = \left[t E_1 + \sum_{i=2}^{n} \left(\frac{\exp(\lambda_i t) - 1}{\lambda_i} \right) E_i \right] Q_{CO}^{*} \mathbf{1} \quad (t \geq 0)$$

and

$$\begin{aligned} \boldsymbol{h}(t) = 2 \Bigg[& \tfrac{1}{2} t^2 E_1 E_1^{*} + \sum_{i=2}^{n} \left(\frac{\exp(\lambda_i t) - 1}{\lambda_i^2} - \frac{t}{\lambda_i} \right) (E_1 E_i^{*} + E_i E_1^{*}) \\ & + \sum_{i=2}^{n} \sum_{j=2}^{n} \left(\frac{1 - \exp(\lambda_i t)}{\lambda_i \lambda_j} E_i E_j^{*} \right) + \sum_{i=2}^{n} \left(\frac{t \exp(\lambda_i t)}{\lambda_i} E_i E_i^{*} \right) \\ & + \sum_{i=2, i \neq j}^{n} \sum_{j=2}^{n} \left(\frac{\exp(\lambda_i t) - \exp(\lambda_j t)}{\lambda_j (\lambda_i - \lambda_j)} E_i E_j^{*} \right) \Bigg] \mathbf{1} \quad (t \geq 0). \end{aligned}$$

In this expression for $\boldsymbol{h}(t)$ it is assumed that the eigenvalues $\lambda_2, \lambda_3, \ldots, \lambda_n$, are distinct. If this is not the case, say $\lambda_i = \lambda_j$, then the factor $(\exp(\lambda_i t) - \exp(\lambda_j t)) / \lambda_j (\lambda_i - \lambda_j)$ in the final component of this expression is replaced by its limit as $\lambda_i \to \lambda_j$, this being $(t \exp(\lambda_j t)) / \lambda_j$ (see Ball and Sansom (1987)).

Ball and Sansom (1987) also give the asymptotic expression

$$\lim_{t \to \infty} \left(\frac{\mathrm{Var}[N(t)]}{\mathrm{E}[N(t)]} \right) = 1 - \frac{2 \sum_{i \in C} \pi_i \sum_{j \in O} q_{ij} \sum_{l \in C} \sum_{k=2}^{n} \lambda_k^{-1} (E_k)_{jl} \sum_{m \in O} q_{lm}}{\sum_{i \in C} \pi_i \sum_{j \in O} q_{ij}}, \qquad (2.39)$$

which is independent of the initial state of the process.

2.1.5.2 Clustering of Bursts of Openings

In this section, we state the formulae derived in Ball and Davies (1997) for the measures (2.38) when $\{N(t)\}$ is the point process describing the starts of bursts of channel openings. First it is convenient to give a more precise definition of a burst of openings. We now suppose that the closed states are partitioned into just short-lived and long-lived closed states, the latter being the union of what were referred to above as long-lived and very long-lived closed states, and that the class of short-lived closed states is denoted C and the class of long-lived closed states is denoted L. Then a burst is a group of successive sojourns of the channel in $O \cup C$. Thus bursts are separated by one or more sojourns of the channel in L, and a burst is deemed to commence at the start of its first open sojourn.

Ball and Davies (1997) use an approach based on an augmented continuous-time Markov chain to obtain a direct derivation of expressions for (2.38) when $\{N(t)\}$ is the point process describing the starts of bursts of channel openings. Whether or not a given opening corresponds to the start of a burst requires knowledge of the history of the channel process. However, the state space of the underlying single channel process can be augmented so that when the channel is in a short-lived closed state, it is also recorded whether the current sojourn in the short-lived

closed states was entered from the open states or from the long-lived closed states. The resulting process is still Markov but the number of short-lived closed states is doubled. The state space can now be partitioned into open, closed-open (short-lived closed states entered from the open states), closed-long (short-lived closed states entered from the long-lived closed states) and long-lived closed states. Denote these classes of states by O, C_O, C_L and L, respectively and let $\tilde{Q}$ be the transition matrix of this augmented process. Then

$$\tilde{Q} = \begin{pmatrix} \tilde{Q}_{\tilde{O}\tilde{O}} & \tilde{Q}_{\tilde{O}\tilde{C}_O} & \tilde{Q}_{\tilde{O}\tilde{C}_L} & \tilde{Q}_{\tilde{O}\tilde{L}} \\ \tilde{Q}_{\tilde{C}_O\tilde{O}} & \tilde{Q}_{\tilde{C}_O\tilde{C}_O} & \tilde{Q}_{\tilde{C}_O\tilde{C}_L} & \tilde{Q}_{\tilde{C}_O\tilde{L}} \\ \tilde{Q}_{\tilde{C}_L\tilde{O}} & \tilde{Q}_{\tilde{C}_L\tilde{C}_O} & \tilde{Q}_{\tilde{C}_L\tilde{C}_L} & \tilde{Q}_{\tilde{C}_L\tilde{L}} \\ \tilde{Q}_{\tilde{L}\tilde{O}} & \tilde{Q}_{\tilde{L}\tilde{C}_O} & \tilde{Q}_{\tilde{L}\tilde{C}_L} & \tilde{Q}_{\tilde{L}\tilde{L}} \end{pmatrix} = \begin{pmatrix} Q_{OO} & Q_{OC} & 0 & Q_{OL} \\ Q_{CO} & Q_{CC} & 0 & Q_{CL} \\ Q_{CO} & 0 & Q_{CC} & Q_{CL} \\ Q_{LO} & 0 & Q_{LC} & Q_{LL} \end{pmatrix}. \qquad (2.40)$$

The number of bursts commencing in $(0, t]$ is then given by the number of transitions into the open states, from either the long-lived closed states or the closed-long states, made by the augmented process in $(0, t]$. Then from Ball and Davies (1997), we obtain, for $t > 0$,

$$\frac{\text{Var}[N(t)]}{\text{E}[N(t)]} = 1 + \frac{2\,\tilde{\pi}^{\top} Q^{*} \tilde{Z} Q^{*} \mathbf{1}}{\tilde{\pi}^{\top} Q^{*} \mathbf{1}} - \frac{2\,\tilde{\pi}^{\top} Q^{*} \tilde{Z}^{2} (I - \exp(\tilde{Q}t)) Q^{*} \mathbf{1}}{\tilde{\pi}^{\top} Q^{*} \mathbf{1}\, t}$$

and

$$\lim_{t \to \infty} \left(\frac{\text{Var}[N(t)]}{\text{E}[N(t)]} \right) = 1 + \frac{2\,\tilde{\pi}^{\top} Q^{*} \tilde{Z} Q^{*} \mathbf{1}}{\tilde{\pi}^{\top} Q^{*} \mathbf{1}},$$

where $\tilde{\pi}$, the equilibrium distribution of the augmented process, is given by

$$\tilde{\pi}_i = \begin{cases} \pi_i & i = 1,\ldots,n_O \\ \pi_i(-Q_{CC}^{-1}Q_{CO}\mathbf{1})_{i-n_O} & i = n_O+1,\ldots,n_O+n_C \\ \pi_{i-n_C}\left(1 - (-Q_{CC}^{-1}Q_{CO}\mathbf{1})_{i-n_O-n_C}\right) & i = n_O+n_C+1,\ldots,n_O+2n_C \\ \pi_{i-n_C} & i = n_O+2n_C+1,\ldots,n \end{cases}$$

and

$$Q^* = \begin{pmatrix} 0 & 0 & 0 & 0 \\ 0 & 0 & 0 & 0 \\ Q_{CO} & 0 & 0 & 0 \\ Q_{LO} & 0 & 0 & 0 \end{pmatrix},$$

$$Q^*\tilde{Z}Q^* = \begin{pmatrix} 0 & 0 & 0 & 0 \\ 0 & 0 & 0 & 0 \\ Q_{CO}\tilde{Z}_{\tilde{O}\tilde{C}_L}Q_{CO} + Q_{CO}\tilde{Z}_{\tilde{O}\tilde{L}}Q_{LO} & 0 & 0 & 0 \\ Q_{LO}\tilde{Z}_{\tilde{O}\tilde{C}_L}Q_{CO} + Q_{LO}\tilde{Z}_{\tilde{O}\tilde{L}}Q_{LO} & 0 & 0 & 0 \end{pmatrix}$$

and

$$\tilde{Z} = -\mathbf{1}\,\tilde{\pi}^\top + (\mathbf{1}\,\tilde{\pi}^\top - \tilde{Q})^{-1}.$$

Note that $\tilde{Z}$ is the fundamental matrix (see, for example, Keilson (1979), p107) of the augmented process (with transition matrix $\tilde{Q}$) which records both the state

of the channel process $\{X(t)\}$ and whether short-lived closed sojourns were entered from the open states or from the long-lived closed states.

The matrix $\tilde{Z}_{OC_L}$ is given by

$$\tilde{Z}_{OC_L} = (-\mathbf{1}\,\pi^{\top})_{OL}\, Q_{LC}\, Q_{CC}^{-2} + \sum_{i=2}^{n} \lambda_i^{-1}\, [E_i]_{OL}\, Q_{LC}\, Q_{CC}^{-1},$$

the matrix $\tilde{Z}_{OL}$ is given by

$$\tilde{Z}_{ij} = \left(\sum_{k=2}^{n} -\lambda_k^{-1} E_k \right)_{i,\, j - n_C} \qquad (i \in O,\, j \in L),$$

and $\tilde{Z}\exp(\tilde{Q}\,t)$ is given as follows. Partitioning $\tilde{Z}\exp(\tilde{Q}\,t)$ in a similar fashion to equation (2.40), we give expressions for $[\tilde{Z}\exp(\tilde{Q}\,t)]_{EF}$ where $\tilde{E}, \tilde{F} = \tilde{O}, \tilde{C}_O, \tilde{C}_L, \tilde{L}$. Using the notation that if $\tilde{E} = \tilde{O}, \tilde{C}_O, \tilde{C}_L, \tilde{L}$ then $E = O, C, C, L$, respectively, and similarly for $\tilde{F}, F$, we have

$$\left[\tilde{Z}\exp(\tilde{Q}\,t)\right]_{\tilde{E}\tilde{F}} = \left[Z\exp(Qt)\right]_{EF}$$

for $t \geq 0$, $\tilde{E} = \tilde{O}, \tilde{C}_O, \tilde{C}_L, \tilde{L}$ and $\tilde{F} = \tilde{O}, \tilde{L}$, where

$$Z = -\sum_{i=2}^{n} \lambda_i^{-1} E_i \quad \text{and} \quad Z\exp(Qt) = -\sum_{i=2}^{n} \lambda_i^{-1} \exp(\lambda_i t)\, E_i\,.$$

Further, the matrix Q_{CC} also admits a spectral representation, given by

$$Q_{CC} = \sum_{i=1}^{n_C} \mu_i F_i ,$$

say, where μ_i and F_i ($i = 1, 2,..., n_C$) are, respectively, the eigenvalues of Q_{CC} and the corresponding projection matrices (see, for example, Fredkin *et al.* (1985)).

If $\lambda_i \neq \mu_j$ for all i and j, and $\tilde{E} \neq \tilde{C}_L$, then, for $t \geq 0$,

$$\begin{aligned} \left[\tilde{Z}\exp(\tilde{Q}\,t)\right]_{\tilde{E}\tilde{C}_L} &= -[\mathbf{1}\ \pi^{\top}]_{EL}\, Q_{LC}\, Q_{CC}^{-2} \exp(Q_{CC}\,t) \\ &\quad - \sum_{i=2}^{n} \sum_{j=1}^{n_C} [E_i]_{EL}\, Q_{LC}\, F_j\, \lambda_i^{-1} (\mu_j - \lambda_i)^{-1} [\exp(\mu_j t) - \exp(\lambda_i t)] \qquad (2.41) \\ &\quad - Z_{EL}\, Q_{LC}\, Q_{CC}^{-1} \exp(Q_{CC}\,t). \end{aligned}$$

If $\lambda_i = \mu_j$ for some i and j, then the term $(\mu_j - \lambda_i)^{-1}[\exp(\mu_j t) - \exp(\lambda_i t)]$ in the above is replaced by $t \exp(\lambda_i t)$. If $\tilde{E} = \tilde{C}_L$, then, for $t \geq 0$,

$$\begin{aligned} \left[\tilde{Z}\exp(\tilde{Q}\,t)\right]_{\tilde{C}_L\tilde{C}_L} &= -[\mathbf{1}\ \pi^{\top}]_{CL}\, Q_{LC}\, Q_{CC}^{-2} \exp(Q_{CC}\,t) \\ &\quad - \sum_{i=2}^{n} \sum_{j=1}^{n_C} [E_i]_{CL}\, Q_{LC}\, F_j\, \lambda_i^{-1} (\mu_j - \lambda_i)^{-1} [\exp(\mu_j t) - \exp(\lambda_i t)] \qquad (2.42) \\ &\quad - Z_{CL}\, Q_{LC}\, Q_{CC}^{-1} \exp(Q_{CC}\,t) - Q_{CC}^{-1} \exp(Q_{CC}\,t), \end{aligned}$$

with the same modification if $\lambda_i = \mu_j$ for some i and j. For $\tilde{E} = \tilde{O}, \tilde{C}_L, \tilde{L}$ and $\tilde{F} = \tilde{C}_O$, the sub-matrices $[\tilde{Z}\exp(\tilde{Q}\,t)]_{EF}$ and $[\tilde{Z}\exp(\tilde{Q}\,t)]_{FF}$ are given by equations (2.41) and (2.42) respectively, but with the subscript L replaced by the subscript O throughout.

2.2 Data Acquisition and Time Interval Omission

In practice, there is a major problem with single channel analysis. The limited frequency response and filtering effect of the electronic recording system, together with noise and sampling the signal at regularly spaced points in time, results in failure to detect very brief channel sojourns in either the open or closed classes of states, a phenomenon known as time interval omission.

2.2.1 Data Acquisition

The current through an ion channel is assumed to consist of rectangular pulses with infinitely short transition times. In order to analyse channel activity it is necessary to estimate the amplitudes and transition times in the measured currents. Cell physiologists Erwin Neher and Bert Sakmann (winners of the 1991 Nobel Prize in Physiology or Medicine) developed a technique (Neher and Sakmann (1976)) that allows the measurement of the electrical currents of magnitude *ca.* 10^{-12} Amp that pass through ion channels. This technique, known as the patch-clamp technique, has caused a revolutionary advancement of many areas of membrane and cell biology. The basic approach requires a low-noise recording procedure. This is achieved by using suction to tightly seal a glass microelectrode onto the plasma membrane of an intact cell, thereby isolating a small patch. The currents flowing through ion channels enclosed by a pipette tip

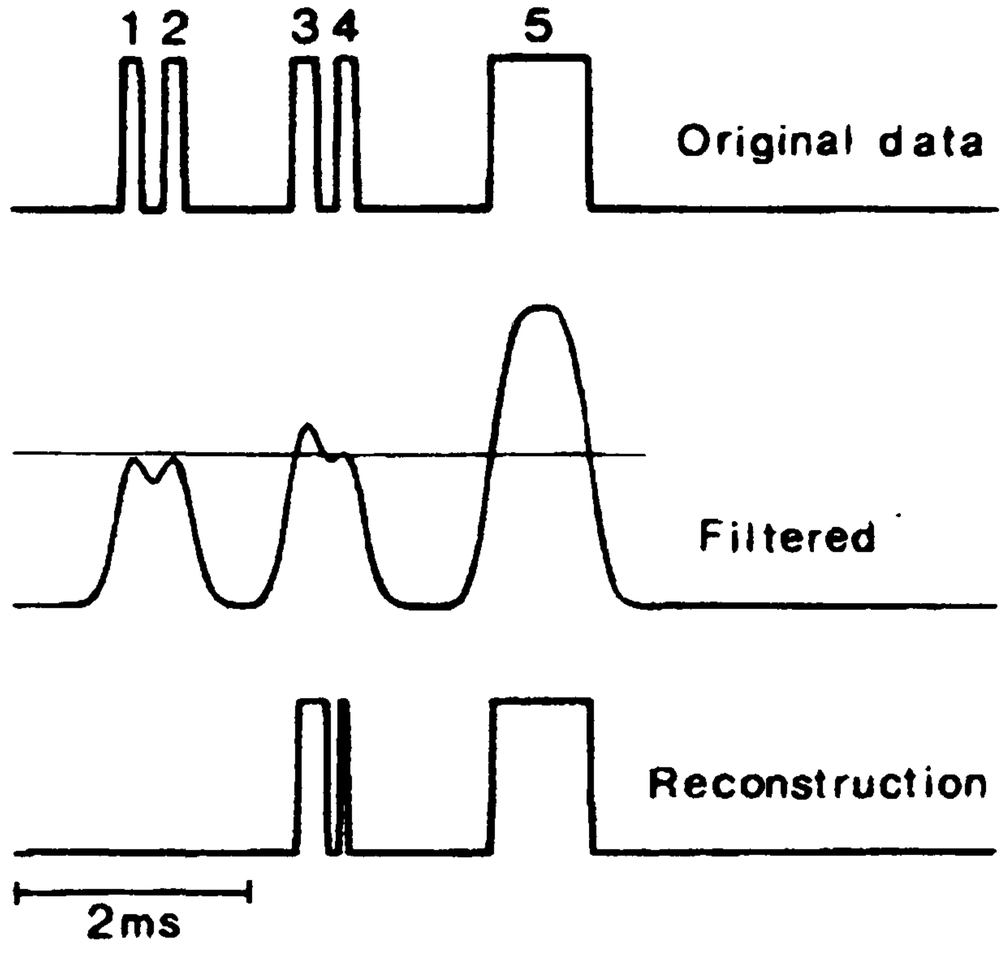

Figure 2.1. Threshold analysis of closely spaced events. Simulated rectangular events (top trace) were filtered and displayed (middle trace) and the reconstruction obtained from the threshold-crossing analysis is shown in the lower trace. Events 1 and 2 were just below threshold and thus not detected, event 4 was even shorter, but was detected because it followed event 3 by a sufficiently short closed interval. [From Colquhoun and Sigworth (1983).]

within that patch are measured using a patch-clamp amplifier. In practice the current signal from a patch-clamp amplifier is filtered (Figure 2.1 and Colquhoun and Sigworth (1983)). Firstly the patch-clamp amplifier places a limit on its frequency response (say < 100 kHz) so that its output is a filtered version of the true current signal. Secondly all the various types of tape recorders used to record the data incorporate some sort of filter. Finally, the data are filtered again to reduce the background noise enough to enable openings and closings to be

detected and identified. This is an important step since the basic problem in identifying channel activity is that short channel openings cannot be differentiated from random noise fluctuations about the baseline and that short closings cannot be distinguished from fluctuations away from the level of current associated with channel openings. The data are always obtained initially in the form of a voltage signal and are subsequently converted to digital form for storage on a digital tape or for computer analysis. The analog-to-digital converter used for this purpose samples the voltage at discrete times. Typically, the sampling interval is of the order of 100 microseconds, whereas the durations of openings are of the order of milliseconds. If the sample rate is not sufficiently high, rapid changes in current may be missed.

The list of the estimates of the times and amplitudes of transitions in the current record is known as an idealised record. These data approximate the channel activity and are often used for statistical analysis of ion channel kinetics. Although this analysis can incorporate corrections for missed events (see below), it is important that the idealised record is as complete and unbiased as possible. Often, in practice, the two operations of finding events and fitting the transitions are carried out separately. For example, a transition finder can scan a channel record for activity and then, once the events are found, they can be fitted to an idealised time course (Colquhoun and Sigworth (1983)). The latter step of computing a theoretical time course for the current can be very time-consuming

and may conceivably require the data to be filtered differently. Alternatively, a simple threshold detector may be used to combine the processes of detection and characterisation of channel events. The use of a simple threshold detector is the most widely employed method of single channel analysis (particularly for channels without multiple conductance levels). Firstly the channel amplitude is estimated and this estimate is used to set a threshold level. Commonly this threshold level is set to half the estimated channel amplitude. Then each crossing of the threshold is interpreted as an opening or a closing of the channel, with all time spent above the threshold taken to be an estimate of the time that the channel has spent in the open class of states (see Figure 2.1). The filter risetime is informally defined to be the minimum length of a pulse to which the filter gives a nearly full-amplitude response (e.g. 90% of full-amplitude), and events shorter than a dead time, τ say, of approximately half the filter risetime will be missed since, after filtering, they will never reach the threshold. The exact value of τ for this detection technique may be either measured experimentally, or be calculated by determining the length of the pulse to which the recording system gives a half-amplitude response. Note that, although this threshold-crossing technique should exclude events whose true pulse width is less than τ, the effect of noise will be to include some of these events and, similarly, to exclude some longer events. However, this problem is not too serious if τ is sufficiently small. Indeed, the threshold-crossing technique performs best when τ is reduced as much as possible to reduce the number of missed events. The length τ of the minimum

detectable sojourn is known in ion channel literature as the resolution of the data. Note that this minimum length may not be so clearly defined for other less common detection techniques.

2.2.2 Modelling Time Interval Omission

One effect of time interval omission is to make openings appear longer than they really are if short closings are undetected since several openings separated by undetected closings will be counted as a single opening, often referred to as an apparent or observed open sojourn. A similar effect in which the lengths of closed sojourns are distorted may occur when short openings are missed, but this is not considered to be as serious as the distortion of open sojourn lengths since the channel openings are of far greater interest than the lengths of closings. Time interval omission is usually modelled by assuming that any sojourn of duration less than the resolution τ fails to be detected. Thus an observed open sojourn is defined as beginning with an actual open sojourn of duration at least τ, followed by a number of pairs of closed and open sojourns with the closed sojourns each having length less than τ, and is immediately followed by a closed sojourn of duration at least τ. An observed closed sojourn is defined analogously.

A general semi-Markov framework for analysing single channel data incorporating time interval omission has been developed by Ball *et al.* (1991,

1993a). This framework is based on a process, analogous to the process $\{J_k, T_k\}$ discussed in section 2.1, which is an embedded semi-Markov process $\{\tilde{J}_k, \tilde{T}_k\}$ say, where $\tilde{J}_k$ ($k = 0, 1,...$) are the gateway states for observable sojourns, $\tilde{T}_0 = 0$ and $\tilde{T}_k$ ($k = 0, 1,...$) are the successive sojourn times in the open and closed classes of states. The properties of the observed single channel record incorporating time interval omission are completely determined by the associated semi-Markov kernel. In practice, only the Laplace transform of this kernel is readily available and it is generally not possible to invert this analytically to obtain a closed form expression for the kernel (see next paragraph). Whilst some observed channel properties, such as moments and correlation functions of observed sojourns are derivable from this Laplace transform, the probability density functions of observed open and closed sojourns are not, although they can be derived from the kernel itself. Further, the kernel is also required for exact likelihood based inference.

We now restrict our attention to the case in which the underlying single channel is Markov and discuss methods of overcoming the problem of the non-existence of a non-recursive, closed form expression for the kernel. Blatz and Magleby (1986), Yeo *et al.* (1988) and Crouzy and Sigworth (1990) described various approximate methods of predicting the distributions of observed open and closed sojourn lengths. These methods all involved approximating the distributions by mixtures of exponential distributions. Roux and Sauvé (1985) considered an

approximation in which the lengths of undetected open (closed) sojourns within an observed closed (open) sojourn are ignored and they also considered numerical inversion of the Laplace transform of the kernel. Ball (1990) considered the case in which the resolution is not constant, but instead follows a negative exponential distribution. Hawkes *et al.* (1990) obtained exact recursive expressions for the open and closed sojourn probability density functions by term-wise inversion of an infinite series expansion for the Laplace transform. These probability density functions, $\tilde{f}_O(t)$ and $\tilde{f}_C(t)$ say, each take the form of a sum of exponentials multiplied by polynomials in t, with a different form holding over each different range of length τ. So, for example, over the interval $[k\tau < t < (k + 1)\tau]$ $(k = 1, 2,...)$, the multiplying polynomials are of degree $(k - 1)$ and the density is zero for $[0 < t < \tau]$. Unfortunately, this exact expression is numerically unstable even for moderate values of t. Other derivations of this expression have subsequently been provided by Ball *et al.* (1993b) and Ball (1997). Ball and Yeo (1994) considered an alternative approach based on the numerical solution of a system of renewal type integral equations, which can also be used when the underlying process is semi-Markov. Ball *et al.* (1993b) further showed that the exact recursive expression of Hawkes *et al.* (1990) can also be extended into this more general semi-Markov setting, although in terms of functions that generally do not admit closed form expressions. Jalali and Hawkes (1992a, 1992b) used Tauberian theorems to obtain asymptotic expressions for the probability density functions $\tilde{f}_O(t)$ and $\tilde{f}_C(t)$ as $t \to \infty$. These expressions are extremely accurate for all

but very small values of t. The exact and approximate expressions for the kernel can therefore be used in combination to closely approximate the kernel for all values of t. For example, Hawkes *et al.* (1992) recommend using the exact form for $t \leq 3\tau$ and the asymptotic form for $t > 3\tau$. Ball (1997) showed that the kernel satisfies a system of linear delay differential equations and exploited the theory of series expansions for the solutions of such equations to explain why the asymptotic expression of Jalali and Hawkes (1992a, 1992b) is accurate even for small t.

2.3 Inference

One of the main aims of the analysis of single ion channels is to make inferences regarding the structure and the parameter values of the continuous-time Markov chain used in modelling the ion channel gating kinetics. The inference method often consists of two steps: (i) experimental data on channel structure (e.g. number of subunits), together with the forms of the open and closed sojourn time probability density functions and the correlation functions, are used to postulate an underlying model, and (ii) the parameters of the postulated model are estimated. The majority of studies (including this thesis) have based inference on the reconstructed sequence of open and closed sojourns described in section 2.2, although several authors have based inference directly on the current record (ie. on the noisy digitised data), thus avoiding the problems of time interval

omission.

2.3.1 Inference based directly on Current Records

Most approaches to current record-based inference have used the theory of hidden Markov models. Using hidden Markov models, Fredkin and Rice (1992a) investigated maximum likelihood parameter estimation and formulated a non model-based technique to determine the conductance levels of the channel and the mean sojourn times at each such level. Chung *et al.* (1990) used hidden Markov models to identify channel conductance levels and both Chung *et al.* (1990) and Fredkin and Rice (1992b) used these models to restore sequences of channel sojourns. Magleby and Weiss (1990a, 1990b) explicitly modelled the effects of filtering and noise using a simulation-based estimation method. More recently, Ball *et al.* (1999) and Hodgson (1999) have both considered the use Markov chain Monte Carlo methods for making Bayesian inferences directly from current records.

2.3.2 Inference based on Sequences of Reconstructed Sojourns

The success of inference based directly on the current record is, to some extent, dependent on the signal to noise ratio in the data and on whether the seal resistance can be kept constant during the recording period to avoid a change in

the baseline current. Whilst it is not yet known whether identifiability problems arise with inference based directly on current records, inference based on reconstructed sojourns tends to be fraught with identifiability problems. Time interval omission, in particular, is a great problem. Ball *et al.* (1993a) point out that structural inferences whose origin is in the structure of the gateway process, such as correlation functions, are likely to be robust to time interval omission, whereas information owing to the parametric form of the semi-Markov kernel of the gateway process, such as sojourn time probability density functions, may be considerably more difficult to recover when time interval omission is present. In the absence of time interval omission, the likelihood of a sequence of sojourn times can be derived relatively easily (see Appendix A for details) and this likelihood function can then be maximised using numerical procedures (see Horn and Lange (1983), Fredkin *et al.* (1985), Chay (1988) and Ball and Sansom (1989)). The main problem in extending the method of maximum likelihood to the case in which time interval omission is present has been the difficulty in calculating the likelihood function posed by the absence of a closed form for the semi-Markov kernel. Several authors have therefore considered maximum likelihood estimation based on approximations to the kernel (e.g. Roux and Sauvé (1985), Blatz and Magleby (1986), Yeo *et al.* (1988)). Due to the difficulties associated with maximum likelihood-based inference, alternative methods of inference have been considered. These include Laplace transform based inference, the derivation of parameter estimates from the forms of observed two-

dimensional open-closed and closed-open sojourn time probability density functions (Magleby and Weiss (1990a, 1990b)), and a method involving Poisson sampling (Ball *et al.* (1992)).

2.3.3 Identifiability Problems

As already mentioned in section 1.3.2, three main identifiability problems arise in making inferences for ion channel gating mechanisms.

2.3.3.1 Structural Non-identifiability

Firstly there is a problem with structural non-identifiability since in some cases two distinct Markov models yield aggregated processes which possess identical probabilistic properties. Kienker (1989) gave necessary and sufficient conditions, in terms of the transition rate matrix of the underlying process and under mild regularity conditions, for two distinct models to give rise to probabilistically indistinguishable aggregated processes. Edeson *et al.* (1994) examine some of the structural properties which underlie this type of non-identifiability and show that the conditions of Kienker (1989) can be used to determine whether or not a given model is identifiable. Edeson *et al.* (1994) also point out that there are cases in which multiple sets of model parameter values give rise to not only the same marginal density functions, but also the same joint density of open and

closed sojourn times.

2.3.3.2 Overparameterised Models

Fredkin *et al.* (1985) considered the problem of determining the maximum number of parameters on which an identifiable model can depend. They considered the marginal open and closed sojourn time probability density functions, the joint open-closed and closed-open sojourn time probability density functions, the closed-open-closed and open-closed-open sojourn time joint probability functions, and so on, and showed that, under the same mild regularity conditions as those considered later by Kienker (1989), the parameters of all joint probability density functions of dimension greater than two can be obtained from just the parameters of the joint open-closed and closed-open sojourn time probability density functions. Fredkin *et al.* (1985) then determined the number of free parameters in these latter joint probability density functions and showed that in order for a model to be identifiable its number of parameters must be no more than twice the product of the numbers of open and closed states. The more stringent result that this number must be at most $n_O n_C + n_O + n_C - 1$ holds for time reversible models (Bates *et al.* (1990)).

2.3.3.3 Non-identifiability induced by Time Interval Omission

Time interval omission not only causes considerable computational problems, but also introduces identifiability problems even for mechanisms which have distinguishable aggregated processes in the absence of time interval omission. It creates difficulties with parameter estimation, in that there is sometimes more than one set of parameter estimates which yield a maximum value of the likelihood function. In this situation the heights of the maxima of the likelihood function are not generally identical but are often very nearly equal. In such cases it is necessary to determine which set of parameter estimates corresponds to the true model parameters. This problem was outlined in section 1.3.2 and will be discussed in detail in Chapter 4 for a Markov model with just one open state and one closed state.

2.4 Ion Channel Biophysics

Biophysicists recognise that voltage-gated channels, such as Na^+, K^+ and Ca^{2+} channels, have some functional similarities and thus regard these as a super-family of related ion channels. Likewise, ligand-gated channels gated by acetylcholine, glutamate, glycine and γ-aminobutyric acid seem similar and are regarded as another super-family. In chapter 3 we model the molecular structure of one type of ligand-gated channel, the nicotinic acetylcholine receptor (nAChR)

channel, and one type of voltage-gated channel, the Ca^{2+}-activated potassium ion channel.

2.4.1 The Nicotinic Acetylcholine Receptor

The acetylcholine-activated channels found in the vertebrate neuromuscular junction are by far the best studied ligand-gated channels. They are specialised for mediating fast chemical synaptic transmission and, whilst they gate ion movements and generate electrical signals, they do so in response to the chemical neurotransmitter acetylcholine. Since the alkaloid nicotine imitates the effects of acetylcholine in acetylcholine channels at the neuromuscular junction, they are termed nicotinic. The nicotinic acetylcholine receptor is a term which refers to an entire macromolecule comprising the pore and the associated acetylcholine binding sites.

The subunit composition and amino acid sequence of nAChR channels from muscle-derived tissue were the first to be established (Conti-Tronconi and Raftery (1982), Changeux *et al.* (1984)). It was found that the polypeptides α, β, γ and δ exist in a pentameric stoichiometry, $\alpha_2\beta\gamma\delta$. The two α-subunits carry the binding sites for acetylcholine and the antagonist (blocker) α-bungarotoxin. More recently the subunit composition of nAChR channels from neurons has been investigated (Lindstrom *et al.* (1987), Steinbach and Ifune (1989)). It

appears that these channels are also pentameric, but are made up of only two classes of subunits and have an $\alpha_2\beta_3$ stoichiometry.

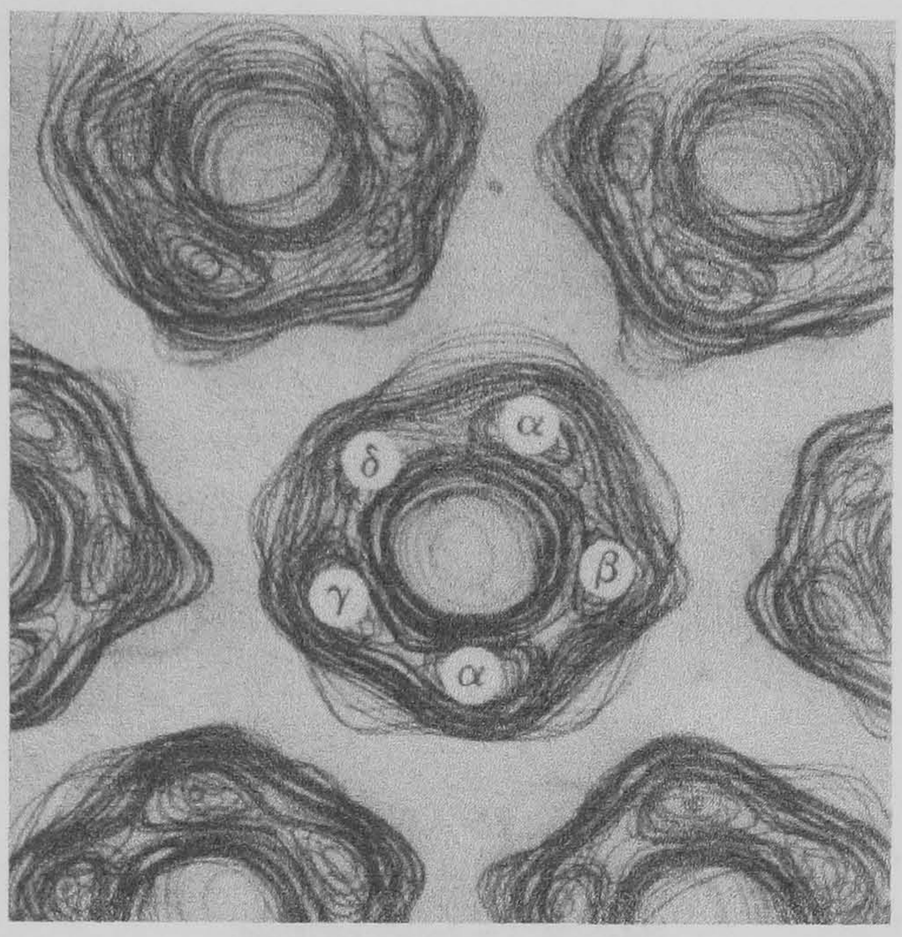

Figure 2.2. Three-dimensional details of the nicotinic acetylcholine receptor (see text). [From Brisson and Unwin (1985).]

The overall shape of the nAChR from the electric ray has been determined by using low-angle x-ray diffraction and electron-microscope image reconstruction using crystallographic methods on a two-dimensional lattice formed by channel proteins which were highly concentrated in lipid bilayers (Kistler *et al.* (1982), Toyoshima and Unwin (1988)). Viewed face-on, as in Figure 2.2, the molecule has a rosette appearance with a central well. The five subunits form a pentagonal complex through the membrane with the void between them presumably being part of the aqueous pore (see Figures 2.2 and 2.3). The five subunits are structurally similar and each occupies an equivalent position in the symmetrical complex. Brisson and Unwin (1985) contains a figure of a face-on view of a

nAChR channel from an electric ray and gives a probable identification of the subunits with the two α-subunits separated by a β-subunit (Figure 2.2). This identification is confirmed in a three-dimensional study by Beroukhim and Unwin (1995). More recent studies (Unwin (1995)) have revealed further structural details, as summarised in Figure 2.3.

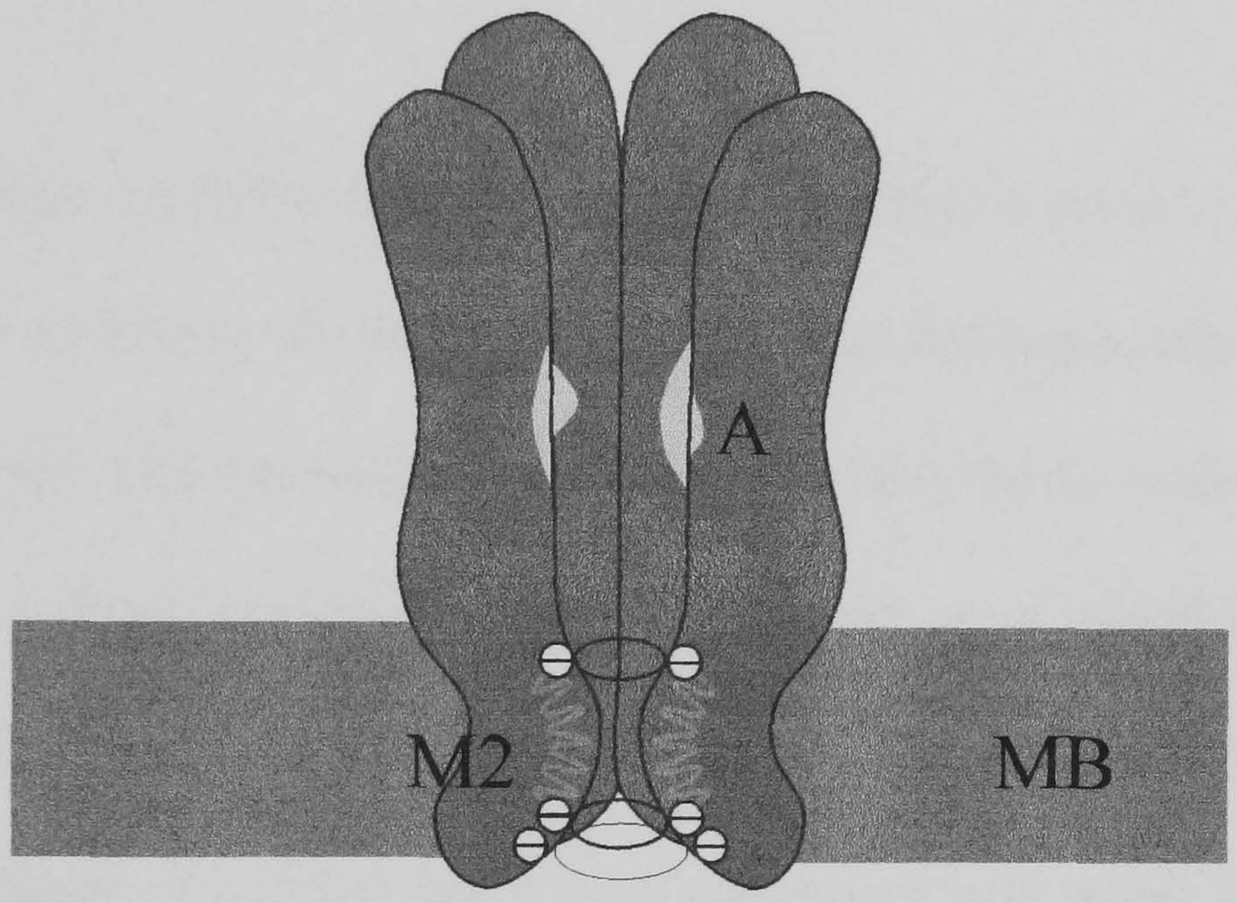

Figure 2.3. Simplified diagram showing the shape of the subunits of the nicotinic acetylcholine receptor. [Drawn after Hucho *et al.* (1996).] A section through the pentameric assembly is shown, cut parallel to the pore axis. So that the pore between the subunits can be seen, only four subunits are displayed. The kinked transmembrane rods, thought to be the M2 segment are shown (M2), as is the approximate position of an acetylcholine binding site (A). The rectangle (MB) represents the membrane bilayer.

The above information regarding the molecular structure of the nicotinic acetylcholine receptor is the basis for the main nAChR channel model formulated

and analysed in Chapter 3. This model assumes an $\alpha_2\beta_3$ subunit stoichiometry and can be used as a possible model either for nAChR in mammalian neurons ($\alpha_2\beta_3$) or, noting that there is very little known about any differences between the behaviour of β, γ, and δ-subunits, for nAChR in muscle tissue ($\alpha_2\beta\gamma\delta$).

2.4.2 The Calcium-activated Potassium Ion Channel

Prominent large conductance calcium-activated potassium ion channels occur in nearly every vertebrate excitable cell. Their long and large unitary currents are easily recorded and therefore these channels have been well-studied in the literature (e.g. Blatz and Magleby (1987), Latorre *et al.* (1989)). These large conductance channels are known as BK channels, where the 'B' denotes 'big', and, in this thesis, it is these that we are concerned with rather than the 'small' (SK) and intermediate ones which were discovered later and have different properties (Romey and Lazdunski (1984), Pennefather *et al.* (1985), Blatz and Magleby (1987)). Single BK channel records show the intrinsic voltage dependence clearly and the gating rates and resulting probability of being open are also sensitive functions of the number of calcium ions bound. The microscopic gating kinetics of BK channels have been investigated in more detail than for any other channel (Moczydlowski and Latorre (1983), Magleby and Pallotta (1983a, 1983b), McManus and Magleby (1988), Rothberg and Magleby (1999)) and the proposed gating mechanisms are remarkably complex with

numerous kinetic states. Section 3.6 contains a discussion of how known results regarding the gating kinetics of BK channels can be taken into account for modelling purposes.

All potassium ion channels show core similarities to each other and are believed to have the same underlying structure. Whilst there have been very few studies of the molecular structure of the BK channel, the potassium ion channel (KcsA) from the bacterium *Streptomyces lividans* has an amino acid sequence similar to that of all known K^+ channels including Ca^{2+}-activated K^+ channels and, with a subunit size of only 160 amino acids, KcsA is amenable to structural studies (Doyle *et al.* (1998), Sansom (1998)). X-ray analysis has been used to determine detailed structural information, such as pore architecture and, more specifically, to explore the selectivity filter which allows the passage of potassium ions, but not of smaller sodium ions. It is known that potassium channels are tetrameric (MacKinnon (1991)) and that typically the four subunits are identical (Ketchum *et al.* (1995)). The four subunits of KcsA exhibit four-fold symmetry about a central pore and the inner helices are tilted so that the subunits open like the petals of a flower facing the outside of the cell (Doyle *et al.* (1998)). Moreover, the known structure of the KcsA potassium ion channel is in excellent agreement with results from functional and mutagenesis studies on Shaker channels from *Drosophila*. The term *homology* is commonly used by molecular biologists to indicate the degree of similarity between two genetically related sequences and

it is believed that the high degree of homology between BK channels and the more-studied KcsA and Shaker channels implies that BK channels are almost certainly tetrameric. Experimentally calculated Hill coefficients (see Appendix B, Hill (1909)) suggest that a BK channel has a minimum of four calcium binding sites (e.g. Barrett *et al.* (1982), Magleby and Pallotta (1983a, 1983b), McManus and Magleby (1991), Golowasch *et al.* (1986) and Oberhauser *et al.* (1988)) and Schreiber and Salkoff (1997) report that BK channels have one or more Ca^{2+} binding sites per subunit. Although the total number of binding sites on a BK channel is as yet unknown, the known symmetry of the related KcsA channel has heightened the belief that a BK channel must have a binding site on each subunit. The known information regarding the structure of the BK channel together with the likely assumption that a BK channel has one binding site per subunit is the basis for the BK channel model formulated and discussed in Chapter 3. Section 3.6.3 contains a discussion of how the model for a BK channel with one binding site per subunit can be adapted to model the situation in which each subunit has two calcium ion binding sites.

3 Models based on the Molecular Structure of Ion Channels

3.1 Introduction

The majority of this chapter is concerned with the formulation and analysis of a model for the nicotinic acetylcholine receptor which incorporates information concerning the structure of the corresponding receptor-channel protein, and uses ideas derived from the sequential model for allosteric proteins developed by Koshland *et al.* (1966). As discussed in section 2.4.1, the nAChR channel is composed of 5 similar subunits which form a ring-like structure surrounding a central pore (Jackson (1993)). For simplicity, we assume that these subunits comprise two α-subunits and three β-subunits, as in mammalian neurons, rather than assuming the more complex $\alpha_2\beta\gamma\delta$ stoichiometry of nAChR in muscle tissue. There are two binding sites for acetylcholine, one on each α-subunit. In the gating model of nAChR discussed below each of the five subunits may switch between an 'open' and a 'closed' conformation. In the light of the results of Unwin (1995), this conformational change may correspond to kinking of the pore-lining M2 helices. In our gating model, conformational changes of subunits are only partially coupled, and channel states containing mixtures of 'open' and 'closed' subunits are possible. However, interactions between neighbouring

subunits occur, so that conformational changes of adjacent subunits are not entirely independent. We use this model to predict the gating kinetics of the acetylcholine receptor. Our numerical examples (section 3.4), based on parameter values determined according to biophysiological considerations and derived indirectly from Jackson (1989), show that the model performs well in its prediction of channel behaviour.

Section 3.6 contains the formulation of a model for the large conductance calcium-activated potassium ion channel. This model is based on the molecular structure and known Ca^{2+}-binding properties of the BK channel. The BK channel is known to consist of 4 identical α-subunits which are believed to be arranged in a square formation. There are four binding sites for Ca^{2+}, one on each α-subunit. In the model presented in section 3.6 each of the four subunits may switch between an 'open' and a 'closed' conformation. As for the related model of nAChR, channel states containing mixtures of 'open' and 'closed' subunits are possible and interactions between neighbouring subunits occur. The model presented may be used to predict the gating behaviour of the BK channel.

The majority of earlier studies of single-channel kinetics of receptor-gated ion channels employed underlying gating mechanisms with, typically, between 2 and 10 states. However basing models on such a small number of states causes difficulties when a channel may exist in many non-identical closed states. In this

case a large state-space is needed to accurately describe ion channel behaviour. Although it is possible to develop 'traditional' Markov models with a larger number of states, this results in a commensurate proliferation of model parameters and this causes problems in parameter estimation. Alternative models with a large number of states have been developed by a number of authors, including Läuger (1988), Millhauser *et al.* (1988) and Doster *et al.* (1990), who treat channel gating in terms of diffusion-like processes. Whilst these large state-space models have few free parameters, their relationship to the underlying structural properties of channels is unclear. This chapter exploits our understanding of the structural biology of ion channel proteins as the basis for structurally reasonable, large state-space gating models which allow single-channel kinetic behaviour to be characterised in terms of a small number of free parameters.

In this chapter, we first formulate a model for acetylcholine receptors, explaining how the model features, including parameters, relate to the underlying channel structure. We then employ the mathematical framework of section 2.1 to derive a number of channel properties, considering also a special case of our model in which no interactions between subunits occur, and a more general case of our model in which the five subunits may comprise any combination of α-subunits and β-subunits. We present some results of numerical computations showing that our model agrees with experimental observations and we give a biophysical

discussion of the model. Next we formulate a model for calcium-activated potassium ion channels, discuss its relationship to biophysiological channel properties and channel structure, and we explore how the model can be adapted to take into account experimental findings. Finally, we consider the relationship between our large state space models based on molecular channel structure and the work of other authors who have considered large state space models.

3.2 Formulation of the Model for Acetylcholine Receptors

3.2.1 Model Description

The acetylcholine channel models developed in this chapter satisfy the following criteria:

(i) they have large state-spaces so as to agree with a range of experimental/statistical studies of ion channel closed time distributions;

(ii) they are based upon *realistic* molecular proposals for channel gating mechanisms;

(iii) they are defined in terms of a small number of free parameters in order to minimise difficulties when attempting to obtain parameter estimates from

experimental data.

3.2.1.1 States, Subunits and Substates

3.2.1.1.1 $\alpha_2\beta_3$ Model

The $\alpha_2\beta_3$ model described in this chapter assumes that a channel consists of 5 subunits arranged in a ring, reflecting the known structure of the nicotinic acetylcholine receptor (nAChR). Two of these subunits are α-subunits and can have an agonist molecule bound to them. The remaining 3 subunits are β-subunits and cannot have agonist molecules bound to them. In line with studies of the molecular structure of nAChR (e.g. Brisson and Unwin (1985)), it is assumed that, for the $\alpha_2\beta_3$ model, the positions of the two types of subunits within the ring are as given in the channel representation given in Figure 3.1.

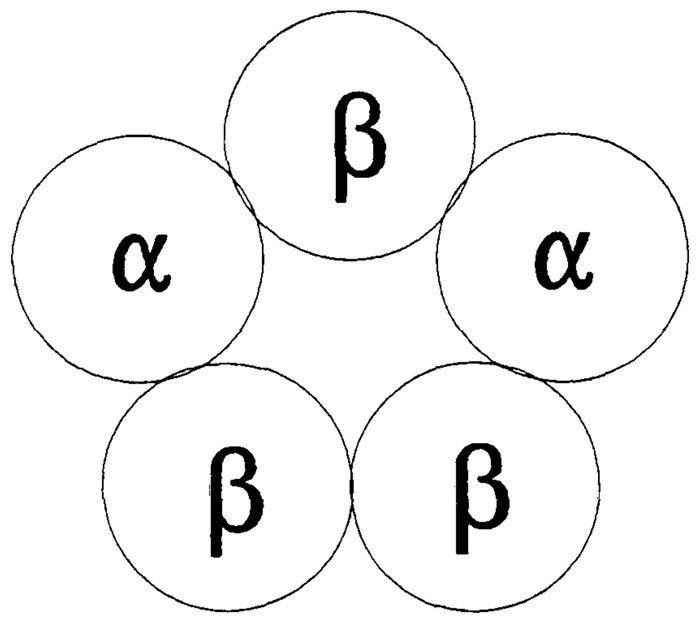

Figure 3.1. Positions of α-subunits and β-subunits within the subunit ring for the nAChR model.

We refer to the state occupied by a channel subunit at any given time as its *substate*. Each subunit may exist in either a closed substate, C, or an open substate, O. In addition, if an α-subunit with an agonist molecule bound to it is closed, it occupies substate CA, and if it is open, it occupies substate OA. Since each of the 2 α-subunits can occupy any one of the 4 substates C, O, CA and OA, and each of the 3 β-subunits can occupy either of the 2 substates C and O, there are $4^2 \times 2^3 = 128$ possible combinations of substates occupied by the 5 channel subunits. Each of these 128 combinations corresponds to a different channel state. Further, the channel is in an open state if and only if all 5 subunits are in open substates, regardless of the number of agonist molecules bound to the channel (see Jackson (1986) who observes spontaneous openings of an nAChR channel in cultured mouse muscle in the absence of agonist), otherwise it is in a closed state. Statistical properties and numerical examples based on the $\alpha_2\beta_3$ model are given in sections 3.3.1 and 3.4.1, respectively.

3.2.1.1.2 $\alpha_r\beta_{5-r}$ Model

In section 3.3.3, the $\alpha_2\beta_3$ model is generalised to $\alpha_r\beta_{5-r}$, where r ($r = 0, 1, 2, 3, 4$ or 5) is the number of α-subunits and the number of β-subunits is $5 - r$, reflecting discussion of α_5, $\alpha_3\beta_2$ and $\alpha_4\beta$ models for acetylcholine channels in ion channel literature (e.g. Couturier *et al.* (1990)). The general $\alpha_r\beta_{5-r}$ model thus formulated and analysed in this chapter also assumes that a channel consists of 5 subunits

arranged in a ring and it encompasses the $\alpha_2\beta_3$ model and several other related models. Note that if $r = 2$ or 3, two distinct models exist - one model with the property that all the α-subunits are adjacent to each other in the subunit ring and one model without this property. The substates which can be occupied by each α-subunit or β-subunit are the same as those for $\alpha_2\beta_3$ model. Since each of the r α-subunits can occupy any one of 4 substates and each of the $5 - r$ β-subunits can occupy either of 2 substates, there are $4^r \times 2^{5-r}$ possible different channel states and the channel is open if and only if all 5 subunits are in open substates.

The case in which $r = 5$ is of special interest for several reasons (Sansom *et al.* (1998)). Firstly, α_5 channels are known to exist in the brain of insects, e.g. locusts. Secondly, they have been seen *in vitro* in experiments in which five α-subunits obtained from a chick's brain (known in the literature as $\alpha 7$ for historical reasons) have been expressed in a frog's egg resulting in the formation of a nAChR channel. Thirdly, they have been the subject of a number of molecular modelling studies since their homopentameric nature gives fivefold rotational symmetry which simplifies modelling procedures. Statistical properties of the general $\alpha_r\beta_{5-r}$ model are discussed in section 3.3.3 and numerical results for this model when $r = 5$ are compared with those for the $\alpha_2\beta_3$ model in section 3.4.2.

3.2.1.2 Transitions

There are 4 types of transitions which an α-subunit can undergo:

(i) The opening of a subunit in a closed substate,

(ii) The closing of a subunit in an open substate,

(iii) The loss of an agonist molecule from a subunit in CA or OA,

(iv) The binding of an agonist molecule to a subunit in C or O.

A β-subunit can undergo only transitions (i) and (ii). Whenever any channel subunit undergoes a transition from one substate to another, the channel enters a different state. The rate for such a channel transition is given by the corresponding subunit transition rate, which may or may not be dependent upon the substates occupied by neighbouring subunits, and is given by Figure 3.2 for an α-subunit and by Figure 3.3 for a β-subunit, where a is the concentration of the agonist acetylcholine, and the parameters h, k_{ON}, K_B, α, L_i and β are defined and explained in section 3.2.2.

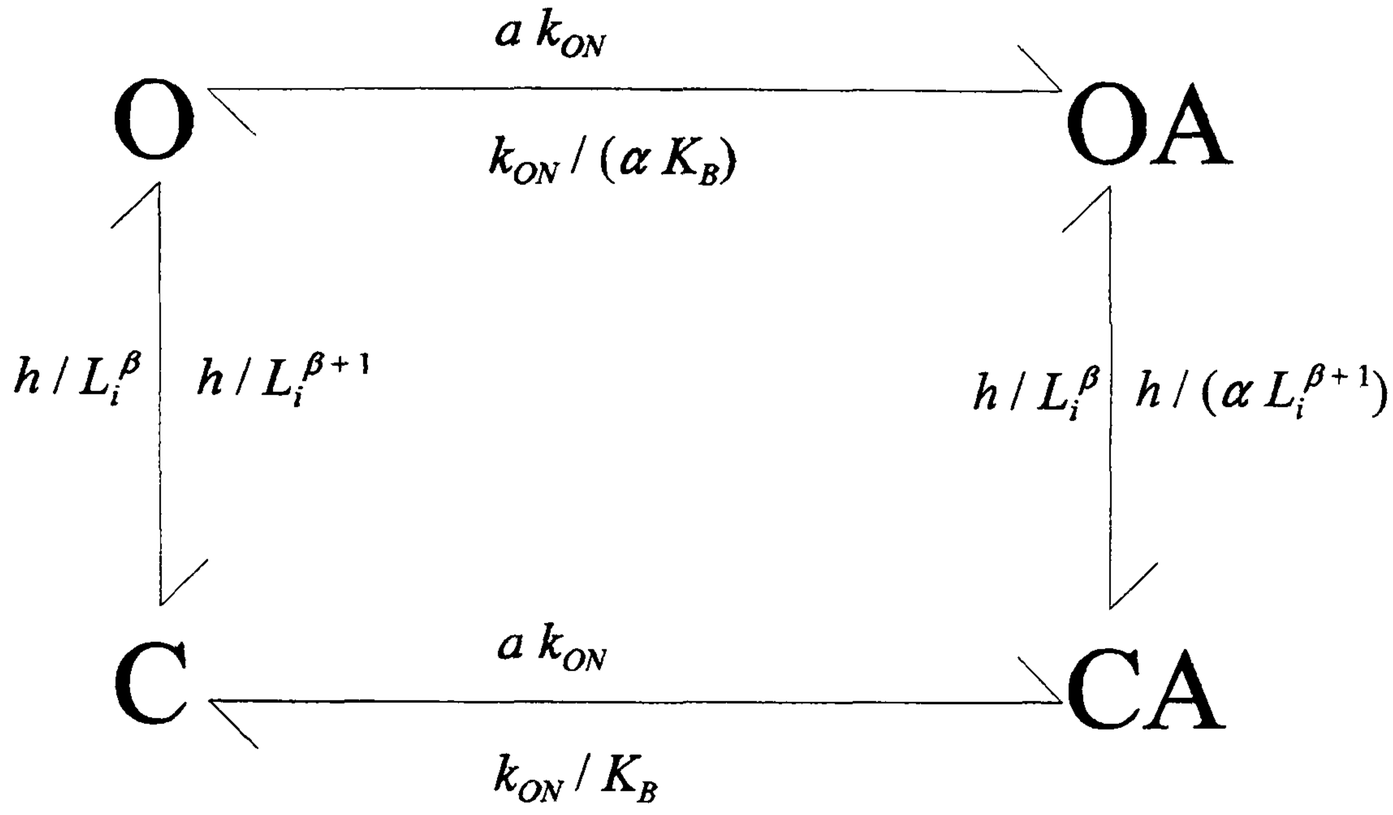

Figure 3.2. Transition rates for α-subunits for a nAChR channel.

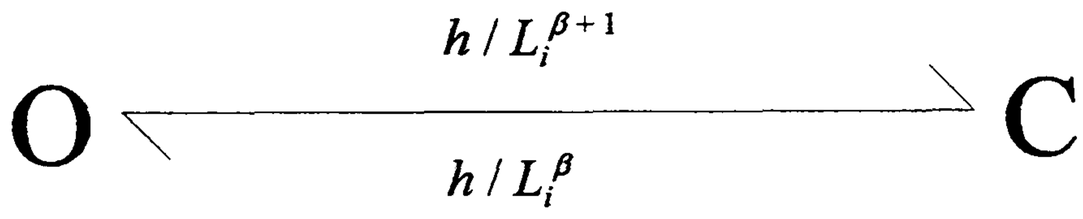

Figure 3.3. Transition rates for β-subunits for a nAChR channel.

3.2.1.3 Subunit Interactions between Nearest Neighbours

The treatment of allosteric globular proteins by Koshland *et al.* (1966) includes interactions between neighbouring subunits. The assumption that neighbouring subunits interact whereas non-neighbouring subunits do not directly interact is

realistic since changes in subunit conformations are associated with changes in subunit shape and a change in the shape of a subunit is likely to affect only neighbouring subunits (Hucho *et al.* (1996)). Such interactions are incorporated into our model via the equilibrium constant L_i, described further in section 3.2.2.2. Essentially a subunit's opening rate, closing rate, or both, are modelled to vary according to whether zero, one or two of the subunits which lie adjacent to that subunit in the subunit ring are open.

3.2.2 Definition and Explanation of Parameters

The parameters of our model are defined and explained below. These parameters may, in principle, be estimated using maximum likelihood estimation. However parameter estimation for our model is outside the scope of this thesis.

3.2.2.1 K_B, k_{ON}, h and α

If an α-subunit is closed then association and disassociation of an agonist molecule occur at rates ak_{ON} and k_{ON}/K_B, respectively, where a denotes the agonist concentration, k_{ON} is an agonist molecule association rate and K_B is an affinity constant. If an α-subunit is open then association and disassociation of an agonist molecule occur at rates ak_{ON} and $k_{ON} / (\alpha K_B)$, respectively, where the parameter α reflects the increased affinity of an open subunit for agonist. The parameter h

is an intrinsic transition rate of the conformational change of subunit opening and closing. Its value can be chosen to set the mean length of an open sojourn and it is scaled according to subunit interactions in order to obtain subunit opening and closing rates.

3.2.2.2 L_i, K_T, K_{OO}, K_{OC} and K_{CC}

In the ion channel literature, models are often described in terms of equilibrium constants, the equilibrium constant for a given transition being the ratio of the transition rates for that transition and the reverse transition. Thus the equilibrium constant for a given subunit to open (ie. to go from state C to state O, or from state CA to state OA) is L_i. We introduce nearest neighbour subunit dependency into our model by varying the equilibrium constant L_i according to the substates occupied by the two nearest neighbours of the subunit in question. This is achieved by letting $i = 0$, 1 or 2, according to whether the subunit in question has 0, 1 or 2 open neighbouring subunits, and defining L_0, L_1 and L_2 by

$$L_0 = K_T K_{OC}^2 K_{CC}^{-2},$$

$$L_1 = K_T K_{OO} K_{CC}^{-1}$$

and

$$L_2 = K_T K_{OO}^2 K_{OC}^{-2},$$

where K_T relates to the transition of a subunit from an open substate to a closed substate, or vice versa, and K_{OO}, K_{OC} and K_{CC} relate to the strengths of interactions between 2 open subunits, between an open subunit and a closed subunit, and

between 2 closed subunits, respectively. So, for example, in order to increase the opening rate (with respect to the closing rate) of a subunit with one open neighbouring subunit and one closed neighbouring subunit, it is necessary to increase the value of L_1 by increasing K_{OO} with respect to K_{CC}. An interpretation of the equilibrium constant L_1 in terms of the strengths of subunit interactions and the corresponding parameters is represented diagrammatically in Figure 3.4. This figure represents the fact that $K_{OC}^{-1}K_{CC}^{-1}$ and $K_{OO}K_{OC}$ are associated with the strengths of interactions between neighbouring subunits for a closed subunit with one open neighbour and for an open subunit with one open neighbour, respectively. Additionally, the reciprocal $K_{OC}^{-1}K_{CC}^{-1}$ is associated with the loss of subunit interactions (open-closed and closed-closed) associated with the transition out of the original channel substate, whereas $K_{OO}K_{OC}$ is associated with the new interactions (open-open and open-closed) gained by the transition to the new channel substate. The parameter K_T is an intrinsic equilibrium constant for the closing of the open subunit and is independent of subunit interactions. The equilibrium constant L_1 is given by multiplication of $K_{OC}^{-1}K_{CC}^{-1}$, K_T, and $K_{OO}K_{OC}$. The equilibrium constants L_0 and L_2 have similar interpretations.

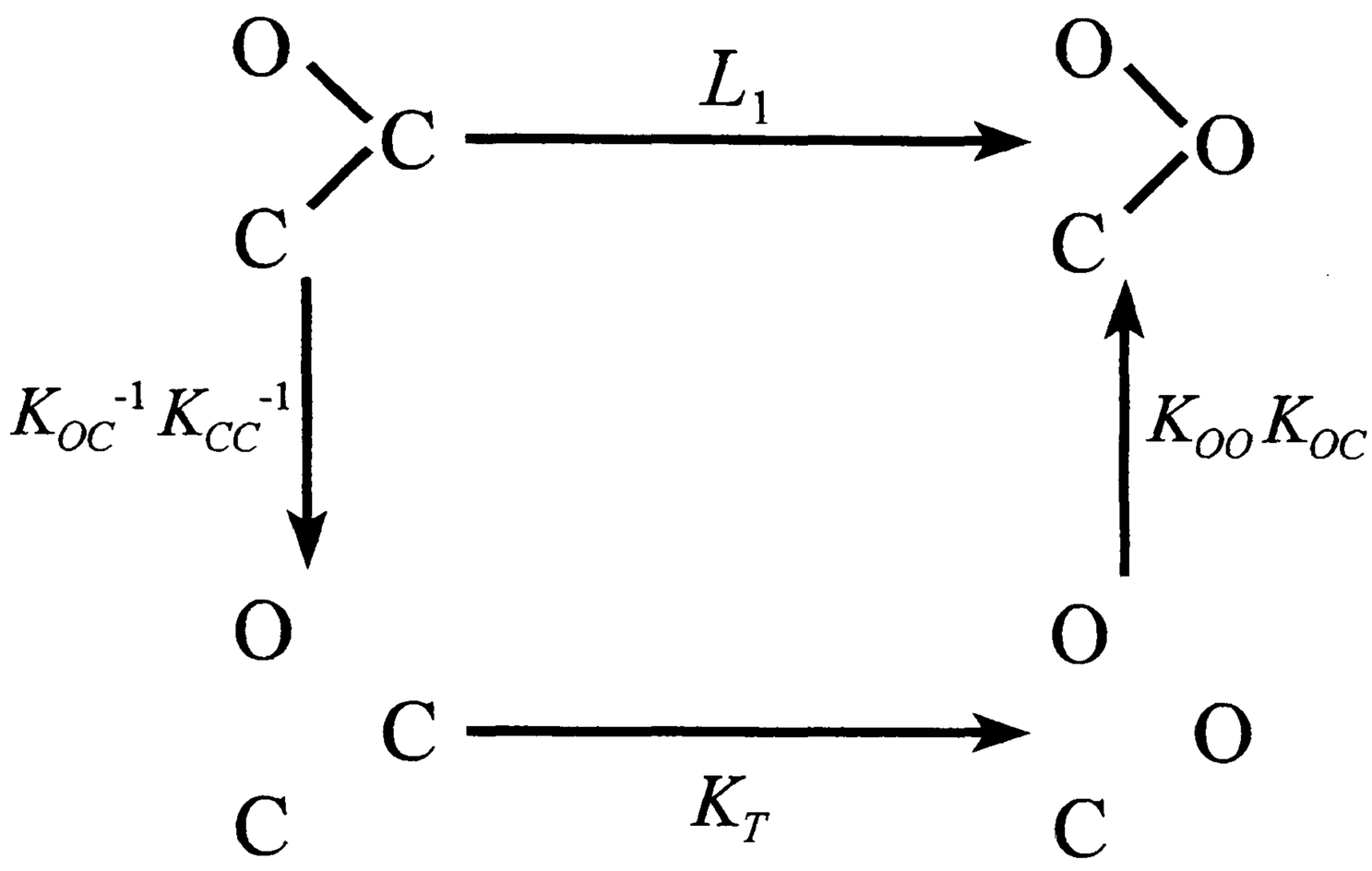

Figure 3.4. Diagrammatic interpretation of the parameter L_1.

It should be noted that if the equilibrium constants L_0, L_1 and L_2 satisfy $L_0 = L_1 = L_2$, then each of the 5 subunits behaves independently of the other 4 subunits. This gives the special case, discussed in section 3.3.2, of a model in which there are no interactions between channel subunits.

3.2.2.3 β

As shown in Table 3.1, the value of β determines whether and how the subunit closing rate (when $\beta = 0$), the subunit opening rate (when $\beta = -1$), or both of these rates (when $\beta \neq 0$ or -1) are dependent upon the substates occupied by neighbouring subunits. It is worth noting that the ratio of closing rate to opening rate for a given subunit remains constant as β varies.

β	Effect of an increase in L_i on the subunit opening and closing rates	
	Opening Rate	Closing Rate
$\beta = 0$	Constant	Decreases
$\beta = -1$	Increases	Constant
$\beta \in (-1, 0)$	Increases	Decreases
$\beta < -1$	Increases	Increases
$\beta > 0$	Decreases	Decreases

Table 3.1. Effect on opening and closing rates of increasing L_i for different values of β.

3.3 Mathematical Treatment

3.3.1 Formulation of a Mathematical Model for $\alpha_2\beta_3$

We now return to the $\alpha_2\beta_3$ structure of channel subunits described in section 3.2.1.1 and consider how it may be modelled using the framework described in section 2.1. We first introduce some notation. Label the channel subunits 1, 2,..., 5, assigning labels in a clockwise direction around the subunit ring, starting from the β-subunit situated in-between the two α-subunits. Thus the α-subunits are numbered 2 and 5, and the β-subunits are numbered 1, 3 and 4. Let $Z_i(t)$ be the substate of subunit i at time t, where

$$Z_i(t) = \begin{cases} \text{O or C} & \text{if } i = 1, 3 \text{ or } 4, \\ \text{O, OA, C or CA} & \text{if } i = 2 \text{ or } 5, \end{cases}$$

and the notation of substates O, C, OA and CA is as described in section 3.2.1.1.1. Then $\boldsymbol{Z}(t) = (Z_1(t),Z_2(t),...,Z_5(t))$ describes the state of the channel at time t.

As pointed out in section 3.2.1.1.1, the number of distinct channel states, n, is 128. A channel is open if and only if all 5 channel subunits are in open substates. Thus (O,O,O,O,O), (O,OA,O,O,O), (O,O,O,O,OA) and (O,OA,O,O,OA) are the possible open states of a channel. Therefore the number of open states, n_O, is 4, and the number of closed states, n_C, is 124. As in section 2.1, let m_O and m_C denote the numbers of open and closed gateway states, respectively. The transition of a channel from an open state to a closed state consists of the closure of one open subunit. Therefore, each open state is an open gateway state, yielding $m_O = 4$. Since a channel in any one of the 4 open states can enter a distinct closed state by closing any one of its 5 subunits, there are 4×5 closed gateway states, ie. $m_C = 20$, and it follows that the set of closed gateway states comprises all closed states in which the channel has precisely one closed subunit.

Label the channel states 1, 2,..., 128 so that $O = \{1, 2, 3, 4\}$ and $C = \{5, 6,..., 128\}$. The precise labelling is not important at this stage and will be described in more detail later. Let $\{X(t); t \geq 0\}$ be the integer-valued Markov chain which records the label X(t) of the state occupied by the channel at time t, ie. X(t) is the number assigned to the state Z(t).

In order to determine the off-diagonal elements q_{ij} of the 128 × 128 transition rate matrix Q of the process $\{X(t); t \geq 0\}$, we require some more notation. Let $Y_k^{(i)}$ be the substate of subunit k when the channel is in state i, where

$$Y_k^{(i)} = \begin{cases} \text{O or C} & \text{if } k = 1, 3 \text{ or } 4, \\ \text{O, OA, C or CA} & \text{if } k = 2 \text{ or } 5. \end{cases}$$

Then $\mathbf{Y}^{(i)} = (Y_1^{(i)}, Y_2^{(i)}, ..., Y_5^{(i)})$ describes state i in terms of the substates occupied by the 5 subunits of a channel in that state. For $i \neq j$, consider the vectors $\mathbf{Y}^{(i)}$ and $\mathbf{Y}^{(j)}$ which describe states i and j. Each possible channel transition involves the transition, from one substate to another, of exactly one of its subunits, so if $\mathbf{Y}^{(i)}$ and $\mathbf{Y}^{(j)}$ differ in more than one of their corresponding elements, then $q_{ij} = 0$. This represents the fact that it is not possible for two or more subunits to change substate simultaneously. Further, if states i and j differ in only one subunit, subunit k say, but substate $Y_k^{(j)}$ cannot be reached from substate $Y_k^{(i)}$ in a single transition by that subunit, again $q_{ij} = 0$. Suppose now that states i and j differ in subunit k only and that substate $Y_k^{(j)}$ can be reached directly from substate $Y_k^{(i)}$. Then the transition rate q_{ij} of the channel process $\{X(t); t \geq 0\}$ is given by the subunit transition rate from substate $Y_k^{(i)}$ to substate $Y_k^{(j)}$ given in Figure 3.2 for an α-subunit or in Figure 3.3 for a β-subunit. For example, if $Y_k^{(i)} = \text{O}$ and $Y_k^{(j)} = \text{OA}$, then $q_{ij} = ak_{\text{on}}$. Note that if $Y_k^{(i)}$ is an open substate and $Y_k^{(j)}$ is a closed substate, or vice versa, the channel transition rate q_{ij} will be dependent on the number of open subunits neighbouring subunit k. The diagonal

elements of the transition rate matrix Q are given by $q_{ii} = -\sum_{j \neq i} q_{ij}$.

3.3.1.1 Equilibrium Distribution

Assume $\mathbf{Y}^{(1)}$ = (O,O,O,O,O) and suppose for the time being that π_1, the equilibrium probability that a channel is in state 1, is known. We show how to calculate π_1 later. Clearly it is possible for a channel in state 1 to reach any other state in 7 or fewer transitions. Let i be any state other than state 1, and suppose that a channel, starting from state 1, visits states $j_1, j_2, \ldots, j_{n_i - 1}$ followed by state i in n_i consecutive transitions, where $j_1, j_2, \ldots, j_{n_i - 1}$ are appropriate state labels, in the order in which the corresponding states are visited. We assume now that the process $\{X(t); t \geq 0\}$ is time reversible, an assumption we justify later. Then, by repeated application of the detailed balance conditions (2.4),

$$\pi_i = \pi_1 \left(\frac{q_{1\, j_1}}{q_{j_1\, 1}} \right) \left(\prod_{k=1}^{n_i - 2} \frac{q_{j_k\, j_{k+1}}}{q_{j_{k+1}\, j_k}} \right) \left(\frac{q_{j_{n_i - 1}\, i}}{q_{i\, j_{n_i - 1}}} \right),$$

which can be rewritten as

$$\pi_i = \pi_1 \, K_{1\, j_1} \left(\prod_{k=1}^{n_i - 2} K_{j_k\, j_{k+1}} \right) K_{j_{n_i - 1}\, i}, \tag{3.1}$$

where $K_{jk} = q_{jk} / q_{kj}$ is defined to be the equilibrium constant for the channel transition from state j to state k. Note that, by Kolmogorov's criterion for

reversibility (see, for example, Kelly (1979)), this product of equilibrium constants is independent of the particular states visited by a channel on its path from state 1 to state i.

Given a single channel transition from state j to state k, it is easy to verify that the corresponding equilibrium constant K_{jk} can be written in the form

$$K_{jk} = (aK_B)^{I_A} \alpha^{I_{OA}} L_0^{-I_0} L_1^{-I_1} L_2^{-I_2},$$

where the exponents I_A, I_{OA}, I_0, I_1 and I_2 are all zero unless the transition involves the binding of an agonist molecule to an α-subunit, in which case $I_A = 1$, or the entrance of an α-subunit into substate OA, in which case $I_{OA} = 1$, or, for $r = 0$, 1 or 2, the closing of an open subunit with r open neighbouring subunits, in which case $I_r = 1$. Since $L_0 L_2 = L_1^2$, we can rewrite the product $L_0^{-I_0} L_1^{-I_1} L_2^{-I_2}$ as $L_1^{-2I_0-I_1} L_2^{I_0-I_2}$. Thus π_i can be expressed in the form

$$\pi_i = \pi_1 (aK_B)^{x_1^{(i)}} \alpha^{x_2^{(i)}} L_1^{-x_3^{(i)}} L_2^{-x_4^{(i)}} \qquad (i = 2, 3, \ldots, 128) \tag{3.2}$$

for some $x_k^{(i)}$ ($k = 1, 2, 3, 4$), which we shall now determine.

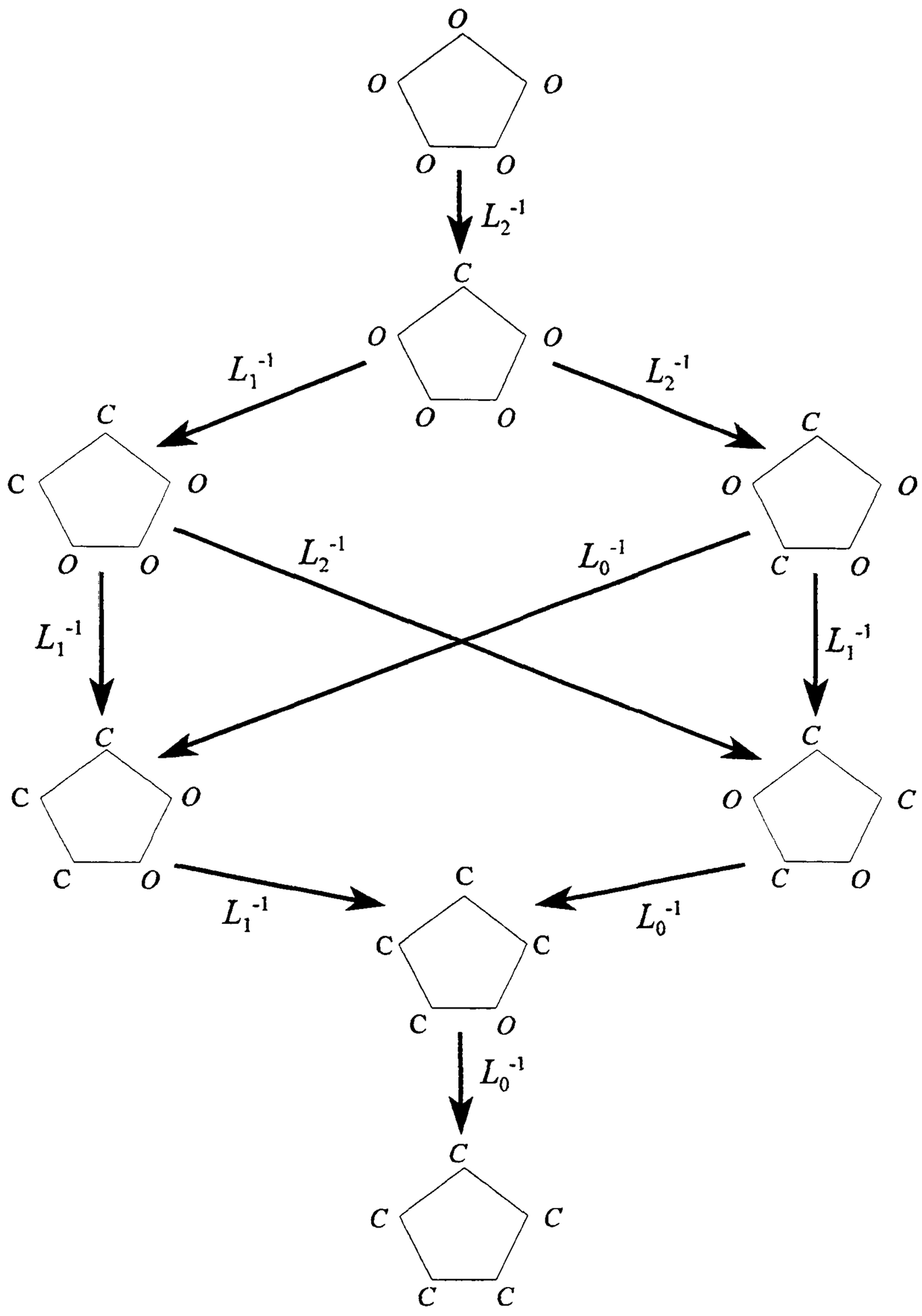

Figure 3.5. Equilibrium constants for open-closed subunit transitions (see text).

If a channel in state i has no closed subunits, then, clearly, $x_3^{(i)}$ and $x_4^{(i)}$ are both zero. Suppose that a channel in state i has r_i $(1 \le r_i \le 5)$ closed subunits and that the states visited by a channel on its path from state 1 to state i are chosen so that the first r_i transitions undergone by the channel, to states $j_1, j_2, \ldots, j_{r_i}$, say, each

consist of the closing of one open subunit, and the remainder of the transitions each consist of the binding of one agonist molecule to an α-subunit. Then $K_{1j_1} K_{j_1j_2} \dots K_{j_{r_{i-1}}j_{r_i}}$, the product of the equilibrium constants for the first r_i transitions, equals $L_1^{-x_3^{(i)}} L_2^{-x_4^{(i)}}$.

In Figure 3.5, the pentagon with all 5 vertices labelled O represents state 1, and, similarly, the pentagon with all 5 vertices labelled C represents the state in which a channel has all its subunits in substate C. For each of the 6 remaining pentagons in Figure 3.5, number its vertices 1 to 5 in a clockwise direction starting from any vertex, and, for $k = 1, 2, \dots, 5$, let v_k be the label of vertex k, ie. v_k is either O or C. Then the pentagon with consecutive vertices labelled v_1, v_2, v_3, v_4 and v_5 represents the 5 states (v_1,v_2,v_3,v_4,v_5), (v_2,v_3,v_4,v_5,v_1), (v_3,v_4,v_5,v_1,v_2), (v_4,v_5,v_1,v_2,v_3) and (v_5,v_1,v_2,v_3,v_4). Moreover, each of the 32 distinct states in which a channel has no agonist molecules bound is represented by exactly one of the 8 pentagons in Figure 3.5.

Suppose a channel undergoes a transition from state j to state k. Then the corresponding equilibrium constant K_{jk} is given by the label on the arrow from the pentagon representing state j to the pentagon representing state k in Figure 3.5.

Given states $j_1, j_2, \dots, j_{r_i}$, the product $K_{1j_1} K_{j_1j_2} \dots K_{j_{r_{i-1}}j_{r_i}}$ can be calculated by multiplication of the appropriate equilibrium constants given in Figure 3.5. It is readily verified that $x_3^{(i)}$ equals the number of pairs of adjacent closed subunits of a channel in state i, and $x_4^{(i)} = r_i - x_3^{(i)}$.

The factor aK_B will appear in $x_1^{(i)}$ of the equilibrium constants in equation (3.1), where $x_1^{(i)}$ is the number of agonist molecules which must necessarily become bound to a channel in order for that channel to undergo the transition(s) from state j_{r_i} to state i. It follows that $x_1^{(i)}$ is the number of agonist molecules bound to a channel in state i. Similarly, the factor α will appear in $x_2^{(i)}$ of the equilibrium constants in equation (3.1), where $x_2^{(i)}$ is the number of α-subunits which must enter substate OA in order for a channel to undergo the transition(s) from state j_{r_i} to state i. Thus, $x_2^{(i)}$ is the number of α-subunits in substate OA when a channel is in state i.

We now show that $q_{kj} / q_{jk} = \pi_j / \pi_k$ ($q_{kj}, q_{jk} \neq 0; j, k = 1, 2, \ldots, 128$), thus justifying our earlier assumption that the process $\{X(t); t \geq 0\}$ is time reversible. Clearly, a transition by a channel from state k to state j corresponds to a single subunit of that channel undergoing a single corresponding substate transition according either to one of the entries, or to the reverse of one of the entries, in the first column of Table 3.2. Since the detailed balance conditions (2.4) for states k and j are symmetrical in k and j, it is not necessary to consider separately channel transitions which correspond to subunit transitions which are the reverse of those considered in Table 3.2. Then the third column of Table 3.2 contains an expression for q_{kj} / q_{jk}, obtained using Figure 3.2 and/or Figure 3.3, as appropriate, for each type of subunit transition and for each possible number i say, where $i \in \{0, 1, 2\}$, of neighbouring open subunits of the subunit undergoing the

transition. From equation (3.2), we have

$$\pi_j / \pi_k = (aK_B)^{y_1^{(j,k)}} \alpha^{y_2^{(j,k)}} L_1^{-y_3^{(j,k)}} L_2^{-y_4^{(j,k)}} \qquad (j, k = 1, 2, \ldots, 128),$$

where $y_m^{(j,k)} = x_m^{(j)} - x_m^{(k)}$ $(m = 1, 2, 3, 4)$ and values of $y_m^{(j,k)}$ are displayed in columns 4 to 7 of Table 3.2. These values are used to determine π_j / π_k, shown in the final column of Table 3.2. Using the fact that $L_0 L_2 = L_1^2$, it is immediately clear that $q_{kj} / q_{jk} = \pi_j / \pi_k$ for all states j and k that directly communicate. Hence the detailed balance conditions (2.4) are satisfied and the process $\{X(t); t \geq 0\}$ is time reversible.

Subunit Transition	i	q_{kj} / q_{jk}	$y_1^{(j,k)}$	$y_2^{(j,k)}$	$y_3^{(j,k)}$	$y_4^{(j,k)}$	π_j / π_k
O → C	0	L_0^{-1}	0	0	2	-1	$L_1^{-2}L_2$
	1	L_1^{-1}	0	0	1	0	L_1^{-1}
	2	L_2^{-1}	0	0	0	1	L_2^{-1}
OA → CA	0	$(\alpha L_0)^{-1}$	0	-1	2	-1	$\alpha^{-1}L_1^{-2}L_2$
	1	$(\alpha L_1)^{-1}$	0	-1	1	0	$\alpha^{-1}L_1^{-1}$
	2	$(\alpha L_2)^{-1}$	0	-1	0	1	$\alpha^{-1}L_2^{-1}$
O → OA	0, 1, 2	$a\alpha K_B$	1	1	0	0	$a\alpha K_B$
C → CA	0, 1, 2	aK_B	1	0	0	0	aK_B

Table 3.2. Values used in showing that $\{X(t); t \geq 0\}$ is time reversible. For details, see text.

Summing the equilibrium probabilities, we obtain that

$$\sum_{i=1}^{128} \pi_1 (aK_B)^{x_1^{(i)}} \alpha^{x_2^{(i)}} L_1^{-x_3^{(i)}} L_2^{-x_4^{(i)}} = 1,$$

from which it follows, after a little algebra, that π_1, the equilibrium probability that a channel is in state 1, can be expressed as

$$\begin{aligned} \pi_1 = 25 [& h_5^2 + 5h_5 L_2^{-1}(h_3 + h_1 (L_1^{-1} + L_2^{-1})) \\ & + 25 (\alpha - 1)^2 (aK_B)^2 (1 + L_1^{-1}) L_2^{-2} \\ & + 5h_0 L_1^{-1} L_2^{-1} (h_4 (L_1^{-1} + L_2^{-1}) + h_2 L_1^{-2}) + h_0^2 L_1^{-5}]^{-1}, \end{aligned} \tag{3.3}$$

where

$$h_i = (aK_B \alpha) i + aK_B (5 - i) + 5 \quad (i = 0,1,...,5). \tag{3.4}$$

It follows from equation (3.2) that P_O, the equilibrium probability of a channel being open, is given by

$$P_O = \pi_1 (1 + aK_B \alpha)^2. \tag{3.5}$$

Recall that an expression for $P_O(t)$, the probability that the channel is open at time t, is given by equation (2.3).

3.3.1.2 Hill Coefficient

The Hill Coefficient (see Appendix B of this thesis, Hill (1909)) is frequently

calculated in ion channel literature and is interpreted as giving, firstly, a lower bound for the number of agonist binding sites and, secondly, an indication of whether or not there is cooperativity between the agonist molecules, i.e. whether or not binding of one agonist molecule promotes binding of another. The Hill Coefficient, n_H, can therefore be used to aid comparison of this model with other literature examples. It is defined by $n_H = H(a^*)$ where a^* is the value of the agonist concentration for which $P_O = 0.5$ and

$$H(a) = \frac{\mathrm{d}}{\mathrm{d}X}\left[\log_{10}\left(\frac{P_O}{1 - P_O}\right)\right],$$

where $X = \log_{10} a$.

Setting $A = aK_B\alpha$, the Hill Coefficient for our model is given by

$$H(a) = \left(\frac{\pi_1^{-1}(1 + A)^{-2} - 1}{\ln 10}\right)\frac{\mathrm{d}}{\mathrm{d}X}\left[\frac{1}{\pi_1^{-1}(1 + A)^{-2} - 1}\right].$$

Following some elementary differentiation, we obtain

$$H(a) = \frac{\left(\frac{\mathrm{d}}{\mathrm{d}X}(\pi_1^{-1})\right)(1 + A)^{-2} - 2\,\pi_1^{-1}(1 + A)^{-3} A \ln 10}{-\ln 10\,(\pi_1^{-1}(1 + A)^{-2} - 1)}, \qquad (3.6)$$

where

$$\left(\frac{\mathrm{d}}{\mathrm{d}X}\,(\pi_1{}^{-1})\right) = \frac{1}{25}\Big[\,2\,h_5 H_5 + 5\,H_5 L_2{}^{-1}(h_3 + h_1(L_1{}^{-1} + L_2{}^{-1}))$$

$$+ 5\,h_5 L_2{}^{-1}(H_3 + H_1(L_1{}^{-1} + L_2{}^{-1}))$$

$$+ 25\,(\alpha - 1)^2\,(a K_B)^2\,(2 \ln 10)\,L_2{}^{-2}(1 + L_1{}^{-1})$$

$$+ 5\,H_0 L_1{}^{-1} L_2{}^{-1}(h_4(L_1{}^{-1} + L_2{}^{-1}) + h_2 L_1{}^{-2})$$

$$+ 5\,h_0 L_1{}^{-1} L_2{}^{-1}(H_4(L_1{}^{-1} + L_2{}^{-1}) + H_2 L_1{}^{-2}) + 2\,h_0 H_0 L_1{}^{-5}\,\Big],$$

with

$$H_i = a\,K_B \ln 10\,(\alpha_i + 5 - i) \qquad (i = 0, 1, \ldots, 5).$$

3.3.1.3 Mean Sojourn Lengths

The unconditional mean open sojourn length μ_O is given by equation (2.22). The numerator of equation (2.22) is simply the equilibrium probability of a channel being open. Assume (O,O,O,O,O), (O,OA,O,O,O), (O,O,O,O,OA) and (O,OA,O,O,OA) are states 1, 2, 3 and 4 respectively. Then, using equation (3.2) in the denominator of equation (2.22), we obtain

$$\mu_O = \frac{(1 + aK_B\alpha)^2}{\sum_{j\in C} q_{1j} + (aK_B\alpha)\left(\sum_{j\in C} q_{2j} + \sum_{j\in C} q_{3j}\right) + (aK_B\alpha)^2 \sum_{j\in C} q_{4j}}.$$

If a channel in open state k has a_k agonist molecules bound to it, its closing rate

is given by

$$\sum_{j \in C} q_{kj} = (5 - a_k)\left(\frac{h}{L_2^{\beta+1}}\right) + a_k\left(\frac{h}{\alpha L_2^{\beta+1}}\right).$$

Hence it follows that

$$\mu_O = \frac{L_2^{\beta+1}(1 + aK_B\alpha)}{h(5 + 3aK_B\alpha + 2aK_B)}. \tag{3.7}$$

Using equations (2.23) and (3.7), the mean length of a closed sojourn can be expressed as

$$\mu_C = \frac{L_2^{\beta+1}(1 - \pi_1(1 + aK_B\alpha)^2)}{h\pi_1(5 + 3aK_B\alpha + 2aK_B)(1 + aK_B\alpha)}.$$

Recall that the variances of open and closed sojourn lengths are given by equations (2.24) and (2.25), respectively.

3.3.1.4 Reduction of State Space Size

In order to determine channel properties such as sojourn time probability density functions and autocorrelation and cross-correlation functions, it is necessary to carry out computations involving the submatrices of the Q-matrix partitioned in

equation (2.1). Since the channel process $\{X(t); t \geq 0\}$ can be in any one of 128 states, computational difficulties may arise. However, by exploiting the symmetry properties of the transition rate matrix, we can reduce our 128-state model to an equivalent model with only 72 states, resulting in a smaller Q-matrix and therefore a saving in computing time.

Let S denote the state space of the 128-state model discussed above and consider, for example, the states (C,C,O,C,OA) and (C,OA,C,O,C) in S. The substates occupied by a channel's α-subunits and β-subunits, the interactions of its neighbouring subunits, and hence its transition rates and observed properties, are the same regardless of which of these two states it occupies. Thus the two states are equivalent and we can formulate a 'reduced state space model' in which we do not distinguish between them. This type of symmetry is present in many pairs of states in S, and hence the state space, S^R, of this reduced model will contain a significantly smaller number of states than the state space S.

We now proceed more formally. If i is the label of a state in S, let $T(i)$ be the label of the state in S which is the mirror image of state i when reflected in the dotted line in Figure 3.6. For example, if $\mathbf{Y}^{(i)}$ = (O,OA,C,O,C), then $\mathbf{Y}^{(T(i))}$ = (O,C,O,C,OA). The states of S fall into two categories. Let i be a state in S. Then we term i a type 1 state if $T(i) = i$, and we term i a type 2 state otherwise. In the reduced model we do not distinguish between type 2 states i

and j with the property that $T(i) = j$. Hence we replace any pair of states in S, i, j say, which satisfy this equation, by a single state in S^R which is occupied by a channel if and only if that channel is in either state i or state j in S. In addition, for each type 1 state, i say, in S, the reduced state space S^R contains a state which is occupied by a channel if and only if that channel is in state i in S.

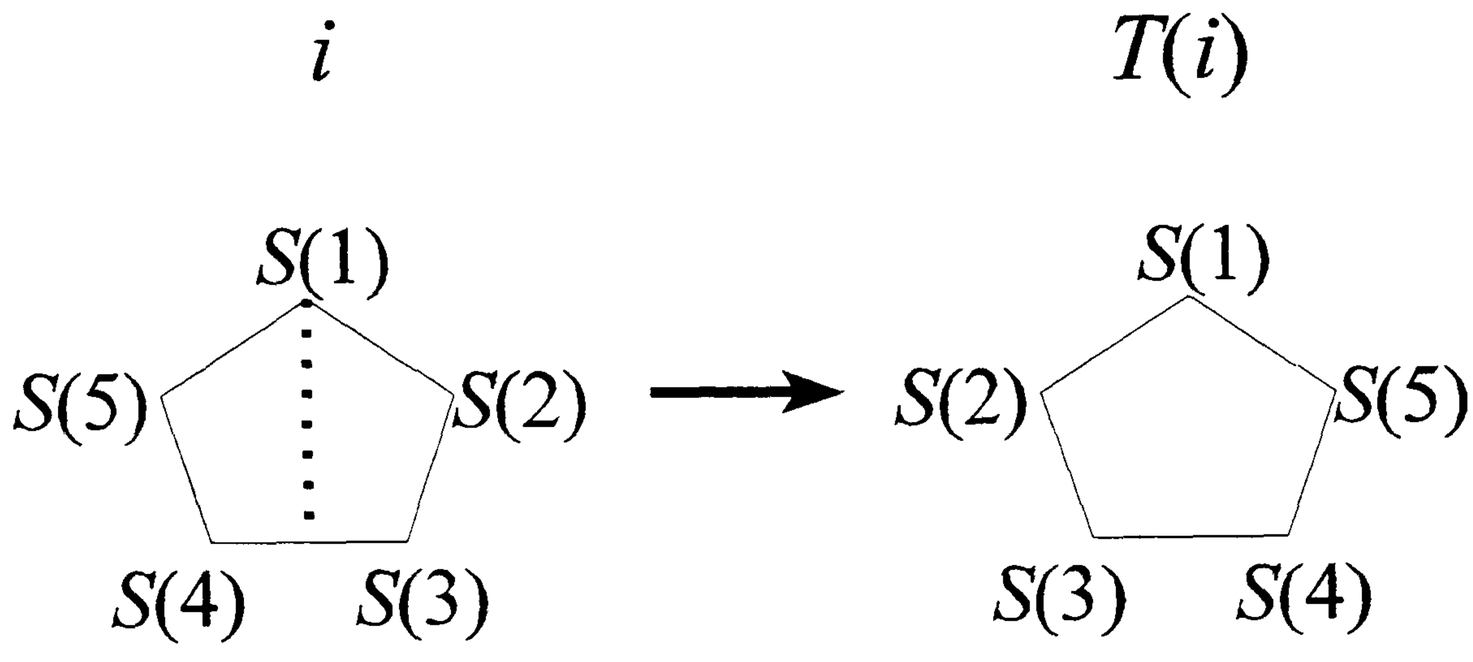

Figure 3.6. Reduction of state space size. For k = 1, 2, 3, 4 and 5, let $S(k)$ be the substate occupied by subunit k when the channel is in state i. Then a channel in state i and a channel in state $T(i)$, the reflection of i in the dotted line, have identical properties (see text).

We now calculate the size of the reduced state space S^R. If i is a type 1 state in S, then subunits 2 and 5 of a channel in state i occupy the same substate as each other, as do subunits 3 and 4. Since subunits 1 and 3 can occupy either of substates O and C, and subunit 2 can occupy any one of substates O, C, OA and CA, there are $2 \times 4 \times 2 = 16$ type 1 states in S. Each of these 16 states is also a state of S^R. This leaves 112 type 2 states in S. Arrange these type 2 states into pairs, i and j say, such that $T(i) = j$. Then each of these 56 pairs in S is equivalent

to a single state in S^R. Thus S^R contains a total of 16 + 56 = 72 states. These 72 states are comprised of 3 open states and 69 closed states. Note that it is not possible to reduce the state space to fewer than 72 states since there are no further symmetries to exploit.

To each type 1 state in S, i say, assign the vector $\mathbf{Y}^{(i)}$, and to each pair, i, j say, of type 2 states in S such that $T(i) = j$, assign the vector $\mathbf{Y}^{(\min(i,j))}$. This procedure gives 72 distinct vectors, which we shall use to describe the 72 states of S^R. (For example, the vector (O,CA,O,O,C) describes the single state in S^R occupied by a channel if and only if that channel occupies one of the 2 states (O,CA,O,O,C) and (O,C,O,O,CA) in S.) Re-label these vectors $\mathbf{Y}_R^{(1)}$, $\mathbf{Y}_R^{(2)}$,..., $\mathbf{Y}_R^{(72)}$ and label the states of S^R described by these vectors 1, 2,..., 72 respectively so that $O^R = \{1, 2, 3\}$ are the open states of S^R and $C^R = \{4, 5,..., 72\}$ are the closed states of S^R. We now give an explicit labelling of the gateway states in S^R for use in the sequel. Let 1, 2 and 3 be the labels of the open gateway states (O,O,O,O,O), (O,OA,O,O,O) and (O,OA,O,O,OA) respectively, and let 4, 5,..., 14 be the labels of the closed gateway states (O,C,O,O,O), (C,O,O,O,O), (O,O,C,O,O), (C,OA,O,O,O), (O,OA,C,O,O), (O,OA,O,C,O), (O,CA,O,O,O), (O,OA,O,O,C), (C,OA,O,O,OA), (O,OA,C,O,OA) and (O,OA,O,O,CA) respectively. We do not give an explicit labelling of the remaining states of S^R since this is not necessary for the sequel.

In the remainder of this chapter, we work in the reduced state space S^R, unless specified otherwise, and use the same notation as we have used for working in S, except that we embellish symbols with the superfix (or suffix) R, where appropriate. We now determine the elements of Q^R, the 72 × 72 transition rate matrix of the integer-valued Markov chain $\{X^R(t); t \geq 0\}$ which records the label $X^R(t)$ of the state of S^R occupied by the channel at time t. Let i and j be states of S^R. Then the transition rate q_{ij}^R is determined by a method identical to that for determining elements of Q (described in the paragraph immediately preceding section 3.3.1.1) with the exception that if $T(i) = i$ and $T(j) \neq j$, then q_{ij}^R equals twice the rate given by this method. For example, if $\mathbf{Y}_R^{(i)}$ = (C,OA,O,O,O) and $\mathbf{Y}_R^{(j)}$ = (C,OA,O,C,O), then $q_{ij}^R = hL_2^{-(\beta+1)}$, whereas if $\mathbf{Y}_R^{(i)}$ = (C,OA,O,O,OA) and $\mathbf{Y}_R^{(j)}$ = (C,OA,O,C,OA), then $q_{ij}^R = 2hL_2^{-(\beta+1)}$ since the single state (C,OA,O,C,OA) in S^R represents two states of S.

3.3.1.5 Open and Closed Entry Process Equilibrium Distributions

Let π_i^O be the equilibrium probability that the open class of states is entered via the ith open state of S^R. Then it follows immediately from relation (2.16) that

$$\pi_i^O \propto \pi_i^R \sum_{j \in C^R} q_{ij}^R \qquad (i \in O^R). \tag{3.8}$$

Using equation (3.2), it is easy to show that the equilibrium probabilities π_1^R, π_2^R

and π_3^R equal π_1, $2\pi_1(aK_B\alpha)$ and $\pi_1(aK_B\alpha)^2$ respectively, where π_1 is given by equation (3.3). Summing the transition rates to the closed states, out of each of the open states, we obtain that

$$\sum_{j\in C^R} q_{1j}^R = 5hL_2^{-(\beta+1)},$$

$$\sum_{j\in C^R} q_{2j}^R = (4 + \alpha^{-1})hL_2^{-(\beta+1)}$$

and

$$\sum_{j\in C^R} q_{3j}^R = (3 + 2\alpha^{-1})hL_2^{-(\beta+1)}.$$

Thus the open entry process equilibrium distribution π^O is given by

$$\pi^O = R^{-1}(5,\ 2aK_B\alpha(4 + \alpha^{-1}),\ (aK_B\alpha)^2(3 + 2\alpha^{-1}))^\top, \tag{3.9}$$

where

$$R = (5 + 3aK_B\alpha + 2aK_B)(1 + aK_B\alpha). \tag{3.10}$$

Similarly, it can be shown that the closed entry process equilibrium distribution, π^C say, is given by

$$\begin{aligned}\pi^C = R^{-1}(&2,\ 1,\ 2,\ 2aK_B\alpha,\ 2aK_B\alpha,\ 2aK_B\alpha,\ 2aK_B,\\ &2aK_B\alpha,\ (aK_B\alpha)^2,\ 2(aK_B\alpha)^2,\ 2\alpha(aK_B)^2)^\top,\end{aligned} \tag{3.11}$$

where the ith element of this vector is the equilibrium probability that the class

of closed states is entered via state $n_O{}^R + i$ of S^R.

3.3.1.6 Sojourn Time Density Functions and Correlation Functions

In this section, we give an explicit formula for the open sojourn time probability density function $f_O^R(t)$. The corresponding closed sojourn time probability density function $f_C^R(t)$ is a sum of 69 exponential terms, and is therefore not given explicitly here. Note that, in practice, $f_C^R(t)$ can usually be fitted quite accurately by a mixture of, say, 2 or 3 exponentials (see section 3.4.1.7) since many of the (necessarily negative) eigenvalues of Q_{CC}^R will be relatively large in modulus.

It is convenient to write the matrix Q_{OO}^R in the form

$$Q_{OO}^R = \begin{pmatrix} X+Y & 2A & 0 \\ B & X & A \\ 0 & 2B & X-Y \end{pmatrix},$$

where

$$A = ak_{ON},$$

$$B = k_{ON}(\alpha K_B)^{-1},$$

$$X = -B - A - (4 + \alpha^{-1})\, h\, L_2^{-(\beta+1)},$$

and

$$Y = B - A + (\alpha^{-1} - 1)\, h\, L_2^{-(\beta + 1)}.$$

Let $W_O^R = \mathrm{diag}(\pi_1^R, \pi_2^R, \pi_3^R)$. Then

$$(W_O^R)^{1/2} Q_{OO}^R (W_O^R)^{-1/2} = \begin{pmatrix} X+Y & \sqrt{2AB} & 0 \\ \sqrt{2AB} & X & \sqrt{2AB} \\ 0 & \sqrt{2AB} & X-Y \end{pmatrix}.$$

It follows after a little algebra that $(W_O^R)^{1/2}\, Q_{OO}^R\, (W_O^R)^{-1/2}$ has eigenvalues $\omega_1 = X - T$, $\omega_2 = X$ and $\omega_3 = X + T$, where $T = (Y^2 + 4AB)^{1/2}$, and corresponding orthonormal eigenvectors $\boldsymbol{b}_i$ $(i = 1, 2, 3)$ given by

$$\boldsymbol{b}_i = s_i^{-1} \left((2 - i)\, T + Y,\ \frac{(2 - i)^2 T^2 - Y^2}{\sqrt{2AB}},\ (2 - i)\, T - Y \right)^{\mathrm{T}}, \qquad (3.12)$$

where, for $i = 1, 2, 3$,

$$s_i = 4T^2 (2 - i)^2 + \left(\frac{Y^2 T^2}{2AB} \right) (1 - (2 - i)^2).$$

Then, using equations (2.18) and (3.12), we obtain

$$\begin{aligned} f_O^R(t) = -\sum_{i=1}^{3} [&5B((2 - i)T + Y) + (4 + \alpha^{-1})((2 - i)^2 T^2 - Y^2) \\ &+ A(3 + 2\alpha^{-1})((2 - i)T - Y)] \\ &\times [(2 - i)(A + B)T + (B - A)Y + (2 - i)^2 T^2 - Y^2] \\ &\times [X + (2 - i)T] R^{-1} B^{-2} s_i^{-2} \exp((X + (2 - i)T)t), \end{aligned}$$

where R is given by equation (3.10).

Formulae for open and closed sojourn autocorrelation functions and for dwell time cross-correlation functions are given by equations (2.29), (2.30) and (2.31) after appropriate substitution for the Q-matrix of our present model.

3.3.1.7 Clustering

Experimental studies (e.g. Sakmann *et al.* (1980)) have found that channel openings are grouped together in bursts, and further, that these bursts of channel openings are themselves grouped together in clusters. Ball and Sansom (1987) derived an expression (see section 2.1.5.1) for a simple descriptive measure which indicates whether or not a given model does indeed display clustering of openings, and Ball and Davies (1997) derived an equivalent expression (see section 2.1.5.2) to determine whether or not a given model displays clustering of bursts of openings. Note that, although the results of sections 2.1.5.1 and 2.1.5.2 have been stated in the notation of the unreduced state space, equivalent results for the reduced state space hold when the derivations of these expressions are based on the transition matrix Q^R.

In order to use the theory outlined in section 2.1.5.2 to examine clustering of bursts of openings for the $\alpha_2\beta_3$ model, we need to partition the closed states into short-lived and long-lived closed states. In practice there is, of course, no way of telling whether a given closed sojourn is entirely within the short-lived closed

states, entirely within the long-lived closed states or neither of these two. This problem has been addressed by Colquhoun and Hawkes (1981), who use Bayes' theorem to calculate the probability that a given closed sojourn is part of a burst, and by Colquhoun and Sakmann (1981) and Colquhoun and Hawkes (1982), who allocate closed sojourns to within bursts and between bursts according to whether they are less than or greater than some critical duration. However, for the $\alpha_2\beta_3$ model, examination of simulated realisations of the model strongly suggests that closed sojourns in which the channel has two agonist molecules bound are gaps within a burst, closed sojourns in which the channel has one agonist molecule bound are gaps between bursts within a cluster of bursts, and closed sojourns in which the channel has no agonist molecules bound are gaps between clusters of bursts. Thus to calculate the degree of clustering of bursts for the model, we shall assume that the short-lived closed states correspond to two agonist molecules being bound to the channel, whilst the long-lived closed states correspond to zero or one agonist molecules bound. It follows that, working in the reduced state-space, the model has 19 short-lived closed states and 50 long-lived closed states.

Colquhoun and Hawkes (1982) derive expressions for a large number of observable characteristics of bursts of openings and also give an analogous theory for the case when bursts of openings are grouped into clusters. These results are used to obtain the numerical results in section 3.4.1.9.3 (see also Appendix C) for the $\alpha_2\beta_3$ model. The application of the theory of Colquhoun and Hawkes (1982)

to the calculation of properties of clusters of bursts of openings for the $\alpha_2\beta_3$ model is based on the following categorisations of closed states. It is assumed, as above, that the channel is in a short-lived closed state whenever it is closed with two agonist molecules bound. However, the long-lived closed states are partitioned further into long-lived closed states which represent gaps between bursts within a cluster of bursts and very long-lived closed states which represent gaps between clusters of bursts. It is assumed that the channel is in a long-lived closed state whenever it is closed with one agonist molecule bound, and that it is in a very long-lived closed state if it is closed with no agonist molecules bound. Hence, working in the reduced state-space, the model has 19 short-lived closed states, 31 long-lived closed states and 19 very long-lived closed states. When calculating properties of bursts of openings, the partition into long-lived closed states and very long-lived closed states is not required.

3.3.2 A Special Case: The $\alpha_2\beta_3$ Model with Independent Subunit Behaviour

In this section we examine the special case in which the parameters L_1, L_2 and L_3 satisfy $L_1 = L_2 = L_3 = L$, say. In this case all the transition rates for a given channel subunit will be independent of the substates occupied by any of the other 4 channel subunits. This assumption allows some simplifications in the calculation of single channel properties.

First, it is possible to determine a simpler expression for the equilibrium distribution π. Using the detailed balance conditions (2.4), it is easy to calculate the equilibrium probabilities that (i) a given α-subunit is in each of the substates O, C, OA and CA, and (ii) a given β-subunit is in each of the substates O and C. Appropriate multiplication of these probabilities yields that the equilibrium probability that a channel occupies state i (i = 1, 2,..., 128) is given by

$$\pi_i = (1 + L)^{-3}(1 + L + LaK_B\alpha + aK_B)^{-2}L^{x_1}(LaK_B\alpha)^{x_2}(aK_B)^{x_3},$$

where x_1, x_2 and x_3 are the number of channel subunits in substates O, OA and CA, respectively, when a channel is in state i. Thus the equilibrium probability P_O that a channel is open is given by

$$P_O = \sum_{i=1}^{4} \pi_i = \left(\frac{L}{1 + L}\right)^3 \left(\frac{L + LaK_B\alpha}{1 + L + LaK_B\alpha + aK_B}\right)^2.$$

Second, the symmetries arising from the assumption of independent subunit behaviour can be exploited to reduce the state space size to 40, which decreases the necessary CPU time for computations. Since the interactions of neighbouring subunits are no longer of interest, the positions of α-subunits and β-subunits in the subunit ring are irrelevant. Thus all states in S with the same numbers of α-subunits in each of the substates O, C, OA and CA, and with the same number of open β-subunits, are equivalent to each other and can be replaced by a single state in a reduced state space which we denote by S^L. For example, the 6 states

(O,CA,C,C,OA), (O,OA,C,C,CA), (C,CA,O,C,OA), (C,OA,C,O,CA), (C,CA,C,O,OA) and (C,OA,O,C,CA) in S are equivalent to a single state of S^L. Since the 2 (unordered) α-subunits of a channel can occupy any one of 10 distinct combinations of substates, and the channel can have either 0, 1, 2 or 3 open β-subunits, the number of states in S^L is $10 \times 4 = 40$. In particular, the state space S^L comprises 3 open states and 37 closed states, of which all 3 open states, and 7 closed states, are gateway states. An integer-valued Markov chain on S^L, analogous to $\{X^R(t); t \geq 0\}$ on S^R, can be set up and its 40×40 transition rate matrix Q^L determined in order to calculate statistical properties of a single nAChR channel under a model in which its subunits are assumed to behave independently.

3.3.3 A More General Case: Model Formulation for $\alpha_r\beta_{5-r}$ ($r = 0, 1, \ldots, 5$)

In this section, following Couturier *et al.* (1990), we consider more general models for ion channels whose subunit rings consist of r α-subunits and $5 - r$ β-subunits, where r is 0, 1, 2, 3, 4 or 5 (as discussed in section 3.2.1.1.2). Since a channel with 2 α-subunits and 3 β-subunits can have its subunits arranged so that its 2 α-subunits are either adjacent to each other or are separated by a β-subunit, there are 2 distinct models in the case $r = 2$. However, these 2 models are closely related and many of their statistical properties will be identical.

Similarly there are 2 possible models when $r = 3$. As there is a unique ordering of r α-subunits and $5 - r$ β-subunits in a subunit ring when r is 0, 1, 4 or 5, there are, in total, eight distinct models with r α-subunits and $5 - r$ β-subunits to be considered.

r	Number of states (gateway states) for the $\alpha_r\beta_{5-r}$ model	
	Open	Closed
0	1 (1)	31 (5)
1	2 (2)	62 (10)
2	4 (4)	124 (20)
3	8 (8)	248 (40)
4	16 (16)	496 (80)
5	32 (32)	992 (160)

Table 3.3. Number of states and number of gateway states for a channel with r α-subunits and $5 - r$ β-subunits.

Table 3.3 gives the numbers of distinct open and closed states which can be occupied by a channel with r α-subunits and $5 - r$ β-subunits. Suppose that these numbers are n_O^r and n_C^r respectively, and label the channel states $1, 2, \ldots, n_O^r + n_C^r$ so that $\{1, 2, \ldots, n_O^r\}$ is the set of open states and $\{n_O^r + 1, n_O^r + 2, \ldots, n_O^r + n_C^r\}$ is the set of closed states. For each of the required channel models, we can set up an integer-valued Markov chain analogous to $\{X(t); t \geq 0\}$ in section 3.3.1 and, using the method described in that section, we can determine the elements of the

associated transition rate matrix. Hence it is possible to derive expressions for the statistical properties of a channel under each of the eight models.

3.3.3.1 Equilibrium Distribution

An expression for the equilibrium distribution for the $\alpha_r\beta_{5-r}$ model ($r = 0, 1,..., 5$) can be determined as in section 3.3.1.1 for the $\alpha_2\beta_3$ model. Suppose that a channel in state i has $x_1^{(i)}$ agonist molecules bound to it, $x_2^{(i)}$ of its α-subunits in substate OA, $x_3^{(i)}$ pairs of adjacent closed subunits, and a total of $x_3^{(i)} + x_4^{(i)}$ closed subunits. Then the equilibrium probability that a channel with r α-subunits and $5 - r$ β-subunits is in state i is given by

$$\pi_i^{(r)} = \pi_1^{(r)} (aK_B)^{x_1^{(i)}} \alpha^{x_2^{(i)}} L_1^{-x_3^{(i)}} L_2^{-x_4^{(i)}},$$

where $\pi_1^{(r)}$, the probability that all 5 channel subunits are in substate O, can be obtained by summing the equilibrium probabilities, and hence can be expressed in the form

$$\pi_1^{(r)} = [u^r + u^{r-1} h_{5-r} L_2^{-1} + c_1^{(r)} L_1^{-1} L_2^{-1} + c_2^{(r)} L_2^{-2} + c_3^{(r)} L_1^{-1} L_2^{-2} + c_4^{(r)} L_1^{-2} L_2^{-1} + v^{r-1} h_r L_1^{-3} L_2^{-1} + v^r L_1^{-5}]^{-1},$$

where $u = aK_B\alpha + 1$, $v = aK_B + 1$, h_i ($i = 0,1,...,5$) is given by equation (3.4) and, for $r = 0, 1,..., 5$, expressions for $c_1^{(r)}$, $c_2^{(r)}$, $c_3^{(r)}$ and $c_4^{(r)}$ are given in Table 3.4. Note that, in the cases when the α-subunits are adjacent to each other and $r = 2$

or 3 , $c_1^{(r)}$ and $c_2^{(r)}$ must be interchanged, as must $c_3^{(r)}$ and $c_4^{(r)}$. Further, the equilibrium probability that the channel is open is $\pi_1^{(r)} u^r$.

r	$c_1^{(r)}$	$c_2^{(r)}$	$c_3^{(r)}$	$c_4^{(r)}$
0	5	5	5	5
1	$3u + 2v$	$3u + 2v$	$2u + 3v$	$2u + 3v$
2	$u\,(u + 4v)$	$u\,(u + 4v) + (u - v)^2$	$v\,(4u + v) + (u - v)^2$	$v\,(4u + v)$
3	$uv\,(4u + v)$	$u\,[v\,(4u + v) + (u - v)^2]$	$v\,[u\,(u + 4v) + (u - v)^2]$	$u\,v\,(u + 4v)$
4	$u^2\,v\,(2u + 3v)$	$u^2\,v\,(2u + 3v)$	$u\,v^2\,(3u + 2v)$	$u\,v^2\,(3u + 2v)$
5	$5\,u^3\,v^2$	$5\,u^3\,v^2$	$5\,u^2\,v^3$	$5\,u^2\,v^3$

Table 3.4. Coefficients in the expression for $\pi_1^{(r)}$ (see text).

3.3.3.2 Mean Sojourn Lengths

For a channel with r α-subunits and $5 - r$ β-subunits ($r = 0, 1,..., 5$), let $\mu_O^{(r)}$ and $\mu_C^{(r)}$ be the equilibrium mean lengths of sojourns in the open and closed classes of states respectively. Then, by a similar argument to that of section 3.3.1.3, the mean length of an open sojourn is given by

$$\mu_O^{(r)} = \frac{h_5 L_2^{\beta + 1}}{5\, h_{5-r} h},$$

where h_i ($i = 0, 1,..., 5$) is given by equation (3.4), and, using equation (2.23), the mean length of a closed sojourn is given by

$$\mu_C^{(r)} = \mu_O^{(r)} [(\pi_1^{(r)} u^r)^{-1} - 1].$$

3.3.3.3 Reduction of State Space Size

r	Number of states (gateway states) in unreduced state space		Number of states (gateway states) in reduced state space	
	Open	Closed	Open	Closed
0	1 (1)	31 (5)	1 (1)	7 (1)
1	2 (2)	62 (10)	2 (2)	38 (6)
2	4 (4)	124 (20)	3 (3)	69 (11)
3	8 (8)	248 (40)	6 (6)	138 (22)
4	16 (16)	496 (80)	10 (10)	262 (42)
5	32 (32)	992 (160)	8 (8)	128 (20)

Table 3.5. Number of states and number of gateway states for the reduced state space $\alpha_r\beta_{5-r}$ model.

As in the $\alpha_2\beta_3$ model discussed in detail above, the size of the state space in each of the other 7 models can be reduced in order to facilitate computations. This reduction can be carried out in a manner identical to that described in section 3.3.1.4, although when *r* is 0 or 5, the state space size can be reduced still further since all 5 channel subunits are of the same type and it is therefore no longer necessary to distinguish between states which are rotations of each other. For example, a channel with its 5 subunits in substates O, C, C, C and C occupies one

of 5 states in an unreduced state space, depending on which of its subunits is in substate O. However, when r is 0 or 5, these 5 states can be replaced by a single state, in a reduced state space, which is occupied by the channel if and only if the channel is in one of these 5 states in the original state space. For each value of r, the numbers of open and closed states in these reduced state spaces are given in the fourth and fifth columns of Table 3.5.

3.3.3.4 Open and Closed Entry Process Equilibrium Distributions

We do not give the open and closed entry process equilibrium distributions based on either the unreduced or the reduced state space here, since in order to do so it would be necessary to give an explicit labelling of the gateway states for each model, and this would be rather lengthy, as can be seen from the number of open and closed gateway states for each model given in Table 3.5. However, we give here the open entry process equilibrium probabilities for aggregations of all open states with the same number of agonist molecules bound, which is still of interest since it allows us to confirm whether or not the channel is more likely to open with a higher number rather than a lower number of agonist molecules bound, but it is less lengthy to display. For this derivation, let the label of an aggregation of channel states be k ($k = 1, 2,..., r + 1$) if and only if a channel in any state in that aggregation is open and has exactly k - 1 agonist molecules bound to it, noting that not all open states with the same number of agonist molecules bound share

identical statistical properties. Suppose $r \neq 0$, since clearly the result is trivial for $r = 0$, and embellish symbols with the superfix A, where appropriate, to denote that states are aggregated as described above. Then, summing the equilibrium probabilities for the unreduced state space, we obtain that the equilibrium probability that a channel is open with k - 1 agonist molecules bound is given by

$$\pi_k^A = \pi_1 (a K_B \alpha)^{k-1} \binom{r}{k-1}.$$

Further, in obvious notation, it is easy to show that

$$\sum_{j \in C^A} q_{kj}^A = \left((k-1)(\alpha^{-1} - 1) + 5\right) h L_2^{-(\beta+1)}.$$

For $r = 1, 2, \ldots, 5$, let the vector $\pi^O(r) = (\pi_1^O(r), \pi_2^O(r), \ldots, \pi_{r+1}^O(r))^\top$ be the open entry process equilibrium distribution based on the state aggregations described above. Then using the above results together with an equation identical to equation (3.8) but with the superfix R replaced by the superfix A throughout, it follows that, for $k = 1, 2, \ldots, r + 1$, the equilibrium probability $\pi_k^O(r)$ that a channel in an open sojourn entered the class of open states via state k, is given by

$$\pi_k^O(r) = \frac{(a K_B \alpha)^{k-1} \binom{r}{k-1} (5 + (k-1)(\alpha^{-1} - 1))}{(1 + a K_B \alpha)^{r-1} h_{5-r}}.$$

3.3.3.5 Sojourn Time Density Functions and Correlation Functions

A formula for the unconditional open sojourn time probability density function is given by equation (2.18), with a similar result holding for the unconditional closed sojourn time probability density function. Formulae for open and closed sojourn autocorrelation functions and for dwell time cross-correlation functions are given in equations (2.29), (2.30) and (2.31).

3.4 Numerical Examples

3.4.1 $\alpha_2\beta_3$ Model

3.4.1.1 Parameter Values

Each parameter value that we use in the numerical examples for the $\alpha_2\beta_3$ model is chosen either according to biophysical considerations or by theoretically matching observable properties of our model to those of the model of Jackson (1989). Let $P(O_i)$ ($P(C_i)$) be the equilibrium probability that a channel is open (closed) with i agonist molecules bound, where i is 0 or 2. Then, using values of equilibrium constants from Scheme I of Jackson (1989), we obtain the equations

$$P(O_0) = 5 \times 10^{-6} \times P(C_0) \tag{3.13}$$

and

$$\mathrm{P}(O_2) \;=\; 14 \times \mathrm{P}(C_2). \tag{3.14}$$

Using equation (3.2), and setting $x = L_2^{-1}$ and $y = L_1^{-1}$, equations (3.13) and (3.14) can be written as

$$5(1+y)x^2 \;+\; 5(1+y+y^2+y^3)x \;+\; (y^5 - 2\times 10^5) \;=\; 0 \tag{3.15}$$

and

$$\begin{aligned}\left[\left(2+\frac{2}{\alpha}+\frac{1}{\alpha^2}\right)+\left(1+\frac{2}{\alpha}+\frac{2}{\alpha^2}\right)y+\left(\frac{2}{\alpha}+\frac{3}{\alpha^2}\right)y^3\right]x^2 \\ +\left[\left(3+\frac{2}{\alpha}\right)+\left(1+\frac{4}{\alpha}\right)y+\left(\frac{4}{\alpha}+\frac{1}{\alpha^2}\right)y^2\right]x \;+\; \left[\frac{y^5}{\alpha^2}-\frac{1}{14}\right] \;=\; 0,\end{aligned} \tag{3.16}$$

respectively. Clearly solutions of equation (3.15) with $x > 0$ and $y > 0$ lie on a decreasing curve in the x-y plane and solutions of equation (3.16) with $x > 0$ and $y > 0$ lie on a second decreasing curve in the x-y plane. Plotting these two curves for a range of values of α, it can be seen that, for reasonable values of L_1 and L_2, they intersect exactly once if the value of y when $x = 0$ is greater for the curve given by (3.16) than for the curve given by (3.15), and that they do not intersect otherwise. This yields the condition $\alpha > 200 \times \sqrt{70}$. In the numerical examples in this section we use the value $\alpha = 5000$ which is consistent with this condition. Solving equations (3.15) and (3.16) numerically, gives the values $L_1 = 0.08706$ and $L_2 = 231.2$.

In order to reflect the observed increased stability of substates in which a subunit has open neighbours, we assume that $1 = K_{CC} < K_{OC} < K_{OO}$ (Koshland *et al.* (1966)). Together with the definitions of L_1 and L_2 in section 3.2.2.2, this implies that

$$K_T < \min(L_1^2 L_2^{-1}, L_2) = 3.8 \times 10^{-5}.$$

Conforming with this inequality, we set $K_T = 10^{-5}$. This yields

$$K_{OO} = L_1 / K_T = 8706$$

and

$$K_{OC} = L_1 / \sqrt{K_T L_2} = 1.81.$$

It follows that

$$L_0 = K_T K_{OC}^2 = 3.28 \times 10^{-5}.$$

The parameter value $K_B = 10^5$ M^{-1} is consistent with equivalent kinetic parameter values used in ion channel literature (e.g. Ogden *et al.* (1987)). The parameter value k_{ON} is set to $k_{ON} = 10^7$ s^{-1} M^{-1} which lies between the estimate of 5×10^6 s^{-1} M^{-1} of Jackson (1989) and the limit of 10^8 s^{-1} M^{-1} set by diffusion (see Jackson (1989)). We use the values $\beta = 0$ and $\beta = -1$ in our calculations in order to obtain channel properties under the respective assumptions that subunit closing

rates (only) and subunit opening rates (only) are dependent upon the substates occupied by neighbouring subunits, noting that there is insufficient information at the molecular level to identify the most realistic value for β. We concentrate mainly on values of agonist concentration in the range 10^{-7}M to 10^{-5}M (see section 3.4.1.2), although we show results for a wider range of values when appropriate. Hille (1992, Chapter 6) describes a number of experiments drawn from ion channel literature and, from the results, concludes that the mean open lifetime for the nAChR channel is approximately 1 ms. Therefore we determine values for h when $\beta = -1$ and $\beta = 0$ by imposing the restriction that the mean length of an open sojourn is 10^{-3} s when $a = 10^{-6}$ M. Using equation (3.7), this yields $h = 330s^{-1}$ for $\beta = -1$ and $h = 77000s^{-1}$ for $\beta = 0$.

3.4.1.2 Equilibrium Distribution

Figure 3.7 demonstrates that the equilibrium probability that a channel is open varies from approximately its minimum to its mid-height to its maximum as the agonist concentration increases from 10^{-7} to 10^{-6} to 10^{-5} M, which is consistent with experimental findings. Therefore, throughout section 3.4, these are the three main values used to compare channel properties as agonist concentration varies.

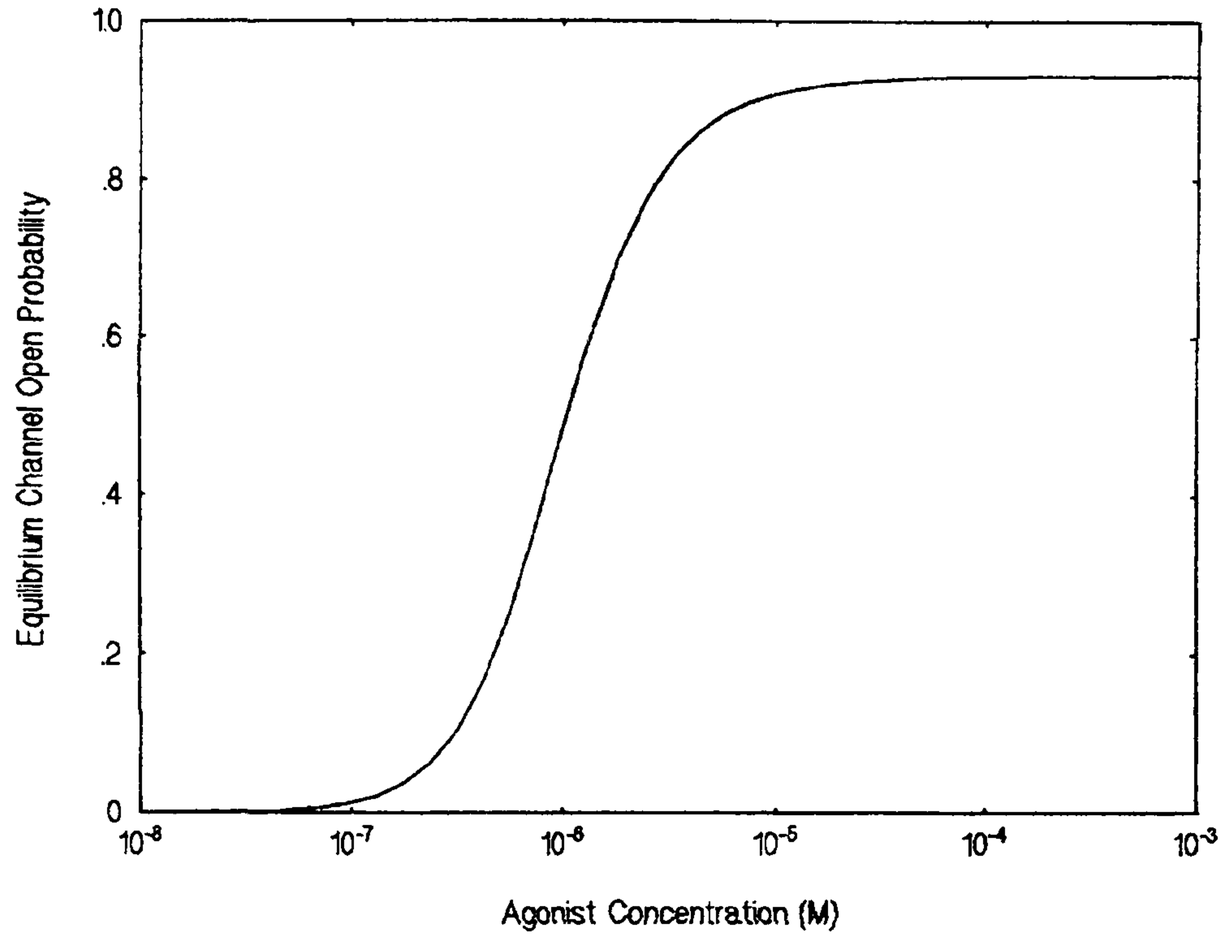

Figure 3.7. Equilibrium channel open probability as agonist concentration varies.

Figures 3.8a and 3.8b are bar charts of the channel equilibrium distribution when $a = 10^{-5}$ M and $a = 10^{-7}$ M, respectively. For $i = 0, 1, \ldots, 5$ and $j = 0, 1$ and 2, each figure gives the equilibrium probability that a channel will occupy a state in which it has i open subunits and j agonist molecules bound. Note that, from equation (3.2), it can be verified that the equilibrium probability that a channel is in any given state is independent of β. It can be seen from Figures 3.8a and 3.8b that for high agonist concentrations the channel is predominantly open with two agonist molecules bound, whereas for low agonist concentrations it is predominantly closed with no agonist molecules bound. These figures also demonstrate that, at each agonist concentration, an open channel usually has two agonist molecules bound and that the number of agonist molecules bound to a closed channel tends to decrease as the number of closed subunits increases.

These results are consistent with those of Colquhoun and Sakmann (1985) who observe recordings which suggest that the channel is sometimes open with fewer than two agonist molecules bound, although they note that these recordings also

Figure 3.8. Aggregated equilibrium probabilities when the agonist concentration is (a) 10^{-5} M and (b) 10^{-7} M.

suggest that open channels usually have two agonist molecules bound.

3.4.1.3 Time-dependent Channel Open Probability following a jump in Agonist Concentration

Although *in vitro* experiments on ion channels are under predominantly equilibrium conditions, synapses and action potentials do not function in a steady state and so it is important to understand channel behaviour in the transient state before equilibrium is attained. Furthermore, such considerations provide more stringent tests of possible models. In experiments, it is common to mimic a synaptic current by applying a very brief rectangular pulse of agonist to a patch and to measure the first latency, i.e. the time that elapses before the channel opens. We restrict attention to the case when the transition rates between states do not vary with time and the agonist concentration is constant other than at a stepwise jump at time $t = 0$, say. We examine the behaviour of a channel following such a jump in agonist concentration from a very low concentration at which the channel is almost always closed to a higher concentration at which it is more frequently open. Thus we calculate the probability that a channel is open as time varies, using the equilibrium distribution for a channel at an agonist concentration of 10^{-14} M as the initial vector, $\mathbf{p}(0)$ in equation (2.3), and using a higher agonist concentration when calculating the entries of the transition matrix Q in that equation. Since first latency experiments are frequently illustrated by

plots of the macroscopic current which represents the sum or average of a set of single channel records (see, for example, Colquhoun and Hawkes (1995)), a graph of the probability that a channel is open as time varies, under our model, can be used to compare the behaviour of a channel under our model with experimental results.

For $\beta = -1$, Figure 3.9a shows plots of the probability that a channel is open, as time varies, following a jump in agonist concentration at time $t = 0$ from (i) $a = 10^{-14}$ M to $a = 10^{-5}$ M, (ii) $a = 10^{-14}$ M to $a = 10^{-6}$ M and (iii) $a = 10^{-14}$ M to $a = 10^{-7}$ M. As expected, a jump to a higher agonist concentration results in a higher probability that the channel is open at time t for all values of $t > 0$. However, when $\beta = -1$ the curves do not near their maximum values for over 100 seconds. This is not consistent with the values of the first latency found experimentally which are typically very short (e.g. 2 ms) for nicotinic receptors. Figure 3.9b is a similar graph for the case $\beta = 0$. For this value of β, the equivalent functions near their maximum values much quicker, suggesting that, in practice, the $\alpha_2\beta_3$ model may be more consistent with experimental results when $\beta = 0$ than when $\beta = -1$.

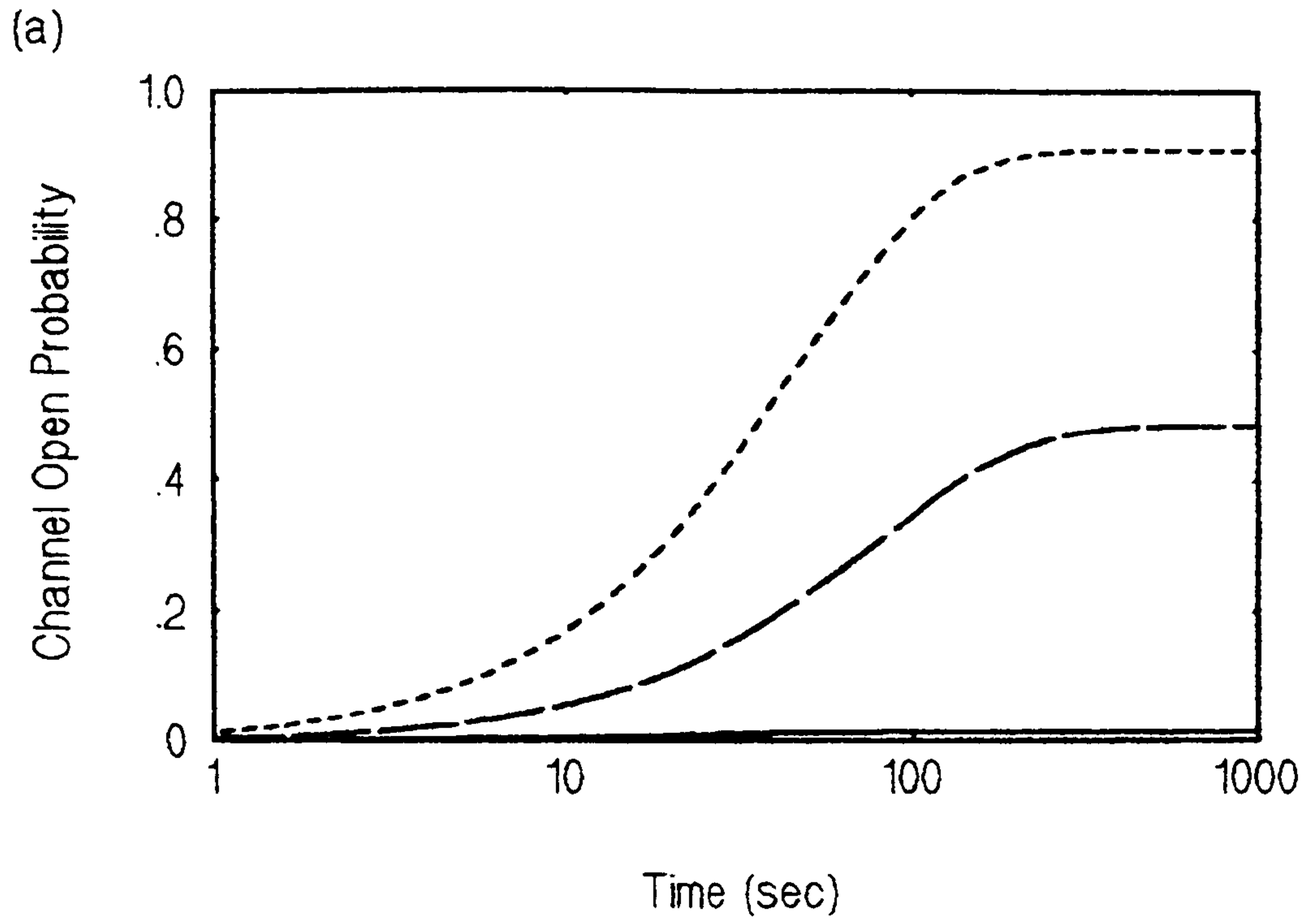

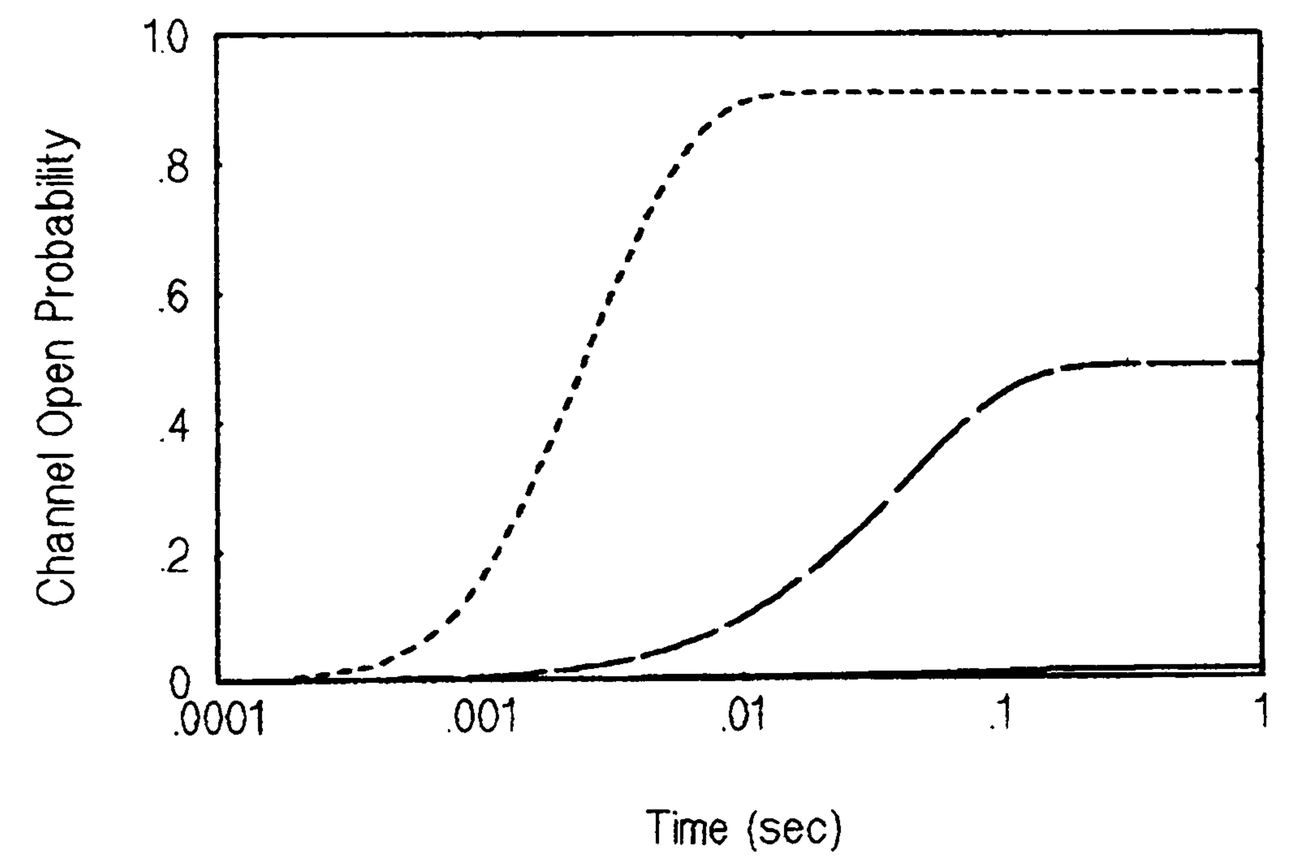

Figure 3.9. Channel open probability as time varies following a jump in agonist concentration from $a = 10^{-14}$ M to $a = 10^{-5}$ M (dotted line), $a = 10^{-6}$ M (dashed line) and $a = 10^{-7}$ M (solid line) for (a) $\beta = -1$ and (b) $\beta = 0$.

3.4.1.4 Hill Coefficient

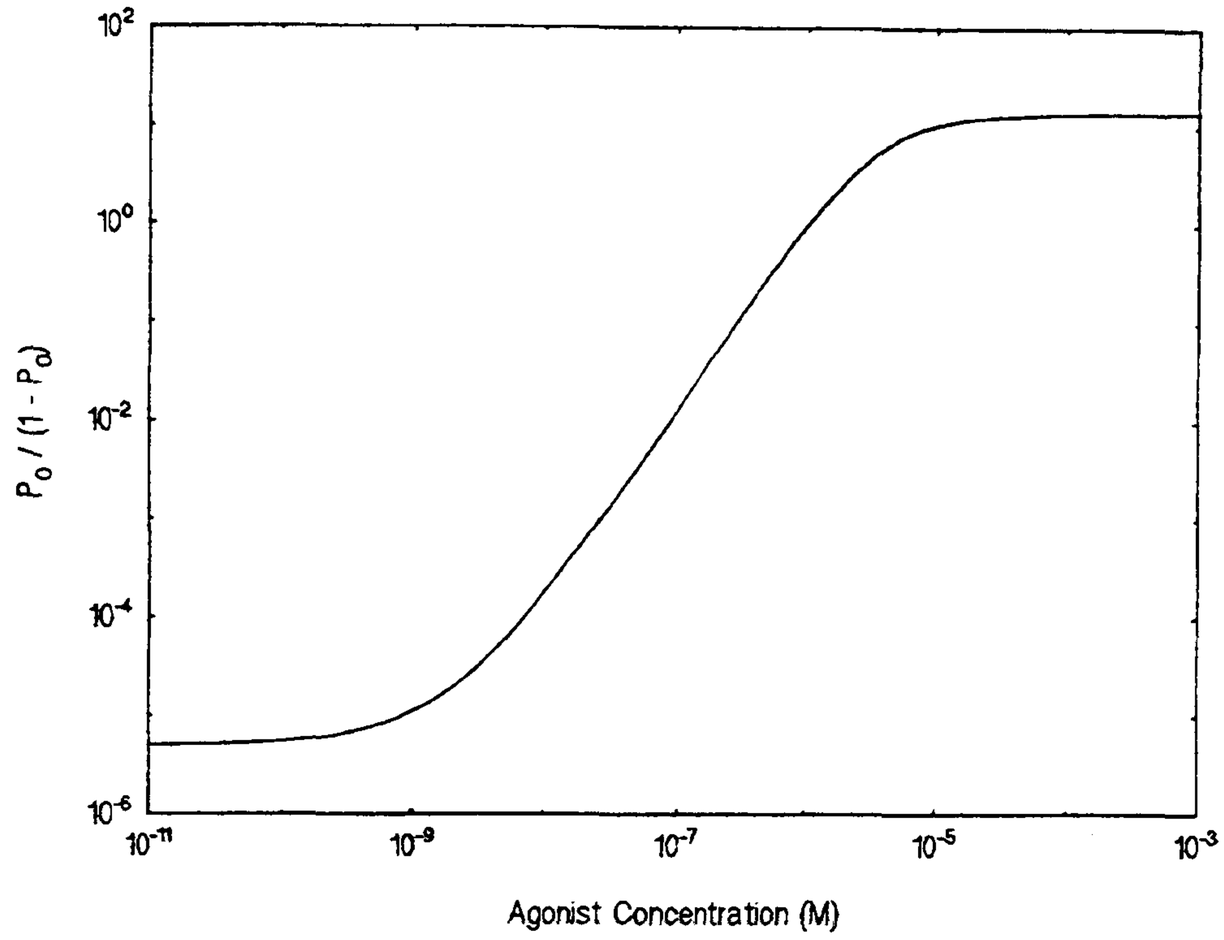

Figure 3.10. Hill Plot.

The Hill Coefficient n_H is determined by evaluating $H(a)$, using equation (3.6), at $a = a^*$ where a^* is the value of a for which the equilibrium probability that a channel is open is 0.5. Substituting our parameter values into equation (3.5) and setting $P_O = 0.5$, we obtain $a^* = 1.019 \times 10^{-6}$ M. Thus the Hill Coefficient, which represents the gradient of the corresponding Hill Plot (see Appendix B), displayed in Figure 3.10 when $a = 1.019 \times 10^{-6}$ M, is $n_H = 1.55$. This is entirely consistent with the structure of the modelled nicotinic acetylcholine channel since n_H is interpreted as a lower bound for the number of agonist binding sites on the channel (see section 3.3.1.2 and Appendix B). This value of the Hill coefficient

is similar to experimental results calculated using Hill plots in which the proportion of time that a channel is open is plotted against agonist concentration on logarithmic scales. Jackson (1993, Chapter 7) gives two examples of experimentally determined Hill coefficients: $n_H = 1.6$, calculated at $a = 2 \times 10^{-5}$ M, for channels in mouse cells and $n_H = 1.7$, calculated at $a = 7.7 \times 10^{-5}$ M, for electric ray receptors and Dionne *et al.* (1978) give similar results with values of n_H in the range 1.5 to 2.

3.4.1.5 Mean Sojourn Lengths

Table 3.6 shows that, for both $\beta = 0$ and $\beta = -1$, the mean length of an open sojourn remains approximately constant as the agonist concentration varies in the range of interest, whereas the mean length of a closed sojourn varies considerably. Recall that the parameter values of h for $\beta = 0$ and for $\beta = -1$ are determined in section 3.4.1.1 by imposing the restriction that the mean length of an open sojourn is 1 ms (Hille (1992, Chapter 6)) when $a = 10^{-6}$ M, thus ensuring that the mean open sojourn lengths are realistic. Problems arise when calculating closed sojourn lengths experimentally since it is not always known how many channels are contained in a patch. Hence there is a paucity of data with which to compare the mean closed sojourn lengths obtained here.

β	Agonist Concentration (M)	Mean Length of Open Sojourn (ms) (Standard Deviation (ms))	Mean Length of Closed Sojourn (ms) (Standard Deviation (ms))
0	10^{-7}	0.99 (0.99)	77.83 (452.19)
0	10^{-6}	1.00 (1.00)	1.06 (10.94)
0	10^{-5}	1.00 (1.00)	0.10 (0.42)
-1	10^{-7}	0.91 (0.93)	78.56 (13496.82)
-1	10^{-6}	1.00 (1.00)	1.07 (540.07)
-1	10^{-5}	1.01 (1.01)	0.10 (55.98)

Table 3.6. Mean open and closed sojourn lengths.

3.4.1.6 Open and Closed Entry Process Equilibrium Distributions

From equations (3.9) and (3.11), it can be seen that the open and closed entry process equilibrium distributions are independent of β. The results given in this subsection are based on an agonist concentration of 10^{-7} M and our calculations show that, for our parameter values, the entry process equilibrium distributions do not vary greatly as agonist concentration varies within a physiologically sensible range. The proportion of entries into the open class of states which are made via the open state in which the channel has two agonist molecules bound is 94.9%, with nearly 5.1% of entries being made via the open states in which the channel has one agonist molecule bound. Unfortunately, there is a shortage of experimental data with which to compare these results, although the results do seem consistent with the findings of Colquhoun and Sakmann (1985) and Jackson (1986, 1988) who note that, although most transitions from the closed class of

states to the open class of states occur when the channel has two agonist molecules bound, experimental findings indicate that it is also possible for the channel to open when one or zero agonist molecules are bound. Note that, since channel gating in the $\alpha_2\beta_3$ model is assumed to be consistent with microscopic reversibility, the proportion of entries into the closed class of states which are made via the closed state(s) in which the channel has a given number of agonist molecules bound is the same as the proportion of entries into the open class of states made via the open state(s) in which the channel has that number of agonist molecules bound. Further, the probability that the closed class of states is entered via a closed state in which the channel has an agonist molecule bound to the closed subunit is only 0.000129, reflecting the model property that a subunit with no agonist molecule bound has a much higher closing rate than a subunit with an agonist molecule bound.

3.4.1.7 Open and Closed Sojourn Probability Density Functions

Using the results of section 3.3.1.6 with $\beta = 0$ and $a = 10^{-6}$ M, the open sojourn time probability density function is given by

$$f_O(t) = 0.001004 \exp(-1684.23\, t) + 6.76 \exp(-1341.47\, t) + 993.67 \exp(-998.71\, t).$$

Figure 3.11 is a graph of this open time probability density function drawn on a log-log scale as is common in ion channel literature (see McManus *et al.* (1987)).

From this graph, we can see that, although the probability density function is a sum of three exponential terms, one exponential term is dominant. This is a consequence of, firstly, the coefficient of one of the three exponential terms being significantly larger than the other two coefficients, and, secondly, one of the three eigenvalues of Q_{OO}^{R} being significantly larger than the other two eigenvalues. Our calculations demonstrate that as the agonist concentration varies in our range of interest, the largest eigenvalue of Q_{OO}^{R} remains approximately constant, whereas the other two eigenvalues vary whilst remaining considerably smaller than the largest eigenvalue. Similarly, when $\beta = -1$ and $a = 10^{-6}$ M, the dominant term of $f_O(t)$ is 987.11 exp(-990.44 t) and hence the graph of $f_O(t)$ for $\beta = -1$ is very similar to that for $\beta = 0$.

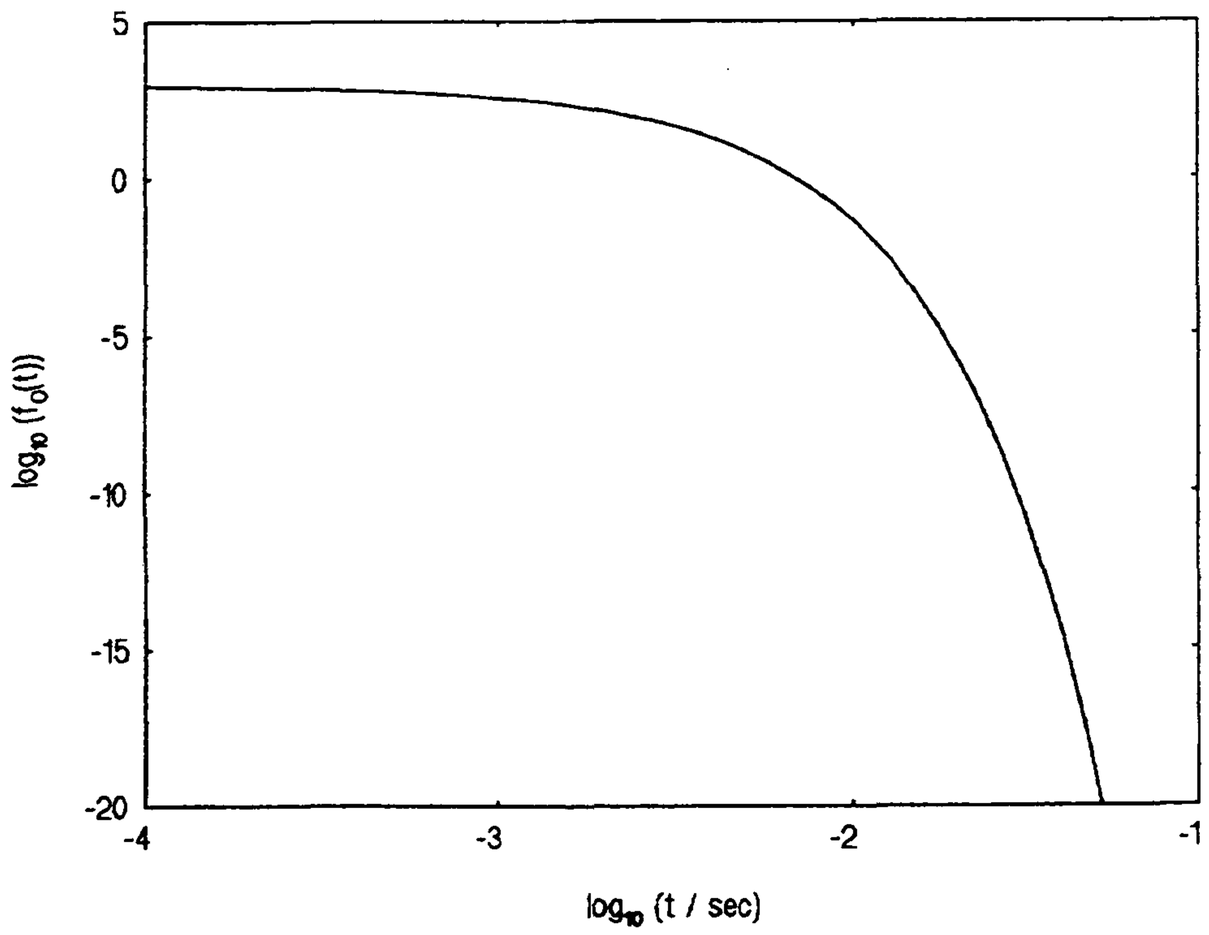

Figure 3.11. Open sojourn time probability density function. The graph is based on an agonist concentration of 10^{-6} M and $\beta = 0$. Graphs for agonist concentrations 10^{-5} M and 10^{-7} M and for $\beta = -1$ appear very similar to this graph (see text) and are not shown here.

It is interesting to note from our numerical results that $f_O(t)$ is a mixture of negative exponential distributions whose time constants form an arithmetic progression. This has been shown (not presented in this thesis) to always be a feature of probability density functions of open sojourn times for a more general $\alpha_r\beta_{n-r}$ ($r = 0, 1,..., n$; $n = 2, 3, 4,...$) model.

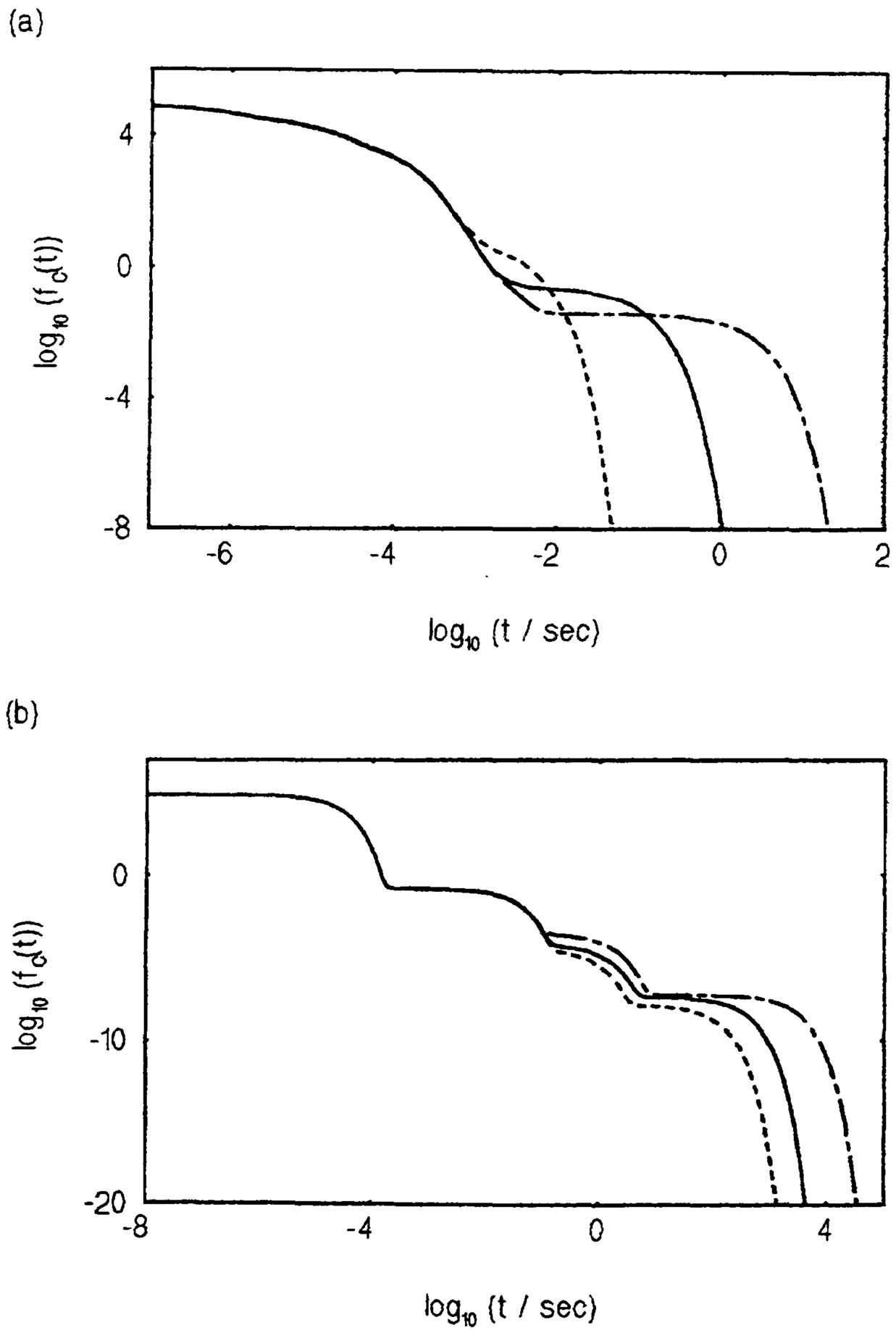

Figure 3.12. Closed sojourn time probability density functions for agonist concentrations of 10^{-5} M (dotted line), 10^{-6} M (solid line) and 10^{-7} M (dashed line) when (a) $\beta = 0$ and (b) $\beta = -1$.

The closed sojourn time probability density function is a sum of 69 exponential terms and we have determined an expression (not given here) for this function using a computer. We note that, basing all calculations on the 72-state reduced state space discussed in section 3.3.1.4, our software (written using FORTRAN 77 employing the NAG library of numerical subroutines and run on a VAX 11/785) determined this expression in approximately 5 seconds, compared with several hours when calculations were based on the 128-state unreduced state-space. From Figures 3.12a and 3.12b, we can see that, in practice, the closed sojourn time probability density function can be fitted quite accurately by a mixture of 2 to 4 exponentials, depending on the value of β. We have found that Q_{CC}^R has just a few eigenvalues which are negative and of small absolute value and the remainder of the eigenvalues of Q_{CC}^R are negative and of large absolute value. Thus the shape of the graph of $f_C(t)$, which is determined by $\exp(Q_{CC}^R)$, is ultimately dependent on the values of the few eigenvalues of small modulus. Figures 3.12a and 3.12b are consistent with the results of a large number of experimental studies which predict that the closed sojourn time probability density function can be approximated by a sum of 2 to 6 exponential components. As a result of such experimental studies, many models postulated in the ion channel literature have been based on a small number of closed states (see, for example, Colquhoun and Sigworth (1995), Horn and Lange (1983)). It is interesting to note that the time constants of the closed sojourn probability density function occur in distinct batches that can be related to the structure of the

matrix Q^R_{CC}.

3.4.1.8 Autocorrelation and Cross-Correlation Functions

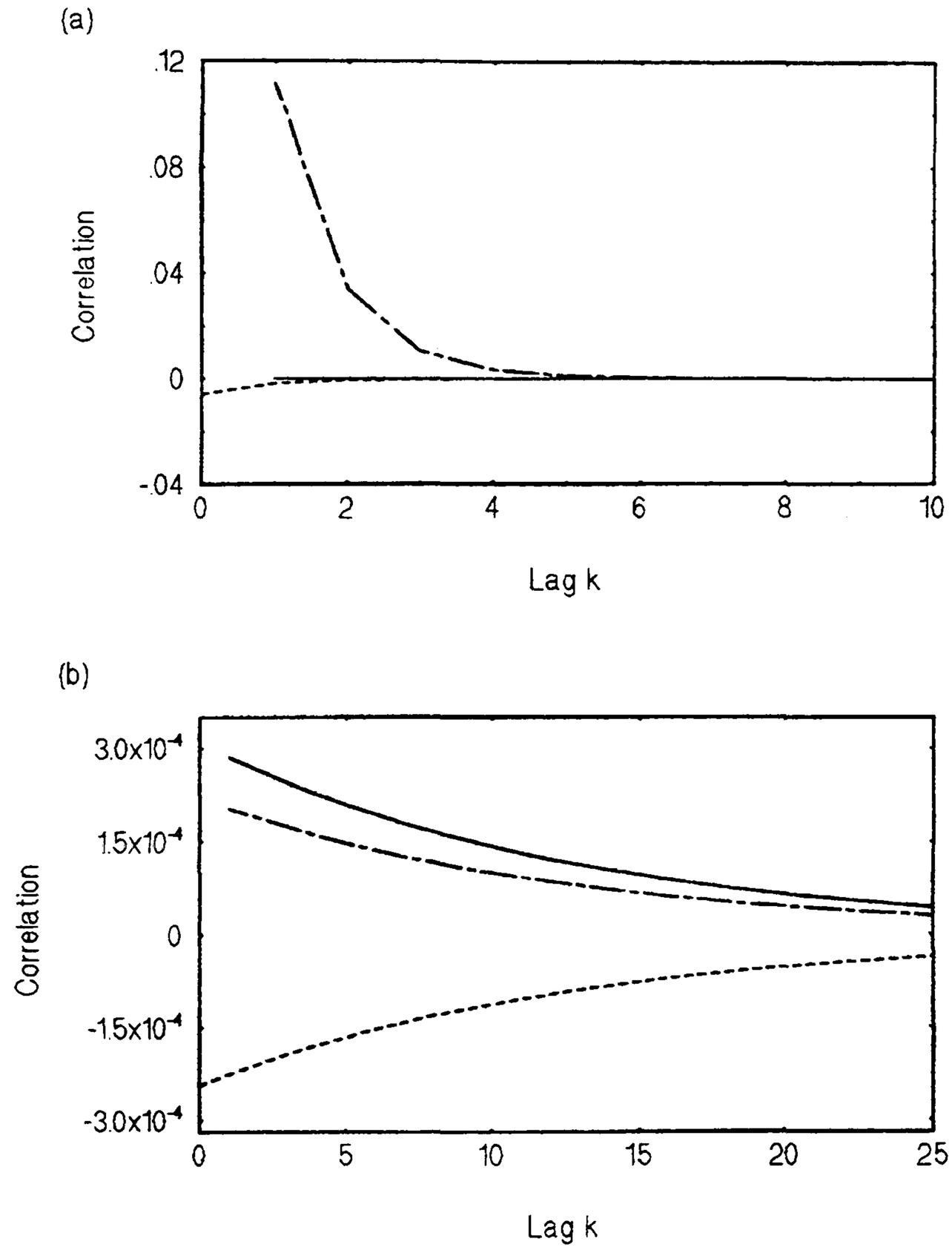

Figure 3.13. Open sojourn (solid line) and closed sojourn (dashed line) autocorrelation functions and open-closed (dotted line) cross-correlation functions for an agonist concentration of 10^{-6} M when (a) $\beta = 0$ and (b) $\beta = -1$. The lag value on the horizontal axis indicates which sojourns' correlation is plotted. For example, when the lag is 2, the correlation between the kth open / closed sojourn and the (k + 2)th open / closed sojourn is plotted.

Figure 3.13 confirms that the open sojourn and closed sojourn autocorrelation functions are decreasing, non-negative, and convex (see section 2.1.4). As reported in ion channel literature (e.g. Jackson (1988)), long open sojourns tend to be adjacent to short closed sojourns, and vice versa, and this is consistent with the negative values taken by the cross-correlation function in Figure 3.13a. Figure 3.13b shows that sojourn lengths are subject to lower correlations when $\beta = -1$ than when $\beta = 0$.

Figure 3.14 shows the effect upon the closed autocorrelation function of varying the agonist concentration within the range 10^{-7} M to 10^{-5} M when $\beta = 0$. As the agonist concentration decreases within this range, the lengths of closed sojourns become more highly correlated. Our studies have shown that open sojourn autocorrelation functions and cross-correlation functions also take higher values as the agonist concentration decreases within the same range and that similar results hold for $\beta = -1$. These results are a consequence of the reductions in agonist binding rates and the resultant decrease in the time spent by the channel in states in which it has one or more agonists bound, and thus the decrease in the number of different transition pathways between the open and the closed classes of states predominantly used by the channel. Note that, as the agonist concentration approaches zero, the class of open states is almost always exited via the open state in which the channel has no agonist molecules bound, and that, as the agonist concentration approaches infinity, the open states are almost always

exited via the open state in which the channel has two agonist molecules bound. Hence, as the agonist concentration approaches zero or infinity, all the correlation functions approach zero.

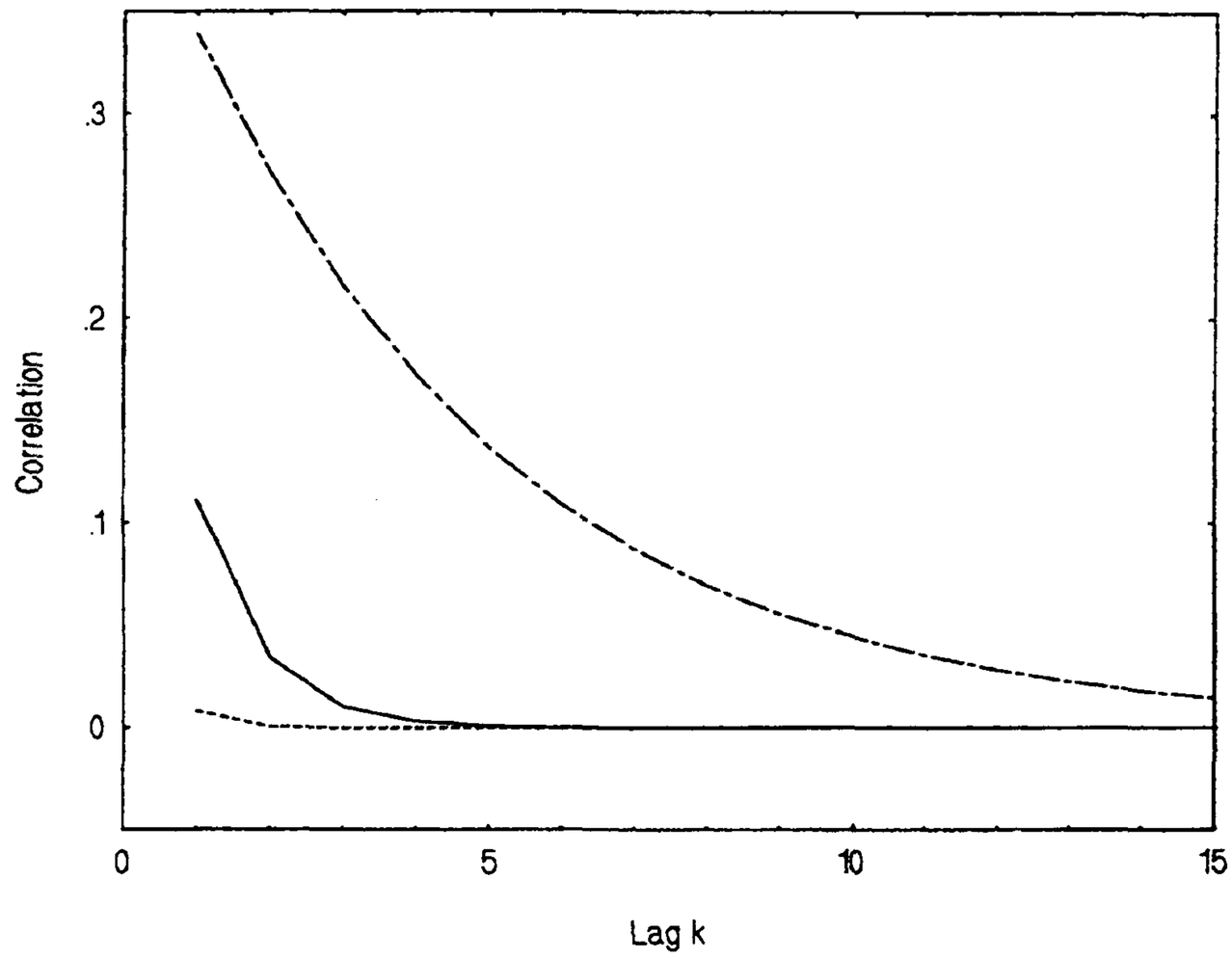

Figure 3.14. Closed sojourn autocorrelation functions for agonist concentrations of 10^{-7} M (dashed line), 10^{-6} M (solid line) and 10^{-5} M (dotted line) when $\beta = 0$.

3.4.1.9 Clustering

The study of characteristics of clusters of channel openings and clusters of bursts of openings yields useful information about the chemical reactions which govern channel behaviour. These properties have been widely studied in ion channel literature since membrane patches often contain multiple channels and, although it cannot be guaranteed that only one channel is being observed, it is extremely

likely that all the openings in any given burst are from a single channel with openings in preceding and subsequent bursts possibly being from a different channel. To date however there is a shortage of experimental studies quantifying the degree of clustering of openings and the degree of clustering of bursts of openings and hence we are currently unable to compare the numerical results of this section with experimental data.

3.4.1.9.1 Clustering of Openings

Let $\{N(t)\}$ be the point process describing the starts of channel openings. Then, for $\beta = 0$ and $\beta = -1$ respectively, Figures 3.15a and 3.15b show the value of $\lim_{t\to\infty} \mathrm{Var}[N(t)] / \mathrm{E}[N(t)]$, given by equation (2.39), as the agonist concentration varies. For each of these values of β, these figures demonstrate that our model does indeed predict that, in the agonist concentration range of interest, channel openings will be highly clustered in time. This model feature is consistent with many experimental studies (e.g. Sakmann *et al.* (1980), Colquhoun and Sakmann (1985) and Dionne and Leibowitz (1982)). Further, the degree of clustering of openings is greater for the case $\beta = -1$ than for the case $\beta = 0$.

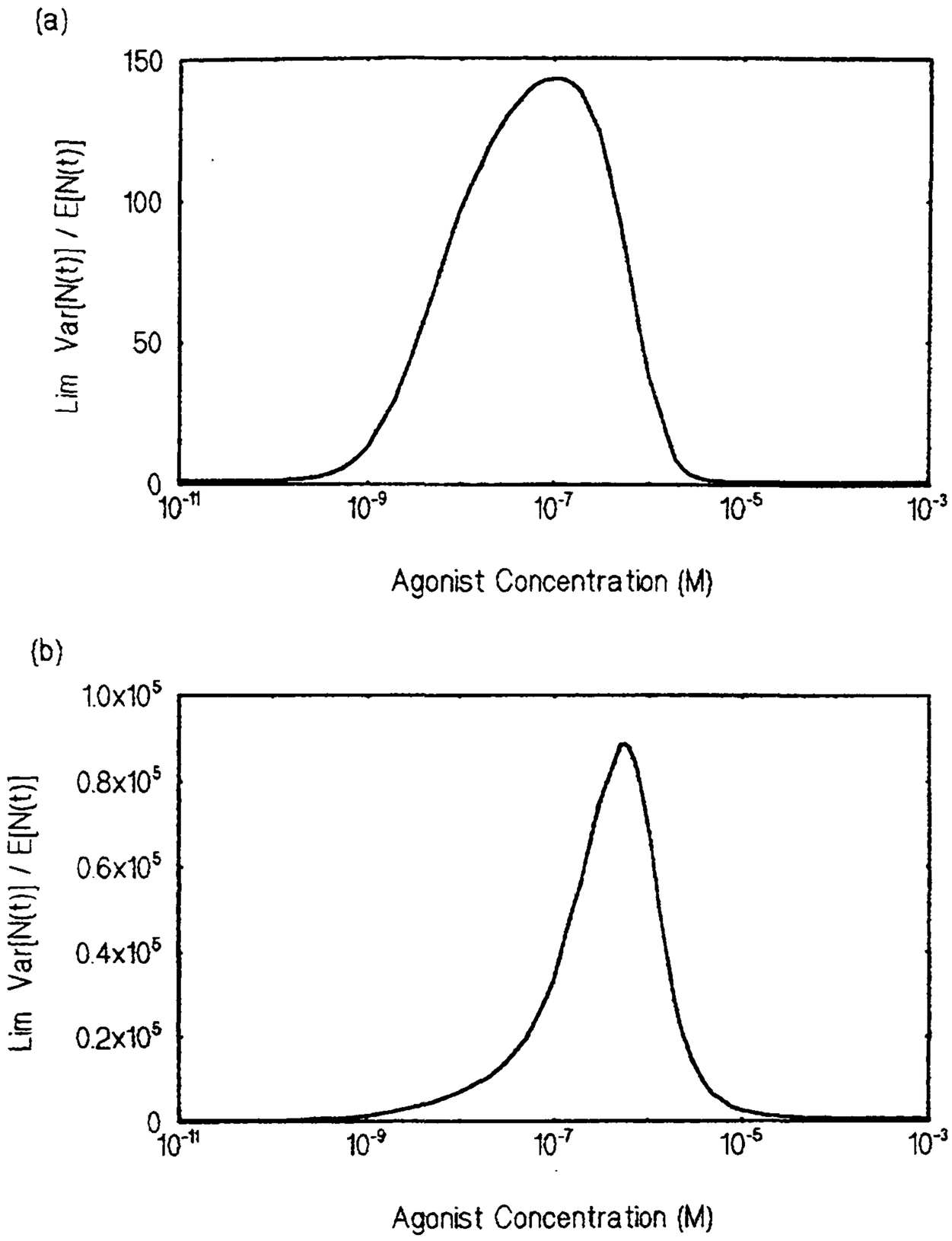

Figure 3.15. Clustering of channel openings: $\lim_{t\to\infty} \mathrm{Var}[N(t)]/\mathrm{E}[N(t)]$ as a function of agonist concentration when (a) $\beta = 0$ and (b) $\beta = -1$.

For $a = 10^{-6}$ M, Figure 3.16a ($\beta = 0$) and Figure 3.16b ($\beta = -1$) show the value of $\mathrm{Var}[N(t)]/\mathrm{E}[N(t)]$ as t varies (see section 2.1.5.1). For $a = 10^{-6}$ M, and also for $a = 10^{-7}$ M (not shown), the function $\mathrm{Var}[N(t)]/\mathrm{E}[N(t)]$ is monotonically increasing for both $\beta = 0$ and $\beta = -1$. However, this is not generally the case for

higher agonist concentrations when openings are not clustered. For example, when $\beta = 0$ and $a = 10^{-5}$ M, Var[$N(t)$]/E[$N(t)$] decreases from 1 at $t = 0$ to 0.915 at $t = 0.000852$ before increasing to 0.970 for large values of t.

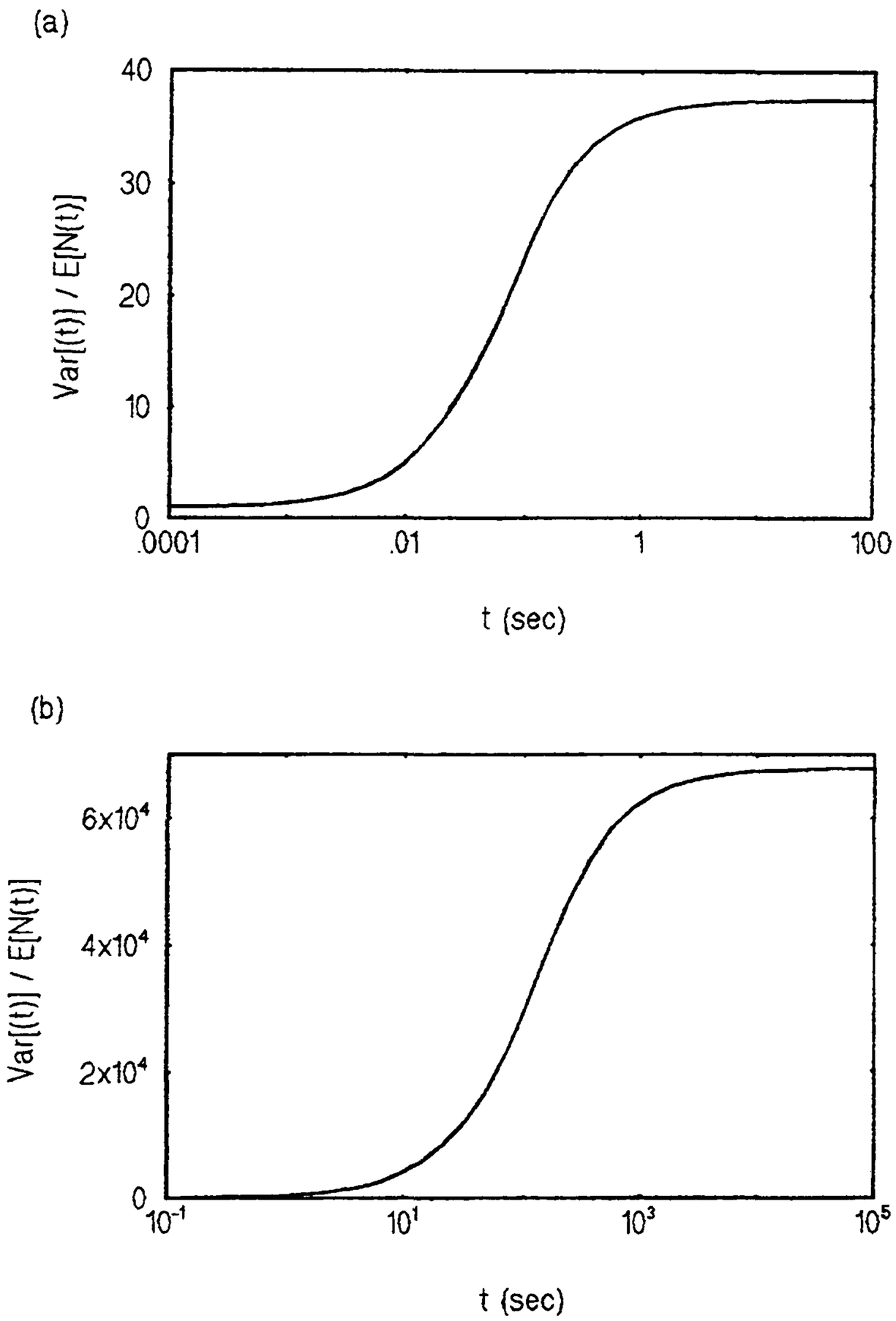

Figure 3.16. Clustering of channel openings: Var[$N(t)$]/E[$N(t)$] as a function of time when agonist concentration is 10^{-6} M for (a) $\beta = 0$ and (b) $\beta = -1$.

3.4.1.9.2 Clustering of Bursts of Openings

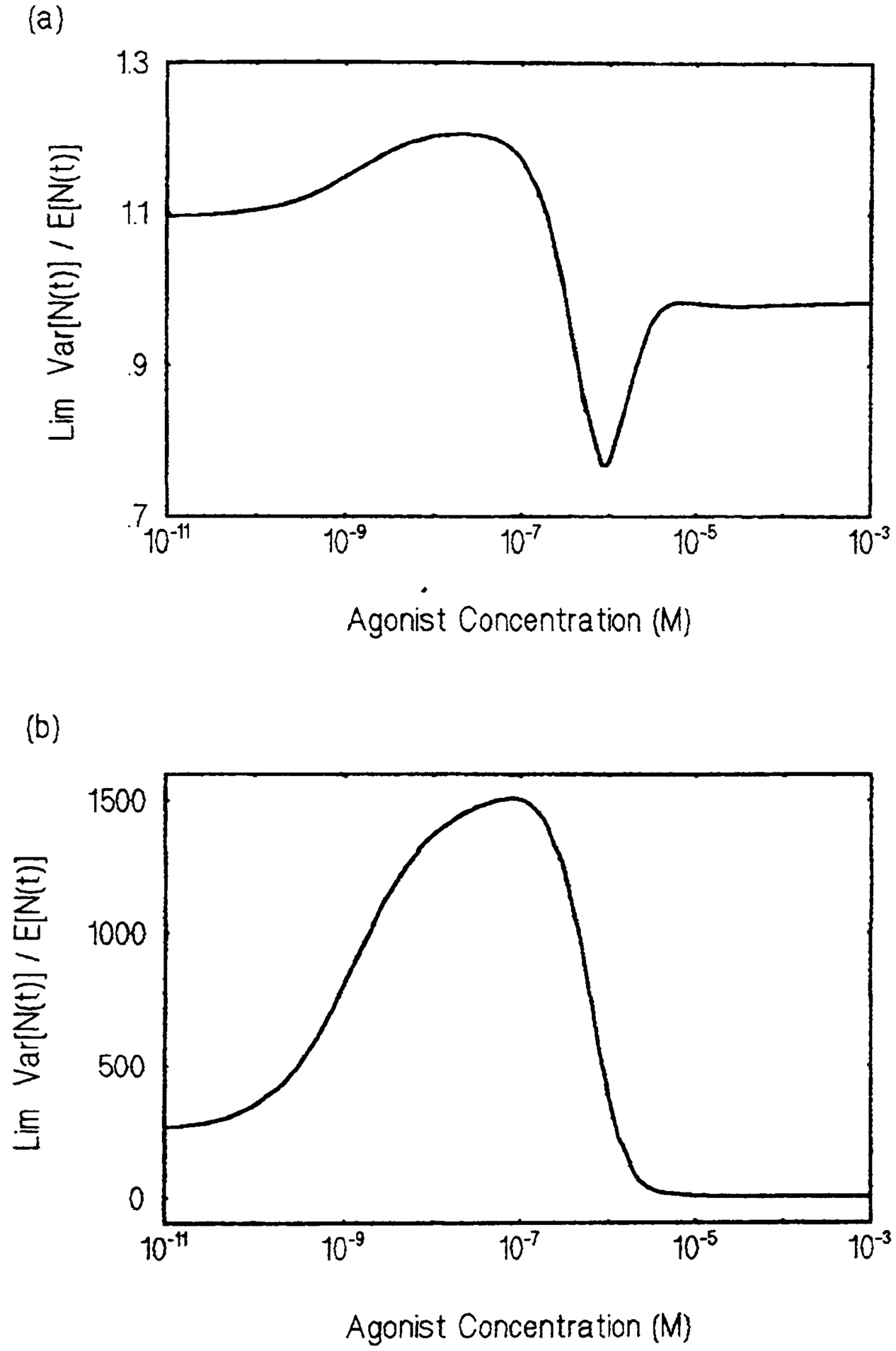

Figure 3.17. Clustering of bursts of channel openings: $\lim_{t\to\infty} \mathrm{Var}[N(t)]/\mathrm{E}[N(t)]$ as a function of agonist concentration when (a) $\beta = 0$ and (b) $\beta = -1$.

Now let $\{N(t)\}$ be the point process describing the starts of bursts of channel openings (see section 2.1.5.2 and section 3.3.1.7). Figure 3.17a ($\beta = 0$) and

Figure 3.17b (β = -1) show $\lim_{t\to\infty}$Var[$N(t)$]/E[$N(t)$] as a function of agonist concentration. Bursts of openings are not clustered in the β = 0 model, except very slightly for $a \approx 10^{-7}$ M. However, they are very highly clustered in the β = -1 model, notably when $a \approx 10^{-7}$ M.

Figure 3.18 shows Var[$N(t)$]/E[$N(t)$] as a function of time when $a = 10^{-6}$ M and β = -1. Although Var[$N(t)$]/E[$N(t)$] is monotonically increasing with t when $a \approx 10^{-6}$ M, this is not the case when β = 0 nor when β = -1 for much higher values of agonist concentration (e.g. $a = 10^{-3}$ M) at which bursts of openings are not clustered. Note that $\lim_{t\to 0}$Var[$N(t)$]/E[$N(t)$] = 1 (see Ball and Davies (1997)).

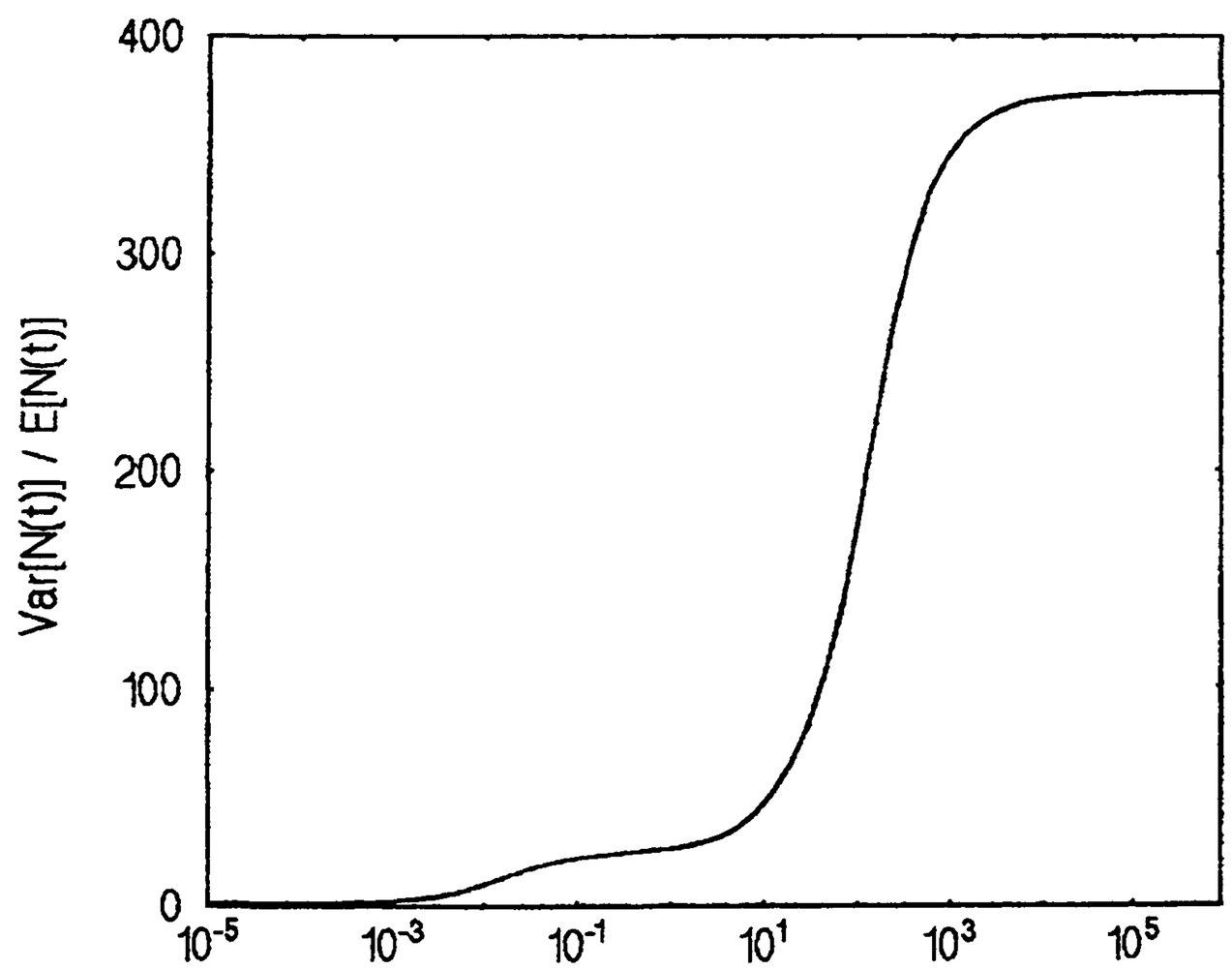

Figure 3.18. Clustering of bursts of channel openings: the function Var[$N(t)$]/E[$N(t)$] when agonist concentration is 10^{-6} M for the case β = -1.

Two mechanisms widely employed to investigate the nicotinic acetylcholine receptor are the 5-state model of Colquhoun and Hawkes (1982, 4.1) and the 4-state linear model studied by Ball and Sansom (1989, Mechanism I). For both these models we have calculated that $\lim_{t\to 0}\mathrm{Var}[N(t)]/\mathrm{E}[N(t)]$ takes values between 0.4 and 1.01 for all realistic values of agonist concentration, indicating that they predict that bursts of channel openings are not clustered, contrary to experimental findings (e.g. Sakmann *et al.* (1980)). Thus, in this respect, the $\alpha_2\beta_3$ model, particularly with $\beta = -1$, is an improvement on these smaller state space models.

3.4.1.9.3 Properties of Bursts of Openings and of Clusters of Bursts of Openings

Appendix C contains numerical results for the $\alpha_2\beta_3$ model based on the expressions for various observable characteristics of bursts of openings and clusters of bursts of openings derived by Colquhoun and Hawkes (1982). These results are obtained by categorising each closed state according to whether a sojourn in that state represents a closing within a burst, a closing between bursts of openings or a closing between clusters of bursts of openings (see section 3.3.1.7).

We do not discuss these results in detail here since there are currently a number

of difficulties in assessing whether they accurately predict channel behaviour. Firstly, although the $\alpha_2\beta_3$ model lends itself to 'natural' definitions of bursts of openings and of clusters of bursts of openings in terms via the categorisation of closed states described in section 3.3.1.7, such definitions have caused difficulty when interpreting observed ion channel data. Most such definitions categorise closed sojourns according to whether or not they are greater than specified critical sojourn lengths, but the method by which such a critical value is chosen varies widely (e.g. Colquhoun and Sakmann (1985), Jackson *et al.* (1983) and Magleby and Palotta (1983b)) and in some cases makes a very significant difference to the interpretation of observations. Other methods used include the use of Bayes' theorem by Colquhoun and Hawkes (1981) to calculate the probability that a particular closed sojourn is within a burst. These variations in definitions will clearly affect the interpretation of data. Secondly, due to the presence of time interval omission, it is not possible in practice to observe many of the shorter channel openings and closings. In most cases, many sojourns are of shorter duration than the detection limit and it is not possible to obtain accurate experimental results with which to compare the results in Appendix C. This situation was observed, for example, by Colquhoun and Sakmann (1985), who measured apparent open times which were often made up of several open sojourns separated by undetected closed sojourns rather than measuring open sojourns themselves. Thirdly, in most experiments it is not known how many channels are being observed and, if, for example, two successive openings

originate from different channels, the closed sojourn between them is likely to be incorrectly interpreted.

3.4.2 Comparison of the α_5 Model with the $\alpha_2\beta_3$ Model

In this section we examine numerical results for the α_5 model by comparing them with those for the $\alpha_2\beta_3$ model. Such a comparison is of value since channels with α_5 stoichiometry exist in the form of insect nAChR channels and there is speculation (e.g. Aidley and Stanfield (1996)) that the original nAChR in some of the earliest multi-cellular animals had α_5 stoichiometry and that the subunits of nAChR channels underwent an evolutionary divergence from each other which started over a billion years ago, resulting in channels with $\alpha_2\beta_3$ stoichiometry.

We use the same parameter values as detailed in section 3.4.1.1, with the exception of K_B, which we reduce to 2206.31 M^{-1} so that the equilibrium channel open probability for the α_5 model, shown in Figure 3.19, reaches half its maximum height at the same agonist concentration as for the $\alpha_2\beta_3$ model and the dose response curve (see Appendix B) appears realistic.

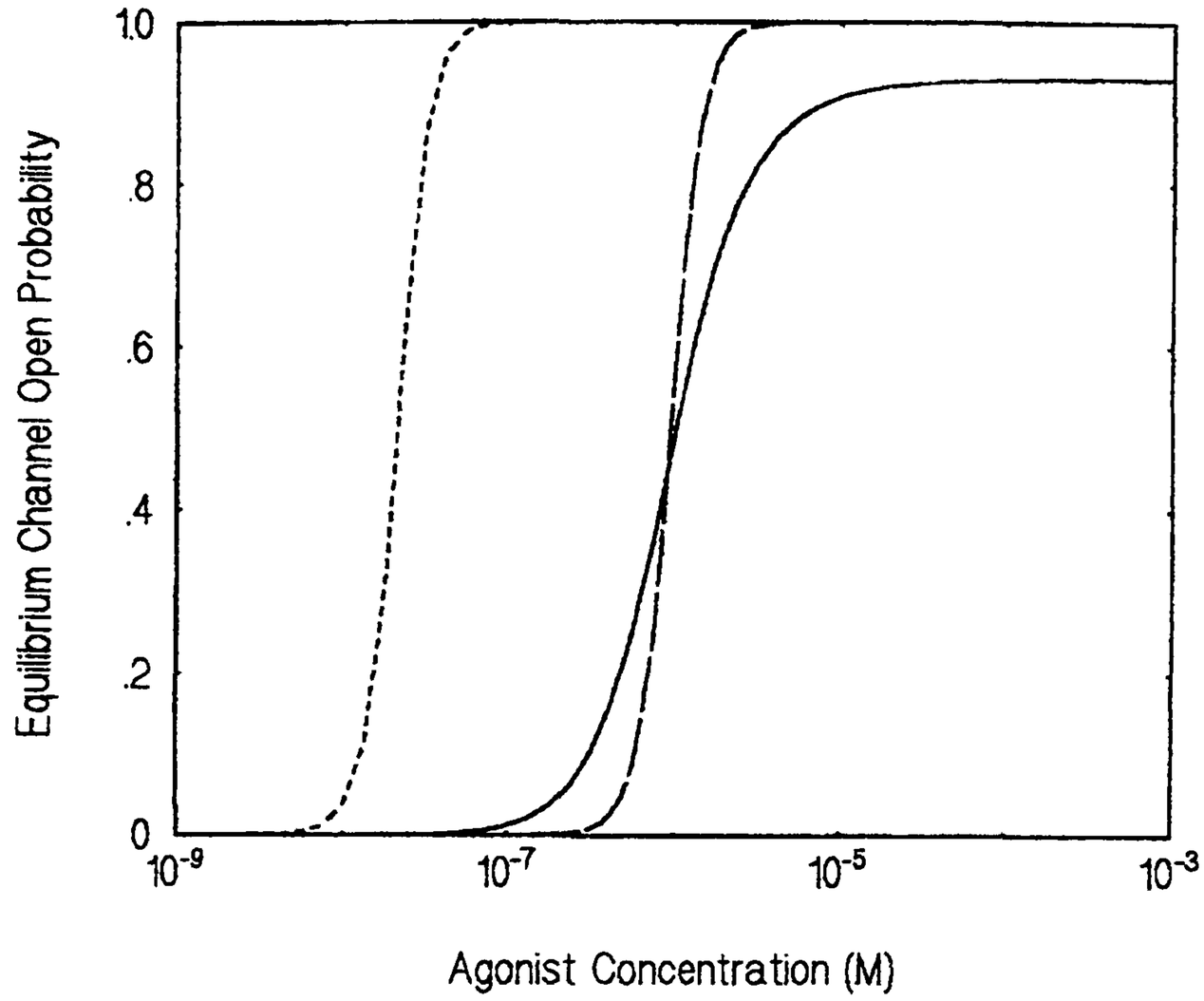

Figure 3.19. Channel open probability as agonist concentration varies. The solid line shows the channel open probability for the $\alpha_2\beta_3$ model with $K_B = 100000\ M^{-1}$, the dotted line corresponds to the α_5 model with $K_B = 100000\ M^{-1}$ and the dashed line corresponds to the α_5 model with $K_B = 2206.31\ M^{-1}$.

We make the following observations:

- The equilibrium distribution for the α_5 model is similar to that for the $\alpha_2\beta_3$ model in that at low agonist concentrations the channel predominantly occupies the closed state in which it has no agonist molecules bound and at high agonist concentrations it tends to occupy the open state with an agonist molecule bound at each binding site.

- Graphs of the α_5 model time-dependent probability that a channel is open following an initial jump in agonist concentration from $a = 10^{-14}$ M to $a = 10^{-5}$ M, 10^{-6} M or 10^{-7} M are very similar to Figure 3.9a (when $\beta = -1$) and Figure 3.9b (when $\beta = 0$), although, as t increases, the probability that the channel is open approaches a higher value for the α_5 model than for the $\alpha_2\beta_3$ model. This result concurs with expectation since the α_5 model has three agonist binding sites more than the $\alpha_2\beta_3$ model.

- The Hill coefficient for the α_5 model is $n_H = 4.5387$. Given the interpretation of n_H, this value is consistent with the five agonist binding sites assumed by our model. Unfortunately, there are very few experimental data with which to compare this result due to a problem known as 'run down' in which continued stimulation of receptors causes channels to disappear so that sufficient data cannot be collected.

- In contrast with the $\alpha_2\beta_3$ model, the mean length of an open sojourn varies with agonist concentration under the α_5 model. Further, the mean length of a closed sojourn varies with agonist concentration to a greater extent under the α_5 model than under the $\alpha_2\beta_3$ model. This variation, demonstrated in Table 3.7, can be explained by examining the forms of the formulae for mean sojourn lengths given in section 3.3.3.2. Such results have not been reported in the ion channel literature and it is likely

that they are not realistic. However, no experiments which can confirm or refute these results have yet been carried out.

β	Agonist Concentration (M)	Mean Length of Open Sojourn (ms) (Standard Deviation (ms))	Mean Length of Closed Sojourn (ms) (Standard Deviation (ms))
0	10^{-7}	1.26 (2.20)	6144.57 (14857.11)
0	10^{-6}	7.21 (16.61)	5.83 (113.46)
0	10^{-5}	65.39 (83.49)	0.02 (0.18)
-1	10^{-7}	1.27 (2.21)	6202.25 (190043.26)
-1	10^{-6}	7.28 (16.70)	5.88 (1232.37)
-1	10^{-5}	66.01 (84.11)	0.02 (6.65)

Table 3.7. Mean open and closed sojourn lengths for the α_5 model.

- For each of the agonist concentrations 10^{-5} M and 10^{-7} M, Figure 3.20 shows the probabilities (independent of the value of β) that a channel has 0, 1, 2, 3, 4 and 5 agonist molecules bound when it enters the class of open states. In contrast with the $\alpha_2\beta_3$ model, the open entry process equilibrium probabilities are highly dependent on agonist concentration within the range of realistic values of agonist concentration, with a greatly increased probability of the channel having more agonist molecules bound when it opens at high agonist concentrations than at low agonist concentrations. Further, we note that, when $a = 10^{-5}$ M, the open states are usually entered from the closed state in which the four open subunits

each have one agonist molecule bound but the closed subunit has no agonist molecule bound.

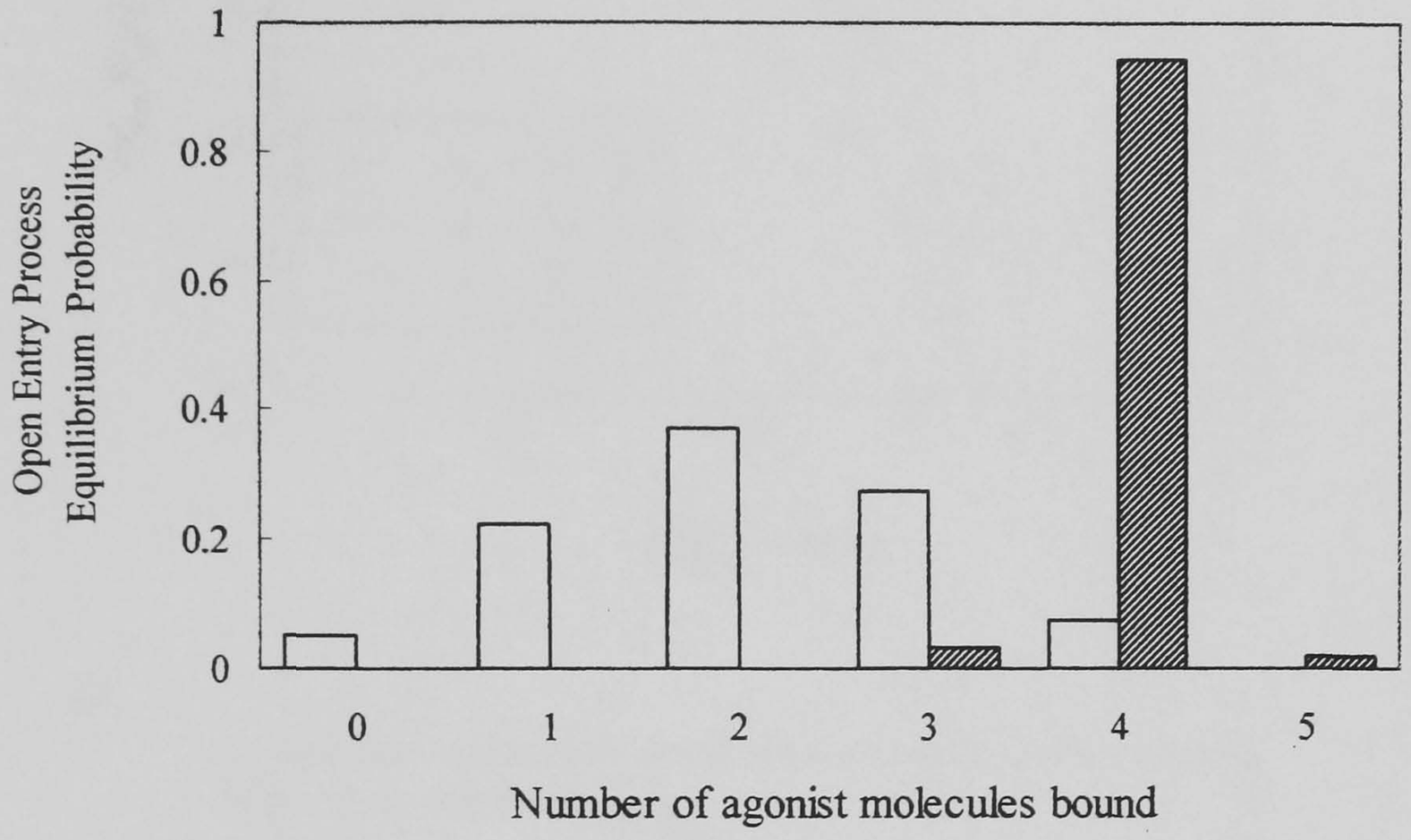

Figure 3.20. Open entry process equilibrium probabilities (as functions of the number of agonist molecules bound to the channel) for the α_5 model. The white bars represent values for an agonist concentration of 10^{-7} M and the darker bars represent values for an agonist concentration of 10^{-5} M.

- In comparison with the $\alpha_2\beta_3$ model, an increased number of exponential terms dominate both the open and closed sojourn time probability density functions in the α_5 model, as can be seen in Figure 3.21. While there is a lack of experimental data with which to compare these figures, these results serve as a prediction.

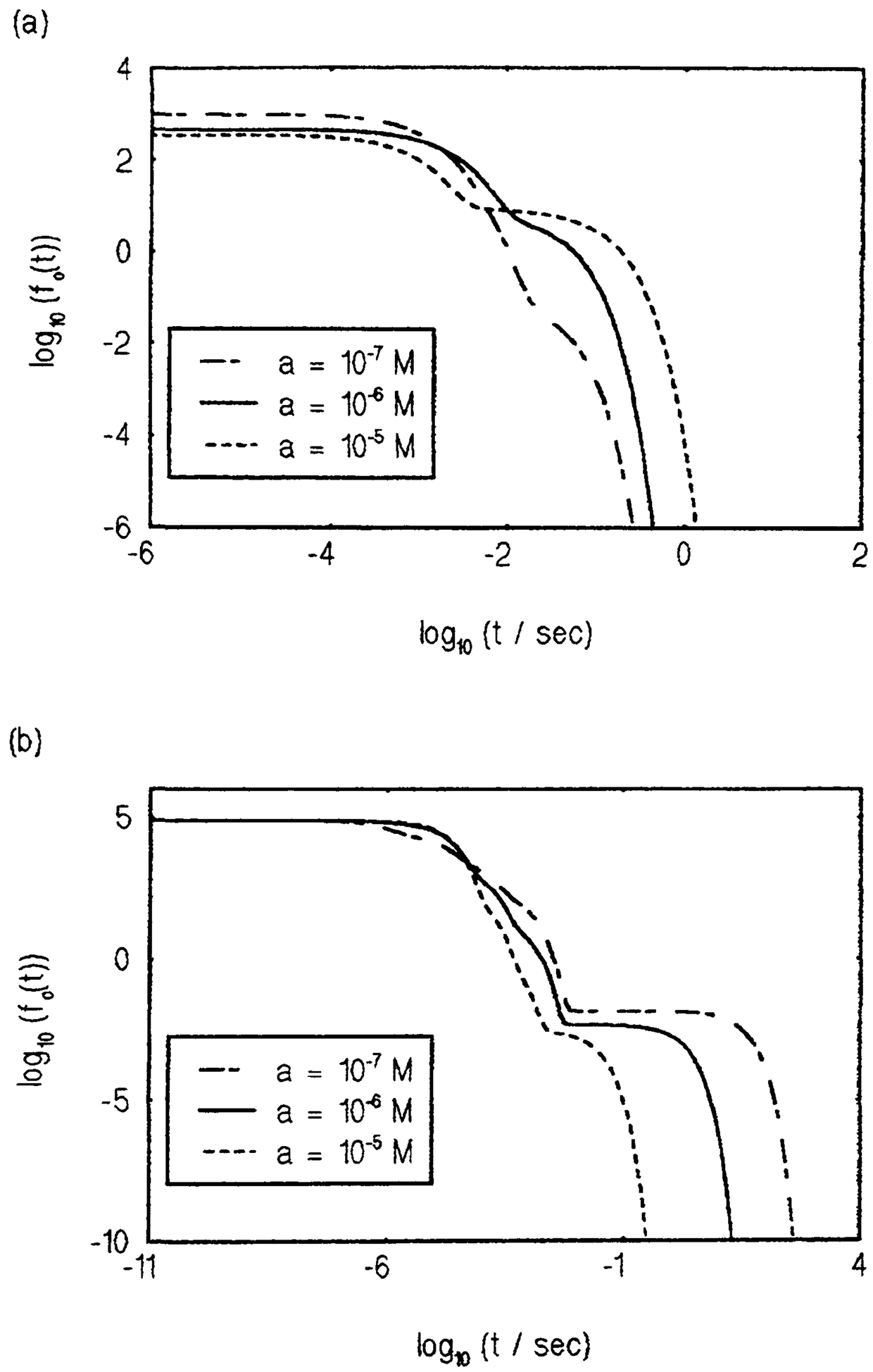

Figure 3.21. Open (a) and closed (b) sojourn time probability density functions for the α_5 model for agonist concentrations of 10^{-5} M, 10^{-6} M and 10^{-7} M when $\beta = 0$.

- The open and closed sojourn autocorrelation functions and the open-closed cross-correlation function for the α_5 model are very similar to those for the $\alpha_2\beta_3$ model.

3.5 Biophysical Discussion of the nAChR Models

3.5.1 Channel Structure

The nicotinic acetylcholine receptor models discussed above are valid in terms of the structure of the channels being modelled. The models incorporate a pentameric channel structure, identification and positioning of α-subunits and β-subunits within a subunit ring as reported for nAChR, and nearest neighbour subunit interactions. Thus, in terms of the known structural information regarding nAChR, these models are realistic.

3.5.2 Channel Physiology

It is not so easy to judge the above nAChR models in terms of their agreement with physiological data. This is chiefly due to a lack of relevant data in the ion channel literature, and, in particular, a lack of data relating single acetylcholine channel behaviour to agonist concentration. Recent experimental work has tended to be concentrated on other types of ion channels, particularly glutamate receptors and potassium channels.

One reason for the lack of recent physiological studies of nAChR is that there is a problem with collecting sufficient data to enable discrimination between models

since the channels are prone to a phenomenon known as *desensitization*. When acetylcholine is continuously present at the neuromuscular junction, it becomes insensitive to further application and the channels will no longer open. This desensitization is evident in single channel records as long periods of inactivity interrupted by clusters of channel openings. At high agonist concentrations a channel may spend most of its time in the desensitized state, with agonist molecules bound but the channel closed. In such circumstances measurements are restricted to clusters when investigating characteristics of the active channel. This yields further problems if multiple channels may be present since different clusters may appertain to different channels. As a result of desensitization, the typical number of nAChR openings recorded is usually only several thousand, whereas it is possible to record hundreds of thousands of openings of a BK channel. A second phenomenon that occurs at high agonist concentrations is an increase in the number of very brief channel closings. These may be caused by the temporary blockage of the channel pore by acetylcholine molecules themselves (Aidley and Stanfield (1996)) and appear on channel records as rapid flickering between openings and closings. The frequency of the flicker is too high to be detected by the recording equipment and the currents are noisy and reduced in amplitude. Thirdly, like a number of other types of ion channel, nAChR channels sometimes display subconductance states in which channel conductance is lower than normal (e.g. Colquhoun and Sakmann (1985)). This behaviour has yet to be explained but may indicate 'subunit by subunit' changes

in channel conformation, consistent with one of the assumptions underlying our model.

With all these complexities in nicotinic acetylcholine channel kinetics there has been little recent progress in kinetic analysis of nAChR behaviour. Further progress may result from more experiments in which a very brief pulse of agonist is applied to a patch resulting in a jump in agonist concentration from a low concentration at which the channel is almost always closed to a higher concentration at which it is more frequently open. Desensitization can be incorporated into ion channel models by inclusion of a third class of states in the semi-Markov model of Ball *et al.* (1991, 1993a) (described in section 2.1 of this thesis). Thus the state space would consist of open states, closed states and desensitized (or absorbing) states which, once entered by a channel, are never exited. Although the semi-Markov process does not possess open and closed entry process equilibrium distributions, progress can still be made in determining certain model properties. For example, using an initial vector relating to states occupied at a very low (pre-jump) agonist concentration, and transition matrices whose entries relate to a higher (post-jump) agonist concentration, we have determined formulae for properties such as the expected number of openings following an agonist concentration jump before desensitization, the expected length of time between an agonist concentration jump and desensitization, etc.

3.5.3 Relationship to Macroscopic Allosteric Models

The most well-known models (Monod *et al.* (1965), Koshland *et al.* (1966), Eigen (1968)) associated with allosteric proteins were originally developed to explain observations in haemoglobin and in the kinetic behaviour of various enzymes and there has been much discussion (e.g. Newsholme and Start (1973)) regarding the relative validity of these models. As early as 1967 it was suggested that the ideas behind these types of models could be applied to ion channels (Karlin (1967)), although, of course, there was very little information regarding detailed ion channel structure until more recently, and hence earlier applications of these ideas were unable to incorporate the structural features that are incorporated in the models described in this chapter.

In 1965, Monod, Wyman and Changeux (MWC) published a classic paper (Monod *et al.* (1965)) in which they proposed a molecular model to explain cooperative behaviour in allosteric proteins. Their model assumes that an allosteric protein comprises a number of separate subunits which each occupy an equivalent position within the protein and that each subunit possesses one ligand binding site. All binding sites are assumed to be equivalent to each other and the binding of ligand to any individual subunit in a particular protein state has no influence on the binding of ligand to the other subunits in the protein in that state. It is assumed that two conformations of the protein exist in the absence of ligand

and that these two conformations differ in their ability to bind ligand. Positive cooperativity of ligand binding is explained by the transition from the conformation in which subunits have less affinity for ligand to that in which they have a greater affinity for ligand. In terms of pentameric acetylcholine channels, the state space of the MWC model comprises states in which either all subunits are in open conformations or all subunits are in closed conformations. Any number of the subunits may have agonist bound in either case, although the channel will have a greater affinity for agonist when all subunits are in open conformations.

The model of Koshland *et al.* (1966) provides a different explanation for the cooperative behaviour in allosteric proteins. In this model any subunit exists in either conformation A say, with no ligand bound, or in conformation B say, with ligand bound. Hence this model requires the existence of only one state of the protein in the absence of ligand and this state is the one in which all subunits are in conformation A. It is further assumed that a conformational change induced by ligand binding to one subunit can modify the conformation of another subunit without ligand bound. The binding of ligand by one subunit therefore produces a conformational change that is transferred to another subunit so that the latter is able to bind ligands more easily. The binding of the second ligand molecule stabilizes this conformation in the second subunit, and influences the conformation of a third subunit. The binding of ligand becomes progressively

easier in this sequential process. Thus, in terms of acetylcholine channels, the state space of the Koshland model comprises all states in which the channel has a combination of open subunits with agonist molecules bound and closed subunits with no agonist molecules bound, and there is positive cooperativity of agonist molecule binding as a result of a subunit with agonist bound interacting with the remaining subunits so that their agonist binding rates are increased.

Eigen (1968) presents a more general model which encompasses both the MWC model and the Koshland model. In this model any protein subunit may exist in either of two conformations and when in either conformation may exist with or without ligand bound. However, this model has a large number of independent parameters and so is rarely used in practice.

The nAChR models formulated in this chapter have state spaces akin to that of the Eigen model, i.e. subunits may be open or closed and may, in either of these conformations have no agonist molecule bound, or, provided that the subunit has an agonist binding site, may have one agonist molecule bound. Thus our nAChR models are without the aforementioned restrictions of the MWC model or the Koshland model. The neighbouring subunit interactions incorporated into our models use ideas adapted from the treatment of allosteric globular proteins by Koshland *et al.* (1966). Whilst there has been a deficit of recent studies comparing the consistency of these particular types of large state space models

for the nicotinic acetylcholine channel, Rothberg and Magleby (1999) examine various kinetic schemes for the Ca^{2+}-activated potassium ion channel drawn from the MWC model and the Eigen model. They conclude that MWC-type models are too simple to account for certain details of BK channel gating. They also find that several models based on the general model of Eigen are not consistent with experimental data at high levels of Ca^{2+} concentration, but that an extended 50-state Eigen model has sufficiently many states and transition pathways to describe many features of the data. Thus the basis of our modelling and the large state spaces of our models for nicotinic acetylcholine channels are in line with the conclusions of Rothberg and Magleby (1999) regarding BK channel models.

3.6 Formulation of a Model for Calcium-activated Potassium Ion Channels

3.6.1 Model Description

Many of the features of our model for the nicotinic acetylcholine receptor can be adapted and used to formulate models for other types of ion channels which reflect the underlying structural properties of those channels. In this section, we describe the formulation of such a model for calcium-activated potassium ion channels. In common with the models already discussed in this chapter, the BK

channel model presented below satisfies the three criteria listed at the beginning of section 3.2.1. Statistical properties of the BK channel based on this model can be determined using a Markov framework analogous to that used to analyse the nAChR channel model. However, detailed mathematical and numerical results for the BK channel are not given in this thesis as they can be obtained in a manner identical to that for the results obtained in sections 3.3 and 3.4 for the nAChR channel. Instead we focus on how the model is formulated and adapted to best describe experimental findings and how it improves on previous studies based on smaller state-space models of calcium-activated potassium ion channel gating.

3.6.1.1 States, Subunits and Substates

The BK channel model presented here assumes that a channel consists of four α-subunits arranged in a square, reflecting the known structure of potassium ion channels. Many authors (e.g. Barrett *et al.* (1982), Magleby and Pallotta (1983a, 1983b), McManus and Magleby (1991), Golowasch *et al.* (1986) and Oberhauser *et al.* (1988)) have conducted experiments to calculate Hill coefficients for the BK Channel. Although there is some variation in the values of the Hill coefficients calculated (caused for example by obtaining data at different pH values), the mean Hill coefficients were between three and four, suggesting that the channel has a minimum of four calcium binding sites. Hence in our model we assume that each of the four subunits has a calcium binding site to which at

most one calcium ion may be bound.

Further, experimental findings (e.g. Methfessel and Boheim (1982), Magleby and Pallotta (1983a), Moczydlowski and Latorre (1983)) have noticed Ca^{2+}-dependent shifts in the time constants of both the open and closed exponential components of the probability density functions, indicating that both open and closed channel states should be capable of binding and unbinding Ca^{2+}, a property which is reflected in our model. As in the model of the acetylcholine channel, we refer to the state occupied by a channel subunit at any given time as its *substate*. Each subunit may exist in either a closed substate, C, or an open substate, O. In addition, we use the notation that if a subunit with a calcium ion bound to it is closed, it occupies substate C_{Ca}, and if it is open, it occupies substate O_{Ca}.

Since each of the 4 subunits can occupy any one of the 4 substates C, O, C_{Ca} and O_{Ca}, there are $4^4 = 256$ possible combinations of substates occupied by the 4 channel subunits, each combination corresponding to a different channel state. Further, we assume that the channel is in an open state if and only if all 4 subunits are in open substates, regardless of the number of calcium ions bound to the channel. Thus the state space comprises 16 open states and 240 closed states.

3.6.1.2 Transitions

There are 4 types of transitions which a subunit can undergo:

(i) The opening of a subunit in a closed substate,

(ii) The closing of a subunit in an open substate,

(iii) The loss of a calcium ion from a subunit in substate C_{Ca} or substate O_{Ca},

(iv) The binding of a calcium ion to a subunit in substate C or substate O.

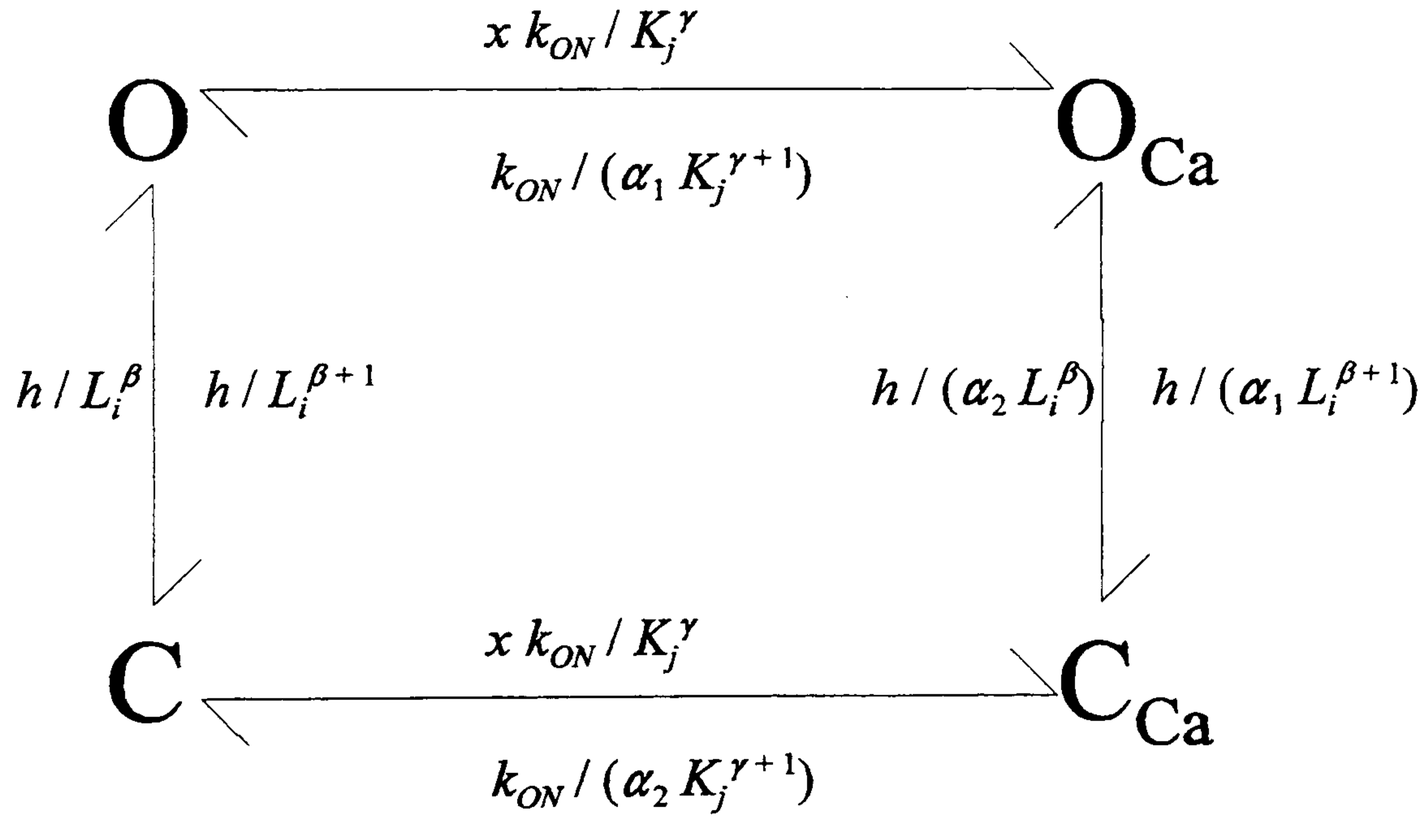

Figure 3.22. Transition rates for a BK channel subunit

Whenever any channel subunit undergoes a transition from one substate to another, the channel enters a different state. The rate for such a channel transition

is given by the corresponding subunit transition rate, which may or may not be dependent upon the substates occupied by neighbouring subunits, and is given by Figure 3.22, whose parameters are defined and explained in section 3.6.1.4.

3.6.1.3 Subunit Interactions between Nearest Neighbours

In the model for the acetylcholine receptor, described in section 3.2, subunits' opening rates, closing rates, or both, are modelled to vary according to whether zero, one or two of the subunits which lie adjacent to that subunit in the subunit ring are open. This type of subunit interaction is incorporated into the BK channel model via the equilibrium constant L_i in exactly the same manner as for the nAChR model. As for the nAChR model, the assumption that only neighbouring subunits interact is based on the fact that a change in subunit conformation corresponds to a change in subunit shape which is likely to affect only touching subunits.

Additionally, the Ca^{2+} binding and unbinding rates for a subunit are modelled to take different values depending upon the number of adjacent subunits which already have Ca^{2+} bound. The equilibrium constant K_i is incorporated into the Ca^{2+} binding and unbinding rates to allow this second form of nearest neighbour subunit interaction and its use is described in more detail in the next subsection.

3.6.1.4 Definition and Explanation of Parameters

If a subunit is closed then association and disassociation of a calcium ion occur at rates xk_{ON}/K_j^{γ} and $k_{ON}/(\alpha_2 K_j^{\gamma+1})$, respectively, where x is the Ca^{2+} concentration, k_{ON} is the association rate, K_j is an affinity constant (see below), the value of γ determines the nature of the dependence of Ca^{2+} binding and unbinding on the number of neighbouring subunits with Ca^{2+} bound (see below) and the parameter $\alpha_2 < 1$ reflects the decreased affinity of a closed subunit for Ca^{2+}. If a subunit is open then association and disassociation of an agonist molecule occur at rates xk_{ON}/K_j^{γ} and $k_{ON}/(\alpha_1 K_j^{\gamma+1})$, respectively, where the parameter $\alpha_1 > 1$ reflects the increased affinity of an open subunit for Ca^{2+}. The parameters h, L_i, K_T, K_{OO}, K_{OC} and K_{CC} and β are exactly as defined in section 3.2.2 for the nAChR model.

The equilibrium constant for a given subunit to bind a calcium ion (ie. to undergo a transition from state O to state O_{Ca}, or from state C to state C_{Ca}) is the ratio of the transition rates for that transition and the reverse transition and is thus K_j. McManus and Magleby (1991) conclude from experimental results that independent Ca^{2+} binding sites are inconsistent with the data and that there must be some form of cooperative interaction among binding sites. It is not yet known whether this cooperative interaction is based on four equivalent Ca^{2+} binding sites or is a feature of sequential binding occurring when the binding at a site induces a conformational change which either exposes the next site or increases the

binding constant of the next site from a negligible value. We will model this cooperative interaction by the introduction of nearest neighbour subunit dependency of binding and unbinding of Ca^{2+} which incorporates a variation in the value of K_j according to the substates occupied by the two subunits adjacent to the subunit in question. So let $j = 0$, 1 or 2, according to whether the subunit in question has 0, 1 or 2 neighbouring subunits with Ca^{2+} bound and set the values of K_j accordingly. McManus and Magleby (1991) conducted experiments using large-conductance calcium-activated potassium ion channels from rat skeletal muscle and found that the effective equilibrium constant for Ca^{2+} binding increased approximately 6-fold for the binding of the second calcium ion and then increased another 60-fold for the binding of the third calcium ion, with the fourth binding being many times faster than at least the first two. In order for the model to display the property that calcium ions are more likely to be bound to subunits whose neighbours already have calcium ions bound, the values of K_j must satisfy $K_2 > K_1 > K_0$. It should be noted that our BK channel model can be shown to be time reversible using a similar argument to that used in section 3.3.1.1 for the $\alpha_2\beta_3$ model and that Kolmogorov's criterion for reversibility imposes the condition $K_0 K_2 = K_1^2$. It should also be noted that, if the parameters satisfy $K_0 = K_1 = K_2$, then each of the 4 subunits binds and unbinds Ca^{2+} independently of its neighbouring subunits.

The value of γ determines whether and how the Ca^{2+} binding rate ($\gamma = -1$) for a

subunit, the Ca^{2+} unbinding rate ($\gamma = 0$) for a subunit, or both of these rates ($\gamma \neq 0$ or -1) are dependent upon the substates occupied by neighbouring subunits. McManus and Magleby (1991) have found experimentally that both Ca^{2+} binding and unbinding rates vary according to the number of Ca^{2+} already bound, suggesting that $\gamma \neq 0$ or -1. It is worth noting that the ratio of Ca^{2+} binding rate to Ca^{2+} unbinding rate for a given subunit remains constant as γ varies.

3.6.2 Biophysical Discussion of Model Properties

In this section we discuss properties of the BK channel model formulated above and show that they are consistent with the results of experimental studies of large conductance BK channels in the ion channel literature.

3.6.2.1 Reversible Markov Process

Studies by McManus and Magleby (1991) of skeletal muscle potassium ion channels suggest that the gating should be consistent with a Markov process in which the transition rates from any given state depend only on the state that the channel is in and not on the history of the preceding transitions. Support consistent with Markov gating comes from the observation that the time constants of the components in the open-time and closed-time probability distributions are

independent of previous channel activity (McManus and Magleby (1989)). Further, the gating should be consistent with microscopic reversibility, as indicated by the observation that the relationship between the durations of adjacent open and closed intervals is independent of the time direction of analysis (McManus and Magleby (1989)). As discussed in section 3.6.1.4, our BK channel model is time reversible.

3.6.2.2 Numbers of Channel Open and Closed States

In the $\alpha_2\beta_3$ nAChR model, states which can be pictorially represented as reflections of each other (see section 3.3.1.4 and Figure 3.6) are aggregated to form a single state in a reduced state space. In the BK channel model, some further reduction of the state space is possible since all four subunits are α-subunits and are modelled as having identical behaviour to each other, therefore yielding further symmetry to exploit. In this model, states which can be pictorially represented as rotations of each other are also aggregated together to give a single state in the reduced state space. Thus it can be shown that the reduced state space for the BK channel model comprises 55 states, compared with the unreduced state space which comprises 256 states. Assuming that all four subunits must be in open substates in order for the channel to be open, these 55 states comprise 6 open states and 49 closed states.

The numbers of exponential components fitted by McManus and Magleby (1988) to the dwell-time distributions that they obtained experimentally indicate that the BK channel should have at least three or four open states and at least six to eight closed states. Note that the observed number of exponential components in the dwell-time distributions is entirely consistent with a large state space model in which many of the states have similar kinetic properties and are thus not detected. McManus and Magleby (1991) consider a number of small state space models and comment that it is possible that the inability of these simpler schemes to give theoretically perfect descriptions of the data arises because the gating has some of the features of models with larger state spaces. In particular, Rothberg and Magleby (1999) examine a number of possible small state space models and find that they cannot accurately describe the dependency between lengths of adjacent sojourns at high Ca^{2+} concentrations. Rothberg and Magleby (1999) also investigate a possible 50-state model for the BK channel and find that the additional kinetic complexity gives a model capable of capturing a greater range of experimental channel behaviour. Thus the numbers of open and closed states in our model of the BK channel are consistent with the conclusions of McManus and Magleby (1988), McManus and Magleby (1991) and Rothberg and Magleby (1999).

3.6.2.3 Durations of Channel Openings and Closings

When Ca^{2+} is bound to a subunit, its closing rate is $h / (\alpha_1 L_i^{\beta+1})$, whereas its closing rate is $h / L_i^{\beta+1}$ when no Ca^{2+} is bound. Since in our model we set $\alpha_1 > 1$, the closing rate of a subunit with Ca^{2+} bound is less than its closing rate with no Ca^{2+} bound, and hence, on average, a subunit remains open for longer when it has a calcium ion bound. Similarly, given a value of $\alpha_2 < 1$, consideration of the opening rates enables us to verify that, on average, subunits remain in a closed state for less time when they have Ca^{2+} bound than when they have no Ca^{2+} bound. Magleby and Pallotta (1983a) reported that openings in the longer duration open states required a BK channel to have more calcium ions bound than openings in the briefer duration open states. Conversely, they found that closings in the longer duration closed states required a BK channel to have less calcium ions bound than closings in the briefer duration closed states. Our assumptions regarding the values of α_1 and α_2, and their resulting impact on the subunit, and hence channel, opening and closing rates are consistent with these results. It should also be noted that increasing the calcium ion concentration, x, in our model drives each subunit, and hence the channel, from the longer duration closed states to the briefer duration closed states and from the briefer duration open states to the longer duration open states, which is again consistent with the experimental findings of Magleby and Pallotta (1983a).

In a realistic model, parameters take values such that Ca^{2+} binding and unbinding rates are relatively small compared to subunit opening and closing rates. This means that a closing (opening) of a subunit with Ca^{2+} bound will usually be adjacent to an opening (closing) in which that subunit has a Ca^{2+} bound. A similar phenomenon occurs when no calcium ion is bound to the subunit. Since a subunit with Ca^{2+} bound has, on average, longer openings and shorter closings than when no Ca^{2+} is bound, one feature of this model will be an inverse relationship between the durations of adjacent openings and closings of each subunit, and hence of a channel. This inverse relationship is a feature supported by the experimental findings of McManus *et al.* (1985) who, for a large conductance calcium-activated potassium ion channel in skeletal muscle, plot the mean duration of all open intervals adjacent to closed intervals within a specified range of durations against the mean duration of the specified closed intervals (see McManus *et al.* (1985) Figure 1). As the specified closed intervals become longer, the mean durations of the adjacent open intervals become shorter. McManus *et al.* (1985) also found a similar inverse relationship between the durations of adjacent open and closed intervals when the mean closed intervals adjacent to specified ranges of open intervals were determined (see McManus *et al.* (1985) Figure 2). Note that these experimental findings exclude models for the BK channel in which there is only one transition pathway between the open and closed states since such models require that the mean durations of adjacent open and closed intervals be independent.

3.6.3 Model Variations suggested by Experimental Studies

Since the model developed above is based so closely upon channel structure and has parameters which can be interpreted directly in terms of channel biophysiological properties, it is easy to adapt it to reflect different assumptions which may be suggested by experimental data. This feature makes our model an improvement on smaller state Markov models previously considered in the literature whose parameters had an unclear relationship to the underlying structural properties of the ion channels involved and hence could not be so easily adapted. Further, an increase in the complexity of channel properties to be described by our model does not necessarily result in a commensurate proliferation of model parameters, as demonstrated in the two examples below.

3.6.3.1 Channels to which more than four calcium ions may be bound

In two of thirteen experiments conducted by McManus and Magleby (1991), Hill coefficients greater than four (4.1 and 5.0) were observed, suggesting that a minimum of five Ca^{2+} binding sites may be required in some cases. In particular, an increase in the Hill coefficient has been observed when the pH level at which the data have been obtained has been decreased (e.g. Cook *et al.* (1984), Christensen and Zeuthen (1987), Blatz (1989), Kume *et al.* (1990) and Laurido *et al.* (1990)).

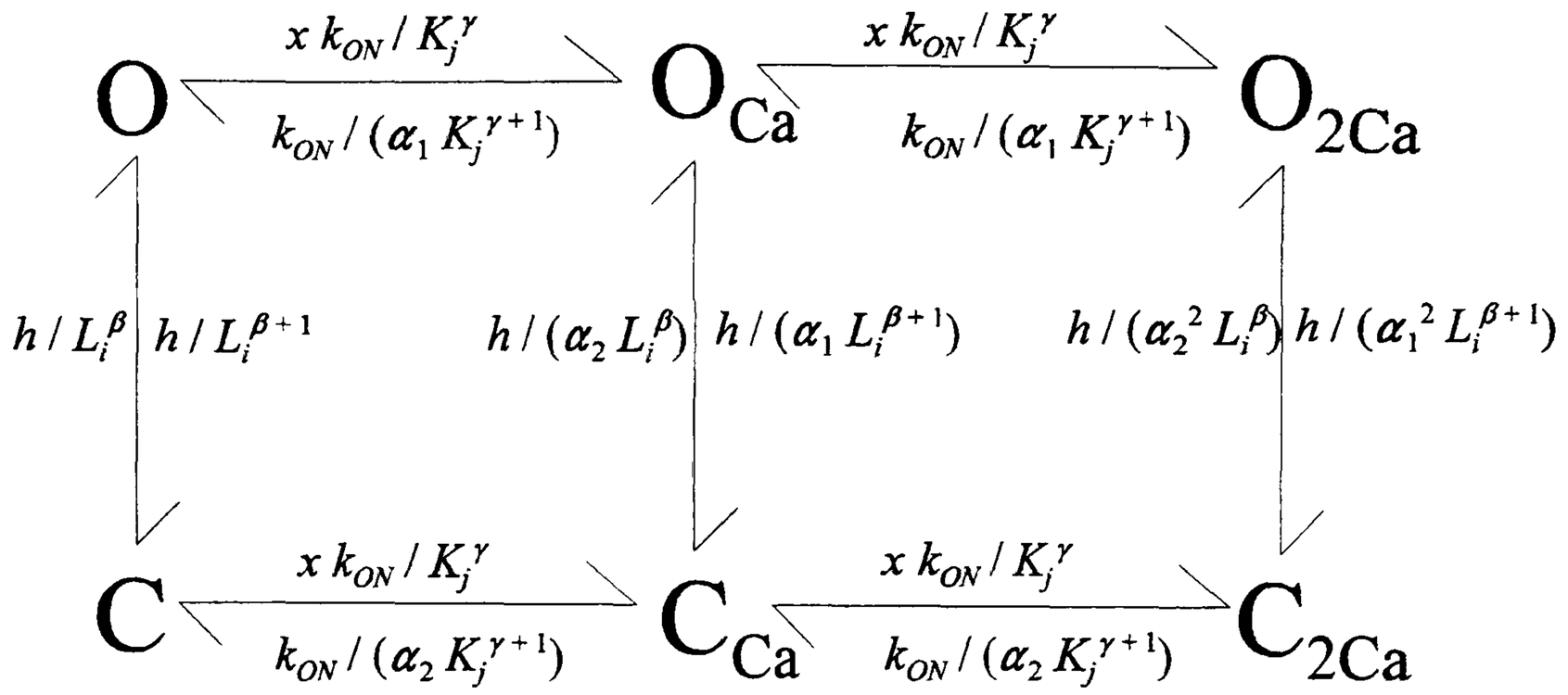

Figure 3.23. A possible scheme of transition rates for a BK channel subunit which can bind two calcium ions.

One way in which possible binding of an increased number of Ca^{2+} ions to a channel may be incorporated into our model is by increasing the number of Ca^{2+} which may be bound to one or more subunits, or, equivalently, increasing the number of substates which one or more subunits may occupy. Although this will result in an increased state space size, it is not necessary to increase the number of parameters if, for example, we proceed as follows. Let O_{2Ca} and C_{2Ca} denote open and closed substates, respectively, in which a subunit has two Ca^{2+} bound. Then the transition rates for that subunit could be defined by Figure 3.23, where all parameters retain their biophysical interpretation as given above. Note that the opening and closing rates for a subunit with two Ca^{2+} bound contain the factors $1/\alpha_2^2$ and $1/\alpha_1^2$, respectively, since experimental data suggest that a BK channel

has a faster opening rate when more calcium ions are bound (McManus and Magleby (1991)). The incorporation of these factors also ensures that the model retains its microscopic reversibility property. Using this new transition rate scheme, we can calculate equilibrium distributions and statistical properties as for the original model.

3.6.3.2 Channels which open only when calcium ions are bound

Although Hill coefficients calculated experimentally can give an indication of the minimum number of calcium ions which are bound to the channel when it is fully activated, it is not known for certain whether a BK channel requires a minimum number of calcium ions to be bound in order for that channel to be open. McManus and Magleby (1991, Scheme X) give an 8-state model with 3 open and 5 closed states such that the channel can open only with 2, 3 or 4 Ca^{2+} bound and comment that since their data suggest that the duration of the open state increases with the number of Ca^{2+} bound, it may well be the case that the channel can also open with zero or one Ca^{2+} bound but that the durations of the openings in these cases will be so brief that they are not detected experimentally. Our model can easily be adapted to cater for a requirement in which a minimum number of Ca^{2+} are required for the channel to open by relaxing the assumption that a channel with 4 open subunits is always open. For example, for a model in which a channel requires two Ca^{2+} to be bound for it to open, the reduced state space will consist of 4 open and 51 closed states instead of 6 and 49 respectively, the two

extra closed states being those in which all 4 subunits are in open substates but the channel has zero or one Ca^{2+} bound. This reclassification of some open states as closed states affects neither the total number of states nor the transition rates between those states and it is therefore very simple to recalculate channel properties under this model variation.

3.7 Discussion of Large State Space Models based on Molecular Structure

All the models examined in this chapter are based on simple postulates and yet have resulted in a relatively high level of complexity, particularly regarding the number of states required to accurately describe the channels being modelled. The requirement for this level of kinetic complexity is supported by Rothberg and Magleby (1999) who reject a variety of small state space BK channel models which cannot replicate experimental results in favour of a model with 50 states. However, Rothberg and Magleby (1999) point out that even this 50 state model is a reduced model compared with the likely actual gating mechanism since states with similar properties (which they term *isoforms*) are not all included in their model. Inclusion of these states would increase the state space size to 110. Further, Rothberg and Magleby (1998, 1999) suggest that BK channels may have additional brief lifetime closed states which, when included in their model, improve the description of the Ca^{2+} dependence of the kinetic structure and give

rise to the majority of the brief closings (flickers) in the gating. The inclusion of these states increases the state space by a further 50%. Recent improvements in technology have allowed analysis of increasingly large data samples (e.g. 500,000 openings) and Silberberg *et al.* (1996) have found that BK channels exhibit a further feature, termed *wanderlust kinetics*, in which slow changes in kinetics occur over a time course of tens of seconds to minutes. This feature could be modelled by allowing several kinetic modes with different levels of open probability, introducing more states, more parameters, and thus yet more complexity into the modelling process.

Although BK channel models have been examined in some detail, models of some other types of ion channels have not been investigated in such depth. However, the small state space models of various types of ion channels which have been studied tend not to have the ability to fully describe channel data. Whilst larger state space models may be more successful in describing certain features of experimental data, it seems that as further experimental research has resulted in an increase in known channel kinetic properties, the models accounting for such properties have become increasingly complex. The models formulated in this chapter attempt to describe known features of channel kinetics using a large state space whilst remaining simple in terms of their number of free parameters and the postulates upon which they are based. As is the case with any model, as further information becomes available, these models will require refinement.

4 Inference for a Two-state Ion Channel Model

4.1 Introduction

4.1.1 Model

As discussed in section 2.1, the gating behaviour of a single ion channel is usually modelled by a continuous-time Markov chain with a finite state space. The complete process is unobservable; rather the state space is partitioned into two classes, termed 'open' and 'closed' corresponding to the channel being respectively open or closed, and it is possible to observe only which class the process is in. In this chapter, a two-state Markov model with one open state and one closed state is considered. Open and closed sojourns are assumed to be independent negative exponential random variables with means μ_O and μ_C. Let $T_1, S_1, T_2, S_2, \ldots$ be the durations of successive open and closed sojourns of the channel. It is assumed that short sojourns in either state fail to be detected (see section 2.2). In particular, it is assumed that there are known constants τ_O and τ_C such that any open (closed) sojourn of duration less than τ_O (τ_C) is undetected.

Under this model, an observed open sojourn, $\tilde{T}$ say, is defined as commencing with an open sojourn of duration at least τ_O, followed by a random number, N

say, of arbitrary open sojourns separated by undetected closed sojourns, and terminated as soon as there is a detected closed sojourn. Hence

$$\tilde{T} = T' + \sum_{i=1}^{N} (T_{i+1} + S_i^*), \tag{4.1}$$

where T' has the same distribution as T_1 conditional on T_1 being greater than τ_O, S_i^* $(i = 1, 2,...)$ has the same distribution as S_i conditional on S_i being at most τ_C and the sum is omitted if $N = 0$.

In practice it is more convenient to work with adjusted observed open and closed sojourns, defined respectively by $\tilde{U} = \tilde{T} - \tau_O$ and $\tilde{V} = \tilde{S} - \tau_C$.

4.1.2 Distribution of Observed Open and Closed Sojourns

4.1.2.1 Moment-generating Functions, Means and Variances

For $i = 1, 2,...,$ let $f_{T_i}(t)$, $f_{S_i}(t)$, $f_{S_i^*}(t)$ and $f_{T'}(t)$ be the probability density functions of T_i, S_i, S_i^* and T', respectively, and let $F_{S_1}(t)$ and $F_{T_1}(t)$ be the distribution functions of S_1 and T_1, respectively (Milne *et al.* (1988)). Then since T_i $(i = 1, 2,...)$ are exponentially distributed with mean μ_O,

$$f_{T_i}(t) = \begin{cases} 0 & t \leq 0 \\ \mu_O^{-1} \exp(-t/\mu_O) & t > 0, \end{cases}$$

with a similar expression holding for $f_{S_i}(t)$. For $i = 1, 2,...$, the sojourn length T' has the same distribution as T_i conditional on T_i being greater than τ_O. Therefore

$$f_{T'}(t) = f_{T_1}(t)\ (1 - F_{T_1}(\tau_O))^{-1}$$

for $t > \tau_O$ and so

$$f_{T'}(t) = \begin{cases} 0 & t \le \tau_O \\ \mu_O^{-1} \exp(-(t - \tau_O)/\mu_O) & t > \tau_O. \end{cases}$$

For $i = 1, 2,...$, the sojourn length S_i^* has the same distribution as S_i conditional on S_i being no more than τ_C. Therefore $f_{S_i^*}(t) = f_{S_i}(t)\ (F_{S_1}(\tau_C))^{-1}$ for $0 < t \le \tau_C$ and hence

$$f_{S_i^*}(t) = \begin{cases} 0 & t \le 0 \text{ and } t > \tau_C \\ [\mu_C(1 - \exp(-\tau_C/\mu_C))]^{-1} \exp(-t/\mu_c) & 0 < t \le \tau_C. \end{cases}$$

The number N of undetected closed sojourns in an observed open sojourn $\tilde{T}$ has a geometric distribution with parameter $1 - F_{S_1}(\tau_C) = \exp(-\tau_C/\mu_C)$. Thus

$$\mathbf{P}(N = k) = \exp(-\tau_C/\mu_C)(1 - \exp(-\tau_C/\mu_C))^k \qquad (k = 0, 1,...)$$

and, for $0 \le s \le 1$, the probability generating function, $G_N(s)$, of N is given by

$$G_N(s) = \sum_{k=0}^{\infty} s^k \exp(-\tau_C/\mu_C)(1 - \exp(-\tau_C/\mu_C))^k$$

$$= \exp(-\tau_C/\mu_C)(1 - (1 - \exp(-\tau_C/\mu_C))s)^{-1}.$$

Recalling the standard theory that, if $S = X_1 + X_2 + \ldots + X_N$, where $X_1, X_2, \ldots, X_N$ are independent identically distributed random variables with moment-generating function $\Phi_X(\theta)$, and N has probability generating function $H_N(s)$, then the moment-generating function of S is given by $H_N(\Phi_X(\theta))$, it follows, by independence of successive sojourns, that the moment-generating function, $\Phi_{\tilde{U}}(\theta) = \mathbf{E}[\exp(-\tilde{U}\theta)]$ say, of the adjusted observed open sojourn length $\tilde{U}$ is given by

$$\Phi_{\tilde{U}}(\theta) = \mathbf{E}[\exp(-T'\theta)]\,\mathbf{E}[\exp(-\theta\sum_{i=1}^{N}(T_{i+1} + S_i^*))]\,\mathbf{E}[\exp(\tau_O\theta)]$$

$$= \Phi_{T'}(\theta)\; G_N[\Phi_{T_1}(\theta)\;\Phi_{S_1^*}(\theta)]\;\exp(\tau_O\theta) \qquad (\theta \geq 0),$$

where, for $\theta \geq 0$, the moment-generating functions $\Phi_{T'}(\theta)$, $\Phi_{T_1}(\theta)$ and $\Phi_{S_1^*}(\theta)$ of T', T_1 and S_1^* respectively, are given by

$$\Phi_{T'}(\theta) = \int_{\tau_O}^{\infty}\exp(-t\theta)\,\mu_O^{-1}\exp(-(t-\tau_O)/\mu_O)\,dt$$

$$= \exp(-\tau_O\theta)(1 + \mu_O\theta)^{-1} \qquad (\theta \geq 0),$$

$$\Phi_{T_1}(\theta) = \int_{0}^{\infty}\exp(-t\theta)\,\mu_O^{-1}\exp(-t/\mu_O)\,dt$$

$$= (1 + \mu_O\theta)^{-1} \qquad (\theta \geq 0),$$

and

$$\begin{aligned}\Phi_{S_{1^*}}(\theta) &= \int_0^{\tau_C} \exp(-t\theta)\,\mu_C^{-1}\,(1 - \exp(-\tau_C/\mu_C))^{-1}\exp(-t/\mu_C)\,dt \\ &= (1 - \exp(-\tau_C/\mu_C))^{-1}\,(1 + \mu_C\theta)^{-1} \\ &\qquad \times (1 - \exp(-(\theta + \mu_C^{-1})\,\tau_C)) \qquad (\theta \geq 0).\end{aligned}$$

Hence, for $\theta \geq 0$,

$$\Phi_{\tilde{U}}(\theta) = \frac{(1 + \mu_C\theta)}{[\mu_O\mu_C\theta^2 + (\mu_O + \mu_C)\theta]\exp(\tau_C/\mu_C) + \exp(-\theta\tau_C)}. \qquad (4.2)$$

Since the mean and variance, ν_O and $\tilde{\sigma}_O^2$ say, of $\tilde{U}$ are given by $-\Phi'_{\tilde{U}}(0)$ and $\Phi''_{\tilde{U}}(0) - (\Phi'_{\tilde{U}}(0))^2$ respectively, where $'$ denotes differentiation, it follows that

$$\nu_O = (\mu_O + \mu_C)\exp(\tau_C/\mu_C) - \mu_C - \tau_C \qquad (4.3)$$

and

$$\begin{aligned}\tilde{\sigma}_O^2 &= [(\mu_O + \mu_C)\exp(\tau_C/\mu_C) - \tau_C]^2 \\ &\qquad - 2\,\mu_O\mu_C\exp(\tau_C/\mu_C) - \mu_C^2 - \tau_C^2.\end{aligned} \qquad (4.4)$$

Similarly, the mean and variance, ν_C and $\tilde{\sigma}_C^2$, of adjusted observed closed sojourns are given by

$$\nu_C = (\mu_O + \mu_C)\exp(\tau_O/\mu_O) - \mu_O - \tau_O \qquad (4.5)$$

and

$$\tilde{\sigma}_C^2 = [(\mu_O + \mu_C)\exp(\tau_O/\mu_O) - \tau_O]^2 - 2\mu_O\mu_C\exp(\tau_O/\mu_O) - \mu_O^2 - \tau_O^2. \quad (4.6)$$

4.1.2.2 Approximations

Let $\tilde{T}_1$, $\tilde{S}_1$, $\tilde{T}_2$, $\tilde{S}_2$,... be the durations of successive observed open and closed sojourns and let $\tilde{U}_1$, $\tilde{V}_1$, $\tilde{U}_2$, $\tilde{V}_2$,... be the corresponding adjusted observed sojourn lengths. Note that $\tilde{U}_1$, $\tilde{V}_1$, $\tilde{U}_2$, $\tilde{V}_2$,... inherit mutual independence from $\tilde{T}_1$, $\tilde{S}_1$, $\tilde{T}_2$, $\tilde{S}_2$,... Suppose we wish to make inferences concerning (μ_O, μ_C) from a random sample $\tilde{u}_1$, $\tilde{v}_1$, $\tilde{u}_2$, $\tilde{v}_2$,...$\tilde{u}_n$, $\tilde{v}_n$ of n successive pairs of adjusted observed open and closed sojourns. Exact likelihood-based inference is difficult since $\Phi_{\tilde{U}}(\theta)$ and $\Phi_{\tilde{V}}(\theta)$ cannot easily be inverted analytically in the presence of time interval omission (but see Hawkes *et al.* (1990) and Jalali and Hawkes (1992a)) and thus there are no simple expressions for the probability density functions, $f_{\tilde{U}}(t)$ and $f_{\tilde{V}}(t)$ say, of adjusted observed open and closed sojourns. Yeo *et al.* (1988) considered maximum likelihood estimation of (μ_O, μ_C) based on various approximations to $f_{\tilde{U}}(t)$ and $f_{\tilde{V}}(t)$, three of which are discussed below.

4.1.2.2.1 Approximation derived by ignoring Undetected Sojourns

Roux and Sauvé (1985) considered an approximation to $\tilde{T}$ in which the contribution of the undetected closed sojourns, S_i^* ($i = 1, 2,..., N$), is ignored in equation (4.1). Although this is not an unreasonable approach if τ_C is very small compared to μ_O, estimation based on this approximation will clearly be biased. Let $\Phi_{\tilde{U}}^{(1)}(\theta)$ be the moment-generating function of an adjusted observed open sojourn under this approximation. Then adapting the derivation of $\Phi_{\tilde{U}}(\theta)$ to ignore undetected closed sojourns, it immediately follows that

$$\begin{aligned} \Phi_{\tilde{U}}^{(1)}(\theta) &= \Phi_{T'}(\theta)\, G_N[\Phi_{T_1}(\theta)] \exp(\tau_O \theta) \\ &= (1 + \mu_O \exp(\tau_C / \mu_C)\, \theta)^{-1} \qquad (\theta \geq 0), \end{aligned}$$

which is readily recognised as the moment-generating function of a negative exponential distribution with density function $f_{\tilde{U}}^{(1)}(t)$ given by

$$f_{\tilde{U}}^{(1)}(t) = \begin{cases} 0 & t \leq 0 \\ \nu_1^{-1} \exp(-t/\nu_1) & t > 0, \end{cases} \tag{4.7}$$

where

$$\nu_1 = \mu_O \exp(\tau_C / \mu_C). \tag{4.8}$$

Similarly the density function $f_{\tilde{V}}^{(1)}(t)$ of adjusted observed closed sojourns is given by

$$f_{\tilde{V}}^{(1)}(t) = \begin{cases} 0 & t \leq 0 \\ \nu_2^{-1} \exp(-t/\nu_2) & t > 0, \end{cases}$$

where

$$\nu_2 = \mu_C \exp(\tau_O/\mu_O). \tag{4.9}$$

4.1.2.2.2 Approximation using Exponential Distributions with True Means

Yeo *et al.* (1988) also study a natural approximation which improves on equation (4.7) by replacing ν_1 with ν_O, the true mean duration of an adjusted observed open sojourn, given in equation (4.3). Let $f_{\tilde{U}}^{(2)}(t)$ denote the probability density function for adjusted open sojourns under this approximation.

4.1.2.2.3 Bi-exponential Approximation

Another approximation to $f_{\tilde{U}}(t)$ is derived by expanding $\exp(-\theta\tau_C)$ in $\Phi_{\tilde{U}}(\theta)$ in equation (4.2) to the term in θ^2 and inverting the resulting moment-generating function using partial fractions. Again the mean duration of an adjusted observed open sojourn coincides with its true mean and this approximation is usually good since τ_C is small.

Yeo *et al.* (1988) state that, under this approximation, the density function $f_{\tilde{U}}^{(3)}(t)$ say, for adjusted observed open sojourns is given by

$$f_{\tilde{U}}^{(3)}(t) = \begin{cases} 0 & t \leq 0 \\ (\alpha_1/\alpha_2)\ \exp(-t/\alpha_2) + (\alpha_3/\alpha_4)\ \exp(-t/\alpha_4) & t > 0, \end{cases}$$

where

$$\alpha_1 = (\alpha_2 - \mu_C)\,(\alpha_2 - \alpha_4)^{-1},$$

$$\alpha_3 = 1 - \alpha_1,$$

and

$$\alpha_2,\ \alpha_4 = \tfrac{1}{2}\,(p \pm (p^2 - 4q)^{\frac{1}{2}}) \qquad (\alpha_2 > \alpha_4),$$

where

$$p = (\mu_O + \mu_C)\exp(\tau_C / \mu_C) - \tau_C$$

and

$$q = \mu_O \mu_C \exp(\tau_C / \mu_C) + \tfrac{1}{2}\tau_C^2.$$

4.1.3 Inference from Observed Sojourn Times

4.1.3.1 Maximum Likelihood Estimators and Method-of-Moments Estimators

Consider the approximations of sections 4.1.2.2.1 and 4.1.2.2.2, under which durations of successive adjusted observed open sojourns, U_1, U_2,...,U_n say, are

assumed to be independent identically distributed random variables having negative exponential distribution with mean $\nu_O = \nu_O(\mu)$ where μ denotes (μ_O, μ_C). Let $u_1, u_2, \ldots, u_n$ be the realisations of $U_1, U_2, \ldots, U_n$ and let $\bar{u}$ denote the sample mean given by

$$\bar{u} = \frac{1}{n}\sum_{i=1}^{n} u_i .$$

Define $V_1, V_2, \ldots, V_n$ with mean $\nu_C = \nu_C(\mu)$, realisations $v_1, v_2, \ldots, v_n$ and sample mean $\bar{v}$, analogously for adjusted observed closed sojourns.

Then the likelihood function, $L(\mu)$ say, is given by

$$\begin{aligned} L(\mu) &= \prod_{i=1}^{n} (\nu_O(\mu))^{-1} \exp[-(\nu_O(\mu))^{-1} u_i] \\ &\qquad \times \prod_{i=1}^{n} (\nu_C(\mu))^{-1} \exp[-(\nu_C(\mu))^{-1} v_i] \\ &= L_1(\nu_O(\mu))\, L_2(\nu_C(\mu)), \text{ say.} \end{aligned}$$

The log-likelihood functions $\ln [L_1(\nu_O(\mu))]$ and $\ln [L_2(\nu_C(\mu))]$ are given by

$$\ln[L_1(\nu_O(\mu))] = -n(\ln(\nu_O) + \bar{u}/\nu_O)$$

and

$$\ln[L_2(\nu_C(\mu))] = -n(\ln(\nu_C) + \bar{v}/\nu_C),$$

and are maximised at $\nu_O(\mu) = \bar{u}$ and $\nu_C(\mu) = \bar{v}$, respectively. Let $\nu(\mu) = (\nu_O(\mu), \nu_C(\mu))$. If values of μ_O and μ_C exist which satisfy $\nu(\mu) = (\bar{u}, \bar{v})$, then those values maximise $L(\mu)$ and the maximum likelihood estimator of μ coincides with the method-of-moments estimator of μ.

Let $\nu = h(\mu) = (h_O(\mu), h_C(\mu))$, where the function h is determined according to which approximation is under consideration. For the approximation discussed in section 4.1.2.2.1, the function h_O is determined by setting $h_O = \nu_1$ where ν_1 is given by equation (4.8) and, for the approximation discussed in section 4.1.2.2.2, it is determined by setting $h_O = \nu_O$ where ν_O is given by equation (4.3). The function h_C is determined using similar equations for closed sojourns. For the approximation of section 4.1.2.2.2, in which adjusted observed sojourns are assumed to follow negative exponential random variables having the correct means, it is proved in Theorem 4.1 of section 4.2.2 that the equation $h(\mu) = \nu$ has either zero, one or two solutions according to the position of the point (ν_O, ν_C) in relation to a particular strictly decreasing function $\nu_C = \tilde{f}(\nu_O)$, say. Define sets

$$O = \{(x, y) \in (\mathbb{R}^+)^2 : y = \tilde{f}(x)\},$$

$$T = \{(x, y) \in (\mathbb{R}^+)^2 : y > \tilde{f}(x)\}$$

and

$$Z = \{(x, y) \in (\mathbb{R}^+)^2 : y < \tilde{f}(x)\}.$$

Then, by Theorem 4.1, the equation $h(\mu) = \nu$ has one solution for $\nu \in O$, two

solutions for $\nu \in T$ and zero solutions for $\nu \in Z$. Equivalent results hold for the approximation considered in 4.1.2.2.1 (see Yeo *et al.* (1988)).

In the case $(\bar{u}, \bar{v}) \in O(T)$, the method-of-moments estimating equations have one (two) solution(s) giving the maximum likelihood estimator(s) of μ. Now consider the case in which $(\bar{u}, \bar{v}) \in Z$ and the method-of-moments cannot be used to provide maximum likelihood estimators of μ. In order to determine the maximum likelihood estimator(s) of μ, we proceed by maximising $L(\nu) = L_1(\nu_O)L_2(\nu_C)$ for $\nu \in O \cup T$. First suppose that $\nu' = (\nu_O', \nu_C') \in \{\nu \in T: \nu_O \geq \bar{u}$ and $\nu_C \geq \bar{v}\}$. Let ν^* denote the point of intersection of O with the straight line joining ν' and $(\bar{u}, \bar{v})$. It is easily shown that, for $\nu_O > \bar{u}$, $L_1(\nu_O)$ increases as ν_O decreases and therefore that $L_1(\nu_O^*) \geq L_1(\nu_O')$. Similarly, $L_2(\nu_C^*) \geq L_2(\nu_C')$, and hence $L(\nu^*) \geq L(\nu')$. Next suppose that $\nu'' = (\nu_O'', \nu_C'') \in \{\nu \in T: \nu_O \geq \bar{u}$ and $\nu_C < \bar{v}\}$ and let $\nu' = (\nu_O', \nu_C')$ now denote the point of intersection of the two straight lines $\nu_O = \nu_O''$ and $\nu_C = \bar{v}$, noting that $\nu' \in \{\nu \in T: \nu_O \geq \bar{u}$ and $\nu_C \geq \bar{v}\}$. Clearly, $L_1(\nu_O') = L_1(\nu_O'')$, and it is easily shown that, for $\nu_C < \bar{v}$, $L_2(\nu_C)$ increases as ν_C increases and therefore that $L_2(\nu_C') > L_2(\nu_C'')$. Hence $L(\nu') > L(\nu'')$. Finally, suppose $\nu'' \in \{\nu \in T: \nu_O < \bar{u}$ and $\nu_C \geq \bar{v}\}$. Then a similar argument shows that there is again a point ν' say, in $\{\nu \in T: \nu_O \geq \bar{u}$ and $\nu_C \geq \bar{v}\}$ with $L(\nu') > L(\nu'')$. It follows that, for any $\nu \in O \cup T$, there is a point $\nu^* \in O$ such that $L(\nu^*) \geq L(\nu)$. Thus the problem is reduced to locating the maximum of $L(\nu')$ subject to $\nu_C = \tilde{f}(\nu_O)$ and $\bar{u} \leq \nu_O \leq \tilde{f}^{-1}(\bar{v})$. This problem

can be solved using an appropriate numerical software package.

4.1.3.2 Identifiability Problems

Section 4.1.3.1 raises a problem with inference for the two-state model. Time interval omission induces non-identifiability in that, whenever $\nu \in T$, there are two solutions to the method-of-moments estimating equations, corresponding to two peaks of almost equal height of the likelihood surface. In Theorem 4.2 of section 4.2.3, we show that $\nu \in T$ is the usual situation when the number of observed sojourns is sufficiently large.

For the approximation discussed in section 4.1.2.2.1, Yeo *et al.* (1988) prove that the method-of-moments estimating equations have zero, one or two solutions depending on the value of ν (see Section 4.2.4.1). Yeo *et al.* (1988) also prove that the bi-exponential approximation of section 4.1.2.2.3 yields an identifiable model. Further, it is conjectured by Yeo *et al.* (1988) that the approximation considered in section 4.1.2.2.2 yields method-of-moments estimating equations with zero, one or two solutions. This conjecture is proved in section 4.2.

Two methods have been proposed for overcoming the above identifiability problem. In practice, the sequence of open and closed sojourns of the channel is reconstructed from the observed single channel record by using a filter and an

associated threshold crossing algorithm. A computationally highly intensive simulation-based method has been suggested by Magleby and Weiss (1990a) which involves modelling the true effects of the filter. Another method proposed by Colquhoun and Sigworth (1983), Blatz and Magleby (1986) and Yeo *et al.* (1988) involves using samples with different minimum detectable sojourn lengths and estimating (μ_O, μ_C) for each sample. Then, as the detection limit varies, one estimate of (μ_O, μ_C) remains approximately constant while the other varies significantly, thereby allowing the true solution to be determined.

In section 4.3 two new methods of overcoming the identifiability problem are discussed. The first bears resemblance to the method of using samples with different minimum detectable sojourn lengths limits but instead uses samples with different agonist concentrations. The mean length of a closed sojourn of an agonist-activated channel is modelled as $a^{-1}\mu_C$, where a is the agonist concentration, which is assumed to be known. In order to use the methods which involve varying the detection limit or varying the agonist concentration, it is necessary to observe single channel records under different experimental conditions. As, in practice, records of reconstructed sojourn times are frequently used to fit models, it is clearly beneficial to have a method of discriminating between the two solutions on the basis of one such record. The second new method proposed in section 4.3 does not require taking samples under different experimental conditions but instead uses observed open and closed sojourn length

sample variances to discriminate between the two solutions. Numerical examples based on simulated data provide evidence that these two new methods will work in practice.

4.1.3.3 Asymptotic Behaviour of Method-of-Moments Estimators

Clarke *et al.* (1993) investigate local asymptotic theory for situations when there are multiple solutions of the likelihood equations and apply this to obtain simultaneous consistency and asymptotic normality results for the maximum likelihood estimators for μ under the approximate models of sections 4.1.2.2.1 and 4.1.2.2.2. As stated in section 4.1.3.1, under these approximate models these maximum likelihood estimators correspond to method-of-moments estimators. In section 4.2, a framework is developed for analysing the asymptotic behaviour of these method-of-moments estimators under the *exact* model as the numbers of observed open and closed sojourns become large. This framework can be used to shed light on the origin of the non-identifiability discussed in section 4.1.3.2 and makes possible an evaluation of the accuracy of the simultaneous confidence sets given in Clarke *et al.* (1993), which were based on the approximate model discussed in section 4.1.2.2.2. Further, this framework can be used to give a formal justification of the methods for overcoming the identifiability problem which involve using multiple samples with varying detection limits or agonist concentrations.

4.2 Method-of-Moments Estimators

4.2.1 Notation

In this section, a direct argument is used to derive asymptotic results for the method-of-moments estimators under the *exact* model. Modifying the notation of section 4.1.3, let $\boldsymbol{\mu} = (\mu_O, \mu_C)^\top$ and $\boldsymbol{\nu} = (\nu_O, \nu_C)^\top$. Then $\boldsymbol{\nu} = h(\boldsymbol{\mu}) = (h_O(\boldsymbol{\mu}), h_C(\boldsymbol{\mu}))^\top$, where the functions h_O and h_C are determined by equations (4.3) and (4.5). The method-of-moments estimators, $\hat{\boldsymbol{\mu}}_n$ say, of $\boldsymbol{\mu}$, based on a sample of n pairs of observed adjusted open and closed sojourns, are obtained by solving $h(\boldsymbol{\mu}) = \hat{\boldsymbol{\nu}}_n$, where

$$\hat{\boldsymbol{\nu}}_n^{\top} = \left(\frac{1}{n}\sum_{i=1}^{n} \tilde{u}_i, \frac{1}{n}\sum_{i=1}^{n} \tilde{v}_i \right) = (\hat{\nu}_{nO}, \hat{\nu}_{nC})$$

say. Before asymptotic properties of the estimator $\hat{\boldsymbol{\mu}}_n$ are derived, some facts are required concerning the function h. These facts are collected together in Theorem 4.1 below. First some further notation is needed.

Let

$$H^{(1)}(\boldsymbol{\mu}) = \begin{pmatrix} \frac{\partial h_O}{\partial \mu_O} & \frac{\partial h_O}{\partial \mu_C} \\ \frac{\partial h_C}{\partial \mu_O} & \frac{\partial h_C}{\partial \mu_C} \end{pmatrix} (\boldsymbol{\mu})$$

and $J(\mu) = |H^{(1)}(\mu)|$ be respectively the Jacobian matrix and the Jacobian of the transformation h. By elementary differentiation of (4.3) and (4.5), it follows that

$$\frac{\partial h_O}{\partial \mu_O} = \exp(\tau_C / \mu_C), \tag{4.10a}$$

$$\frac{\partial h_O}{\partial \mu_C} = \exp(\tau_C / \mu_C)\,(1 - \tau_C \mu_C^{-2}(\mu_O + \mu_C)) - 1, \tag{4.10b}$$

$$\frac{\partial h_C}{\partial \mu_O} = \exp(\tau_O / \mu_O)\,(1 - \tau_O \mu_O^{-2}(\mu_O + \mu_C)) - 1, \tag{4.10c}$$

and

$$\frac{\partial h_C}{\partial \mu_C} = \exp(\tau_O / \mu_O). \tag{4.10d}$$

Let $A \subseteq \mathbb{R}^2$ be an open set. For $r \in \mathbb{N}$, a function $h : A \to \mathbb{R}^2$ is of class $C^{(r)}$ on A (see Stromberg (1981), p367) if all the rth-order partial derivatives of h_O and h_C are defined, finite and continuous on A. Further, h is of class $C^{(\infty)}$ on A if it is of class $C^{(r)}$ on A for all $r \in \mathbb{N}$.

4.2.2 The Identifiability Problem

Theorem 4.1 provides a proof of the conjecture of Yeo *et al.* (1988) concerning the number of solutions of the moment estimating equations and proves some facts concerning the function h which are needed in order to analyse the

behaviour of the method-of-moments estimators of μ.

Theorem 4.1 (see Figure 4.1)

(a) For all $\nu \in (\mathbb{R}^+)^2$ the equation $h(\mu) = \nu$ has either zero, one or two solutions in $(\mathbb{R}^+)^2$.

(b) The equation $J(\mu) = 0$ implicitly defines a function $\mu_C = f(\mu_O)$ on $(0, \infty)$ that is strictly decreasing, with $\lim_{x \to 0}\{f(x)\} = \infty$ and $\lim_{x \to \infty}\{f(x)\} = 0$.

Let

$$L = \{(x, y) \in (\mathbb{R}^+)^2 : y = f(x)\},$$

$$S = \{(x, y) \in (\mathbb{R}^+)^2 : y > f(x)\},$$

and

$$F = \{(x, y) \in (\mathbb{R}^+)^2 : y < f(x)\}.$$

The image, O say, of L under h implicitly defines a strictly decreasing function $\tilde{f} : \mathbb{R}^+ \to \mathbb{R}^+$ by $\nu_C = \tilde{f}(\nu_O)$. Let $T = \{(x, y) \in (\mathbb{R}^+)^2 : y > \tilde{f}(x)\}$, and let h_S and h_F be the map h restricted to the sets S and F respectively. Then h_S is a bijection from S to T, with inverse function g_S, say. Similarly, h_F is a bijection from F to T, with inverse function g_F, say. Moreover, the functions g_S and g_F are both of class $C^{(\infty)}$ on T.

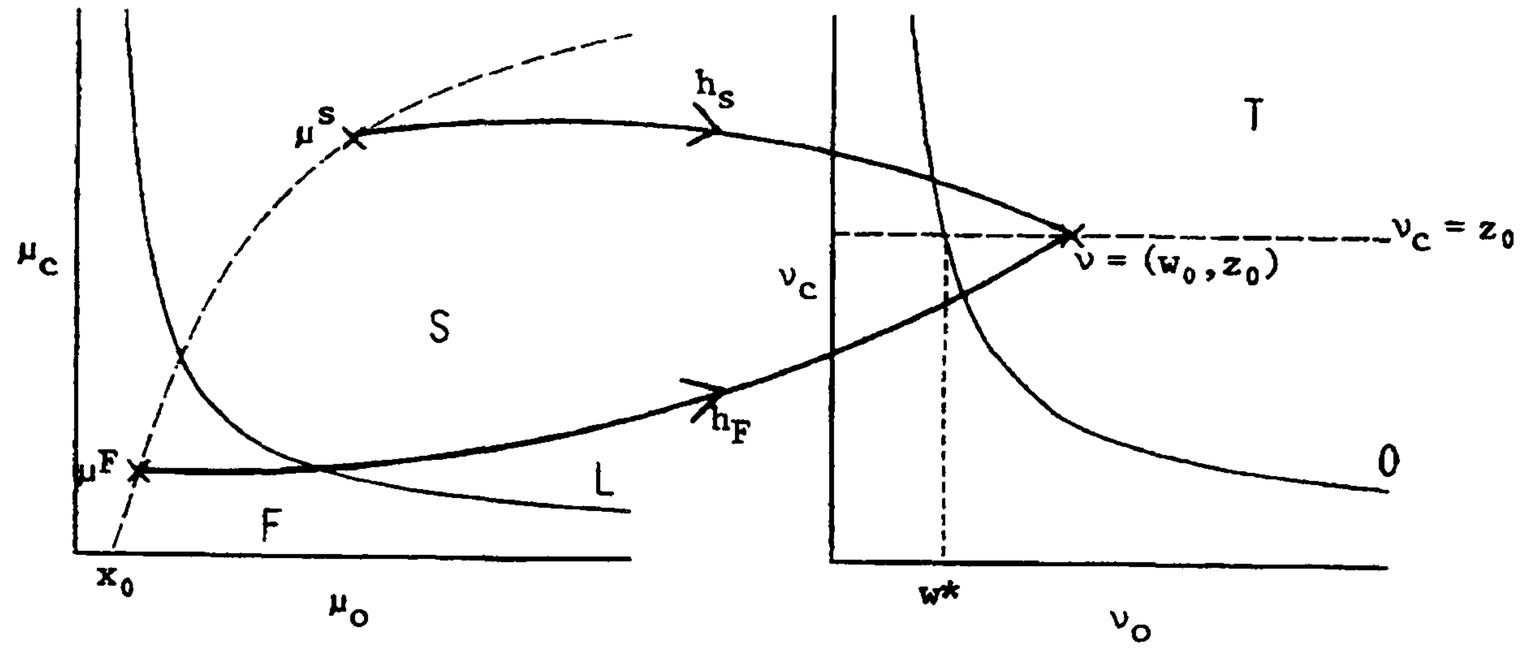

Figure 4.1. Sets F, S, L, T and O, and the bijections h_S and h_F when $\tau_O = \tau_C = 0.1$ ms, illuminating the proof of Theorem 4.1, part (a) (for details, see the statement of, and the text immediately following, Theorem 4.1).

Proof

First we prove the facts in part (b) concerning the equation $J(\mu) = 0$. Using equations (4.10a-d),

$$J(\mu) = \exp\left(\frac{\tau_C}{\mu_C} + \frac{\tau_O}{\mu_O}\right) - \left[\exp\left(\frac{\tau_C}{\mu_C}\right)\left(1 - \frac{\tau_C(\mu_O + \mu_C)}{\mu_C^2}\right) - 1\right] \times \left[\exp\left(\frac{\tau_O}{\mu_O}\right)\left(1 - \frac{\tau_O(\mu_O + \mu_C)}{\mu_O^2}\right) - 1\right]. \tag{4.11}$$

So, letting $u = \mu_O^{-1}$ and $v = \mu_C^{-1}$, equation (4.11) can be rewritten as

$$J(\mu) = \exp(\tau_C v + \tau_O u)\,[1 - G(u, v)],$$

where

$$G(u, v) = \left|\exp(-\tau_C v) - 1 + \tau_C v^2/u + \tau_C v\right| \times \left[\exp(-\tau_O u) - 1 + \tau_O u^2/v + \tau_O u\right].$$

Hence $J(\mu) = 0$ if and only if $G(u, v) = 1$. By elementary partial differentiation of $G(u, v)$ with respect to u, we obtain that

$$\frac{\partial G}{\partial u} = \tau_O\left[\exp(-\tau_C v) - 1 + \tau_C v\right]\left[1 - \exp(-\tau_O u) + 2 u v^{-1}\right] + \tau_O \tau_C v + \tau_C v^2 u^{-2}\left[1 - \exp(-\tau_O u) - \tau_O u \exp(-\tau_O u)\right].$$

Now, for $x > 0$, $\exp(-x) - 1 + x > 0$ and $1 - \exp(-x) - x \exp(-x) > 0$, and so $\partial G / \partial u > 0$ for all $u, v > 0$. Similarly, $\partial G / \partial v > 0$ for all $u, v > 0$.

For $u_0 > 0$,

$$\lim_{v \to 0}\{G(u_0, v)\} = \lim_{v \to 0}\left\{\left(\exp(-\tau_C v) - 1 + \tau_C v^2 u_0^{-1} + \tau_C v\right) \times \left(\exp(-\tau_O u_0) - 1 + \tau_O u_0^2 v^{-1} + \tau_O u_0\right)\right\}$$

$$= \lim_{v \to 0}\left\{\tau_O u_0^2\left(\frac{\exp(-\tau_C v) - 1 + \tau_C v^2 u_0^{-1} + \tau_C v}{v}\right)\right\}$$

$$= \lim_{v \to 0}\left\{\tau_O u_0^2\left(-\tau_C \exp(-\tau_C v) + 2\tau_C v u_0^{-1} + \tau_C\right)\right\},$$

by l'Hôpital's rule, and so $\lim_{v \to 0}\{G(u_0, v)\} = 0$. It is easily shown that $\lim_{v \to \infty}\{G(u_0, v)\} = \infty$. Thus, since $G(u_0, v)$ is strictly increasing in v, there is a unique $v_0 > 0$ such that $G(u_0, v_0) = 1$. Hence for each value of μ_O, there is a

unique value of μ_C such that $J(\mu) = 0$ and therefore $J(\mu) = 0$ implicitly defines a strictly monotone function $\mu_C = f(\mu_O)$ on $(0, \infty)$. Since, for $v_0 > 0$, $G(u, v_0)$ is strictly increasing in u, it follows that $J(\mu)$ is increasing in μ_O for fixed values of μ_C, and similarly $J(\mu)$ is increasing in μ_C for fixed values of μ_O. Thus the function $\mu_C = f(\mu_O)$ is strictly decreasing. By a similar argument, for each $v_1 > 0$, there is a unique $u_1 > 0$ such that $G(u_1, v_1) = 1$. It follows that,

$$\lim_{\mu_O \to 0}\{f(\mu_O)\} = \infty \qquad \text{and} \qquad \lim_{\mu_O \to \infty}\{f(\mu_O)\} = 0.$$

To prove part (a) it is convenient to change our notation slightly. Write x, y, w and z for μ_O, μ_C, ν_O and ν_C, respectively. Then, from equations (4.3) and (4.5), we are interested in the solutions of

$$f_1(x, y) = (x + y)\exp(\tau_C/y) - y - \tau_C = w, \tag{4.12}$$

and

$$f_2(x, y) = (x + y)\exp(\tau_O/x) - x - \tau_O = z, \tag{4.13}$$

for $(w, z) \in (\mathbb{R}^+)^2$. Fix $(w_0, z_0) \in (\mathbb{R}^+)^2$. For $x > 0$, the inverse image of the line $z = z_0$ under the above mapping is given by

$$y = (z_0 + \tau_O + x)\exp(-\tau_O/x) - x = h_1(x) \text{ say.} \tag{4.14}$$

Now

$$h_1'(x) = (z_0 + \tau_O + x)\ \tau_O\, x^{-2} \exp(-\tau_O/x) + \exp(-\tau_O/x) - 1 .$$

For $y > 0$, equation (4.14) implies that $(z_0 + \tau_O + x)\exp(-\tau_O/x) > x$ and so

$$\begin{aligned} h_1'(x) &> \tau_O/x + \exp(-\tau_O/x) - 1 \\ &> 0 . \end{aligned}$$

Now

$$\begin{aligned} \lim_{x\to 0} h_1'(x) &= \lim_{x\to 0}\left[\frac{((z_0 + \tau_O)x^{-2} + x^{-1})\ \tau_O}{\exp(\tau_O/x)} + \frac{1}{\exp(\tau_O/x)} - 1\right] \\ &= \lim_{x\to\infty}\left[\frac{((z_0 + \tau_O)x^2 + x)\ \tau_O}{\exp(\tau_O x)}\right] - 1 \\ &= -1 . \end{aligned}$$

As noted by Yeo *et al.* (1988), $h_1(x)$ has a single zero, at x_0 say, in $(0, \infty)$. Therefore $y = h_1(x)$ is a strictly increasing function defined on (x_0, ∞). Further

$$\begin{aligned} \lim_{x\to\infty} h_1(x) &= (z_0 + \tau_O) + \lim_{x\to\infty}\left|x(\exp(-\tau_O/x) - 1)\right| \\ &= (z_0 + \tau_O) + \lim_{x\to 0}\left[\frac{(\exp(-\tau_O x) - 1)}{x}\right] \\ &= z_0, \end{aligned}$$

again by l'Hôpital's rule.

Now consider the function $w(x)$ defined on (x_0, ∞) by $w(x) = f_1(x, h_1(x))$. Then, by the chain rule,

$$\frac{\mathrm{d}w}{\mathrm{d}x} = \frac{\partial f_1}{\partial x} + \frac{\partial f_1}{\partial y} \cdot \frac{\mathrm{d}h_1}{\mathrm{d}x}, \tag{4.15}$$

evaluated at $(x, h_1(x))$. But h_1 is defined implicitly by $f_2(x, h_1(x)) = z_0$ and so, again by the chain rule,

$$\frac{\mathrm{d}h_1}{\mathrm{d}x} = -\frac{\partial f_2}{\partial x} \Big/ \frac{\partial f_2}{\partial y}, \tag{4.16}$$

evaluated at $(x, h_1(x))$, noting that

$$\frac{\partial f_2}{\partial y} = \exp(\tau_O/x) \neq 0 \text{ or } \infty$$

for $x \geq x_0$. It follows from equations (4.15) and (4.16) that $\frac{\mathrm{d}w}{\mathrm{d}x} = 0$ if and only if

$$\frac{\partial f_1}{\partial x} \cdot \frac{\partial f_2}{\partial y} - \frac{\partial f_1}{\partial y} \cdot \frac{\partial f_2}{\partial x} = 0,$$

or, equivalently, if and only if $J(x, h_1(x)) = 0$. Thus the turning points of $w(x)$ satisfy $J(x, h_1(x)) = 0$ and hence $f(x) = h_1(x)$. But we have shown that h_1 is strictly increasing on $[x_0, \infty)$ with $h_1(x_0) = 0$ and that f is strictly decreasing on $\mathbb{R}^+$ with

$\lim_{x \to -\infty} f(x) = 0$. Therefore $w(x)$ has exactly one turning point.

Now

$$\begin{aligned} \lim_{x \to x_0} w(x) &= \lim_{x \to x_0} \left| f_1(x,\ h_1(x)) \right| \\ &= \lim_{y \to 0} \left[(x_0 + y) \exp(\tau_C / y) - y - \tau_C \right] \\ &= \infty \end{aligned}$$

and

$$\begin{aligned} \lim_{x \to \infty} w(x) &= \lim_{x \to \infty} \left| f_1(x,\ h_1(x)) \right| \\ &= \lim_{x \to \infty} \left[f_1(x,\ z_0) \right] \\ &= \lim_{x \to \infty} \left[(x + z_0) \exp(\tau_O / z_0) - z_0 - \tau_O \right] \\ &= \infty . \end{aligned}$$

Thus the turning point of $w(x)$ must be a minimum. Let $w^* = w^*(z_0)$ be the corresponding minimum value of $w(x)$. Then it follows that equations (4.12) and (4.13), with (w, z) replaced by (w_0, z_0), have zero, one or two solutions according to whether $w_0 < w^*$, $w_0 = w^*$ or $w_0 > w^*$, respectively.

Returning to part (b), and using the above results, any horizontal line $z = z_0$ intersects O at exactly one point. A similar argument shows that the same is true for any vertical line $w = w_0$. Thus O implicitly defines a strictly monotone function $\tilde{f} : \mathbb{R}^+ \to \mathbb{R}^+$, given by $\tilde{f}(z) = w^*(z)$, alternatively written as $\nu_C = \tilde{f}(\nu_O)$.

It is clear from equation (4.14) that the value of $h_1(x)$, at the value of x at which $h_1(x)$ and L intersect, is greater for higher values of z_0. Therefore the shape of the monotone function $\nu_C = \tilde{f}(\nu_O)$ can be determined by considering the value of (ν_O, ν_C) at which $z = z_0$ intersects O as $z_0 \to 0$ and $z_0 \to \infty$, or equivalently as $\mu \to (0, \infty)^\top$ and $\mu \to (\infty, 0)^\top$. By manipulation of equation (4.3),

$$\lim_{\mu \to (0,\infty)^\top} \nu_O = \lim_{\mu \to (0,\infty)^\top} \left[\mu_O \exp\left(\frac{\tau_C}{\mu_C} \right) + \tau_C \left(\frac{\exp(\tau_C/\mu_C) - 1}{\tau_C/\mu_C} \right) - \tau_C \right]$$

$$= 0$$

since, by l'Hôpital's rule,

$$\lim_{\mu_C \to \infty} \left(\frac{\exp(\tau_C/\mu_C) - 1}{\tau_C/\mu_C} \right) = \lim_{x \to 0} \left(\frac{\exp(x) - 1}{x} \right) = 1.$$

It is easy to show that

$$\lim_{\mu \to (0,\infty)^\top} \nu_C = \infty,$$

and therefore, by symmetry,

$$\lim_{\mu \to (\infty,0)^\top} (\nu_O, \nu_C) = (\infty, 0).$$

Hence $\tilde{f}$ is strictly decreasing.

The bijection property of h_F and h_S follows directly from the proof of part (a).

Finally, it is easily verified that h_F and h_S are of class $C^{(\infty)}$ on F and S respectively. It then follows from the Inverse Function Theorem for $\mathbb{R}^2$ (Stromberg (1981), pages 377-378) that g_F and g_S are both of class $C^{(\infty)}$ on T.

4.2.3 Asymptotic Properties of the Method-of-Moments Estimators

This section contains an analysis of the asymptotic behaviour of the method-of-moments estimators as the number of observed open and closed sojourns becomes large. First some more notation is introduced.

For $\nu \in T$, let $\mu^S = g_S(\nu)$ and $\mu^F = g_F(\nu)$ be the two solutions of $h(\mu) = \nu$ where $\mu^S = (\mu_O^S, \mu_C^S)^\top$, $\mu^F = (\mu_O^F, \mu_C^F)^\top$ and $\mu_C^S > \mu_C^F$. Then from equation (4.3) it follows that

$$(\mu_O^S + \mu_C^S)\exp(\tau_C/\mu_C^S) - \mu_C^S = (\mu_O^F + \mu_C^F)\exp(\tau_C/\mu_C^F) - \mu_C^F.$$

This equation can be rearranged to obtain

$$\mu_O^S = \mu_O^F \exp\left[\tau_C\left(\frac{1}{\mu_C^F} - \frac{1}{\mu_C^S}\right)\right] + \exp(-\tau_C/\mu_C^S)\,[\mu_C^F(\exp(\tau_C/\mu_C^F) - 1) - \mu_C^S(\exp(\tau_C/\mu_C^S) - 1)].$$

By considering the series expansions of $\exp(\tau_C/\mu_C^F)$ and $\exp(\tau_C/\mu_C^S)$, it follows

immediately that

$$\mu_C^F(\exp(\tau_C/\mu_C^F) - 1) - \mu_C^S(\exp(\tau_C/\mu_C^S) - 1) > 0,$$

and thus $\mu_O{}^S > \mu_O{}^F$. Hence $\boldsymbol{\mu^S}$ and $\boldsymbol{\mu^F}$ are termed the 'slow' and 'fast' solutions respectively (see also Yeo *et al.* (1988)).

Since h is one-to-one on L, g_S and g_F can be extended to $T \cup O$ by defining $g_S(\boldsymbol{\nu}) = g_F(\boldsymbol{\nu}) = h^{-1}(\boldsymbol{\nu})$ for $\boldsymbol{\nu} \in O$. Estimators $\hat{\boldsymbol{\mu}}_n{}^S$ and $\hat{\boldsymbol{\mu}}_n{}^F$ of $\boldsymbol{\mu^S}$ and $\boldsymbol{\mu^F}$ can now be defined by $\hat{\boldsymbol{\mu}}_n{}^S = g_S(\hat{\boldsymbol{\nu}}_n)$ and $\hat{\boldsymbol{\mu}}_n{}^F = g_F(\hat{\boldsymbol{\nu}}_n)$, where for completeness $\hat{\boldsymbol{\mu}}_n{}^S = \hat{\boldsymbol{\mu}}_n{}^F = \mathbf{0}$ if $\hat{\boldsymbol{\nu}}_n \notin T \cup O$. Let $G_S{}^{(1)}(\boldsymbol{\nu})$ and $G_F{}^{(1)}(\boldsymbol{\nu})$ be the Jacobian matrices of g_S and g_F respectively. Writing $g_S(\boldsymbol{\nu}) = (g_O{}^S(\boldsymbol{\nu}),\ g_C{}^S(\boldsymbol{\nu}))$, it follows by standard theory that

$$G_S^{(1)}(\boldsymbol{\nu}) = \begin{pmatrix} \frac{\partial g_O^S}{\partial \nu_O} & \frac{\partial g_O^S}{\partial \nu_C} \\ \frac{\partial g_C^S}{\partial \nu_O} & \frac{\partial g_C^S}{\partial \nu_C} \end{pmatrix} = \frac{1}{J}\begin{pmatrix} \frac{\partial h_C}{\partial \mu_C^S} & -\frac{\partial h_O}{\partial \mu_C^S} \\ -\frac{\partial h_C}{\partial \mu_O^S} & \frac{\partial h_O}{\partial \mu_O^S} \end{pmatrix},$$

where

$$J = \frac{\partial h_O}{\partial \mu_O^S} \cdot \frac{\partial h_C}{\partial \mu_C^S} - \frac{\partial h_O}{\partial \mu_C^S} \cdot \frac{\partial h_C}{\partial \mu_O^S}.$$

Writing $g_F(\boldsymbol{\nu}) = (g_O{}^F(\boldsymbol{\nu}),\ g_C{}^F(\boldsymbol{\nu}))$, a similar expression holds for $G_F{}^{(1)}(\boldsymbol{\nu})$.

Theorem 4.2

(a) If $\boldsymbol{\mu} \notin L$ then

(i) $\mathbf{P}(\hat{\boldsymbol{\nu}}_n \in T \text{ for all sufficiently large } n) = 1$,

(ii) $\hat{\mu}_n^S \xrightarrow{\text{a.s.}} \mu^S$ and $\hat{\mu}_n^F \xrightarrow{\text{a.s.}} \mu^F$ as $n \to \infty$,

(iii) $$\sqrt{n}\begin{pmatrix} \hat{\mu}_n^S - \mu^S \\ \hat{\mu}_n^F - \mu^F \end{pmatrix} \xrightarrow{\text{D}} N(\mathbf{0}, \boldsymbol{\Sigma}) \text{ as } n \to \infty,$$

where

$$\boldsymbol{\Sigma} = \begin{pmatrix} G_S^{(1)}(\nu) D G_S^{(1)}(\nu)^\top & G_S^{(1)}(\nu) D G_F^{(1)}(\nu)^\top \\ G_F^{(1)}(\nu) D G_S^{(1)}(\nu)^\top & G_F^{(1)}(\nu) D G_F^{(1)}(\nu)^\top \end{pmatrix}$$

and

$$D = \begin{pmatrix} \tilde{\sigma}_O^{\,2} & 0 \\ 0 & \tilde{\sigma}_C^{\,2} \end{pmatrix} \qquad (= \text{diag}(\tilde{\sigma}_O^{\,2}, \tilde{\sigma}_C^{\,2}), \text{ say}).$$

(b) If $\boldsymbol{\mu} \in L$ then

(i) $\lim_{n\to\infty}\{\mathbf{P}(\hat{\boldsymbol{\nu}}_n \in T)\} = \frac{1}{2}$;

(ii) if $\check{\boldsymbol{\mu}}_n^S$ is defined by

$$\check{\mu}_n^S = \begin{cases} \hat{\mu}_n^S & \text{if } \hat{v}_n \in T, \\ \mu & \text{if } \hat{v}_n \notin T, \end{cases}$$

and $\check{\mu}_n^F$ is defined similarly, then

$$\check{\mu}_n^S \xrightarrow{\text{a.s.}} \mu \quad \text{and} \quad \check{\mu}_n^F \xrightarrow{\text{a.s.}} \mu \quad \text{as } n \to \infty.$$

Proof

By the strong law of large numbers,

$$\hat{v}_n \xrightarrow{\text{a.s.}} v \quad \text{as} \quad n \to \infty.$$

Now $\mu \notin L$ implies that $v \in T$, so part (a) (i) follows immediately since T is an open set. Also, since the function g_S is continuous on $T \cup O$,

$$\hat{\mu}_n^S = g_S(\hat{v}_n) \xrightarrow{\text{a.s.}} g_S(v) = \mu^S \quad \text{as} \quad n \to \infty,$$

and similarly

$$\hat{\mu}_n^F \xrightarrow{\text{a.s.}} \mu^F \quad \text{as} \quad n \to \infty.$$

Part (a) (ii) now follows, as does part (b) (ii) on noting that if $\boldsymbol{\mu} \in L$ and $\boldsymbol{\nu} = h(\boldsymbol{\mu})$ then $g_S(\boldsymbol{\nu}) = g_F(\boldsymbol{\nu}) = \boldsymbol{\mu}$.

To prove part (a) (iii), first note that by the Central Limit Theorem

$$\sqrt{n}\,(\hat{\boldsymbol{\nu}}_n - \boldsymbol{\nu}) \xrightarrow{\mathrm{D}} \boldsymbol{Z} \quad \text{as} \quad n \to \infty, \tag{4.17}$$

where $\boldsymbol{Z} \sim \mathrm{N}(\boldsymbol{0}, D)$. Now

$$\begin{pmatrix} \hat{\mu}_n^S - \mu^S \\ \hat{\mu}_n^F - \mu^F \end{pmatrix} = \begin{pmatrix} g_S(\hat{\boldsymbol{\nu}}_n) - g_S(\boldsymbol{\nu}) \\ g_F(\hat{\boldsymbol{\nu}}_n) - g_F(\boldsymbol{\nu}) \end{pmatrix},$$

so since g_S and g_F are both differentiable at $\boldsymbol{\nu}$, it follows using the delta-method (see, for example, Andersen *et al.* (1992), pages 109-110) that

$$\sqrt{n} \begin{pmatrix} \hat{\mu}_n^S - \mu^S \\ \hat{\mu}_n^F - \mu^F \end{pmatrix} \xrightarrow{\mathrm{D}} \begin{pmatrix} G_S^{(1)}(\nu) \\ G_F^{(1)}(\nu) \end{pmatrix} \boldsymbol{Z} \quad \text{as} \quad n \to \infty,$$

and part (a) (iii) follows.

To prove part (b) (i), let $\boldsymbol{\mu}_0 \in L$, $\boldsymbol{\nu}_0 = h(\boldsymbol{\mu}_0) = (\nu_{0O}, \ \nu_{0C})^{\top}$ say,

$$\theta = \tan^{-1}\left\{-\frac{\partial \tilde{f}}{\partial \nu_O}(\nu_{0O})\right\}$$

and

$$M = \begin{pmatrix} \cos\theta & -\sin\theta \\ \sin\theta & \cos\theta \end{pmatrix}.$$

Then the transformation $\boldsymbol{x} = M(\boldsymbol{\nu} - \boldsymbol{\nu}_0)$ maps the curve $\boldsymbol{\nu}_C = \tilde{f}(\boldsymbol{\nu}_O)$ to a curve $x_2 = \tilde{f}_1(x_1)$ (where we have written $\boldsymbol{x} = (x_1, x_2)^\top$) satisfying $\tilde{f}_1(0) = 0$ and $\tilde{f}_1'(0) = 0$, where $\tilde{f}_1'$ is the first derivative of $\tilde{f}_1$ with respect to x_1. For $n = 1, 2, \ldots$, let $\hat{\boldsymbol{x}}_n = M(\hat{\boldsymbol{\nu}}_n - \boldsymbol{\nu}_0)$. Then $\hat{\boldsymbol{\nu}}_n \in T$ if and only if, using obvious notation, $\hat{x}_{n2} > \tilde{f}_1(\hat{x}_{n1})$. Using (4.17),

$$\sqrt{n}\,\hat{\boldsymbol{x}}_n \xrightarrow{D} M\boldsymbol{Z} \quad \text{as} \quad n \to \infty,$$

so since $\tilde{f}_1(0) = 0$ and $\tilde{f}_1'(0) = 0$, application of the delta-method yields that

$$\sqrt{n}\,(\hat{x}_{n2} - \tilde{f}_1(\hat{x}_{n1})) \xrightarrow{D} Z' \quad \text{as} \quad n \to \infty,$$

where $Z' = (0 \;\; 1)M\boldsymbol{Z}$.

Now $\boldsymbol{Z} \sim \mathrm{N}(\boldsymbol{0}, D)$ so $Z' \sim \mathrm{N}(\boldsymbol{0}, \sigma^2)$, where

$$\begin{aligned} \sigma^2 &= (0 \;\; 1)\, M D M^\top (0 \;\; 1)^\top \\ &= \sin^2\theta\, \tilde{\sigma}_O^2 + \cos^2\theta\, \tilde{\sigma}_C^2. \end{aligned}$$

Thus

$$\lim_{n\to\infty} \mathrm{P}\,(\hat{v}_n \in T) = \lim_{n\to\infty} \mathrm{P}\,(\sqrt{n}\,(\hat{x}_{n2} - \tilde{f}_1(\hat{x}_{n1})) > 0)$$

$$= \mathrm{P}(Z' > 0)$$

$$= \tfrac{1}{2},$$

as required.

The following corollary is an immediate consequence of Theorem 4.2, part (a) (iii), and can be used to construct confidence sets for μ^S and μ^F. Let $\Sigma_{S,v} = G_S^{(1)}(v) D G_S^{(1)}(v)^\top$ and define $\Sigma_{F,v}$ similarly.

Corollary 4.1

If $\mu \notin L$ then, as $n \to \infty$,

$$n\,(\hat{\mu}_n^S - \mu^S)^\top \Sigma_{S,v}^{-1} (\hat{\mu}_n^S - \mu^S) \xrightarrow{D} \chi_2^2,$$

and

$$n\,(\hat{\mu}_n^F - \mu^F)^\top \Sigma_{F,v}^{-1} (\hat{\mu}_n^F - \mu^F) \xrightarrow{D} \chi_2^2.$$

Since $F(x) = 1 - \exp(-x/2)$ is the distribution function of a χ^2_2 random variable and hence $F^{-1}(1 - \alpha) = -2 \ln \alpha$, it follows that the ellipses

$$\{ \mu^S \in \mathbb{R}^2 : n(\hat{\mu}_n^S - \mu^S)^\top \Sigma_{S,v}^{-1} (\hat{\mu}_n^S - \mu^S) \leq -2 \ln \alpha \} \qquad (4.18)$$

and

$$\{ \mu^F \in \mathbb{R}^2 : n(\hat{\mu}_n^F - \mu^F)^\top \Sigma_{F,v}^{-1} (\hat{\mu}_n^F - \mu^F) \leq -2 \ln \alpha \}$$

are approximate $100(1 - \alpha)\%$ confidence sets for μ^S and μ^F respectively.

In practice, $\Sigma_{S,v}$ and $\Sigma_{F,v}$ will be unknown and hence will have to be estimated from the data. The matrix $\Sigma_{S,v}$, for example, can be estimated by setting $\hat{\Sigma}_{S,v} = G_S^{(1)}(\hat{v}_n)\hat{D}G_S^{(1)}(\hat{v}_n)^\top$, where $\hat{D}$ is obtained by replacing the variances $\tilde{\sigma}_O^2$ and $\tilde{\sigma}_C^2$ in the definition of D by their corresponding sample variances. Alternatively, $\hat{D}$ could be estimated from equations (4.4) and (4.6) by replacing (μ_O, μ_C) with $\hat{\mu}_n^S$. In either case, $\hat{\Sigma}_{S,v}$ and $\hat{\Sigma}_{F,v}$ are strongly consistent estimators of $\Sigma_{S,v}$ and $\Sigma_{F,v}$, respectively, and application of Slutsky's Theorem shows that Corollary 4.1 still holds with $\Sigma_{S,v}$ and $\Sigma_{F,v}$ replaced by $\hat{\Sigma}_{S,v}$ and $\hat{\Sigma}_{F,v}$, respectively.

4.2.4 Approximations based on Negative Exponential Distributions

4.2.4.1 Approximation derived by ignoring Undetected Sojourns

In the approximation described in section 4.1.2.2.1, the positive contribution of undetected sojourn lengths is ignored in equation (4.1). Therefore the means given by equation (4.8) and (4.9) are less than the true means. Yeo *et al.* (1988) show that, under this approximation, whenever the moment equations

$$\mu_O \exp(\tau_C/\mu_C) = \bar{u} \tag{4.19a}$$

and

$$\mu_C \exp(\tau_O/\mu_O) = \bar{v} \tag{4.19b}$$

have only one solution, then that solution lies on the hyperbola $\tilde{L}$ say, given by $\mu_O\mu_C = \tau_O\tau_C$, and that there is a one-to-one correspondence between values of ν and μ for which equations (4.19a) and (4.19b) have a single solution. Under this mapping, $\tilde{L}$ is transformed to a strictly decreasing convex curve $\tilde{O}$ say, given by $\nu_C = j(\nu_O)$ say, where $j(\nu_O)$ approaches infinity (zero) as ν_O approaches zero (infinity). Further, Yeo *et al.* (1988) prove that equations (4.19a) and (4.19b) have two (zero) solutions whenever ν lies above (below) $\tilde{O}$ and that the curves $\tilde{L}$ and $\tilde{O}$ lie strictly below the curves L and O, respectively. It is clear from their

argument that whenever there are two solutions of equations (4.19a) and (4.19b), they lie on either side of the curve $\tilde{L}$. They also show that these two solutions (μ_O^F, μ_C^F) and (μ_O^S, μ_C^S) say, have the property that $\mu_O^F < \mu_O^S$ and $\mu_C^F < \mu_C^S$.

Let $\tilde{T} = \{(x, y) \in (\mathbb{R}^+)^2 : y > j(x)\}$. By the strong law of large numbers,

$$\hat{\nu}_n \xrightarrow{\text{a.s.}} \nu \quad \text{as} \quad n \to \infty.$$

Since any value of μ is mapped by equations (4.3) and (4.5) to a value of ν that lies on or above O, it follows that ν lies strictly above $\tilde{O}$ and hence $\nu \in \tilde{T}$. Since $\tilde{T}$ is an open set, it follows that, for all μ,

$$\mathbf{P}(\hat{\nu}_n \in \tilde{T} \text{ for all sufficiently large } n) = 1.$$

Let $\tilde{S} = \{(x, y) \in (\mathbb{R}^+)^2 : xy > \tau_O \tau_C\}$ and $\tilde{F} = \{(x, y) \in (\mathbb{R}^+)^2 : xy < \tau_O \tau_C\}$. Let $\tilde{h}(\mu) = (\tilde{h}_O(\mu), \tilde{h}_C(\mu))^\top = (\nu_1, \nu_2)^\top$ where the functions $\tilde{h}_O$ and $\tilde{h}_C$ are determined by equations (4.8) and (4.9), and let $\tilde{h}_S$ and $\tilde{h}_F$ be the map $\tilde{h}$ restricted to the sets $\tilde{S}$ and $\tilde{F}$, respectively. Then $\tilde{h}_S$ ($\tilde{h}_F$) is a bijection from $\tilde{S}$ ($\tilde{F}$) to $\tilde{T}$, with inverse function $\tilde{g}_S$ ($\tilde{g}_F$) say. By the Inverse Function Theorem for $\mathbb{R}^2$ (Stromberg (1981)), $\tilde{g}_S$ and $\tilde{g}_F$ are both of class $C^{(\infty)}$ on $\tilde{T}$. Hence

$$\hat{\mu}_n^S = \tilde{g}_S(\hat{\nu}_n) \xrightarrow{\text{a.s.}} \tilde{g}_S(\nu) \neq \mu^S \quad \text{as} \quad n \to \infty,$$

with a similar result holding for $\hat{\mu}_n^F$. Thus the approximation is asymptotically biased.

Now, the function $\tilde{g}_S$ ($\tilde{g}_F$) maps points in $\tilde{T}$ to points in $\tilde{S}$ ($\tilde{F}$) and maps points on the curve $\tilde{O}$ to points on the curve $\tilde{L}$. In particular, points in $\tilde{T} \cup \tilde{O}$ which lie strictly below O are mapped by $\tilde{g}_S$ ($\tilde{g}_F$) to a connected set $\tilde{L}_S$ ($\tilde{L}_F$) say, which is bounded below (above) by $\tilde{L} \subset \tilde{L}_S$ ($\tilde{L}_F$). Since, asymptotically, $\hat{\boldsymbol{v}}_n$ lies above O and $\tilde{g}_S$ and $\tilde{g}_F$ are bijections, it follows that, asymptotically, $\tilde{g}_S(\hat{\boldsymbol{v}}_n)$ and $\tilde{g}_F(\hat{\boldsymbol{v}}_n)$ do not lie in the connected set $\tilde{L}_S \cup \tilde{L}_F$. Hence there is a set of values which, asymptotically, cannot be taken by estimates of $\boldsymbol{\mu}$ under the approximation derived by ignoring undetected sojourns.

By the Central Limit Theorem

$$\sqrt{n}\,(\hat{\boldsymbol{v}}_n - \boldsymbol{v}) \xrightarrow{D} \boldsymbol{Z} \quad \text{as} \quad n \to \infty,$$

where $\boldsymbol{Z} \sim \mathrm{N}(\boldsymbol{0}, D)$. Now using the delta-method (Andersen *et al.* (1992)), it follows that

$$\sqrt{n}\begin{pmatrix} \hat{\mu}_n^S - \tilde{g}_S(\boldsymbol{v}) \\ \hat{\mu}_n^F - \tilde{g}_F(\boldsymbol{v}) \end{pmatrix} \xrightarrow{D} \begin{pmatrix} \tilde{G}_S^{(1)}(\boldsymbol{v}) \\ \tilde{G}_F^{(1)}(\boldsymbol{v}) \end{pmatrix} \boldsymbol{Z} \quad \text{as} \quad n \to \infty,$$

where $\tilde{G}_S^{(1)}(\boldsymbol{v})$ and $\tilde{G}_F^{(1)}(\boldsymbol{v})$ are given by expressions similar to those for $G_S^{(1)}(\boldsymbol{v})$

and $G_F^{(1)}(v)$, but with h_O and h_C replaced by $\tilde{h}_O$ and $\tilde{h}_C$, respectively, throughout. Thus

$$\sqrt{n}\begin{pmatrix} \hat{\mu}_n^S - \tilde{g}_S(v) \\ \hat{\mu}_n^F - \tilde{g}_F(v) \end{pmatrix} \xrightarrow{D} N(\mathbf{0}, \tilde{\Sigma}) \text{ as } n \to \infty,$$

where

$$\tilde{\Sigma} = \begin{pmatrix} \tilde{G}_S^{(1)}(v) D \tilde{G}_S^{(1)}(v)^\top & \tilde{G}_S^{(1)}(v) D \tilde{G}_F^{(1)}(v)^\top \\ \tilde{G}_F^{(1)}(v) D \tilde{G}_S^{(1)}(v)^\top & \tilde{G}_F^{(1)}(v) D \tilde{G}_F^{(1)}(v)^\top \end{pmatrix}.$$

Table 1 of Yeo *et al.* (1988) gives maximum likelihood estimates of μ_O and μ_C, under this approximation and also under the approximation using exponential distributions with true means, for three examples taken from ion channel literature. Yeo *et al.* (1988) point out that, in their examples, under this approximation, the estimated values of the slow solution are slight over-estimates, and those of the fast solution are substantial under-estimates, compared to the estimates under the approximation using exponential distributions with true means. These results are broadly consistent with our results displayed in Table 4.2 of section 4.3.2.3.2.

4.2.4.2 Confidence Sets based on the Approximation using Exponential Distributions with True Means

Now consider the approximate model described in section 4.1.2.2.2 in which the adjusted observed open and closed sojourns, $\tilde{U}$ and $\tilde{V}$, are assumed to follow negative exponential distributions with means ν_O and ν_C respectively. Thus $\tilde{U}$ and $\tilde{V}$ are now assumed to have variances ν_O^2 and ν_C^2 respectively and Theorem 4.2 and Corollary 4.1 hold for this approximate model provided that D is replaced by $D_1 = \text{diag}(\nu_O^2, \nu_C^2)$. In this section, the asymptotic accuracy of the resulting approximate confidence sets is assessed. Note that these approximate confidence sets coincide with those of Clarke *et al.* (1993) which were derived using a quite different approach.

For ease of exposition, it is convenient to restrict attention to confidence sets for μ^S. Fix $\alpha \in (0, 1)$ and let $I_{n,S}$ be the confidence set estimator for μ^S with coverage probability $1 - \alpha$, given in expression (4.18) for the exact model but with $\Sigma_{S,\nu}$ replaced by $\hat{\Sigma}_{S,\nu}$. Then

$$I_{n,S} = \{ \mu \in \mathbb{R}^2 : n(\hat{\mu}_n^S - \mu)^\top \hat{\Sigma}_{S,\nu}^{-1}(\hat{\mu}_n^S - \mu) \leq F^{-1}(1 - \alpha) \},$$

where $F^{-1}(1 - \alpha) = -2 \ln \alpha$. Let $I'_{n,S}$ be the equivalent set based on the approximate model. Then

$$I'_{n,S} = \{\mu \in \mathbb{R}^2 : n(\hat{\mu}_n^S - \mu)^\top (\hat{\Sigma}'_{S,v})^{-1} (\hat{\mu}_n^S - \mu) \le F^{-1}(1-\alpha)\},$$

where $\hat{\Sigma}'_{S,v} = G_S^{(1)}(\hat{\nu}_n)\hat{D}_1 G_S^{(1)}(\hat{\nu}_n)^\top$ and $\hat{D}_1 = \mathrm{diag}(\hat{\nu}_{nO}^2, \hat{\nu}_{nC}^2)$.

Let $A_{n,S} = \pi F^{-1}(1-\alpha)\,|\hat{\Sigma}_{S,v}|^{1/2}$ and $A'_{n,S} = \pi F^{-1}(1-\alpha)\,|\hat{\Sigma}'_{S,v}|^{1/2}$ be the areas of $I_{n,S}$ and $I'_{n,S}$ respectively. Then $A_{n,S} / A'_{n,S} = |\hat{D}|^{1/2} / |\hat{D}_1|^{1/2}$, which converges almost surely to $c_O c_C$ as $n \to \infty$, where $c_O = \tilde{\sigma}_O^S / \nu_O$ and $c_C = \tilde{\sigma}_C^S / \nu_C$ are respectively the coefficients of variation of adjusted observed open and closed sojourns when $(\mu_O, \mu_C) = (\mu_O^S, \mu_C^S)$. From equations (4.3) and (4.4),

$$\begin{aligned} c_O^2 &= \nu_O^{-2}[(\nu_O + \mu_C^S)^2 - 2\mu_O^S\mu_C^S \exp(\tau_C/\mu_C^S) - (\mu_C^S)^2 - \tau_C^2] \\ &= 1 + 2(\mu_C^S/\nu_O)^2 [\exp(\tau_C/\mu_C^S) - 1 - \tau_C/\mu_C^S - \tfrac{1}{2}(\tau_C/\mu_C^S)^2] \\ &= 1 + 2(\mu_C^S/\nu_O)^2 \sum_{k=3}^{\infty} (\tau_C/\mu_C^S)^k / k!, \end{aligned} \tag{4.20}$$

with a similar expression holding for c_C^2. Hence $c_O > 1$ and $c_C > 1$, and so the confidence sets based on the approximate model will tend to have a smaller area than those based on the exact model.

Let $\psi_n(\alpha)$ be the coverage probability of the approximate confidence set $I'_{n,S}$ under the exact model with $\mu = \mu^S$, and let $\psi(\alpha) = \lim_{n\to\infty}\{\psi_n(\alpha)\}$. Since $\hat{D}_1$ is a strongly consistent estimator of D_1,

$$\psi(\alpha) = \lim_{n\to\infty}[\mathbf{P}\{\, n(\hat{\mu}_n^S - \mu^S)^\top (\hat{\Sigma}'_{S,\nu})^{-1}(\hat{\mu}_n^S - \mu^S) \le F^{-1}(1-\alpha)\,\}]$$

$$= \lim_{n\to\infty}[\mathbf{P}\{\, \boldsymbol{Y}_n^\top \hat{D}_1^{-1}\boldsymbol{Y}_n \le F^{-1}(1-\alpha)\,\}]$$

$$= \lim_{n\to\infty}[\mathbf{P}\{\, \boldsymbol{Y}_n^\top D_1^{-1}\boldsymbol{Y}_n \le F^{-1}(1-\alpha)\,\}],$$

where $\boldsymbol{Y}_n = \{G_S^{(1)}(\boldsymbol{\nu})\}^{-1}(\hat{\mu}_n^S - \mu^S)\sqrt{n}$. By Theorem 4.2, part (a)(iii), $\boldsymbol{Y}_n \xrightarrow{D} \boldsymbol{Y}$ say, as $n \to \infty$, where $\boldsymbol{Y} \sim N(\mathbf{0}, D)$. Hence $D^{1/2}\boldsymbol{Y} \sim N(\mathbf{0}, I)$, where I is the 2×2 identity matrix, and $D^{1/2}\boldsymbol{Y} = \boldsymbol{Z} = (Z_O, Z_C)^\top$ say, where Z_O and Z_C are independent standard normal random variables. It follows that

$$\boldsymbol{Y}^\top D_1^{-1}\boldsymbol{Y} = (D^{1/2}\boldsymbol{Z})^\top D_1^{-1}(D^{1/2}\boldsymbol{Z})$$

$$= \boldsymbol{Z}^\top D^{1/2} D_1^{-1} D^{1/2}\boldsymbol{Z}$$

$$= \boldsymbol{Z}^\top \begin{pmatrix} (\tilde{\sigma}_O^S/\nu_O)^2 & 0 \\ 0 & (\tilde{\sigma}_C^S/\nu_C)^2 \end{pmatrix} \boldsymbol{Z}$$

$$= \boldsymbol{Z}^\top \begin{pmatrix} c_O^2 & 0 \\ 0 & c_C^2 \end{pmatrix} \boldsymbol{Z}$$

$$= c_O^2 Z_O^2 + c_C^2 Z_C^2 .$$

Since $\boldsymbol{Y}_n \xrightarrow{D} \boldsymbol{Y}$ as $n \to \infty$, it follows that $\boldsymbol{Y}_n^\top D_1^{-1}\boldsymbol{Y}_n \xrightarrow{D} \boldsymbol{Y}^\top D_1^{-1}\boldsymbol{Y}$ as $n \to \infty$ and so

$$\psi(\alpha) = \lim_{n\to\infty}[\mathbf{P}\{\, \boldsymbol{Y}_n^\top D_1^{-1}\boldsymbol{Y}_n \le F^{-1}(1-\alpha)\,\}]$$

$$= \mathbf{P}\{\, c_O^2 Z_O^2 + c_C^2 Z_C^2 \le F^{-1}(1-\alpha)\,\}. \qquad (4.21)$$

By conditioning on Z_O, equation (4.21) may be expressed as

$$\begin{aligned}\psi(\alpha) &= \int_{-\sqrt{a}c_O^{-1}}^{\sqrt{a}c_O^{-1}} \mathbf{P}\left\{-c_C^{-1}\sqrt{a - c_O^2 Z_O^2} < Z_C \right. \\ &\qquad \left. < c_C^{-1}\sqrt{a - c_O^2 Z_O^2} \;\middle|\; Z_O = x\right\} \phi(x)\,dx \\ &= \int_{-\sqrt{a}c_O^{-1}}^{\sqrt{a}c_O^{-1}} \left[\Phi\left(c_C^{-1}\sqrt{a - c_O^2 x^2}\right) - \Phi\left(-c_C^{-1}\sqrt{a - c_O^2 x^2}\right)\right] \phi(x)\,dx \\ &= 2\int_0^{\sqrt{a}c_O^{-1}} \left[2\,\Phi\left(c_C^{-1}\sqrt{a - c_O^2 x^2}\right) - 1\right] \phi(x)\,dx, \end{aligned} \tag{4.22}$$

where $a = F^{-1}(1 - \alpha)$, and $\phi(x)$ and $\Phi(x)$ are the standard normal density and distribution functions, respectively. Thus $\psi(\alpha)$ can be calculated numerically by using a quadrature procedure.

Bounds for $\psi(\alpha)$ can be obtained as follows. Let c_1 and c_2 be respectively the minimum and maximum of c_O^{-2} and c_C^{-2}. Then

$$c_2^{-1}(Z_O^2 + Z_C^2) \le c_O^2 Z_O^2 + c_C^2 Z_C^2 \le c_1^{-1}(Z_O^2 + Z_C^2),$$

and so, from equation (4.21),

$$\begin{aligned}&\mathbf{P}\left[c_1^{-1}(Z_O^2 + Z_C^2) \le F^{-1}(1 - \alpha)\right] \le \psi(\alpha) \\ &\qquad \le \mathbf{P}\left[c_2^{-1}(Z_O^2 + Z_C^2) \le F^{-1}(1 - \alpha)\right].\end{aligned}$$

Hence

$$F[c_1 F^{-1}(1 - \alpha)] \leq \psi(\alpha) \leq F[c_2 F^{-1}(1 - \alpha)].$$

But $F(x) = 1 - \exp(-x / 2)$ and $F^{-1}(1 - \alpha) = -2 \ln \alpha$. Thus

$$1 - \alpha^{c_1} \leq \psi(\alpha) \leq 1 - \alpha^{c_2} \qquad (0 < \alpha < 1). \tag{4.23}$$

Since $c_O > 1$ and $c_C > 1$, it follows immediately that $c_1 \leq c_2 < 1$ and hence the confidence sets based on the approximate model will asymptotically have coverage probabilities that are less than the intended $1 - \alpha$. Note from equation (4.20) that, as $\mu_C^F < \mu_C^S$, c_O will be larger for the fast solution than for the slow solution. A similar conclusion holds for c_C. Thus the asymptotic coverage probabilities in the approximate model will be worse for the fast solution μ^F than for the slow solution μ^S.

In most practical situations c_O and c_C will be very close to one (see the numerical examples in section 4.2.5). In such circumstances a good approximation to $\psi(\alpha)$ is obtained by using its Taylor series expansion in (c_O, c_C) about $(1, 1)$ as follows. Let $Y_O = c_O Z_O$ and $Y_C = c_C Z_C$. Then Y_O and Y_C are independent with $Y_O \sim N(0, c_O^2)$ and $Y_C \sim N(0, c_C^2)$, and

$$\psi(\alpha) = \mathbf{P}[(Y_O^2 + Y_C^2) \leq F^{-1}(1 - \alpha)].$$

Now (Y_O, Y_C) has joint probability density function $f_{Y_O Y_C}(y_O, y_C)$ say, where

$$f_{Y_O Y_C}(y_O, y_C) = (2\pi c_O c_C)^{-1} \exp(-\tfrac{1}{2} y_O^2 c_O^{-2} - \tfrac{1}{2} y_C^2 c_C^{-2})$$

for $(-\infty < y_O, y_C < \infty)$. Therefore

$$\psi(\alpha) = \int_D (2\pi c_O c_C)^{-1} \exp(-\tfrac{1}{2} y_O^2 c_O^{-2} - \tfrac{1}{2} y_C^2 c_C^{-2})\, dy_O\, dy_C, \qquad (4.24)$$

where $D = \{(y_O, y_C) : y_O^2 + y_C^2 \le F^{-1}(1 - \alpha)\}$. Let $\psi(\alpha) = \psi(c_O, c_C)$. Then, by Taylor's theorem,

$$\psi(c_O, c_C) \approx \psi(1, 1) + (c_O - 1)\,\psi_{C_O}(1, 1) + (c_C - 1)\,\psi_{C_C}(1, 1), \qquad (4.25)$$

where, for example, the subscript c_O denotes partial differentiation with respect to c_O. Differentiating (4.24) partially with respect to c_O yields

$$\frac{\partial \psi(\alpha)}{\partial c_O} = \int_D (-2\pi c_O^2 c_C)^{-1} \exp(-\tfrac{1}{2} y_O^2 c_O^{-2} - \tfrac{1}{2} y_C^2 c_C^{-2})$$

$$+ (2\pi c_O c_C)^{-1} \exp(-\tfrac{1}{2} y_O^2 c_O^{-2} - \tfrac{1}{2} y_C^2 c_C^{-2})\,(y_O^2 / c_O^3)\, dy_O\, dy_C,$$

and setting $(c_O, c_C) = (1, 1)$ gives

$$\left.\frac{\partial \psi(\alpha)}{\partial c_O}\right|_{(1,\,1)} = \int_D (-2\pi)^{-1} \exp(-\tfrac{1}{2}(y_O^2 + y_C^2))\, dy_O\, dy_C$$

$$+ \int_D (2\pi)^{-1} y_O^2 \exp(-\tfrac{1}{2}(y_O^2 + y_C^2))\, dy_O\, dy_C. \qquad (4.26)$$

By symmetry, the second integral in equation (4.26) can be rewritten so that

$$\left.\frac{\partial \psi(\alpha)}{\partial c_O}\right|_{(1,\,1)} = -\,\mathbf{P}[Z_O^2 + Z_C^2 \le F^{-1}(1-\alpha)] + \tfrac{1}{2}\int_D (2\pi)^{-1}(y_O^2 + y_C^2)\exp(-\tfrac{1}{2}(y_O^2 + y_C^2))\,dy_O\,dy_C,$$

and transforming to polar coordinates gives

$$\left.\frac{\partial \psi(\alpha)}{\partial c_O}\right|_{(1,\,1)} = -\,\mathbf{P}[Z_O^2 + Z_C^2 \le F^{-1}(1-\alpha)] + \tfrac{1}{2}\int_{r=0}^{\sqrt{F^{-1}(1-\alpha)}}\int_{\theta=0}^{2\pi}(2\pi)^{-1} r^3 \exp(-\tfrac{1}{2}r^2)\,d\theta\,dr.$$

Calculating the second integral with respect to θ, and then substituting $u = \frac{1}{2}r^2$ and recalling that $\frac{1}{2}F^{-1}(1-\alpha) = -\ln\alpha$, gives

$$\left.\frac{\partial \psi(\alpha)}{\partial c_O}\right|_{(1,\,1)} = -F[F^{-1}(1-\alpha)] + \int_0^{-\ln\alpha} u\,e^{-u}\,du$$

$$= -(1-\alpha) + [\alpha\ln\alpha - (\alpha - 1)]$$

$$= \alpha\ln\alpha.$$

By symmetry,

$$\left.\frac{\partial \psi(\alpha)}{\partial c_C}\right|_{(1,\,1)} = \left.\frac{\partial \psi(\alpha)}{\partial c_O}\right|_{(1,\,1)}.$$

Substituting these results into expression (4.25) yields

$$\psi(\alpha) \approx (1 - \alpha) + (c_O + c_C - 2)\ \alpha \ln \alpha \qquad (4.27)$$

for $0 < \alpha < 1$.

4.2.5 Numerical Examples

The above theory is now illustrated using simulated data for five examples, taken from the ion channel literature, that have been considered previously by Milne *et al.* (1989). They are CS from Colquhoun and Sigworth (1983), BM_1 and BM_2 based on Blatz and Magleby (1986), and P_1 and P_2 from Prod'hom *et al.* (1987). The results are displayed in Table 4.1 and Figure 4.2.

For each example, the sample mean adjusted open and closed sojourn times $\hat{\nu}_O$ and $\hat{\nu}_C$ are given in Table 4.1, together with the detection limits $\tau = \tau_O = \tau_C$ and the slow and fast method-of-moments estimates, $\hat{\mu}^S$ and $\hat{\mu}^F$. All the values are in milliseconds. For each of the two estimates $\hat{\mu}^S$ and $\hat{\mu}^F$, Table 4.1 also gives the coefficients of variation c_O and c_C, calculated by assuming that the estimates are the true values of μ, and the corresponding asymptotic coverage probability $\psi(0.05)$, calculated numerically from equation (4.22), of the 95% confidence set for μ based on the approximate model described in section 4.1.2.2.2. The Taylor series approximation to $\psi(0.05)$ obtained in approximation (4.27) and the lower

and upper bounds for $\psi(0.05)$, given by inequalities (4.23), are also shown.

Solution	c_O	c_C	$\psi(0.05)$	Approx-imation to $\psi(0.05)$	Lower bound for $\psi(0.05)$	Upper bound for $\psi(0.05)$
Example CS: $\hat{\nu}_O = 0.4$, $\hat{\nu}_C = 1.8$, $\tau = 0.2$						
Slow $\mu = (0.2990, 0.8787)$	1.010	1.002	0.9482	0.9483	0.9470	0.9495
Fast $\mu = (0.1063, 0.2148)$	1.049	1.007	0.9413	0.9417	0.9344	0.9480
Example BM_1: $\hat{\nu}_O = 2.790$, $\hat{\nu}_C = 0.1160$, $\tau = 0.1$						
Slow $\mu = (1.0034, 0.1003)$	1.000	1.013	0.9480	0.9481	0.9462	0.9499
Fast $\mu = (0.1443, 0.0359)$	1.001	1.098	0.9334	0.9351	0.9166	0.9496
Example BM_2: $\hat{\nu}_O = 1.678$, $\hat{\nu}_C = 0.2262$, $\tau = 0.1$						
Slow $\mu = (0.9997, 0.2000)$	1.000	1.003	0.9494	0.9494	0.9490	0.9499
Fast $\mu = (0.0800, 0.0364)$	1.004	1.056	0.9405	0.9411	0.9319	0.9489
Example P_1: $\hat{\nu}_O = 1.165$, $\hat{\nu}_C = 0.125$, $\tau = 0.035$						
Slow $\mu = (0.8647, 0.1194)$	1.000	1.001	0.9499	0.9499	0.9498	0.9500
Fast $\mu = (0.0190, 0.0093)$	1.002	1.040	0.9434	0.9437	0.9372	0.9494
Example P_2: $\hat{\nu}_O = 0.445$, $\hat{\nu}_C = 0.145$, $\tau = 0.035$						
Slow $\mu = (0.3352, 0.1289)$	1.000	1.001	0.9498	0.9498	0.9497	0.9499
Fast $\mu = (0.0191, 0.0128)$	1.007	1.030	0.9444	0.9446	0.9407	0.9480

Table 4.1. Coverage probabilities for confidence sets derived from the approximate model.

For each example, $\psi(0.05)$ is very close to the intended 0.95, indicating that the approximation is very good. Also the Taylor series approximation to $\psi(0.05)$ is always extremely good, as are the lower and upper bounds. All these observations are a consequence of the fact that both c_O and c_C are always very close to one. Note that, as predicted by the theory, these results are always slightly worse for the fast solution than for the slow solution.

The number of observed open and closed sojourns on which $\hat{\nu}$ was based was not generally given in these examples. Figure 4.2 shows 95% confidence sets for μ^S and μ^F for the example BM_1, assuming that $n = 5000$, which is quite typical for single-channel experiments. The confidence sets based on the approximate model are too small, though the difference is very slight, especially for the slow solution.

In the above, we have restricted attention to confidence sets with $\alpha = 0.05$. However, similar results hold for all values of α. Although the approximate model clearly gives very good results in all the examples that we have considered, we still recommend the use of confidence sets based on the exact model, as they are no more difficult to implement.

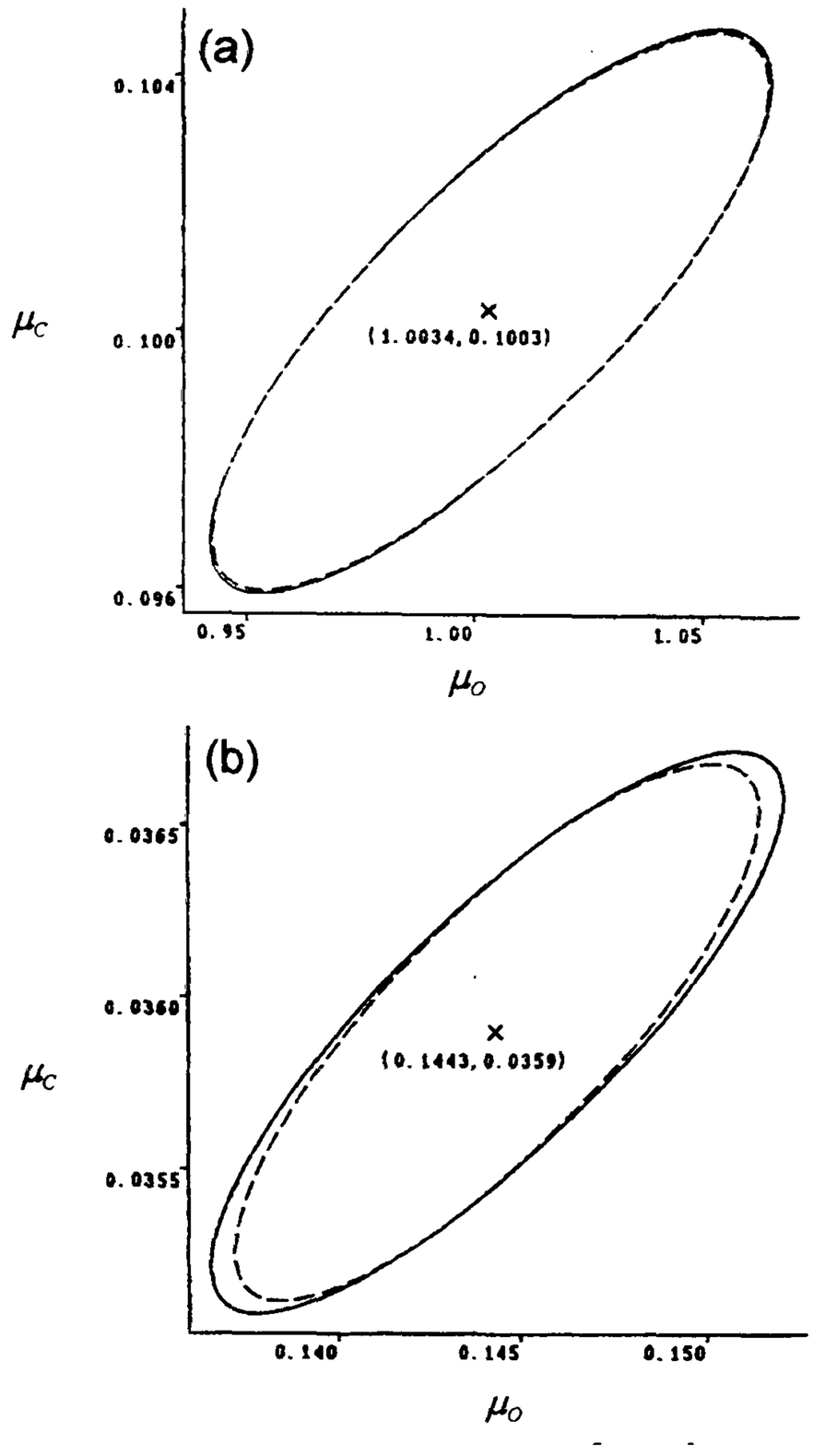

Figure 4.2. (a) Simultaneous confidence sets for the parameters μ_O^S and μ_C^S based on the BM_1 values $\hat{v}_O = 2.790$ ms, $\hat{v}_C = 0.1160$ ms, $\tau_O = \tau_C = 0.1$ and sample size $n = 5000$. The plot shows the 95% confidence set for $\boldsymbol{\mu}^S$ derived from expression (4.18) for the exact model (solid line) and the equivalent confidence set based on the approximate model (dotted line). The method-of-moments estimate $\hat{\boldsymbol{\mu}}_n^S = (1.0034, 0.1003)^\top$ is marked. (b) Simultaneous confidence sets equivalent to those shown in (a), but for the parameters μ_O^F and μ_C^F. The method-of-moments estimate $\hat{\boldsymbol{\mu}}_n^F = (0.1443, 0.0359)^\top$ is marked.

4.3 Resolving the Identifiability Problem

In this section, we discuss various methods of resolving the identifiability problem. We first show that in the method, first proposed by Colquhoun and Sigworth (1983), which involves obtaining estimates of (μ_O, μ_C) for several samples, each with a different detection limit, one estimate is approximately the same for each sample, while the other varies significantly. A similar argument can be used to justify a new method of distinguishing between the two solutions in which maximum likelihood estimates are obtained for several samples, each with a different agonist concentration. This new method is then described, together with results of simulation studies carried out under a variety of conditions. Finally, another new method which uses observed open and closed sojourn length sample variances to discriminate between the two solutions is presented, supported by numerical examples.

4.3.1 Introduction

Of the proposed methods (mentioned in section 4.1.3.2) of overcoming the identifiability problem, two are methods which distinguish between the two solutions on the basis of more than one sample. One of these methods involves using samples with different detection limits and the other involves using samples with different agonist concentrations. Consider the first of these methods and

suppose for ease of exposition that $\tau_O = \tau_C$ (= τ say) and note that the sets L, S and F defined in the statement of Theorem 4.1 depend implicitly on τ. Let $\mu^* = (\mu_O^*, \mu_C^*)$ where μ_O^* and μ_C^* are chosen so that $\mu^* = \tau\mu$. It follows from the shape of the curve $J(\mu) = 0$ that, for fixed μ^*, there exists $\tau_X > 0$ such that $(\mu_O^*/\tau_X, \mu_C^*/\tau_X) \in L$. Since $\mu \in S$ if and only if $\mu_O^*/\tau > \mu_O^*/\tau_X$ or $\mu_C^*/\tau > \mu_C^*/\tau_X$, it follows that $\mu \in S$ if and only if $\tau < \tau_X$. Similarly $\mu \in F$ if and only if $\tau > \tau_X$ and $\mu \in L$ if and only if $\tau = \tau_X$. Now suppose that $\tau < \tau_X$, so that $\mu^S = (\mu_O^S, \mu_C^S)$ is the true value of μ which does not vary as τ varies and $\mu^F = (\mu_O^F, \mu_C^F) = g_F[h_S(\mu^S)]$ is the corresponding false solution. Now the maps g_F and h_S depend implicitly on τ. We will now show that μ^F varies as τ varies. From equation (4.3),

$$v_O + \tau = (\mu_O^S + \mu_C^S)\exp(\tau/\mu_C^S) - \mu_C^S = (\mu_O^F + \mu_C^F)\exp(\tau/\mu_C^F) - \mu_C^F$$

so that

$$\mu_O^F = [(\mu_O^S + \mu_C^S)\exp(\tau/\mu_C^S) - \mu_C^S + \mu_C^F]\exp(-\tau/\mu_C^F) - \mu_C^F. \qquad (4.28)$$

Clearly, either $\frac{d\mu_C^F}{d\tau}$ is non-zero and μ_C^F varies as τ varies, or $\frac{d\mu_C^F}{d\tau}$ is zero. In the latter case, differentiation of equation (4.28) setting $\frac{d\mu_C^F}{d\tau} = 0$ yields

$$\frac{d\mu_O^F}{d\tau} = -\exp(-\tau/\mu_C^F)\,(\mu_C^F\,\mu_C^S)^{-1}\,[(\mu_O^S + \mu_C^S)\exp(\tau/\mu_C^S) - \mu_C^S] \times (\mu_C^S - \mu_C^F)$$

and $\frac{d\mu_O^F}{d\tau}$ is clearly negative since $\mu_C^S > \mu_C^F$. Hence μ_O^F decreases as τ increases.

Therefore μ^F varies as τ varies whenever μ lies in S. Similarly it can be shown that if $\tau > \tau_X$, and therefore the true solution is the fast solution μ^F, that the slow solution μ^S varies as τ varies. This is illustrated for the case $\mu^T = (0.8787, 0.2990)$ by Figure 3 of Yeo *et al.* (1988). In practice, μ^S and μ^F are estimated from the data. However, the consistency results of Theorem 4.2, part (a) (ii), imply that taking samples with different values of τ will enable us to distinguish between the true and false solutions, provided that the sample sizes are sufficiently large. Similar arguments to the above hold when the agonist concentration is varied as in the method described in the next section.

4.3.2 Varying Agonist Concentration

4.3.2.1 Theory

Agonist concentration dependence of channel gating kinetics is incorporated in the two-state Markov model described in section 4.1.1 as follows. Let C represent the closed (unliganded) state of the channel and OA the open (mono-liganded) state. Let the channel opening rate be a/μ_C where a is the agonist concentration and let the channel closing rate be $1/\mu_O$. Then the opening rate is dependent on the agonist concentration, whereas the closing rate is constant. This can be represented as

$$\mathbf{C} \underset{1/\mu_O}{\overset{a/\mu_C}{\rightleftharpoons}} \mathbf{OA}\,. \tag{4.29}$$

Since this is simply the model described in section 4.1.1 with μ_C replaced by μ_C/a, the theory of sections 4.1 and 4.2 hold for this model. In particular, let $f_O^{(1)}(u), f_O^{(2)}(u)$ and $f_O^{(3)}(u)$ denote the probability density functions for adjusted observed open sojourns under the approximations described in sections 4.1.2.2.1, 4.1.2.2.2 and 4.1.2.2.3 respectively with μ_C replaced by μ_C/a in each case. Let $f_C^{(1)}(v), f_C^{(2)}(v)$ and $f_C^{(3)}(v)$ denote the corresponding probability density functions for adjusted observed closed sojourns.

4.3.2.2 Maximum Likelihood Estimation

The model parameters μ_O and μ_C can be estimated using maximum likelihood methods (Horn and Lange (1983), Colquhoun and Sigworth (1983), Ball and Sansom (1989)) based on any of the approximate density functions $f_O^{(1)}(u), f_O^{(2)}(u)$ and $f_O^{(3)}(u)$ ($f_C^{(1)}(v), f_C^{(2)}(v)$ and $f_C^{(3)}(v)$) of adjusted observed openings (closings). As successive openings (closings) are independent for the model in (4.29) (Fredkin *et al.* (1985)), one form of the normalised log-likelihood (see Appendix A and Yeo *et al.* (1988)) is given by

$$l(\mu) = m^{-1} \sum_{i=1}^{m} [\ln f_O(u_i, \mu) + \ln f_C(v_i, \mu)], \tag{4.30}$$

where f_O and f_C represent the probability density functions of adjusted observed openings and closings, respectively, under any one of the three approximations and where there are m adjusted observed open-closed time pairs (u_i, v_i). Thus maximisation of $l(\mu)$ provides a method for estimating μ_O and μ_C.

In the gating model (4.29), the agonist concentration, a, is an experimentally controllable variable. We consider two basic approaches to likelihood estimation. In the first approach μ is estimated independently at each value of a and the behaviour of the resultant estimates is examined. In the second approach a global log-likelihood, corresponding to simultaneous fitting of the model to data obtained at n different agonist concentrations a_j $(j = 1, ..., n)$, is maximised in order to estimate μ. The normalised global log-likelihood is given by

$$l_G(\mu) = \frac{\sum_{j=1}^{n} m_j \, l(a_j, \mu)}{\sum_{j=1}^{n} m_j}, \tag{4.31}$$

where $l(a_j, \mu)$ is the log-likelihood, as defined in equation (4.30), at a single agonist concentration a_j and m_j is the corresponding number of open-closed time pairs.

Parameter error estimates and correlations are obtained by inversion of the corresponding Hessian matrices (see Appendix A) as follows. Let

$$V = \left(m^{-1} \, (l_{OO} \, l_{CC} - l_{OC}^2)^{-1} \begin{pmatrix} l_{CC} & -l_{OC} \\ -l_{OC} & l_{OO} \end{pmatrix} \right)_{[\hat{\mu}_O, \, \hat{\mu}_C]}$$

where subscripts $_O$ and $_C$ denote partial differentiation with respect to μ_O and μ_C respectively. Then the standard deviations of $\hat{\mu}_O$ and $\hat{\mu}_C$ are given by $\sqrt{v_{11}}$ and $\sqrt{v_{22}}$ respectively and the correlation between $\hat{\mu}_O$ and $\hat{\mu}_C$ is given by $v_{12} \, (v_{11} \, v_{22})^{-½}$, where v_{ij} $(i, j = 1, 2)$ is the (i, j)th element of V. Expressions for l_{OO}, l_{OC} and l_{CC} for each of the three approximations of section 4.1.2.2, with agonist concentration dependent opening rates incorporated, are given in Appendix D.

4.3.2.3 Numerical Examples

4.3.2.3.1 Computer-simulated Data

The theory of sections 4.3.2.1 and 4.3.2.2 is illustrated here using data simulated according to the model represented by expression (4.29) for a range of agonist concentrations. The maximum likelihood procedure is used to examine the behaviour of the parameter estimates generated by the three approximations.

In selecting model parameter values for the simulations, two assumptions have been made. Firstly it has been assumed that association of the agonist molecule with the receptor is diffusion limited, yielding $\mu_C = 10^{-4}$ M ms. Secondly, the

dissociation constant for the receptor-agonist complex has been assumed to be 10^{-4} M, yielding $\mu_O = 1$ ms. These values yield agonist-concentration-dependent channel kinetics comparable with examples in the literature (e.g. Ball and Sansom (1989)), and fall within physiologically reasonable limits.

Channel openings were simulated for four different agonist concentrations, $a = 10^{-6}$, 10^{-5}, 10^{-4} and 10^{-3} M, corresponding to channel open probabilities of 0.01, 0.09, 0.50 and 0.91, respectively. This range of concentrations is comparable to that used in experimental studies (e.g. Colquhoun and Ogden (1988) and Kerry *et al.* (1988)). Five thousand observed channel openings and closings were simulated at each concentration. A detection limit $\tau = \tau_O = \tau_C = 0.1$ ms was used, and this resulted in omission of approximately 10% of channel openings at each agonist concentration. The fraction of closings which were undetected ranged from approximately 0.1% at $a = 10^{-6}$ M to approximately 63% at $a = 10^{-3}$ M. The value of τ used is comparable to that used in several literature examples, including Yeo *et al.* (1988).

4.3.2.3.2 Likelihood Surfaces

For each agonist concentration, the normalised log-likelihood was evaluated under each of the three approximations of section 4.1.2.2 for a range of μ_O and μ_C, thus generating a likelihood surface. Contour plots of these likelihood

surfaces are displayed in Figure 4.3 (a-d) for four different values of agonist concentration under the approximation derived by ignoring undetected sojourns. The equivalent contour plots for the other two approximations are not shown here as they are extremely similar. For convenience in displaying the contour plots of the likelihood surfaces, the μ_O and μ_C axes have been transformed according to

$$\phi_O = \ln\left(\frac{\mu_O}{\mu_O^M}\right) \quad \text{and} \quad \phi_C = \ln\left(\frac{\mu_C}{\mu_C^M}\right),$$

where the superscript ^{M} indicates the parameter values used in the model simulation. Typically, values of ϕ_O of between -12 and +12 were used and this corresponds to values of μ_O between $6.1 \times 10^{-6}\ \mu_O^M$ and $1.6 \times 10^5\ \mu_O^M$.

As predicted by the theory of this chapter, at each of the four agonist concentrations, the corresponding log-likelihood surface has two maxima. These are most widely separated at the lower agonist concentrations, but are still distinct at $a = 10^{-3}$ M. As also expected, the 'false' parameter estimates depend on the agonist concentration used, whereas the 'true' parameter estimates remain almost constant as agonist concentration varies.

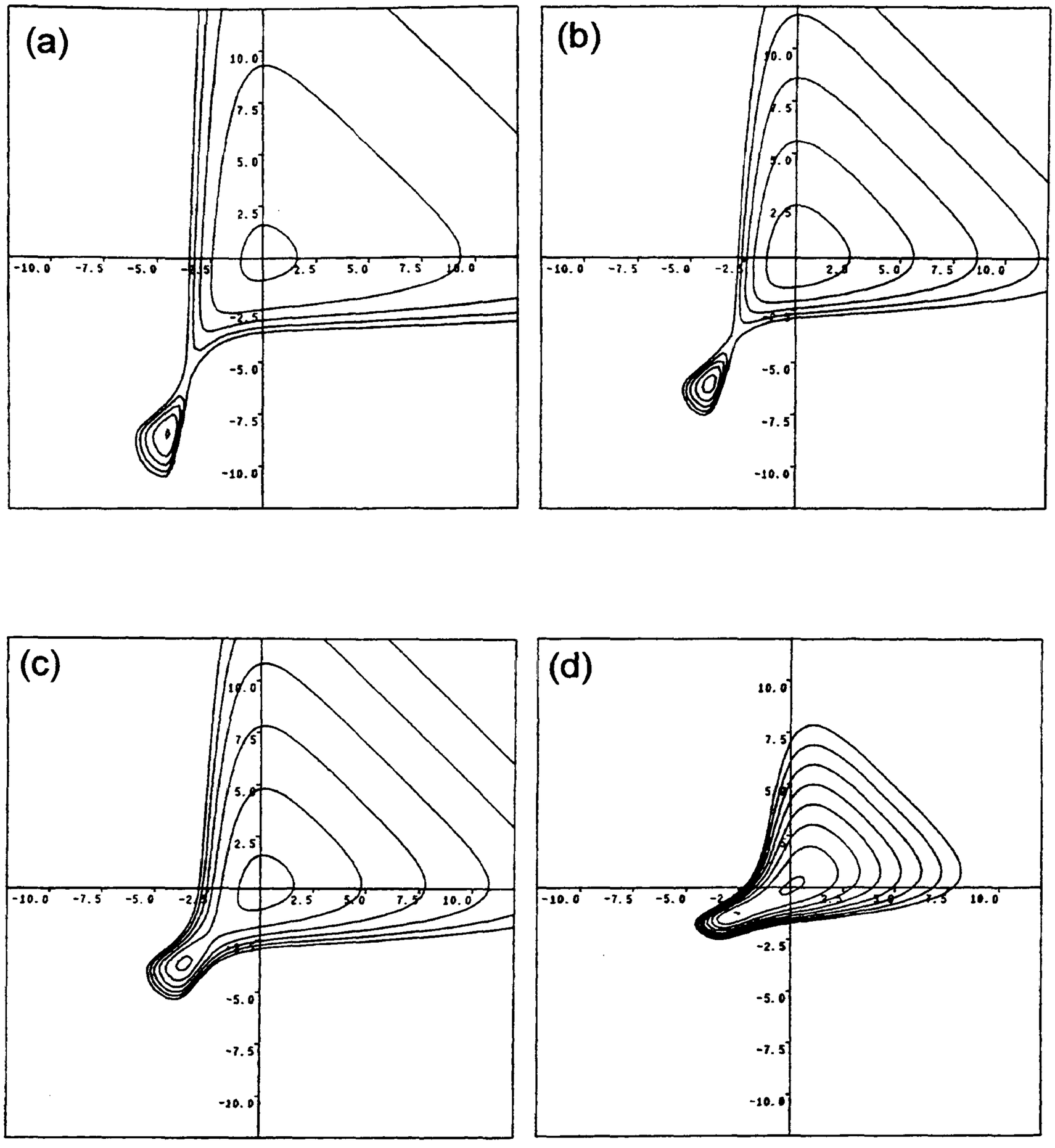

Figure 4.3. Contour plots of the normalised log-likelihood surfaces for four agonist concentrations: (a) $a = 10^{-6}$ M; (b) $a = 10^{-5}$ M; (c) $a = 10^{-4}$ M; (d) $a = 10^{-3}$ M. Values on the horizontal axes correspond to ϕ_O and values on the vertical axes correspond to ϕ_C. The contour intervals are (a) 7.5; (b) 3; (c) 3; (d) 0.95. Other details are as described in the text.

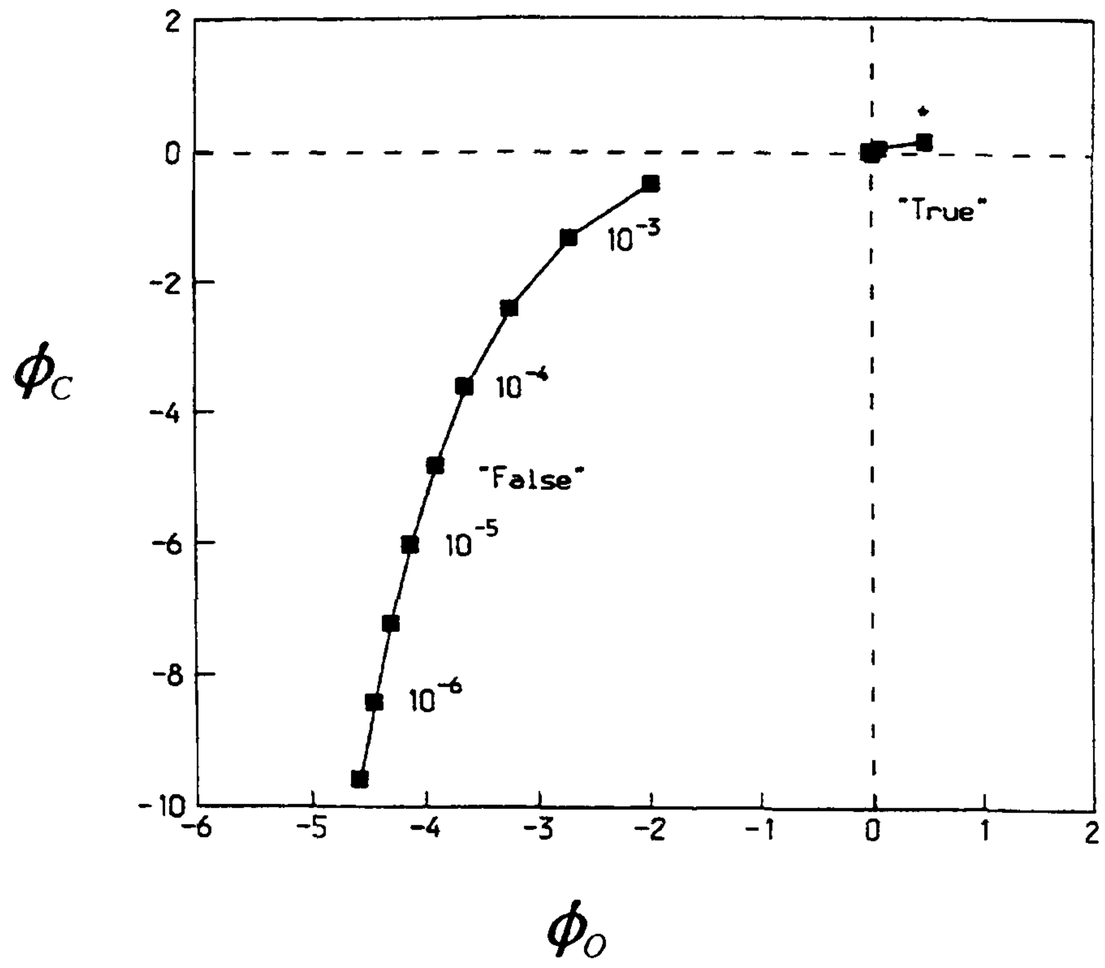

Figure 4.4. Behaviour of the two sets of parameter estimates as functions of agonist concentration. The points for the 'false' estimates are labelled with the corresponding agonist concentrations.

In Figure 4.4, for each agonist concentration, the positions of the two parameter estimates (again under the approximation derived by ignoring undetected sojourns) are plotted in the (ϕ_O, ϕ_C) plane. Two distinct loci can be seen, demonstrating the dependence of the 'false' parameter estimates, but not the 'true' parameter estimates, on the value of agonist concentration. Furthermore, the invariant estimates are tightly clustered about (ϕ_O, ϕ_C) = (0, 0), ie. about the point corresponding to the parameter values used in the simulation. The values of the parameter estimates used to construct Figure 4.4 are given in Table 4.2 (in the rows relating to the approximation of section 4.1.2.2.1), together with the corresponding parameter estimate standard deviations and correlations. The

correlation between the 'true' estimates is smaller than that between the 'false' estimates at all agonist concentrations. At all four agonist concentration levels the 'false' parameter estimates are markedly different from the underlying model values. Note also from Table 4.2 that, at each agonist concentration, the two values of the log-likelihood corresponding to the two values of ($\hat{\mu}_O$, $\hat{\mu}_C$) are identical, or almost identical for the bi-exponential approximation, so that it is not possible to distinguish between the estimates on the basis of the values of the log-likelihood. However, these numerical results confirm that the identifiability problem for this gating model can, in principle, be solved by obtaining data at different levels of agonist concentration, calculating and plotting both sets of estimates against the agonist concentration, and selecting that set which varies least. From Table 4.2 it can be seen that this approach should work for each of the three approximations.

The independence from the agonist concentration of the 'true' parameter estimate starts to break down when the fraction of undetected events reaches exceptionally high levels. For example, in Figure 4.4, the 'true' solution only deviates noticeably from the model parameters for $a > 10^{-3}$ M. For $a = 10^{-2.5}$ M, the 'true' parameters are $\hat{\mu}_O = 1.643\ \mu_O^M$ and $\hat{\mu}_C = 1.170\ \mu_C^M$, so that both estimates (marked with an asterisk in Figure 4.4) are significantly higher than the model values. However, for this agonist concentration, the fraction of undetected closings is extremely high (96%).

a / M	A	True / False	$l(\hat{\mu})$	$\hat{\mu}_O$ / ms (standard deviation)	$\hat{\mu}_C$ / 10^{-4} ms M (standard deviation)	Correlation between $\hat{\mu}_O$ and $\hat{\mu}_C$
10^{-6}	1	True	-6.72	1.015 (0.014)	0.9976 (0.0142)	0.099
		False	-6.72	0.0118 (0.00002)	0.000243 (0.0000008)	0.353
	2	True	-6.72	1.016 (0.014)	0.9985 (0.0142)	0.099
		False	-6.72	0.0128 (0.00002)	0.000305 (0.000001)	0.278
	3	True	-6.72	1.015 (0.014)	0.9978 (0.0142)	0.099
		False	-6.72	0.0127 (0.00002)	0.000306 (0.000001)	0.279
10^{-5}	1	True	-4.41	1.018 (0.014)	0.9861 (0.0140)	0.108
		False	-4.41	0.0164 (0.00004)	0.00242 (0.00001)	0.389
	2	True	-4.41	1.017 (0.014)	0.9846 (0.0140)	0.109
		False	-4.41	0.0186 (0.00005)	0.00319 (0.00002)	0.297
	3	True	-4.41	1.015 (0.014)	0.9851 (0.0140)	0.109
		False	-4.42	0.0186 (0.00005)	0.00320 (0.00002)	0.300
10^{-4}	1	True	-2.24	1.008 (0.014)	1.035 (0.015)	0.194
		False	-2.24	0.0267 (0.0001)	0.0268 (0.0001)	0.499
	2	True	-2.24	1.002 (0.014)	1.029 (0.015)	0.204
		False	-2.24	0.0342 (0.0002)	0.0345 (0.0002)	0.394
	3	True	-2.24	1.003 (0.014)	1.029 (0.015)	0.204
		False	-2.24	0.0342 (0.0002)	0.0345 (0.0002)	0.393
10^{-3}	1	True	-0.86	1.007 (0.023)	1.042 (0.016)	0.756
		False	-0.86	0.0693 (0.0009)	0.2702 (0.0015)	0.764
	2	True	-0.86	0.9927 (0.0251)	0.9872 (0.0175)	0.823
		False	-0.86	0.1468 (0.0030)	0.3600 (0.0033)	0.829
	3	True	-0.86	0.9941 (0.0250)	0.9889 (0.0175)	0.821
		False	-0.87	0.1451 (0.0031)	0.3590 (0.0033)	0.838

Table 4.2. Parameter estimates against agonist concentration for the three approximations. In the column entitled 'A', the labels 1, 2 and 3 indicate whether the approximation given in section 4.1.2.2.1, 4.1.2.2.2 or 4.1.2.2.3, respectively, was used to calculate the likelihood.

4.3.2.3.3 Global-Likelihood Surface

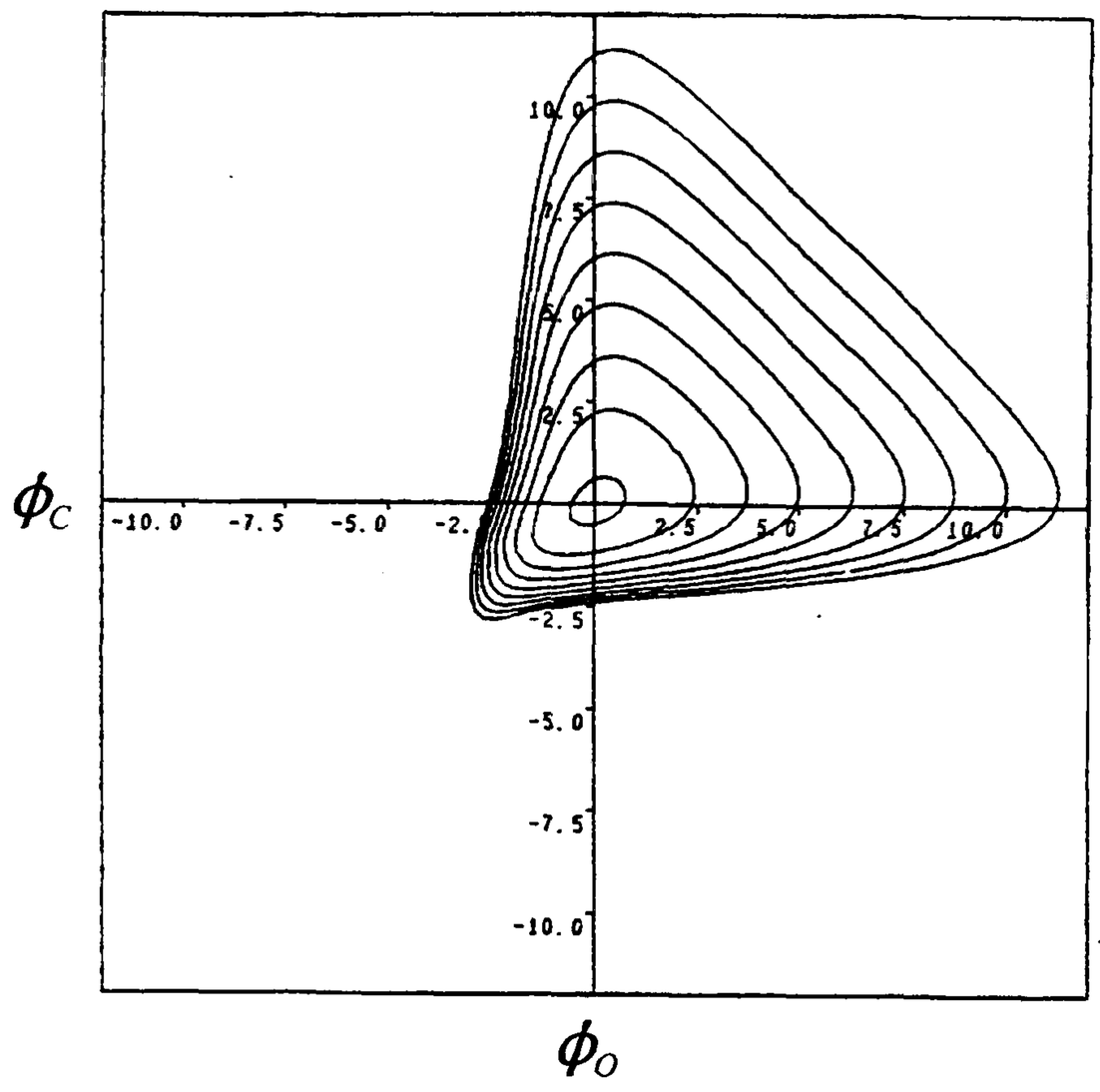

Figure 4.5. Contour plot of the global log-likelihood surface derived from analysis of the same data as that used to construct the surfaces in Figure 4.3. The contour interval is 5.

The surface shown in Figure 4.5 is the global likelihood, defined in equation (4.31), under the approximation derived by ignoring undetected sojourns and corresponding to the four agonist concentrations discussed above. Note that this surface corresponds to a summation of the four surfaces seen in Figure 4.3 (a-d). It is clear that there is only a single maximum on the global surface, corresponding to the 'true' parameter estimate. The position of this single maximum corresponds to $\hat{\mu}_O = 1.017$ ms, $\hat{\mu}_C = 1.017 \times 10^{-4}$ M ms, with standard deviations of 0.0076 ms and 0.0068×10^{-4} M ms, respectively, and a correlation between the parameters of 0.338. Further studies have shown that the global

likelihood surface derived from data simulated at only two different agonist concentrations can also show a single maximum, corresponding to the 'true' parameter estimate.

4.3.2.3.4 Effect of varying the Detection Limit

Using further simulations we have explored the extent to which the success of this approach for identifying the 'true' parameter set is dependent on the value of τ. Experimentally, the value of τ used in processing single-channel recordings depends on the signal to noise ratio for those recordings and realistic values of τ range from less than 0.05 ms, for high signal to noise ratio data, to more than 0.2 ms for poor signal to noise ratio data.

We have explored the behaviour of $(\hat{\mu}_O, \hat{\mu}_C)$ as a function of agonist concentration for values of τ in the range 0.02 ms to 0.5 ms. Other simulation conditions were the same as for the examples discussed above and the results are presented in Figure 4.6 as graphs of $(\hat{\mu}_O, \hat{\mu}_C)$ against agonist concentration for the various values of τ based on the approximation derived by ignoring undetected sojourns. It can be seen that the 'false' values of $(\hat{\mu}_O, \hat{\mu}_C)$ are strongly dependent on τ, whereas the 'true' values of $(\hat{\mu}_O, \hat{\mu}_C)$ are tightly clustered about $(\phi_O, \phi_C) = (0, 0)$ (see Yeo *et al.* (1988)). The exception to this (not shown on Figure 4.6) was for $\tau = 0.5$ ms at agonist concentrations in excess of 10^{-3} M, for

which the 'true' estimates differed considerably from the model parameter values used in the simulation. However, under these conditions the fraction of undetected closings was more than 99%. This situation would be immediately recognisable in experimental data as it would result in poorly resolved, noisy openings of greatly reduced amplitude, which would be difficult to process. However, even in this case, evaluation of the global likelihood surface for τ = 0.5 ms produced only a single maximum at $(\hat{\mu}_O, \hat{\mu}_C)$ = (0.9447 μ_O^M, 1.005 μ_C^M) and the overall approach for identifying the 'true' parameter estimates still appears to work.

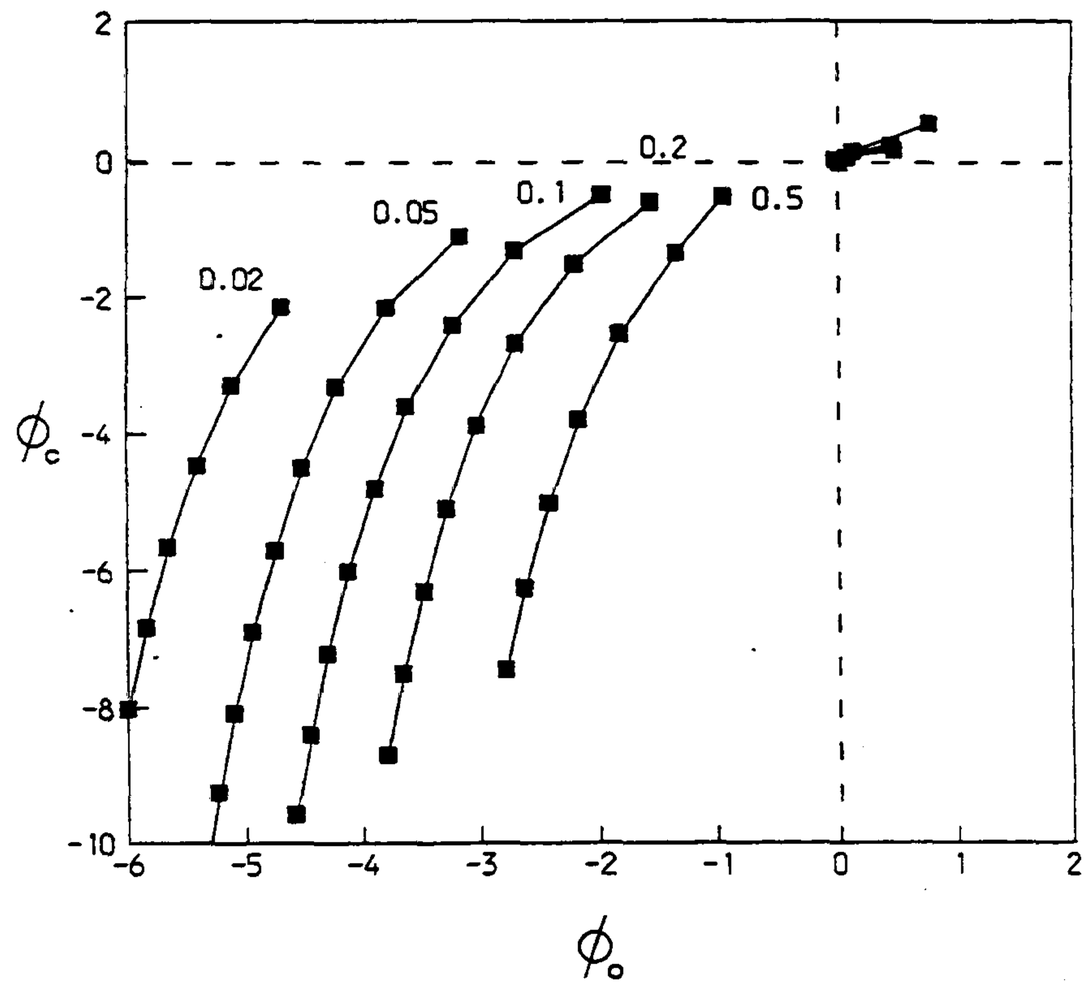

Figure 4.6. Behaviour of the 'true' and 'false' estimates as functions of minimum detectable dwell time τ. For each value of τ, the agonist concentration ranges from $a = 10^{-6.5}$ M to $a = 10^{-2.5}$ M, with the exceptions of $\tau = 0.2$ ms, for which the $a = 10^{-2.5}$ M point has been omitted, and of $\tau = 0.5$ ms, for which points corresponding to $a \geq 10^{-3.0}$ M have been omitted (see text).

4.3.2.3.5 Further Simulation Studies

The above estimation procedures have also been repeated employing (i) smaller sample sizes, (ii) different model parameter values, and (iii) the fast solution as the set of model parameter values for the simulations. In each case the values of the detection limit and agonist concentrations used were as given in section 4.3.2.3.1. Similar results were obtained using each of the three approximations so only results based on the approximation derived by ignoring undetected sojourns are given here.

Table 4.3 shows that the method of identifying the 'true' solution still works reasonably well even when the sample sizes used are much smaller than those typically used in comparable studies. For example, using a sample consisting of 500 observed openings and closings, the single maximum of the global likelihood surface corresponds to $\hat{\mu}_O = 1.001 \ \mu_O^M$ and $\hat{\mu}_C = 1.013 \ \mu_C^M$. Even with a sample size of just 50, maximisation of the global likelihood surface yields parameter estimates of $\hat{\mu}_O = 1.033 \ \mu_O^M$ and $\hat{\mu}_C = 0.8862 \ \mu_C^M$. It is worth recalling that estimation based on the approximation used in these examples is biased so the parameter estimates are likely to differ slightly from the model parameter values no matter how large the sample size used.

Sample Size	a / M	'True'		'False'	
		$\hat{\mu}_O$ / ms	$\hat{\mu}_C$ / (10^{-4} ms M)	$\hat{\mu}_O$ / ms	$\hat{\mu}_C$ / (10^{-4} ms M)
50	10^{-3}	1.148	1.081	0.0671	0.2657
	10^{-4}	0.8448	0.8194	0.0288	0.0286
	10^{-5}	1.095	0.711	0.0173	0.00240
	10^{-6}	0.9008	0.8596	0.0120	0.000232
500	10^{-3}	1.212	1.126	0.0650	0.262
	10^{-4}	0.9941	1.073	0.0264	0.0269
	10^{-5}	0.9095	0.9716	0.0165	0.002496
	10^{-6}	1.020	0.984	0.0118	0.000224

Table 4.3. Parameter estimates for a range of sample sizes. The detection limit used in the simulations is $\tau = 0.1$ ms.

Table 4.4 contains results which demonstrate that the approach is valid for a wide range of model parameter values. In each case, a sample size of 5000 was used. All the results presented so far have used the 'slow' solution as the 'true' solution. However, further simulation studies (not presented here) have also shown that the method of identifying the 'true' solution by using samples with different agonist concentrations works equally well when the 'fast' solution is the 'true' solution.

Model Parameters		a / M	'True'		'False'	
μ_O	μ_C		$\hat{\mu}_O$ / ms	$\hat{\mu}_C$ / (ms M)	$\hat{\mu}_O$ / ms	$\hat{\mu}_C$ / (10^{-4} ms M)
1	0.1	10^{-3}	1.026	0.1016	0.0117	0.2236
		10^{-4}	1.011	0.0995	0.0092	0.0213
		10^{-5}	1.005	0.1016	0.0076	0.00205
		10^{-6}	0.9953	0.1013	0.0064	0.000198
100	0.0001	10^{-3}	97.12	0.0001	0.0466	0.1155
		10^{-4}	100.06	0.000101	0.0225	0.0118
		10^{-5}	101.19	0.000101	0.0147	0.00113
		10^{-6}	99.11	0.0001	0.0110	0.00011
100	0.1	10^{-3}	101.69	0.0999	0.0110	0.1095
		10^{-4}	98.12	0.1010	0.0087	0.0107
		10^{-5}	101.02	0.1010	0.0073	0.00105
		10^{-6}	100.98	0.1000	0.0062	0.000103

Table 4.4. Parameter estimates for a range of model parameters. The detection limit used in the simulations is $\tau = 0.1$ ms.

4.3.3 Sample Variance Discrimination

4.3.3.1 Method

The two methods of overcoming the identifiability problem which are considered in sections 4.3.1 and 4.3.2 require data from more than one channel record to discriminate between the two solutions. In this section, a method which discriminates between the slow and fast solutions on the basis of just one channel

record is described. The idea underlying this method is that, although the means of observed open and closed sojourn times are the same for the two solutions, the corresponding variances differ slightly. Since channel records are typically quite long, it is possible to determine the true solution by comparing the sample variances of observed open and closed sojourns with those predicted by the slow and fast solutions.

Returning to the model (discussed in sections 4.1 and 4.2) without agonist-concentration-dependent opening rates, suppose that we have a random sample of n successive pairs of adjusted observed open and closed sojourns, $u_1, v_1, u_2, v_2, \ldots, u_n, v_n$ say, with respective sample variances s_O^2 given by

$$s_O^2 = \frac{1}{n-1}\sum_{i=1}^{n} u_i^2 - n\left(\frac{1}{n}\sum_{i=1}^{n} u_i\right)^2$$

and s_C^2 given by the same expression but with u_i replaced by v_i. Then $\mathbf{E}[s_O^2] = \tilde{\sigma}_O^2$, where $\tilde{\sigma}_O^2$ is given by equation (4.4), and (Kendall and Stuart (1977), p296) $\mathrm{var}(s_O^2) = n^{-1}\kappa_4 + 2(n-1)^{-1}(\tilde{\sigma}_O^2)^2$, where κ_4 is the fourth cumulant of an adjusted observed open sojourn which is given (Milne *et al.* (1988)) by

$$\begin{aligned}\kappa_4 = {} & 6(\mu_O+\mu_C)^4\exp(4\tau_c/\mu_C) \\ & - 24(\mu_O+\mu_C)^2[(\mu_O+\mu_C)\tau_c+\mu_O\mu_C]\exp(3\tau_c/\mu_C) \\ & + 12[4\tau_c(\mu_O+\mu_C)\mu_O\mu_C + 2\tau_c^2(\mu_O+\mu_C)^2 + \mu_O^2\mu_C^2]\exp(2\tau_c/\mu_C) \\ & - 4\tau_C^2[(\mu_O+\mu_C)\tau_c+3\mu_O\mu_C]\exp(\tau_c/\mu_C) - 6\mu_C^4.\end{aligned}$$

Similar expressions hold for $\mathbf{E}[s_C^2]$ and $\text{var}(s_C^2)$, noting that the fourth cumulant of an adjusted observed closed sojourn has an expression identical to that for κ_4 but with μ_O and μ_C interchanged and τ_C replaced by τ_O.

Let $\boldsymbol{v} = (\tilde{\sigma}_O^2, \tilde{\sigma}_C^2)^\top$ and $\hat{\boldsymbol{v}} = (s_O^2, s_C^2)^\top$. Then, for large n, $\hat{\boldsymbol{v}}$ approximately follows a bivariate normal distribution with mean vector $\boldsymbol{v}$ and dispersion matrix $\tilde{\boldsymbol{\Sigma}} = \text{diag}\{\text{var}(s_O^2), \text{var}(s_C^2)\}$. Note that the off-diagonal elements of $\tilde{\boldsymbol{\Sigma}}$ are zero since successive adjusted observed open and closed sojourns are mutually independent. Let $\boldsymbol{v}_S$ and $\tilde{\boldsymbol{\Sigma}}_S$ be respectively the mean vector and dispersion matrix of $\hat{\boldsymbol{v}}$ given $\mu = \mu^S$, and define $\boldsymbol{v}_F$ and $\tilde{\boldsymbol{\Sigma}}_F$ similarly. Then we wish to determine whether $\hat{\boldsymbol{v}}$ comes from a $\text{N}(\boldsymbol{v}_S, \tilde{\boldsymbol{\Sigma}}_S)$ or a $\text{N}(\boldsymbol{v}_F, \tilde{\boldsymbol{\Sigma}}_F)$ distribution. This can be done by using a linear discriminant function (see, for example, Mardia *et al.* (1979)) and replacing the unknown parameters by their estimates as follows. Suppose that $\tilde{\boldsymbol{\Sigma}}_S = \tilde{\boldsymbol{\Sigma}}_F$ (= $\tilde{\boldsymbol{\Sigma}}$ say). Let $H(\hat{\boldsymbol{v}}) = \boldsymbol{a}^\top(\hat{\boldsymbol{v}} - \frac{1}{2}(\boldsymbol{v}_S + \boldsymbol{v}_F))$, where $\boldsymbol{a} = \tilde{\boldsymbol{\Sigma}}^{-1}(\boldsymbol{v}_S - \boldsymbol{v}_F)$. Then the maximum likelihood discriminant rule allocates $\hat{\boldsymbol{v}}$ to $\text{N}(\boldsymbol{v}_S, \tilde{\boldsymbol{\Sigma}}_S)$, i.e. decides that $\mu = \mu^S$, if $H(\hat{\boldsymbol{v}}) > 0$ and allocates $\hat{\boldsymbol{v}}$ to $\text{N}(\boldsymbol{v}_F, \tilde{\boldsymbol{\Sigma}}_F)$ if $H(\hat{\boldsymbol{v}}) \leq 0$. Since $\tilde{\boldsymbol{\Sigma}}_S \neq \tilde{\boldsymbol{\Sigma}}_F$, we have replaced $\tilde{\boldsymbol{\Sigma}}$ by $\frac{1}{2}(\tilde{\boldsymbol{\Sigma}}_S + \tilde{\boldsymbol{\Sigma}}_F)$ in the discriminant function H. When applying the method, μ^S and μ^F will be unknown and hence $(\boldsymbol{v}_S, \tilde{\boldsymbol{\Sigma}}_S)$ and $(\boldsymbol{v}_F, \tilde{\boldsymbol{\Sigma}}_F)$ are estimated by replacing μ by $\hat{\mu}_n^S$ and $\hat{\mu}_n^F$ respectively.

Since $H(\hat{\boldsymbol{v}})$ follows a $\text{N}(-\frac{1}{2}\boldsymbol{a}^\top\tilde{\boldsymbol{\Sigma}}\boldsymbol{a}, \boldsymbol{a}^\top\tilde{\boldsymbol{\Sigma}}_F\boldsymbol{a})$ distribution whenever $\mu = \mu^F$, it

follows that, for known μ^S and μ^F,

$$\mathbf{P}[\text{decide } \mu = \mu^S \mid \mu = \mu^F] = \Phi\left[\frac{-a^\top(\tilde{\Sigma}_S + \tilde{\Sigma}_F)a}{4\sqrt{a^\top\tilde{\Sigma}_F a}}\right]. \tag{4.32}$$

Similarly

$$\mathbf{P}[\text{decide } \mu = \mu^F \mid \mu = \mu^S] = \Phi\left[\frac{-a^\top(\tilde{\Sigma}_S + \tilde{\Sigma}_F)a}{4\sqrt{a^\top\tilde{\Sigma}_S a}}\right]. \tag{4.33}$$

These misclassification probabilities may be estimated by replacing the unknown parameters in these expressions by their estimates.

The assumption that $\tilde{\Sigma}_S = \tilde{\Sigma}_F$ can be relaxed in determining an allocation rule. This results in a quadratic discriminant function $Q(\hat{v})$ say, (see, for example, Krzanowski (1988)), given by

$$Q(\hat{v}) = \ln\left(\frac{|\tilde{\Sigma}_F|}{|\tilde{\Sigma}_S|}\right) - \hat{v}^\top(\tilde{\Sigma}_S^{-1} - \tilde{\Sigma}_F^{-1})\hat{v}$$
$$+ 2v^\top(\tilde{\Sigma}_S^{-1}\mu^S - \tilde{\Sigma}_F^{-1}\mu^F) - ((\mu^S)^\top\tilde{\Sigma}_S^{-1}\mu^S - (\mu^F)^\top\tilde{\Sigma}_F^{-1}\mu^F).$$

Discrimination based on this quadratic discriminant function classifies μ^S as the true solution if $Q(\hat{v}) > 0$ and μ^F as the true solution if $Q(\hat{v}) \leq 0$. Again the unknown parameters may be replaced by their estimates when applying this

method. It should be noted that the misclassification probabilities based on this quadratic discriminant function method are more difficult to calculate than those based on the linear discriminant function method above.

4.3.3.2 Numerical Examples

4.3.3.2.1 Tests based on Examples from Ion Channel Literature

The theory of section 4.3.3.1 is illustrated using simulated data for the same five examples, taken from the ion channel literature, that were considered in section 4.2.5. The results are displayed in Table 4.5. For each of the five examples CS, BM_1, BM_2, P_1 and P_2, one thousand data sets with $n = 1000$, ie. consisting of 1000 successive pairs of adjusted observed open and closed sojourns, were simulated by using the appropriate model parameter $\boldsymbol{\mu}^S$, given in Table 4.5. For each data set, a discrimination test based on the linear discriminant function and a discrimination test based on the quadratic discriminant function were performed and the misclassification probability for the former test was estimated using the methods described in section 4.3.3.1. This procedure was repeated with data sets simulated using model parameter $\boldsymbol{\mu}^F$, given in Table 4.5, and also with $n = 5000$ and $n = 10000$. For each of the five examples, and for each combination of n and $\boldsymbol{\mu}^S$ or $\boldsymbol{\mu}^F$, Table 4.5 gives the number of correct classifications in the 1000 simulations for each of the two discrimination tests and the mean of the estimated

misclassification probabilities for the tests based on the linear discriminant function. The results show that, for the examples considered, the two discrimination methods are reasonably effective in determining the correct solution. Note that the results of the tests based on the quadratic discriminant function are not, in general, any better than those for the tests based on the linear discriminant function, suggesting that the linear discriminant function should be used in preference to the quadratic discriminant function.

From Table 4.5, it can be seen that the misclassification probabilities shown are considerably overestimated. We investigated this overestimation by repeating our simulation study, but now using the known true values of μ^S and μ^F in calculating both the linear discriminant function $H(\hat{\boldsymbol{v}})$ and the misclassification probabilities. The numbers of misclassifications were now consistent with the calculated misclassification probabilities, indicating that the discrepancy is not a consequence of the normal approximations; rather it is an artefact of replacing μ^S and μ^F by their method-of-moments estimators $\hat{\mu}^S$ and $\hat{\mu}^F$. To estimate the misclassification probabilities, it is necessary to estimate the mean and variance of $H(\hat{\boldsymbol{v}})$. Returning to our original simulation study, we found that, although the mean of $H(\hat{\boldsymbol{v}})$ was being estimated fairly accurately, its variance was always appreciably overestimated, and consequently so were the misclassification probabilities. However, it should be noted that $\hat{\mu}^S$ and $\hat{\mu}^F$ are negatively dependent, and failure to take account of negative dependence is often the cause of overestimation of variance.

Example	Slow / Fast	Sample Size	Number of correct allocations based on $H(\hat{\nu})$ ($Q(\hat{\nu})$)	Mean misclassification probability (based on $H(\hat{\nu})$)
CS $\tau = 0.2$ $\mu^S = (0.2990, 0.8787)^\top$ $\mu^F = (0.1063, 0.2148)^\top$	Slow ($\mu = \mu^S$)	1000	766 (804)	0.3314
		5000	921 (923)	0.1638
		10000	967 (964)	0.0828
	Fast ($\mu = \mu^F$)	1000	701 (655)	0.3433
		5000	899 (896)	0.1823
		10000	971 (973)	0.0999
BM_1 $\tau = 0.1$ $\mu^S = (1.0034, 0.1003)^\top$ $\mu^F = (0.1443, 0.0359)^\top$	Slow ($\mu = \mu^S$)	1000	925 (932)	0.1640
		5000	998 (995)	0.0142
		10000	1000 (1000)	0.0010
	Fast ($\mu = \mu^F$)	1000	901 (894)	0.2062
		5000	995 (997)	0.0330
		10000	1000 (1000)	0.0047
BM_2 $\tau = 0.1$ $\mu^S = (0.9997, 0.2000)^\top$ $\mu^F = (0.0800, 0.0364)^\top$	Slow ($\mu = \mu^S$)	1000	817 (843)	0.2738
		5000	966 (964)	0.0894
		10000	997 (995)	0.0287
	Fast ($\mu = \mu^F$)	1000	772 (743)	0.2945
		5000	964 (968)	0.1134
		10000	994 (995)	0.0438
P_1 $\tau = 0.035$ $\mu^S = (0.8647, 0.1194)^\top$ $\mu^F = (0.0190, 0.0093)^\top$	Slow ($\mu = \mu^S$)	1000	759 (782)	0.3256
		5000	728 (929)	0.1560
		10000	976 (975)	0.0764
	Fast ($\mu = \mu^F$)	1000	699 (674)	0.3372
		5000	897 (897)	0.1740
		10000	972 (972)	0.0922
P_2 $\tau = 0.035$ $\mu^S = (0.3352, 0.1289)^\top$ $\mu^F = (0.0191, 0.0128)^\top$	Slow ($\mu = \mu^S$)	1000	704 (748)	0.3697
		5000	853 (859)	0.2290
		10000	943 (944)	0.1468
	Fast ($\mu = \mu^F$)	1000	626 (573)	0.3769
		5000	831 (825)	0.2418
		10000	932 (931)	0.1610

Table 4.5. Discrimination between the slow and fast solutions on the basis of the sample variances of observed open and closed sojourns.

We carried out further simulation studies using other quantities, including the sums of the squares of simulated observed open and closed sojourn times, the sums of the cubes of these times, their skewness and their kurtosis, as discriminants between the slow and fast solutions. However, since the results obtained indicated that none of these quantities is a better discriminant than the sample variance, the results of these studies are not shown here.

4.3.3.2.2 Effect of varying the Detection Limit

In this section we investigate the dependence of the performance of the sample variance discrimination method on the detection limit. In the examples considered, $\tau_O = \tau_C = \tau$, say. Restricting our attention to the example CS in Table 4.5, we assumed that the slow solution $\boldsymbol{\mu}^S = (0.2990, 0.8787)^T$ is the true solution and, for various values of the detection limit τ, we calculated the corresponding false solutions. For each value of τ and each given record length n, we simulated 1000 data sets from the true model, each consisting of n observed open sojourn times and n observed closed sojourn times. For each data set we calculated $\hat{\boldsymbol{\mu}}^S$ and $\hat{\boldsymbol{\mu}}^F$, discriminated between the two solutions using the linear discriminant function $H(\hat{\boldsymbol{v}})$, and calculated the approximate misclassification probability. We then repeated the procedure but with data sets simulated from the corresponding false model. Note that the true model parameter values (μ_O, μ_C) remain the same for all values of τ, but that the false model parameter values (μ_O, μ_C) vary with τ.

τ	Record Length	Data simulated from true model		Data simulated from false model	
		Number of correct allocations	Mean misclassification probability	Number of correct allocations	Mean misclassification probability
0.05	**True Model: $\mu = (0.2990, 0.8787)$, $\tilde{\sigma}_O^2 = 0.1011$, $\tilde{\sigma}_C^2 = 1.0881$** **False Model: $\mu = (0.01452, 0.02086)$, $\tilde{\sigma}_O^2 = 0.1052$, $\tilde{\sigma}_C^2 = 1.0962$**				
	1000	647	0.4094	630	0.4130
	5000	767	0.3044	765	0.3113
	10000	856	0.2347	861	0.2433
0.1	**True Model: $\mu = (0.2990, 0.8787)$, $\tilde{\sigma}_O^2 = 0.1166$, $\tilde{\sigma}_C^2 = 1.5548$** **False Model: $\mu = (0.03804, 0.06189)$, $\tilde{\sigma}_O^2 = 0.1247$, $\tilde{\sigma}_C^2 = 1.5739$**				
	1000	746	0.3465	673	0.3565
	5000	881	0.1887	896	0.2048
	10000	961	0.1062	937	0.1218
0.15	**True Model: $\mu = (0.2990, 0.8787)$, $\tilde{\sigma}_O^2 = 0.1369$, $\tilde{\sigma}_C^2 = 2.2421$** **False Model: $\mu = (0.06881, 0.1251)$, $\tilde{\sigma}_O^2 = 0.1480$, $\tilde{\sigma}_C^2 = 2.2705$**				
	1000	743	0.3228	700	0.3358
	5000	923	0.1518	899	0.1713
	10000	979	0.07297	981	0.08974
0.2	**True Model: $\mu = (0.2990, 0.8787)$, $\tilde{\sigma}_O^2 = 0.1632$, $\tilde{\sigma}_C^2 = 3.2505$** **False Model: $\mu = (0.1063, 0.2148)$, $\tilde{\sigma}_O^2 = 0.1759$, $\tilde{\sigma}_C^2 = 3.2872$**				
	1000	747	0.3312	714	0.3431
	5000	903	0.1637	917	0.1825
	10000	971	0.08282	957	0.09991
0.3	**True Model: $\mu = (0.2990, 0.8787)$, $\tilde{\sigma}_O^2 = 0.2399$, $\tilde{\sigma}_C^2 = 6.8675$** **False Model: $\mu = (0.2008, 0.4982)$, $\tilde{\sigma}_O^2 = 0.2498$, $\tilde{\sigma}_C^2 = 6.8971$**				
	1000	-	-	-	-
	5000	784	0.3062	739	0.3149
	10000	845	0.2358	830	0.2443

Table 4.6 Results of simulations carried out to investigate the performance of the sample variance discrimination method. For $\tau = 0.3$, v is very close to the curve O of Figure 4.1 and, when the record length is small, e.g. $n = 1000$, $\hat{v}$ often lies below O, and the moment estimating equations have no solution. Thus these cases have been omitted from this table.

The results are shown in Table 4.6. For each combination of detection limit τ and record length n, the number of correct classifications in the 1000 simulations and the mean of the estimated misclassification probabilities are shown when the data are simulated from each of the true model and the false model.

Whilst it can be seen from Table 4.6 that the discriminant method works satisfactorily over a wide range of detection limits, it is also clear that, for fixed record length n, the proportion of correct classifications does not vary monotonically with τ. We examined this relationship by considering the dependence of the misclassification probabilities, as predicted by equations (4.32) and (4.33), on the detection limit τ.

Recall Figure 4.1 of section 4.2.2 and let $p_n(\mu_O, \mu_C, \tau)$ be the misclassification probability calculated from equation (4.32) if (μ_O, μ_C) lies in the region F, or from equation (4.33) if (μ_O, μ_C) lies in the region S, when the detection limit is τ, the record length is n, and μ_O and μ_C are, respectively, the true means of open and closed sojourn times. By re-scaling time so that $\tau = 1$, we obtain that

$$\begin{aligned} p_n(\mu_O, \mu_C, \tau) &= p_n(\tau^{-1}\mu_O, \tau^{-1}\mu_C, 1) \\ &= p_n^*(\tau^{-1}\mu_O, \tau^{-1}\mu_C), \end{aligned} \tag{4.34}$$

say. Hence it is sufficient to examine the behaviour of $p_n^*(\mu_O, \mu_C)$ as (μ_O, μ_C) varies. Figure 4.7(a) is a contour plot of $p_n^*(\mu_O, \mu_C)$ when the record length n is

10000. Note that $p_n^*(\mu_O, \mu_C)$ is close to ½ in the region of the curve L in Figure 4.1 of section 4.2.2, as then the two solutions are very close together and it is therefore difficult to discriminate between them. Figure 4.7(b) shows the cross-section of the surface $p_n^*(\mu_O, \mu_C)$ along the line $0.8787\ \mu_O = 0.2990\ \mu_C$, which corresponds to varying τ in the CS example. The misclassification probability $p_n^*(\mu_O, \mu_C)$ tends to ½ as μ_O (and hence μ_C) tends to zero or infinity. (The limit as μ_O tends to infinity is not clear from Figure 4.7(b), but was verified by further calculations.) The cross-section also has a peak of height ½ at the point where (μ_O, μ_C) crosses the curve L. Thus, for a given model, sample variance discrimination will be poor for values of τ for which (μ_O, μ_C) is near L and for very high and very low values of τ, but it will be good for the remaining values of τ. In the first case, the slow and fast solutions are very close together, so a misclassification may not be too serious. In the second case, very large values of τ do not occur in practice, but it is unfortunate that as τ becomes smaller it becomes more difficult to discriminate between the two solutions. When interpreting Figures 4.7(a) and 4.7(b), it should be remembered that, because of the time re-scaling used in deriving equation (4.34), large (small) values of μ_O and μ_C correspond to small (large) values of τ. Note that generally the misclassification probabilities are considerably smaller in the case when μ_O and μ_C are distinct than in the case when they are the same. Remember also that, whilst the estimated misclassification probabilities are a good indication of whether or not the method is likely to be working well, these probabilities are usually overestimated.

(a)

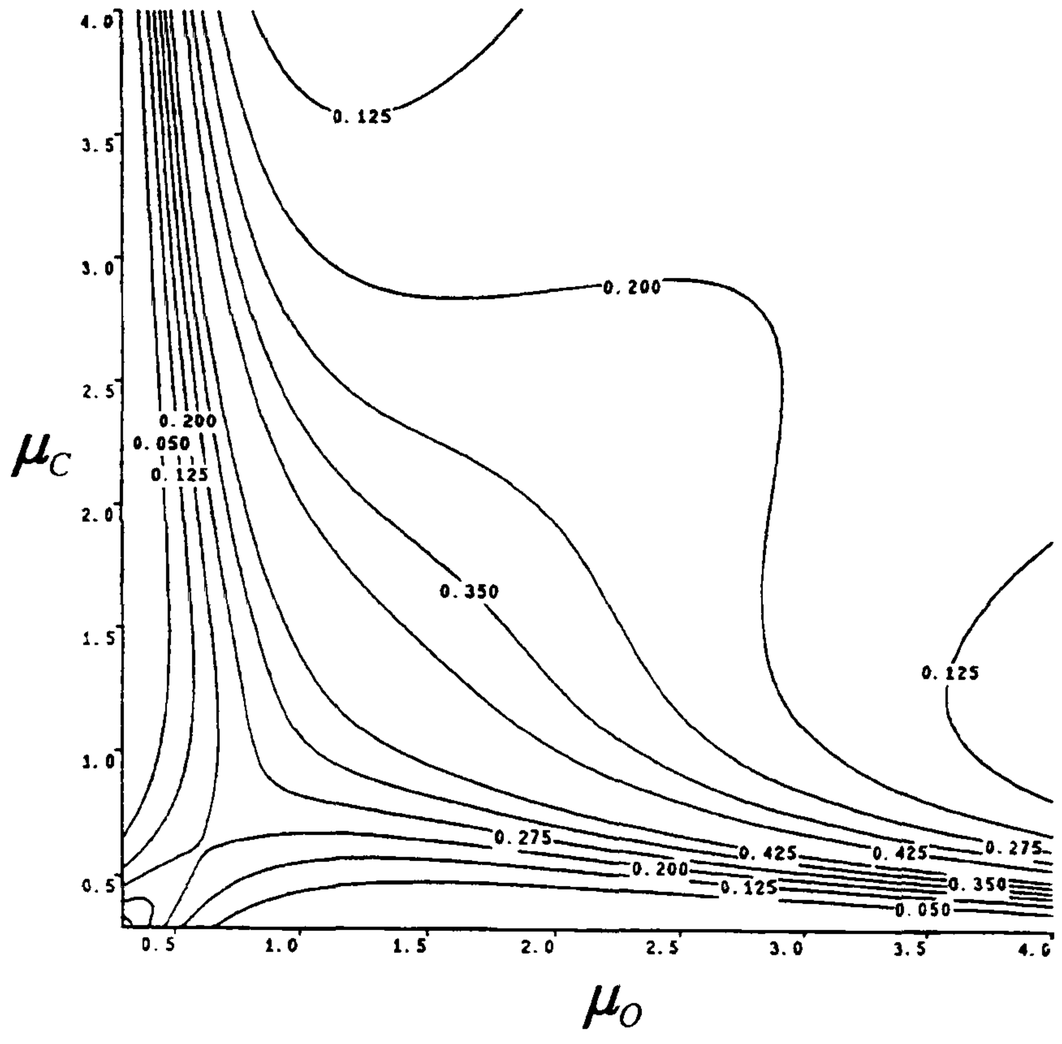

(b)

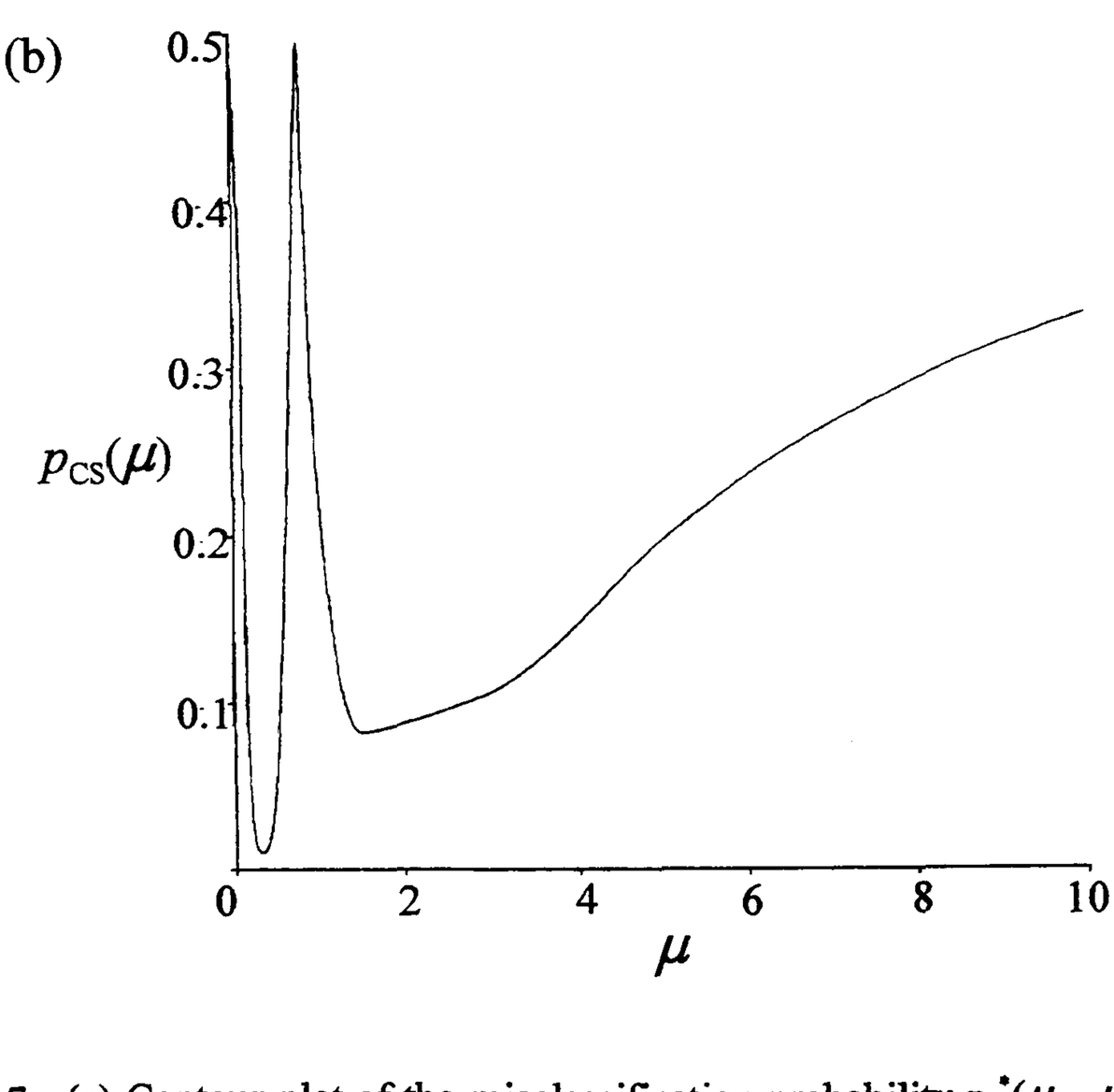

Figure 4.7. (a) Contour plot of the misclassification probability $p_n^*(\mu_O, \mu_C)$ for record length $n = 10000$ and detection limit $\tau = 1.0$. (b) Cross-section of the surface of misclassification probabilities $p_n^*(\mu_O, \mu_C)$ for record length $n = 10000$, along the line $0.8787\mu_O = 0.2990\mu_C$. The line $p_{CS}(\mu) = p_n^*(\mu, 0.8787\mu / 0.2990)$ is plotted for $0 \le \mu \le 10$.

5 Conclusion

5.1 Models based on the Molecular Structure of Ion Channels

In Chapter 3 of this thesis we use continuous-time Markov chains to describe the single-channel kinetics of receptor-gated channels in terms of underlying gating mechanisms. The large state-space models thus formulated incorporate information from biological investigations of ion channel structure. We develop such a model for nicotinic acetylcholine receptors which takes account of the pentameric structure of the membrane proteins and the interaction between neighbouring subunits and we derive expressions for various channel properties. By exploiting symmetries to reduce the size of the state space, and using parameter values chosen by a combination of biophysical considerations and theoretically matching observable properties of our model to those of the model of Jackson (1989), we evaluate these expressions for channel properties. Our results show that our model displays a wider range of observed channel properties than those displayed by simpler models discussed in the literature. We generalise our model so that, in addition to treating those receptor channels with two agonist binding subunits, it may also be applied to systems with an arbitrary number of agonist binding subunits. We further adapt and extend the underlying concepts

to model the BK channel, taking account of its tetrameric structure and more complex subunit interactions.

Our models have the considerable merit of being defined by a relatively small number of parameters which are directly related to the molecular properties of the channel. However, preliminary investigations (not presented in this thesis) for the BK channel model, using simulated data and based on the method of maximum likelihood, find that even this relatively small number of parameters is sufficiently large that significant problems may arise in trying to estimate them. For example, in one of the simplest of these investigations, we assume that all but three parameter values are known and we attempt to estimate the remaining three values (K_T, K_{OO} and K_{OC}) by maximising the log-likelihood using the simplex method (NAG numerical subroutine E04CCF) on a VAX 11/785. We find that problems occur during the estimation procedure since, during the maximisation subroutine, some calculations involve early estimates of parameter values which cause eigenvalues of Q_{CC} to be extremely small and hence, following rounding errors, cause entries of $\exp(Q_{CC}t)$ to be zero. This results in spurious parameter estimates which are dependent on the manually entered estimates used as starting points by the subroutine. Further, our FORTRAN77 programs take a very long time (days) to run even when the sample size is only several hundred. Thus questions of inference remain largely unaddressed for our models.

CONCLUSION

In order to improve our models there are a number of features which could be incorporated. Firstly, we could include time interval omission. For many channel properties this is not problematic and we have indeed calculated values (not presented in this thesis) for a number of channel properties, assuming the presence of time interval omission. However, it is not clear how time interval omission should be modelled when the state space is partitioned into more than two classes (e.g. open, short-lived closed and long-lived closed) as it is in calculations to determine clustering properties. Secondly, there are a number of characteristics of ion channels (e.g. response of BK channels to changes in voltage (Hille (1992))) which have been ignored in formulating our models and incorporation of such features requires further studies. Thirdly, our models do not incorporate desensitization. We have calculated expressions (not presented in this thesis) for several channel properties assuming the existence of three classes (open, closed and desensitized) of states for a semi-Markov model of channel gating in the case in which it is known which states are in the desensitized class and how they are interconnected to each other and to other states. We have also specialised these results to the Markov case. Further work is required to determine how to formulate biologically realistic large state-space models which incorporate desensitized states.

Together with the large number of mathematical problems yet to be solved, if realistic ion channel models are to be developed, there is a strong need for further

experimental research to obtain additional details of the structure, function and behaviour of ion channels. A real understanding of channel physiology at atomic resolution requires simulation studies to provide dynamic images of the events during ion permeation and gating and such studies are reliant on precise knowledge of channel structure. In terms of the models formulated in this thesis, one specific area requiring further study is the behaviour of channels with respect to the binding and unbinding of agonist molecules or calcium ions and the number and location of binding sites within channels. It is not known whether, in some cases, such binding activity is necessary in order for channels to open. More experimental studies are needed to demonstrate the effect of agonist concentration on the gating behaviour of the nicotinic acetylcholine channel and also to determine patterns of clustering of channel openings. Further work is also required to increase understanding of the functions and behaviour of individual channel subunits and this would enable us to more confidently specify our model parameter values. In particular, there is currently insufficient information available for us to specify parameter values for our BK channel model with any real degree of confidence, thus preventing us from evaluating that model by examining predicted channel properties.

We show how the nicotinic acetylcholine channel model formulated in this thesis can be varied to provide us with a model for the BK channel. This illustrates that the new style of model developed in Chapter 3 can be easily adapted to describe

other polymeric ion channels, given sufficient information regarding relevant channel structure. Further studies are needed to specify and evaluate models of other types of channel.

5.2 Inference for a two-state Ion Channel Model

Although a two-state model is undoubtedly only a very crude approximation to the complex dynamical behaviour of an ion channel, analysis of such a relatively simple Markov model is a useful first step towards investigating more complex Markov models, which have proved difficult to analyse theoretically in the presence of time interval omission. Thus this simple model provides a conceptual framework for increasing our understanding of time interval omission and the problems that it causes, as well as for exploring ways to overcome these problems. In Chapter 4 of this thesis we analyse an ion channel model, with one open state and one closed state such that successive open and closed sojourns are independent negative exponential random variables with respective means μ_O and μ_C, incorporating time interval omission. We develop a framework to analyse the behaviour of the method-of-moments estimators of μ_O and μ_C as the number of observed sojourns becomes large. We use the framework to explore and understand the non-identifiability induced by time interval omission and to construct confidence sets for the mean sojourn lengths. We prove a conjecture that the moment estimating equations have zero, one or two solutions and we

devise two new methods to overcome this non-identifiability. We illustrate much of this theory using numerical examples based on simulated data. Thus we resolve the unsolved problems raised by Yeo *et al.* (1988).

The natural extension of this theory is to examine Markov models with more than two states. Unfortunately such an extension presents problems. The presence of time interval omission introduces difficulties with many methods of parameter estimation. In the case of maximum likelihood estimation, it results in the lack of a convenient expression for the likelihood of a sequence of observed sojourn times and, in at least some models, induces the non-identifiability problem examined in detail in this thesis. In the case of the two-state model, we apply the method-of-moments to several different approximate probability density functions of adjusted observed open and closed sojourns, for each of which the method of maximum likelihood yields the same estimators as the method-of-moments. However, this approach is not so easy to apply in models with more than two states. First, it is not clear which moments (e.g. higher moments) should be used in the estimation procedure. Second, a model with more states usually has a larger number of parameters and this results in increased complexity in the equations to be solved. For example, using simulated data, an investigation (not presented in this thesis), based on the method-of-moments, of a three-state linear model with four parameters shows that existing commercially available optimisation software is not generally capable of simultaneously estimating all

four parameters without being fed an initial point that lies very close to the true parameter set. Second, it is extremely difficult to determine whether or not the moment estimating equations have multiple solutions, and there is a possibility that the existence of an identifiability problem may even depend on the choice of moments used.

6 References

Aidley, D. J. and Stanfield, P. R. (1996) Ion Channels: Molecules in Action. Cambridge University Press.

Andersen, P. K., Borgan, Ø., Gill, R. D. and Keiding, N. (1992) Statistical Models based on Counting Processes. Springer-Verlag.

Ball, F. G. (1990) Aggregated Markov processes with negative exponential time interval omission. *Adv. Appl. Prob.*, **22**, 802-830.

Ball, F. G. (1997) Empirical clustering of bursts of openings in Markov and Semi-Markov models of single channel gating incorporating time interval omission. *Adv. Appl. Prob.*, **29**, 909-946.

Ball, F. G., Cai, Y., Kadane, J. B. and O'Hagan, A. (1999) Bayesian inference for ion-channel gating mechanisms directly from single-channel recordings, using Markov chain Monte Carlo. *Proceedings of the Royal Society* A, **455**, 2879-2932.

Ball, F. G., Chen, A. and Sansom, M. S. P. (1992) Poisson sampling based inference for single ion channel data with time interval omission. *Proceedings*

of the Royal Society B, **250**, 263-269.

Ball, F. G., Davies, S. S. and Sansom, M. S. P. (1990) Single-channel data and missed events: analysis of a two-state Markov model. *Proceedings of the Royal Society* B, **242**, 61-67.

Ball, F. G., Davies, S. S. and Sansom, M.S.P. (1994) Ion channel gating and time interval omission: statistical inference for a two-state Markov model. *Proceedings of the Royal Society* B, **255**, 267-272.

Ball, F. G. and Davies, S. S. (1995) Statistical inference for a two-state Markov model of a single ion channel, incorporating time interval omission. *J. R. Statist. Soc.* B, **57**, 269-287.

Ball, F. G. and Davies, S. S. (1997) Clustering of bursts of openings in Markov and semi-Markov models of single channel gating. *Adv. Appl. Prob.*, **29**, 92-113.

Ball, F. G., Kerry, C. J., Ramsey, R. L., Sansom, M. S. P. and Usherwood, P. N. R. (1988) The use of dwell time cross-correlation functions to study single-ion channel gating kinetics. *Biophysical Journal*, **54**, 309-320.

Ball, F. G., Milne, R. K. and Yeo, G. F. (1991) Aggregated semi-Markov

processes incorporating time interval omission. *Adv. Appl. Prob.*, **23**, 772-797.

Ball, F. G., Milne, R. K. and Yeo, G. F. (1993b) On the exact distribution of observed open times in single ion channel models. *J. Appl. Prob.*, **30**, 529-537.

Ball, F. G. and Rice, J. A. (1989) A note on single-channel autocorrelation functions. *Mathematical Biosciences*, **97**, 17-26.

Ball, F. G. and Rice, J. A. (1992) Stochastic models for ion channels: introduction and bibliography. *Mathematical Biosciences,* **112**, 189-206.

Ball, F. G. and Sansom, M. S. P. (1987) Temporal clustering of ion channel openings incorporating time interval omission. *IMA Journal of Mathematics Applied in Medicine and Biology*, **4**, 333-361.

Ball, F. G. and Sansom, M. S. P. (1988a) Aggregated Markov processes incorporating time interval omission. *Adv. Appl. Prob.*, **20**, 546-572.

Ball, F. G. and Sansom, M. S. P. (1988b) Single-channel autocorrelation functions: the effects of time interval omission. *Biophysical Journal*, **53**, 819-832.

REFERENCES

Ball, F. G. and Sansom, M. S. P. (1989) Ion-channel gating mechanisms: model identification and parameter estimation from single channel recordings. *Proceedings of the Royal Society* B, **236**, 385-416.

Ball, F. G. and Yeo, G. F. (1994) Numerical evaluation of observed sojourn time distributions for a single ion channel incorporating time interval omission. *Statist. Comp.*, **4**, 1-12.

Ball, F. G., Yeo, G. F., Milne, R. K., Edeson, R. O., Madsen, B. W. and Sansom, M. S. P. (1993a) Single ion channel models incorporating aggregation and time interval omission. *Biophysical Journal*, **64**, 357-374.

Barrett, J. N., Magleby, K. L. and Palotta, B. S. (1982) Properties of single calcium-activated potassium channels in cultured rat muscle. *Journal of Physiology*, **331**, 211-230.

Bates, S. E., Sansom, M. S. P., Ball, F. G., Ramsey, R. L. and Usherwood, P. N. R. (1990) Glutamate receptor-channel gating - maximum likelihood analysis of gigaohm seal recordings from locust muscle. *Biophysical Journal*, **58**, 219-229.

Bellman, R. (1960) *Introduction to Matrix Analysis.* New York: McGraw-Hill.

REFERENCES

Beroukhim, R. and Unwin, N. (1995) Three-dimensional location of the main immunogenic region of the acetylcholine receptor. *Neuron*, **15**, 323-331.

Bever, C. T. J., Anderson, P. A., Leslie, J., Panitch, H. S., Dhib-Jalbut, S., Khan, O. A., *et al.* (1996) Treatment with oral 3,4 diaminopyridine improves leg strength in multiple sclerosis patients. *Neurology*, **47**, 1457-1462.

Blatz, A. L. (1989) Large conductance Ca-activated K channels in adult rat diaphragm: single channel properties and block by protons. *Biophysical Journal*, **55**, 545a.

Blatz, A. L. and Magleby, K. L. (1986) Correcting single channel data for missed events. *Biophysical Journal*, **49**, 967-980.

Blatz, A. L. and Magleby, K. L. (1987) Calcium-activated potassium channels. *Trends Neurosci.*, **10**, 463-467.

Brisson, A. and Unwin, P. N. T. (1985) Quaternary structure of the acetylcholine receptor. *Nature*, **315**, 474-477.

Changeux, J. -P., Devillers-Thiéry, A. and Chemouilli, P. (1984) Acetylcholine receptor: An allosteric protein. *Science*, **225**, 1335-1345.

REFERENCES

Chay, T. T. (1988) Kinetic modelling for the channel gating process from single channel patch clamp data. *J. Theor. Biol.*, **132**, 449-468.

Christensen, O. and Zeuthen, T. (1987) Maxi K^+ channels in leaky epithelia are regulated by intracellular Ca^{2+}, pH and membrane potential. *Plügers Archiv*, **408**, 249-259.

Chung, S. H., Moore, J. B., Xia, L., Premkumar, L. S. and Gage, P. W. (1990) Characterization of single channel currents using digital signal processing techniques based on hidden Markov models. *Phil. Trans. R. Soc. Lond.* B, **329**, 265-285.

Çinlar, E. (1969) Markov renewal theory. *Adv. Appl. Prob.*, **1**, 123-187.

Çinlar, E. (1975) *Introduction to Stochastic Processes*. Prentice-Hall, Englewood Cliffs, NJ.

Clarke, B. R., Milne, R. K. and Yeo, G. F. (1993) Local asymptotic theory for multiple solutions of likelihood equations, with application to a single ion channel model. *Scand. J. Statist.*, **20**, 133-146.

Colquhoun, D. and Hawkes, A. G. (1977) Relaxation and fluctuations of

membrane currents that flow through drug-operated channels. *Proceedings of the Royal Society* B, **199**, 231-262.

Colquhoun, D. and Hawkes, A. G. (1981) On the stochastic properties of single ion channels. *Proceedings of the Royal Society* B, **211**, 205-235.

Colquhoun, D. and Hawkes, A. G. (1982) On the stochastic properties of bursts of single ion channel openings and of clusters of bursts. *Phil. Trans. R. Soc. Lond.* B, **300**, 1-59.

Colquhoun, D. and Hawkes, A. G. (1983) The principles of stochastic interpretation of ion-channel mechanisms. In *Single-Channel Recording* (First Edition) (eds B. Sakmann and E. Neher), pp. 135-175. New York: Plenum.

Colquhoun, D. and Hawkes, A. G. (1987) A note on correlations in single ion channel records. *Proceedings of the Royal Society* B, **230**, 15-52.

Colquhoun, D. and Hawkes, A. G. (1995) The principles of stochastic interpretation of ion-channel mechanisms. In *Single-Channel Recording* (Second Edition) (eds B. Sakmann and E. Neher), pp. 397-482. New York: Plenum.

Colquhoun, D. and Ogden, D. C. (1988) Activation of ion channels in the frog

end-plate by high concentrations of acetylcholine. *Journal of Physiology, Lond.* **395**, 131-159.

Colquhoun, D. and Sakmann, B. (1981) Fluctuations in the microsecond time range of the current through single acetylcholine receptor ion channels. *Nature*, **294**, 464-466.

Colquhoun, D. and Sakmann, B. (1985) Fast events in single-channel currents activated by acetylcholine and its analogues at the frog muscle end-plate. *Journal of Physiology*, **369**, 501-557.

Colquhoun, D. and Sigworth, F. J. (1983) Fitting and statistical analysis of single-channel records. In *Single-Channel Recording* (First Edition) (eds B. Sakmann and E. Neher), pp. 191-263. New York: Plenum.

Colquhoun, D. and Sigworth, F. J. (1995) Fitting and statistical analysis of single-channel records. In *Single-Channel Recording* (Second Edition) (eds B. Sakmann and E. Neher), pp. 483-587. New York: Plenum.

Conti-Tronconi, B. M. and Raftery, M. A. (1982) The nicotinic cholinergic receptor: Correlation of molecular structure with functional properties. *Annu. Rev. Biochem.*, **51**, 491-530.

REFERENCES

Cook, D. L., Ikeuchi, M. and Fujimoto, W. Y. (1984) Lowering of pH inhibits Ca^{2+}-activated K^+ channels in pancreatic b cells. *Plügers Archiv*, **391**, 85-100.

Couturier, S., Bertrand, D., Matter, J. M., Hernandez, M. -C., Bertrand, S., Millar, N., Valera, S., Barkas, T. and Ballivet, M. (1990) Neuronal nicotinic acetylcholine receptor subunit (α7) is developmentally regulated and forms a homo-oligomeric channel blocked by α-BTX. *Neuron*, **5**, 847-856.

Crouzy, S. C. and Sigworth, F. J. (1990) Yet another approach to the dwell-time omission problem of single-channel analysis. *Biophysical Journal*, **58**, 731-743.

Dabrowski, A. R., McDonald, D. and Rosler, U. (1990) Renewal theory properties of ion channels. *Ann. Statist.*, **18**, 1091-1115.

DiNubile, M. J. and Hokama, Y. (1995) The ciguatera poisoning syndrome from farm-raised salmon. *Ann. Intern. Med.*, **122**, 113-114.

Dionne, V. E., and Leibowitz, M. (1982) Acetylcholine receptor kinetics: a description from single-channel currents at snake neuromuscular junctions. *Biophysical Journal*, **39**, 253-261.

Dionne, V. E., Steinbach, J. H. and Stevens, C. F. (1978) An analysis of the

dose-response relationship at voltage-clamped frog neuromuscular junctions. *Journal of Physiology*, **281**, 421-444.

Doster, W., Schirmacher, W. and Settles, M. (1990) Percolation model of ionic channel dynamics. *Biophysical Journal*, **57**, 681-684.

Doyle, D. A., Cabral, J. M., Pfeutzner, R. A., Kuo, A., Gulbis, J. M., Cohen, S. L., Cahit, B. T., MacKinnon, R. (1998) The structure of the potassium channel: molecular basis of K^+ conduction and selectivity. *Science*, **280**, 69-77.

Edeson, R. O., Ball, F. G., Yeo, G. F., Milne, R. K. and Davies, S. S. (1994) Model properties underlying non-identifiability in single channel inference. *Proceedings of the Royal Society* B, **255**, 21-29.

Eigen, M. (1968) New looks and outlooks on physical enzymology. *Q. Rev. Biophys.*, **1**, 3-33.

Fredkin, D. R., Montal, M. and Rice, J. A. (1985) Identification of aggregated Markovian models: application to the nicotinic acetylcholine receptor. In *Proc. Berkeley Conf. in Honor of Jerzy Neyman and Jack Kiefer* (eds L. M. LeCam and R.A. Olshen), vol. 1, pp. 269-289. Belmont: Wadsworth.

REFERENCES

Fredkin, D. R. and Rice, J. A. (1992a) Maximum likelihood estimation and identification directly from single-channel recordings. *Proceedings of the Royal Society* B, **249**, 125-132.

Fredkin, D. R. and Rice, J. A. (1992b) Bayesian restoration of single channel patch clamp recordings. *Biometrics*, **48**, 427-448.

Fröberg, C. -E. (1969) *Introduction to Numerical Analysis,* (Second Edition). London: Addison-Wesley.

Golowasch, J., Kirkwood, A. and Miller, C. (1986) Allosteric effects of Mg^{2+} on the gating of Ca^{2+}-activated K^{+} channels from mammalian skeletal muscle. *Journal of Experimental Biology*, **124**, 5-13.

Grimmett, G. R. and Stirzaker, D. R. (1982) *Probability and random processes.* Clarendon Press: Oxford.

Hamill, O. P. and Sakmann, B. (1981) Multiple conductance states of single acetylcholine receptor channels in embryonic muscle cells. *Nature*, **294**, 462-464.

Hawkes, A. G., Jalali, A. and Colquhoun, D. (1990) The distributions of the apparent open times and shut times in a single channel record when brief events

cannot be detected. *Phil. Trans. R. Soc. Lond.*, A, **332**, 511-538.

Hawkes, A. G., Jalali, A. and Colquhoun, D. (1992) Asymptotic distributions of apparent open times and shut times in a single channel record allowing for the omission of brief events. *Phil. Trans. R. Soc. Lond.*, B, **337**, 383-404.

Hill, A. V. (1909) The mode of action of nicotine and curare determined by the form of the contraction curve and the method of temperature coefficients. *Journal of Physiology*, **39**, 361-373.

Hille, B. (1992) *Ionic Channels of Excitable Membranes.* (Second Edition.) Sinauer Associates: Sunderland, MA.

Hodgson, M. E. A. (1999) A Bayesian restoration of an ion channel signal. *J. R. Statist. Soc.*, B, **61**, 95-114.

Horn, R. and Lange, K. (1983) Estimating kinetic constants from single channel data. *Biophysical Journal,* **43**, 207-233.

Hucho, F., Tsetlin, V. I. and Machold, J. (1996) The emerging three-dimensional structure of a receptor:- the nicotinic acetylcholine receptor. *Eur. J. Biochem.*, **239**, 539-557.

REFERENCES

Jackson, M. B. (1986) Kinetics of unliganded acetylcholine receptor channel gating. *Biophysical Journal,* **49**, 663-672.

Jackson, M. B. (1988) Dependence of acetylcholine receptor channel kinetics on agonist concentration in cultured mouse muscle fibres. *Journal of Physiology,* **397**, 555-583.

Jackson, M. B. (1989) Perfection of a synaptic receptor: Kinetics and energetics of the acetylcholine receptor. *Proceedings of the National Academy of Sciences of the USA,* **86**, 2199-2203.

Jackson, M. B. (1993) Thermodynamics of Membrane Receptors and Channels. CRC Press.

Jackson, M. B., Wong, B. S., Morris, C. E., Lecar, H. and Christian, C. N. (1983) Successive openings of the same acetylcholine receptor channel are correlated in open time. *Biophysical Journal,* **42**, 109-114.

Jalali, A. and Hawkes, A. G. (1992a) The distribution of apparent occupancy times in a two-state Markov process in which brief events cannot be detected. *Adv. Appl. Prob.*, **24**, 288-301.

REFERENCES

Jalali, A. and Hawkes, A. G. (1992b) Generalised eigenproblems arising in aggregated Markov processes allowing for time interval omission. *Adv. Appl. Prob.*, **24**, 302-321.

Karlin, A. (1967) On the application of a plausible model of allosteric proteins to the receptor for acetylcholine. *J. Theor. Biol.*, **16**, 306-320.

Keilson, J. (1979) *Markov Chain Models - Rarity and Exponentiality.* Springer: New York.

Kelly, F. P. (1979) *Reversibility and Stochastic Networks.* Chichester: Wiley.

Kendall, M. G. and Stuart, A. (1977) The Advanced Theory of Statistics, Vol. I. (4th ed.) Charles Griffin and Company Limited, High Wycombe.

Kerry, C. J., Ramsey, R. L., Sansom, M. S. P. and Usherwood, P. N. R. (1988) Glutamate receptor-channel kinetics: the effect of glutamate concentration. *Biophysical Journal,* **53**, 39-52.

Ketchum, K. A. *et al.* (1995) A new family of outwardly rectifying potassium channel proteins with two pore domains in tandem. *Nature*, **376**, 690-695.

REFERENCES

Kienker, P. (1989) Equivalence of aggregated Markov models of ion channel gating. *Proceedings of the Royal Society* B, **236**, 269-309.

Kijima, S. and Kijima, H. (1987) Statistical analysis of channel current from a membrane patch. I. Some stochastic properties of ion channels or molecular systems in equilibrium. *J. Theor. Biol.*, **128**, 423-434.

Kistler, J., Stroud, R. M., Klymkowsky, M. W., Lalancette, R. A. and Fairclough, R. H. (1982) Structure and function of an acetylcholine receptor. *Biophysical Journal*, **37**, 371-383.

Koshland, D. E. JR., Némethy, G. and Filmer, D. (1966) Comparison of experimental binding data and theoretical models in proteins containing subunits. *Biochem.*, **5**, 365-385.

Krzanowski, W. J. (1988) *Principles of Multivariate Analysis*. Oxford: Clarendon.

Kume, H., Takagi, K., Satake, T., Tokuno, H. and Tomita, T. (1990) Effects of intracellular pH on calcium-activated potassium channels in rabbit tracheal smooth muscle. *Journal of Physiology*, **424**, 445-457.

REFERENCES

Latorre, R., Oberhauser, A., Labarca, P. and Alvarez, O. (1989) Varieties of calcium-activated potassium channels. *Annu. Rev. Physiol.*, **51**, 385-399.

Läuger, P. (1988) Internal motions in proteins and gating kinetics of ionic channels. *Biophysical Journal,* **53**, 877-884.

Läuger, P. (1995) Conformation transitions of ionic channels. In *Single-Channel Recording* (Second Edition) (eds B. Sakmann and E. Neher), pp. 651-662. New York: Plenum.

Laurido, C., Wolff, D. and Latorre, R. (1990) Effect of pH in a Ca^{2+}-activated K^{+} channel [K(Ca)] from rat skeletal muscle. *Biophysical Journal*, **57**, 507a.

Lehmann, E. L. (1983) *Theory of Point Estimation.* New York: John Wiley.

Lindstrom, J. , Schoepfer, R. and Whiting, P. (1987) Molecular studies of the neuronal nicotinic acetylcholine receptor family. *Mol. Neurobiol.*, **1**, 281-337.

MacKinnon, R. (1991) Determination of the subunit stoichiometry of a voltage-activated potassium channel. *Nature*, **350**, 232-235.

Magleby, K. L. and Weiss, D. S. (1990a) Estimating kinetic parameters for single

channels with simulation: a general method that resolves the missed events problem and accounts for noise. *Biophysical Journal*, **58**, 1411-1426.

Magleby, K. L. and Weiss, D. S. (1990b) Identifying kinetic gating mechanisms for ion channels by using two-dimensional distributions of simulated dwell times. *Proceedings of the Royal Society* B, **241**, 220-228.

Magleby, K. L. and Pallotta, B. S. (1983a) Calcium-dependence of open and shut interval distributions from calcium-activated potassium channels in cultured rat muscle. *Journal of Physiology*, **344**, 585-604.

Magleby, K. L. and Pallotta, B. S. (1983b) Burst kinetics of single calcium-activated potassium channels in cultured rat muscle. *Journal of Physiology*, **344**, 605-623.

Mardia, K. V., Kent, J. T. and Bibby, J. M. (1979) *Multivariate Analysis*. London: Academic Press.

McManus, O. B., Blatz, A. L. and Magleby, K. L. (1985) Inverse relationship of the durations of adjacent open and shut intervals for Cl and K channels. *Nature, Lond.* **317**, 625-627.

REFERENCES

McManus, O. B., Blatz, A. L. and Magleby, K. L. (1987) Sampling, log binning, fitting and plotting durations of open and shut intervals from single channels and the effects of noise. *Pfluegers Arch. Eur. J. Physiol.* **410**, 530-553.

McManus, O. B. and Magleby, K. L. (1988) Kinetic states and modes of single large-conductance calcium-activated potassium channels in cultured rat skeletal muscle. *Journal of Physiology*, **402**, 79-120.

McManus, O. B. and Magleby, K. L. (1989) Kinetic time constants independent of previous single-channel activity suggest Markov gating for a large-conductance Ca-activated K channel. *Journal of General Physiology*, **94**, 1037-1070.

McManus, O. B. and Magleby, K. L. (1991) Accounting for the Ca^{2+}-dependent kinetics of single large-conductance Ca^{2+}-activated K^{+} channels in rat skeletal muscle. *Journal of Physiology*, **443**, 739-777.

Methfessel, C. and Boheim, G. (1982) The gating of single calcium-dependent potassium channels is described by an activation/blockade mechanism. *Biophysics of Structure and Mechanism*, **9**, 35-60.

Millhauser, G. L., Salpeter, E. E. and Oswald, R. E. (1988) Diffusion models of ion-channel gating and the origin of power-law distributions from single-channel

recording. *Proceedings of the National Academy of Sciences of the USA,* **85**, 1502-1507.

Milne, R. K., Yeo, G. F., Edeson, R. O. and Madsen, B. W. (1988) Stochastic modelling of a single ion channel: an alternating renewal approach with application to limited time resolution. *Proceedings of the Royal Society* B, **233**, 247-292.

Milne, R. K., Yeo, G. F., Edeson, R. O. and Madsen, B. W. (1989) Estimation of single channel kinetic parameters from data subject to limited time resolution. *Biophysical Journal*, **55**, 673-676.

Moczydlowski, E. and Latorre, R. (1983) Gating kinetics of Ca^{2+}-activated K^{+} channels from rat muscle incorporated into planar lipid bilayers: evidence for two voltage-dependent Ca^{2+} binding reactions. *Journal of General Physiology*, **82**, 511-542.

Monod, J., Wyman, J. and Changeux, J. P. (1965) On the nature of allosteric transitions: a plausible model. *J. Mol. Biol.*, **12**, 88-118.

Neher, E. and Sakmann, B. (1976) Single-channel currents recorded from membrane of denervated frog muscle fibres. *Nature*, **260**, 799-802.

REFERENCES

Newsholme, E. A. and Start, C. (1973) Regulation in Metabolism. Bristol: Wiley.

Oberhauser, A., Alvarez, O. and Latorre, R. (1988) Activation by divalent cations of a Ca^{2+}-activated K^+ channel from skeletal muscle membrane. *Journal of General Physiology*, **92**, 67-86.

Ogden, D. C., Colquhoun, D. and Marshall, C. G. (1987) Activation of nicotinic ion channels by acetylcholine analogues. In *Cellular and molecular basis of cholinergic function* (eds M. J. Dowdall and J. N. Hawthorne), pp. 133-151. Chichester: Ellis Horwood.

Pennefather, P., Lancaster, B., Adams, P. R., and Nicoll, R. A. (1985) Two distinct Ca-dependent K currents in bullfrog sympathetic ganglion cells. *Proc. Natl. Acad. Sci. USA*, **82**, 3040-3044.

Prod'hom, B., Pietrobon, D. and Hess, P. (1987) Direct Measurement of proton transfer rates to a group controlling the dihydropyridine-sensitive Ca^{2+} channel. *Nature*, **329**, 243-246.

Romey, G. and Lazdunski, M. (1984) The coexistence in rat muscle cells of two distinct classes of Ca^{2+}-dependent K^+ channels with different pharmacological

properties and different physiological function. *Biochem. Biophys. Res. Commun.*, **118**, 669-674.

Rose, M. R. (1998) Neurological channelopathies. *BMJ*, **316**, 1104-1105.

Rothberg, B. S. and Magleby, K. L. (1998) Kinetic structure of large-conductance Ca^{2+}-activated K^+ channels suggests that the gating includes transitions through intermediate or secondary states. A mechanism for flickers. *Journal of General Physiology,* **111**, 751-780.

Rothberg, B. S. and Magleby, K. L. (1999) Gating kinetics of single large-conductance Ca^{2+}-activated K^+ channels in high Ca^{2+} suggest a two-tiered allosteric gating mechanism. *Journal of General Physiology,* **114**, 93-124.

Roux, B. and Sauvé, R. (1985) A general solution to the time interval omission problem applied to single channel analysis. *Biophysical Journal,* **48**, 149-158.

Sakmann, B., Patlak, J. and Neher, E. (1980) Single acetylcholine-activated channels show burst-kinetics in presence of desensitizing concentrations of agonist. *Nature*, **286**, 71-73.

Sansom, M. S. P. (1998) Ion channels: A first view of K^+ channels in atomic

glory. *Current Biology,* **8**, R450-R452.

Sansom, M. S. P., Adcock, C. and Smith, G. R. (1998) Modelling and Simulation of Ion Channels: Applications to the Nicotinic Acetylcholine Receptor. *Journal of Structural Biology,* **121**, 246-262.

Sansom, M. S. P., Ball, F. G., Kerry, C. J., McGee, R., Ramsey, R. L. and Usherwood, P. N. R. (1989) Markov, fractal, diffusion and related models of ion channel gating: a comparison with experimental data from two ion channels. *Biophysical Journal,* **56**, 1229-1243.

Schreiber, M. and Salkoff, L. (1997) A novel calcium-sensing domain in the BK channel. *Biophysical Journal,* **73**, 1355-1363.

Sigg, D., Qian, H. and Bezanilla, F. (1999) Kramers' Diffusion Theory Applied to Gating Kinetics of Voltage-Dependent Ion Channels. *Biophysical Journal,* **76**, 782-803.

Silberberg, S. D., Lagrutta, A., Adelman, J. P. and Magleby, K. L. (1996) Wanderlust kinetics and variable Ca^{2+}-sensitivity of Drosophila, a large conductance Ca^{2+}-activated K^+ channel, expressed in oocytes. *Biophysical Journal,* **70**, 2640-2651.

REFERENCES

Silvey, S. D. (1975) *Statistical Inference*. London & New York: Chapman and Hall.

Steinbach, J. H. and Ifune, C. (1989) How many kinds of nicotinic acetylcholine receptor are there? *Trends Neurosci.*, **12**, 3-6.

Steinlein, O. K., Mulley, J. C., Propping, P., Wallace, R. H., Phillips, H. A., Scheffer, I. E., *et al.* (1995) A missense mutation in the neuronal nicotinic acetylcholine receptor alpha 4 subunit is associated with autosomal dominant nocturnal frontal lobe epilepsy. *Nat. Genet.*, **11**, 201-203.

Stromberg, K. R. (1981) *An Introduction to Classical Real Analysis*. Belmont: Wadsworth.

Toyoshima, C. and Unwin, N. (1988) Ion channel of acetylcholine receptor reconstructed from images of postsynaptic membranes. *Nature*, **336**, 247-250.

Unwin, N. (1989) The structure of ion channels in membranes of excitable cells. *Neuron*, **3**, 665-676.

Unwin, N. (1993) Nicotinic acetylcholine receptor at 9Å resolution. *J. Mol. Biol.*, **288**, 765-786.

REFERENCES

Unwin, N. (1995) Acetylcholine receptor channel imaged in the open state. *Nature*, **373**, 37-43.

Weber, G. (1975) Energetics of ligand binding to proteins. *Adv. Protein Chem.*, **29**, 1-83.

Yeo, G. F., Milne, R. K., Edeson, R. O. and Madsen, B. W. (1988) Statistical inference from single channel records: two-state Markov model with limited time resolution. *Proceedings of the Royal Society* B, **235**, 63-94.

Appendix A

This appendix contains a description of the method of maximum likelihood (see section 2.3 and Chapter 4 of this thesis). Parameter estimation in ion channel models has frequently employed the method of maximum likelihood (see, for example, Colquhoun and Sigworth (1983), Horn and Lange (1983), Ball and Sansom (1989) and Yeo *et al.* (1988)). This method can be formulated as follows (see, for example, Silvey (1975)). Consider a probability model in which observable independent random variables $X_1, X_2, ..., X_n$ have respective probability density functions $f_1(x_1, \theta), f_2(x_2, \theta), ..., f_n(x_n, \theta)$, where θ is a k-dimensional row vector of parameters. The joint probability density function of $X_1, X_2, ..., X_n$ is the product of their individual probability density functions and may be regarded as a function of θ, in which case it is known as the likelihood function L of the random sample and we write

$$L(\theta) = f_1(x_1, \theta) f_2(x_2, \theta) \ldots f_n(x_n, \theta).$$

The method of maximum likelihood selects the estimate $\hat{\theta}(x_1, x_2, ..., x_n)$ of θ if $\hat{\theta}(x_1, x_2, ..., x_n)$ is the value of θ which maximises the likelihood function $L(\theta)$. Given an estimate $\hat{\theta}(x_1, x_2, ..., x_n)$ of θ, the corresponding k-vector of random variables $\hat{\theta}(X_1, X_2, ..., X_n)$ is called an estimator of θ. Frequently there will be a unique maximum likelihood estimator $\hat{\theta}(X_1, X_2, ..., X_n)$ of θ, and often it may be obtained by the process of differentiation.

APPENDIX A

Since each of the functions $L(\theta)$ and $\ln L(\theta)$ attains its maximum for the same value of θ, we may instead maximise a normalised version of the likelihood function (Yeo *et al.* (1988)) such as

$$l(\theta) = n^{-1} \ln L(\theta),$$

which we term the normalised log-likelihood function. Let θ_i denote the ith element of the vector θ. Assuming $l(\theta)$ is differentiable, the likelihood equations are given by the equations

$$\frac{\partial l(\theta)}{\partial \theta_i} = 0, \quad (i = 1, 2, \ldots, k),$$

whose solutions are local maxima, local minima, or saddle points of $l(\theta)$. For any local maxima $\hat{\theta}$ which is a solution of these equations, the (per observation) information matrix given by the Hessian

$$J(\hat{\theta}) = \left[\frac{\partial^2 l(\theta)}{\partial \theta_i \partial \theta_j} \right] \Bigg|_{\theta = \hat{\theta}}$$

gives information regarding the precision of $\hat{\theta}(X_1, X_2, \ldots, X_n)$ as an estimator of the true parameter θ. Further, the estimated asymptotic dispersion matrix of the estimator $\hat{\theta}$ is given by the matrix $n^{-1}[J(\hat{\theta})]^{-1}$, whose entries comprise the estimated variances and covariances of $\hat{\theta}_i$, and which can be used to construct confidence regions for θ since the quadratic form $n(\hat{\theta} - \theta) J(\hat{\theta}) (\hat{\theta} - \theta)^{\top}$ has asymptotically a χ^2_k distribution (see section 5.3.2 of Silvey (1975)).

APPENDIX A

Note that under certain regularity conditions (see, for example, Lehmann (1983)), maximum likelihood estimators are consistent, asymptotically normally distributed (with means equal to the true parameter values and dispersion matrix $n^{-1}[J(\hat{\theta})]^{-1}$) and of minimum variance. These asymptotic properties justify the use of the method of maximum likelihood to estimate parameters in ion channel models since the data sets associated with these models are usually very large.

Appendix B

This appendix contains a brief account of elementary ligand-receptor theory (Newsholme and Start (1973), Aidley and Stanfield (1996), Jackson (1993)) based on the model of Hill (1909) for the reaction between haemoglobin and oxygen. We assume here that a channel has n equivalent agonist binding sites and that there are no intermediate states of binding site occupancy, i.e. the number of agonist molecules bound to the channel is either zero or n.

Let $[R]$ be the concentration of receptors with no agonist molecules bound, let $[A_nR]$ be the concentration of receptors with n agonist molecules bound and let $[A]$ (or, equivalently, a) be the concentration of agonist molecules. Then the reaction between n molecules of agonist and a receptor with n agonist binding sites can be described by the equation

$$R + nA \underset{k_{-1}}{\overset{k_{+1}}{\rightleftarrows}} A_nR,$$

where k_{+1} and k_{-1} are transition rate constants. The equilibrium binding constant, $K_b^{(n)}$, equal to k_{+1} / k_{-1}, is given by

$$K_b^{(n)} = \frac{[A_nR]}{[R]\,[A]^n}$$

B.1

so that $[A_nR] = K_b^{(n)} [R] a^n$. Letting p be the proportion of channels that have n agonist molecules bound, we have

$$p = \frac{[A_n R]}{[R] + [A_n R]}$$

$$= \frac{K_b^{(n)} [R] a^n}{[R] + K_b^{(n)} [R] a^n},$$

$$= \frac{a^n}{(K_b^{(n)})^{-1} + a^n},$$

and hence $p / (1 - p) = a^n K_b^{(n)}$. Thus we obtain the Hill equation

$$\log\left(\frac{p}{1 - p}\right) = n \log a + \log K_b^{(n)},$$

which can, in theory, be used to obtain a value for n.

Since, in practice, p cannot be measured directly, some other property has to be used as a measure of agonist-receptor action, and it is common practice to replace p with the channel open probability P_O in the Hill equation. The relation between the agonist concentration and the size of the response (P_O) is called the dose response curve.

A Hill plot consists of a graph of $P_O / (1 - P_O)$ against agonist concentration on logarithmic scales and the Hill coefficient, n_H, is usually obtained by measuring the slope of the Hill plot at the value of agonist concentration for which $P_O = 0.5$.

APPENDIX B

Following Hill (1909), we assumed that the channel can have only zero or n agonist molecules bound to it. This assumption predicts that the Hill plot should be linear with slope equal to n, the number of agonist binding sites on a channel. However, the assumption that partially ligated intermediates can be neglected is unrealistic (Weber (1975)). Hence the Hill coefficient should be interpreted cautiously as a lower bound for the number of binding sites.

The Hill coefficient is also an important and widely used indication of the degree of interaction between the channel subunits, in terms of agonist binding. At the two extremes $P_O = 0$ and $P_O = 1$, n_H takes the value one and there is no cooperativity between the binding sites on each subunit: in the case $P_O \to 0$, almost all the subunits have no agonist molecules bound and as $P_O \to 1$, almost all the subunits have agonist molecules bound. However, in the intermediate range, n_H reaches a maximum and the Hill plot looks roughly linear with $n_H > 1$. It should be noted that the overall shape of the Hill plot is hence sigmoidal. Whereas a value of $n_H = 1$ indicates a complete lack of cooperativity between the agonist molecules, a value of $n_H > 1$ indicates cooperativity in that the binding of one agonist molecule promotes the binding of another, and a value of $n_H < 1$ may indicate the presence of negative cooperativity. If n_H is equal to the number of receptor binding sites, n then there is total cooperativity in that the channel only ever has zero or n agonist molecules bound, as in the assumptions of the model discussed above. A value of n_H greater than one suggests that two or more agonist molecules must be bound to a channel before it becomes fully active.

Appendix C

This appendix contains numerical results for the $\alpha_2\beta_3$ model based on the expressions for various observable characteristics of bursts of openings and of clusters of bursts of openings derived by Colquhoun and Hawkes (1982) (see section 3.4.1.9.3).

C.1 Properties of Bursts of Channel Openings

Tables C.1.1 and C.1.2 contain results of numerical calculations of properties of bursts of channel openings for a range of agonist concentrations when $\beta = 0$ and $\beta = -1$, respectively.

APPENDIX C

Channel Property	Agonist Concentration		
	10^{-5} M	10^{-6} M	10^{-7} M
Probability that a channel has 2 agonist molecules bound at the start of a burst	0.962	0.698	0.109
Probability that a channel has 0 agonist molecules bound at the start of a burst	0.00016	0.0261	0.463
Expected number of openings in a burst	139.104	62.031	9.926
Expected number of openings in a burst starting in an open state in which 2 agonist molecules are bound	140.746	83.61	77.827
Expected number of openings in a burst starting in an open state in which 0 agonist molecules are bound	54.049	2.295	1.016
Expected length of an opening within a burst	1.000	0.999	0.979
Expected length of a closing within a burst	0.0734	0.0688	0.0690
Expected length of a closing between bursts	3.942	63.110	1362.015
Expected burst length	149.300	56.175	10.243
Expected total burst open time	139.165	61.974	9.627
Expected total burst closed time	10.135	4.201	0.615
Expected length of a burst starting in an open state in which 2 agonist molecules are bound	151.060	89.287	83.008
Expected length of a burst starting in an open state in which 0 agonist molecules are bound	57.825	2.012	0.619

Table C.1.1. Properties of bursts of channel openings when $\beta = 0$ for various agonist concentrations. All times are given in milliseconds.

APPENDIX C

Channel Property	Agonist Concentration		
	10^{-5} M	10^{-6} M	10^{-7} M
Probability that a channel has 2 agonist molecules bound at the start of a burst	0.708	0.412	0.0172
Probability that a channel has 0 agonist molecules bound at the start of a burst	0.00017	0.0292	0.777
Expected number of openings in a burst	786958.17	115920.6	3253.762
Expected number of openings in a burst starting in an open state in which 2 agonist molecules are bound	787147.91	119838.79	15956.97
Expected number of openings in a burst starting in an open state in which 0 agonist molecules are bound	431074.21	12803.64	166.66
Expected length of an opening within a burst	1.010	1.009	0.997
Expected length of a closing within a burst	0.0688	0.0878	0.251
Expected length of a closing between bursts	24723.42	68555.94	112612.76
Expected burst length	848819.91	127100.54	4060.43
Expected total burst open time	794695.32	116920.72	3244.33
Expected total burst closed time	54124.61	10179.83	816.10
Expected length of a burst starting in an open state in which 2 agonist molecules are bound	849024.15	131379.85	19577.31
Expected length of a burst starting in an open state in which 0 agonist molecules are bound	464960.84	14039.38	207.70

Table C.1.2. Properties of bursts of channel openings when β = -1 for various agonist concentrations. All times are given in milliseconds.

APPENDIX C

C.2 Properties of Clusters of Bursts of Channel Openings

Tables C.2.1 and C.2.2 contain results of calculations of properties of clusters of bursts of channel openings for a range of agonist concentrations when $\beta = 0$ and $\beta = -1$, respectively.

APPENDIX C

Channel Property	Agonist Concentration		
	10^{-5} M	10^{-6} M	10^{-7} M
Probability that a channel has 2 agonist molecules bound at the start of a cluster	0.962	0.717	0.12
Probability that a channel has 0 agonist molecules bound at the start of a cluster	0	0.0004	0.011
Expected number of openings in a cluster	139.138	63.636	17.427
Expected number of openings in a cluster starting in an open state in which 2 agonist molecules are bound	140.746	83.61	77.827
Expected number of openings in a cluster starting in an open state in which 0 agonist molecules are bound	54.05	2.295	1.016
Expected length of an opening within a cluster	1	0.999	0.988
Expected length of a closing within a cluster	0.734	0.0688	0.0689
Expected length of a closing between clusters	3.942	63.171	1355.279
Expected length of a closing between bursts in a cluster	1.25	1.232	0.489
Expected length of any closing	0.101	1.06	77.833
Expected cluster length	149.337	67.899	18.345
Expected total cluster open time	139.199	63.588	17.212
Expected total cluster closed time	10.138	4.311	1.132
Expected length of a cluster starting in an open state in which 2 agonist molecules are bound	151.061	89.287	83.007
Expected length of a cluster starting in an open state in which 0 agonist molecules are bound	57.825	2.012	0.619
Expected number of bursts in a cluster	1.822	1.133	1.101
Expected number of openings in a burst	76.374	56.143	15.835
Expected burst length	81.408	59.759	16.624
Expected total burst time per cluster	148.31	67.735	18.295

Table C.2.1. Properties of clusters of bursts of channel openings when $\beta = 0$ for various agonist concentrations. All times are given in milliseconds.

Channel Property	Agonist Concentration		
	10^{-5} M	10^{-6} M	10^{-7} M
Probability that a channel has 2 agonist molecules bound at the start of a cluster	0.807	0.235	0.00709
Probability that a channel has 0 agonist molecules bound at the start of a cluster	0.0493	0.461	0.908
Expected number of openings in a cluster	739565.18	69594.9	1435.97
Expected number of openings in a cluster starting in an open state in which 2 agonist molecules are bound	756486.65	119111.66	15945.12
Expected number of openings in a cluster starting in an open state in which 0 agonist molecules are bound	414282.9	12725.98	166.54
Expected length of an opening within a cluster	1.01	1.009	0.997
Expected length of a closing within a cluster	0.0688	0.0878	0.251
Expected length of a closing between clusters	24674.25	68382.04	112454.98
Expected length of a closing between bursts in a cluster	10.896	4.787	3.786
Expected length of any closing	0.102	1.07	78.564
Expected cluster length	797701.16	76307.21	1791.83
Expected total cluster open time	746836.43	70195.13	1431.58
Expected total cluster closed time	50864.69	6112.08	360.25
Expected length of a cluster starting in an open state in which 2 agonist molecules are bound	815952.48	130582.65	19562.8
Expected length of a cluster starting in an open state in which 0 agonist molecules are bound	446849.48	13954.23	207.55
Expected number of bursts in a cluster	420.56	372.1	73.61
Expected number of openings in a burst	1758.53	187.03	19.51
Expected burst length	1885.9	200.3	20.61
Expected total burst time per cluster	793129.52	74530.59	1516.9

Table C.2.2. Properties of clusters of bursts of channel openings when β= -1 for various agonist concentrations. All times are given in milliseconds.

Appendix D

This appendix contains expressions for the second partial derivatives of the normalised log-likelihood defined in equation (4.30) under each of the three approximations described in section 4.1.2.2 but with agonist concentration dependent opening rates incorporated as described in section 4.3.2.1. These derivatives are used to calculate standard deviations and correlations of parameter estimates (see section 4.3.2.2).

D.1 Single Exponential Approximations

Define probability density functions $f_O(u)$ and $f_C(v)$ of adjusted observed openings and closings, respectively, as follows. Let

$$f_O(u) = \begin{cases} 0 & u \leq 0 \\ r^{-1} \exp(-u/r) & u > 0 \end{cases}$$

and

$$f_C(v) = \begin{cases} 0 & v \leq 0 \\ s^{-1} \exp(-v/s) & v > 0, \end{cases}$$

where the definitions of r and s are given in D.1.1 or D.1.2, depending upon which single exponential approximation is under consideration. The normalised

log-likelihood is given by

$$l(\mu) = m^{-1} \sum_{i=1}^{m} [\ln(r^{-1}\exp(-u_i r^{-1})) + \ln(s^{-1}\exp(-v_i s^{-1}))]$$

$$= -[\ln r + \ln s + \bar{u} r^{-1} + \bar{v} s^{-1}],$$

where

$$\bar{u} = m^{-1} \sum_{i=1}^{m} u_i \qquad \text{and} \qquad \bar{v} = m^{-1} \sum_{i=1}^{m} v_i .$$

Throughout this appendix, let the subscripts $_O$ and $_C$ denote partial differentiation with respect to μ_O and μ_C, respectively. Then

$$l_O(\mu) = (\bar{u} r^{-2} - r^{-1}) r_O + (\bar{v} s^{-2} - s^{-1}) s_O,$$

$$l_C(\mu) = (\bar{u} r^{-2} - r^{-1}) r_C + (\bar{v} s^{-2} - s^{-1}) s_C,$$

$$l_{OO}(\mu) = (\bar{u} r^{-2} - r^{-1}) r_{OO} + (r^{-2} - 2\bar{u} r^{-3}) r_O^2$$
$$+ (\bar{v} s^{-2} - s^{-1}) s_{OO} + (s^{-2} - 2\bar{v} s^{-3}) s_O^2,$$

$$l_{CC}(\mu) = (\bar{u} r^{-2} - r^{-1}) r_{CC} + (r^{-2} - 2\bar{u} r^{-3}) r_C^2$$
$$+ (\bar{v} s^{-2} - s^{-1}) s_{CC} + (s^{-2} - 2\bar{v} s^{-3}) s_C^2$$

and

$$l_{OC}(\mu) = (\bar{u}r^{-2} - r^{-1})r_{OC} + (r^{-2} - 2\bar{u}r^{-3})r_O r_C$$
$$+ (\bar{v}s^{-2} - s^{-1})s_{OC} + (s^{-2} - 2\bar{v}s^{-3})s_O s_C .$$

Sections D.1.1 and D.1.2 contain expressions for r, s and their first and second partial derivatives under the approximations described in sections 4.1.2.2.1 and 4.1.2.2.2, but with agonist concentration dependent opening rates incorporated.

D.1.1 Approximation derived by ignoring Undetected Sojourns

Under the approximation described in section 4.1.2.2.1, but with agonist concentration dependent opening rates incorporated,

$$r = \mu_O \exp(a\tau_C/\mu_C) \qquad \text{and} \qquad s = a^{-1}\mu_C \exp(\tau_O/\mu_O).$$

It follows that

$$r_O = \exp(a\tau_C/\mu_C),$$

$$s_O = -a^{-1}\mu_C\mu_O^{-2}\tau_O \exp(\tau_O/\mu_O),$$

$$r_C = -a\mu_O\mu_C^{-2}\tau_C \exp(a\tau_C/\mu_C),$$

$$s_C = a^{-1}\exp(\tau_O/\mu_O),$$

$$r_{OO} = 0,$$

$$s_{OO} = a^{-1}\mu_C\mu_O^{-3}\tau_O\exp(\tau_O/\mu_O)(\tau_O\mu_O^{-1} + 2),$$

$$r_{CC} = a\mu_O\mu_C^{-3}\tau_C\exp(a\tau_C/\mu_C)(a\tau_C\mu_C^{-1} + 2),$$

$$s_{CC} = 0,$$

$$r_{OC} = -a\mu_C^{-2}\tau_C\exp(a\tau_C/\mu_C)$$

and

$$s_{OC} = -a^{-1}\mu_O^{-2}\tau_O\exp(\tau_O/\mu_O).$$

D.1.2 Approximation using Exponential Distributions with True Means

Under the approximation described in section 4.1.2.2.2, but with agonist concentration dependent opening rates incorporated,

$$r = (\mu_O + a^{-1}\mu_C)\exp(a\tau_C/\mu_C) - a^{-1}\mu_C - \tau_C$$

and

$$s = (\mu_O + a^{-1}\mu_C)\exp(\tau_O/\mu_O) - \mu_O - \tau_O.$$

It follows that

APPENDIX D

$$r_O = \exp(a\tau_C/\mu_C),$$

$$s_O = [1 - \mu_O^{-2}\tau_O(\mu_O + a^{-1}\mu_C)]\exp(\tau_O/\mu_O) - 1,$$

$$r_C = [a^{-1} - a\mu_C^{-2}\tau_C(\mu_O + a^{-1}\mu_C)]\exp(a\tau_C/\mu_C) - a^{-1},$$

$$s_C = a^{-1}\exp(\tau_O/\mu_O),$$

$$r_{OO} = 0,$$

$$s_{OO} = \tau_O\mu_O^{-3}[\tau_O + a^{-1}\mu_O^{-1}\mu_C\tau_O + 2a^{-1}\mu_C]\exp(\tau_O/\mu_O),$$

$$r_{CC} = \tau_C\mu_C^{-3}[a\tau_C + a^2\mu_C^{-1}\mu_O\tau_C + 2a\mu_O]\exp(a\tau_C/\mu_C),$$

$$s_{CC} = 0,$$

$$r_{OC} = -a\tau_C\mu_C^{-2}\exp(a\tau_C/\mu_C)$$

and

$$s_{OC} = -a^{-1}\tau_C\mu_O^{-2}\exp(\tau_O/\mu_O).$$

D.2 Bi-exponential Approximation

Incorporating agonist concentration dependence of opening rates into the expression for the approximate probability density function of adjusted observed openings given in section 4.1.2.2.3 and a similar expression for the equivalent probability density function for closings, let

$$f(u) = \begin{cases} 0 & u \le 0 \\ \frac{\alpha_1}{\alpha_2}\exp(-u/\alpha_2) + \frac{\alpha_3}{\alpha_4}\exp(-u/\alpha_4) & u > 0, \end{cases}$$

where

$$\alpha_1 = (\alpha_2 - a^{-1}\mu_C)(\alpha_2 - \alpha_4)^{-1},$$

$$\alpha_3 = 1 - \alpha_1,$$

$$\alpha_2 = \tfrac{1}{2}(p + (p^2 - 4q)^{1/2})$$

and

$$\alpha_4 = \tfrac{1}{2}(p - (p^2 - 4q)^{1/2}),$$

where

$$p = (\mu_O + a^{-1}\mu_C)\exp(a\tau_C/\mu_C) - \tau_C$$

and

$$q = a^{-1}\mu_O\mu_C\exp(a\tau_C/\mu_C) + \tfrac{1}{2}\tau_C^2.$$

Similarly, let

$$g(v) = \begin{cases} 0 & v \le 0 \\ \frac{\beta_1}{\beta_2}\exp(-v/\beta_2) + \frac{\beta_3}{\beta_4}\exp(-v/\beta_4) & v > 0, \end{cases}$$

where

$$\beta_1 = (\mu_O - \beta_2)\,(\beta_4 - \beta_2)^{-1},$$

$$\beta_3 = 1 - \beta_1,$$

$$\beta_2 = \tfrac{1}{2}(x + (x^2 - 4y)^{\frac{1}{2}})$$

and

$$\beta_4 = \tfrac{1}{2}(x - (x^2 - 4y)^{\frac{1}{2}}),$$

where

$$x = (\mu_O + a^{-1}\mu_C)\exp(\tau_O/\mu_O) - \tau_O$$

and

$$y = a^{-1}\mu_O\mu_C \exp(\tau_O/\mu_O) + \tfrac{1}{2}\tau_O^2.$$

Then $f(u)$ and $g(v)$ are the probability density functions of adjusted observed openings and closings, respectively, under this approximation, and the normalised log-likelihood is given by

$$l(\mu) = m^{-1} \sum_{i=1}^{m} [\ln f(u_i) + \ln g(v_i)] .$$

It follows that

$$l_O(\mu) = m^{-1} \sum_{i=1}^{m} \left[\left(\frac{1}{f(u_i)}\right) f_O(u_i) + \left(\frac{1}{g(v_i)}\right) g_O(v_i)\right],$$

$$l_C(\mu) = m^{-1} \sum_{i=1}^{m} \left[\left(\frac{1}{f(u_i)}\right) f_C(u_i) + \left(\frac{1}{g(v_i)}\right) g_C(v_i)\right],$$

APPENDIX D

$$l_{OO}(\mu) = m^{-1} \sum_{i=1}^{m} \left[\left(\frac{1}{f(u_i)} \right) f_{OO}(u_i) - \left(\frac{1}{f(u_i)} \right)^2 (f_O(u_i))^2 + \left(\frac{1}{g(v_i)} \right) g_{OO}(v_i) - \left(\frac{1}{g(v_i)} \right)^2 (g_O(v_i))^2 \right],$$

$$l_{CC}(\mu) = m^{-1} \sum_{i=1}^{m} \left[\left(\frac{1}{f(u_i)} \right) f_{CC}(u_i) - \left(\frac{1}{f(u_i)} \right)^2 (f_C(u_i))^2 + \left(\frac{1}{g(v_i)} \right) g_{CC}(v_i) - \left(\frac{1}{g(v_i)} \right)^2 (g_C(v_i))^2 \right]$$

and

$$l_{OC}(\mu) = m^{-1} \sum_{i=1}^{m} \left[\left(\frac{1}{f(u_i)} \right) f_{OC}(u_i) - \left(\frac{1}{f(u_i)} \right)^2 f_O(u_i) f_C(u_i) + \left(\frac{1}{g(v_i)} \right) g_{OC}(v_i) - \left(\frac{1}{g(v_i)} \right)^2 g_O(v_i) g_C(v_i) \right],$$

where

$$f_O(u) = \sum_{i=1}^{4} \frac{\partial f(u)}{\partial \alpha_i} \cdot \frac{\partial \alpha_i}{\partial \mu_O},$$

$$f_C(u) = \sum_{i=1}^{4} \frac{\partial f(u)}{\partial \alpha_i} \cdot \frac{\partial \alpha_i}{\partial \mu_C},$$

$$f_{OO}(u) = \sum_{j=1}^{4} \left[\left(\sum_{i=1}^{4} \frac{\partial^2 f(u)}{\partial \alpha_i \partial \alpha_j} \cdot \frac{\partial \alpha_i}{\partial \mu_O} \right) \left(\frac{\partial \alpha_j}{\partial \mu_O} \right) + \frac{\partial f(u)}{\partial \alpha_j} \cdot \frac{\partial^2 \alpha_j}{\partial \mu_O^2} \right],$$

$$f_{CC}(u) = \sum_{j=1}^{4} \left[\left(\sum_{i=1}^{4} \frac{\partial^2 f(u)}{\partial \alpha_i \partial \alpha_j} \cdot \frac{\partial \alpha_i}{\partial \mu_C} \right) \left(\frac{\partial \alpha_j}{\partial \mu_C} \right) + \frac{\partial f(u)}{\partial \alpha_j} \cdot \frac{\partial^2 \alpha_j}{\partial \mu_C^2} \right]$$

and

$$f_{OC}(u) = \sum_{j=1}^{4} \left[\left(\sum_{i=1}^{4} \frac{\partial^2 f(u)}{\partial \alpha_i \partial \alpha_j} \cdot \frac{\partial \alpha_i}{\partial \mu_C} \right) \left(\frac{\partial \alpha_j}{\partial \mu_O} \right) + \frac{\partial f(u)}{\partial \alpha_j} \cdot \frac{\partial^2 \alpha_j}{\partial \mu_O \partial \mu_C} \right].$$

Expressions for $g_O(v)$, $g_C(v)$, $g_{OO}(v)$, $g_{CC}(v)$ and $g_{OC}(v)$ are the same as those for $f_O(v), f_C(v), f_{OO}(v), f_{CC}(v)$ and $f_{OC}(v)$ respectively, but with f replaced by g and α_i replaced by β_i ($i = 1, 2, 3, 4$) throughout.

By elementary partial differentiation,

$$\frac{\partial f(u)}{\partial \alpha_1} = \alpha_2^{-1} \exp(-u\alpha_2^{-1}),$$

$$\frac{\partial f(u)}{\partial \alpha_2} = \alpha_1 \alpha_2^{-2} (u\alpha_2^{-1} - 1) \exp(-u\alpha_2^{-1}),$$

$$\frac{\partial f(u)}{\partial \alpha_3} = \alpha_4^{-1} \exp(-u\alpha_4^{-1}),$$

$$\frac{\partial f(u)}{\partial \alpha_4} = \alpha_3 \alpha_4^{-2} (u\alpha_4^{-1} - 1) \exp(-u\alpha_4^{-1}),$$

$$\frac{\partial^2 f(u)}{\partial \alpha_2^{\,2}} = \alpha_1 \alpha_2^{\,-3} (u^2 \alpha_2^{\,-2} - 4u\alpha_2^{\,-1} + 2) \exp(-u\alpha_2^{\,-1}),$$

$$\frac{\partial^2 f(u)}{\partial \alpha_4^{\,2}} = \alpha_3 \alpha_4^{\,-3} (u^2 \alpha_4^{\,-2} - 4u\alpha_4^{\,-1} + 2) \exp(-u\alpha_4^{\,-1}),$$

$$\frac{\partial^2 f(u)}{\partial \alpha_1 \partial \alpha_2} = (u\alpha_2^{\,-3} - \alpha_2^{\,-2}) \exp(-u\alpha_2^{\,-1})$$

and

$$\frac{\partial^2 f(u)}{\partial \alpha_3 \partial \alpha_4} = (u\alpha_4^{\,-3} - \alpha_4^{\,-2}) \exp(-u\alpha_4^{\,-1}).$$

The second partial derivatives of $f(u)$ which are not given above are all zero.

Expressions for the first and second partial derivatives of $g(v)$ are the same as those for the corresponding partial derivatives of $f(v)$, but with α_i replaced by β_i ($i = 1, 2, 3, 4$) throughout.

The first partial derivatives of α_i ($i = 1, 2, 3, 4$) with respect to μ_O and μ_C are given by

$$\frac{\partial \alpha_2}{\partial \mu_O} = \tfrac{1}{2}[p_O + (p^2 - 4q)^{-\frac{1}{2}}(pp_O - 2q_O)],$$

$$\frac{\partial \alpha_4}{\partial \mu_O} = p_O - \frac{\partial \alpha_2}{\partial \mu_O},$$

APPENDIX D

$$\frac{\partial \alpha_1}{\partial \mu_O} = (\alpha_2 - \alpha_4)^{-1} \frac{\partial \alpha_2}{\partial \mu_O} - (\alpha_2 - \alpha_4)^{-2}(\alpha_2 - a^{-1}\mu_C)\left(\frac{\partial \alpha_2}{\partial \mu_O} - \frac{\partial \alpha_4}{\partial \mu_O} \right),$$

$$\frac{\partial \alpha_3}{\partial \mu_O} = - \frac{\partial \alpha_1}{\partial \mu_O},$$

$$\frac{\partial \alpha_2}{\partial \mu_C} = \tfrac{1}{2}[p_C + (p^2 - 4q)^{-\frac{1}{2}}(pp_C - 2q_C)],$$

$$\frac{\partial \alpha_4}{\partial \mu_C} = p_C - \frac{\partial \alpha_2}{\partial \mu_C},$$

$$\frac{\partial \alpha_1}{\partial \mu_C} = (\alpha_2 - \alpha_4)^{-1}\left(\frac{\partial \alpha_2}{\partial \mu_C} - a^{-1} \right)$$

$$- (\alpha_2 - \alpha_4)^{-2}(\alpha_2 - a^{-1}\mu_C)\left(\frac{\partial \alpha_2}{\partial \mu_C} - \frac{\partial \alpha_4}{\partial \mu_C} \right)$$

and

$$\frac{\partial \alpha_3}{\partial \mu_C} = - \frac{\partial \alpha_1}{\partial \mu_C}.$$

The first partial derivatives of β_i (i = 1, 2, 3, 4) with respect to μ_O and μ_C are given by

$$\frac{\partial \beta_2}{\partial \mu_O} = \tfrac{1}{2}[x_O + (x^2 - 4y)^{-\frac{1}{2}}(xx_O - 2y_O)],$$

$$\frac{\partial \beta_4}{\partial \mu_O} = x_O - \frac{\partial \beta_2}{\partial \mu_O},$$

$$\frac{\partial \beta_1}{\partial \mu_O} = (\beta_2 - \beta_4)^{-1}\left(\frac{\partial \beta_2}{\partial \mu_O} - 1\right)$$

$$- (\beta_2 - \beta_4)^{-2}(\beta_2 - \mu_O)\left(\frac{\partial \beta_2}{\partial \mu_O} - \frac{\partial \beta_4}{\partial \mu_O}\right),$$

$$\frac{\partial \beta_3}{\partial \mu_O} = -\frac{\partial \beta_1}{\partial \mu_O},$$

$$\frac{\partial \beta_2}{\partial \mu_C} = \tfrac{1}{2}[x_C + (x^2 - 4y)^{-\frac{1}{2}}(xx_C - 2y_C)],$$

$$\frac{\partial \beta_4}{\partial \mu_C} = x_C - \frac{\partial \beta_2}{\partial \mu_C},$$

$$\frac{\partial \beta_1}{\partial \mu_C} = (\beta_2 - \beta_4)^{-1}\frac{\partial \beta_2}{\partial \mu_C} - (\beta_2 - \beta_4)^{-2}(\beta_2 - \mu_O)\left(\frac{\partial \beta_2}{\partial \mu_C} - \frac{\partial \beta_4}{\partial \mu_C}\right)$$

and

$$\frac{\partial \beta_3}{\partial \mu_C} = -\frac{\partial \beta_1}{\partial \mu_C}.$$

By further elementary partial differentiation, the second partial derivatives of α_i ($i = 1, 2, 3, 4$) are given by

$$\frac{\partial^2 \alpha_2}{\partial \mu_O^2} = \tfrac{1}{2}[p_{OO} + (pp_{OO} + p_O^2 - 2q_{OO})(p^2 - 4q)^{-1/2} - (pp_O - 2q_O)^2 (p^2 - 4q)^{-3/2}],$$

$$\frac{\partial^2 \alpha_4}{\partial \mu_O^2} = p_{OO} - \frac{\partial^2 \alpha_2}{\partial \mu_O^2},$$

$$\frac{\partial^2 \alpha_1}{\partial \mu_O^2} = (\alpha_2 - \alpha_4)^{-1} \frac{\partial^2 \alpha_2}{\partial \mu_O^2} - 2(\alpha_2 - \alpha_4)^{-2} \left(\frac{\partial \alpha_2}{\partial \mu_O}\right)\left(\frac{\partial \alpha_2}{\partial \mu_O} - \frac{\partial \alpha_4}{\partial \mu_O}\right) - (\alpha_2 - a^{-1}\mu_C)(\alpha_2 - \alpha_4)^{-2} \times \left[\left(\frac{\partial^2 \alpha_2}{\partial \mu_O^2} - \frac{\partial^2 \alpha_4}{\partial \mu_O^2}\right) - 2(\alpha_2 - \alpha_4)^{-1}\left(\frac{\partial \alpha_2}{\partial \mu_O} - \frac{\partial \alpha_4}{\partial \mu_O}\right)^2\right],$$

$$\frac{\partial^2 \alpha_3}{\partial \mu_O^2} = -\frac{\partial^2 \alpha_1}{\partial \mu_O^2},$$

$$\frac{\partial^2 \alpha_2}{\partial \mu_C^{\,2}} = \tfrac{1}{2}[p_{CC} + (pp_{CC} + p_C^2 - 2q_{CC})(p^2 - 4q)^{-1/2}$$

$$- (pp_C - 2q_C)^2 (p^2 - 4q)^{-3/2}],$$

$$\frac{\partial^2 \alpha_4}{\partial \mu_C^{\,2}} = p_{CC} - \frac{\partial^2 \alpha_2}{\partial \mu_C^{\,2}},$$

$$\frac{\partial^2 \alpha_1}{\partial \mu_C^{\,2}} = (\alpha_2 - \alpha_4)^{-1} \frac{\partial^2 \alpha_2}{\partial \mu_C^{\,2}} - (\alpha_2 - a^{-1}\mu_C)(\alpha_2 - \alpha_4)^{-2}$$

$$- 2(\alpha_2 - \alpha_4)^{-2} \left(\frac{\partial \alpha_2}{\partial \mu_C} - a^{-1} \right) \left(\frac{\partial \alpha_2}{\partial \mu_C} - \frac{\partial \alpha_4}{\partial \mu_C} \right)$$

$$\times \left[\left(\frac{\partial^2 \alpha_2}{\partial \mu_C^{\,2}} - \frac{\partial^2 \alpha_4}{\partial \mu_C^{\,2}} \right) - 2(\alpha_2 - \alpha_4)^{-1} \left(\frac{\partial \alpha_2}{\partial \mu_C} - \frac{\partial \alpha_4}{\partial \mu_C} \right)^2 \right],$$

$$\frac{\partial^2 \alpha_3}{\partial \mu_C^{\,2}} = - \frac{\partial^2 \alpha_1}{\partial \mu_C^{\,2}},$$

$$\frac{\partial^2 \alpha_2}{\partial \mu_O \partial \mu_C} = \tfrac{1}{2}[p_{OC} + (pp_{OC} + p_O p_C - 2q_{OC})(p^2 - 4q)^{-1/2}$$

$$- (pp_O - 2q_O)(pp_C - 2q_C)(p^2 - 4q)^{-3/2}],$$

$$\frac{\partial^2 \alpha_4}{\partial \mu_O \partial \mu_C} = p_{OC} - \frac{\partial^2 \alpha_2}{\partial \mu_O \partial \mu_C},$$

$$\frac{\partial^2 \alpha_1}{\partial \mu_O \partial \mu_C} = (\alpha_2 - \alpha_4)^{-1} \frac{\partial^2 \alpha_2}{\partial \mu_O \partial \mu_C} - (\alpha_2 - \alpha_4)^{-2}$$

$$\times \left[\frac{\partial \alpha_2}{\partial \mu_O} \left(\frac{\partial \alpha_2}{\partial \mu_C} - \frac{\partial \alpha_4}{\partial \mu_C} \right) + \frac{\partial \alpha_2}{\partial \mu_C} \left(\frac{\partial \alpha_2}{\partial \mu_O} - \frac{\partial \alpha_4}{\partial \mu_O} \right) \right]$$

$$- (\alpha_2 - a^{-1} \mu_C)(\alpha_2 - \alpha_4)^{-2}$$

$$\times \left[\left(\frac{\partial^2 \alpha_2}{\partial \mu_O \partial \mu_C} - \frac{\partial^2 \alpha_4}{\partial \mu_O \partial \mu_C} \right) \right.$$

$$\left. - 2(\alpha_2 - \alpha_4)^{-1} \left(\frac{\partial \alpha_2}{\partial \mu_O} - \frac{\partial \alpha_4}{\partial \mu_O} \right) \left(\frac{\partial \alpha_2}{\partial \mu_C} - \frac{\partial \alpha_4}{\partial \mu_C} \right) \right],$$

and

$$\frac{\partial^2 \alpha_3}{\partial \mu_O \partial \mu_C} = - \frac{\partial^2 \alpha_1}{\partial \mu_O \partial \mu_C}.$$

The second partial derivatives of β_i ($i = 2, 3, 4$) are given by the expressions for the corresponding second partial derivatives of α_i, but with p, q and α replaced by x, y and β, respectively, throughout, and

$$\frac{\partial^2 \beta_1}{\partial \mu_O^2} = (\beta_2 - \beta_4)^{-1} \frac{\partial^2 \beta_2}{\partial \mu_O^2} - 2(\beta_2 - \beta_4)^{-2} \left(\frac{\partial \beta_2}{\partial \mu_O} - 1 \right) \left(\frac{\partial \beta_2}{\partial \mu_O} - \frac{\partial \beta_4}{\partial \mu_O} \right)$$

$$- (\beta_2 - \mu_O)(\beta_2 - \beta_4)^{-2}$$

$$\times \left[\left(\frac{\partial^2 \beta_2}{\partial \mu_O^2} - \frac{\partial^2 \beta_4}{\partial \mu_O^2} \right) - 2(\beta_2 - \beta_4)^{-1} \left(\frac{\partial \beta_2}{\partial \mu_O} - \frac{\partial \beta_4}{\partial \mu_O} \right)^2 \right],$$

$$\frac{\partial^2 \beta_1}{\partial \mu_C^{\,2}} = (\beta_2 - \beta_4)^{-1} \frac{\partial^2 \beta_2}{\partial \mu_C^{\,2}} - 2(\beta_2 - \beta_4)^{-2} \left(\frac{\partial \beta_2}{\partial \mu_C} \right) \left(\frac{\partial \beta_2}{\partial \mu_C} - \frac{\partial \beta_4}{\partial \mu_C} \right)$$

$$- (\beta_2 - \mu_O)(\beta_2 - \beta_4)^{-2}$$

$$\times \left[\left(\frac{\partial^2 \beta_2}{\partial \mu_C^{\,2}} - \frac{\partial^2 \beta_4}{\partial \mu_C^{\,2}} \right) - 2(\beta_2 - \beta_4)^{-1} \left(\frac{\partial \beta_2}{\partial \mu_C} - \frac{\partial \beta_4}{\partial \mu_C} \right)^2 \right]$$

and

$$\frac{\partial^2 \beta_1}{\partial \mu_O \partial \mu_C} = (\beta_2 - \beta_4)^{-1} \frac{\partial^2 \beta_2}{\partial \mu_O \partial \mu_C} - (\beta_2 - \beta_4)^{-2}$$

$$\times \left[\left(\frac{\partial \beta_2}{\partial \mu_O} - 1 \right) \left(\frac{\partial \beta_2}{\partial \mu_C} - \frac{\partial \beta_4}{\partial \mu_C} \right) + \frac{\partial \beta_2}{\partial \mu_C} \left(\frac{\partial \beta_2}{\partial \mu_O} - \frac{\partial \beta_4}{\partial \mu_O} \right) \right]$$

$$- (\beta_2 - \mu_O)(\beta_2 - \beta_4)^{-2} \times \left[\left(\frac{\partial^2 \beta_2}{\partial \mu_O \partial \mu_C} - \frac{\partial^2 \beta_4}{\partial \mu_O \partial \mu_C} \right) \right.$$

$$\left. - 2(\beta_2 - \beta_4)^{-1} \left(\frac{\partial \beta_2}{\partial \mu_O} - \frac{\partial \beta_4}{\partial \mu_O} \right) \left(\frac{\partial \beta_2}{\partial \mu_C} - \frac{\partial \beta_4}{\partial \mu_C} \right) \right].$$

Finally, the first and second derivatives of p, q, x and y are given by

$$p_O = \exp(a \tau_C / \mu_C),$$

$$p_C = \exp(a \tau_C / \mu_C) [a^{-1} - a \tau_C \mu_C^{-2} (\mu_O + a^{-1} \mu_C)],$$

$$p_{OO} = 0,$$

$$p_{CC} = a \tau_C \mu_C^{-3} \exp(a \tau_C / \mu_C) (2\mu_O + a \tau_C \mu_O \mu_C^{-1} + \tau_C),$$

APPENDIX D

$$p_{OC} = -a\tau_C\mu_C^{-2}\exp(a\tau_C/\mu_C),$$

$$q_O = a^{-1}\mu_C\exp(a\tau_C/\mu_C),$$

$$q_C = \exp(a\tau_C/\mu_C)(a^{-1}\mu_O - \tau_C\mu_C^{-1}\mu_O),$$

$$q_{OO} = 0,$$

$$q_{CC} = a\tau_C^2\mu_O\mu_C^{-3}\exp(a\tau_C/\mu_C),$$

$$q_{OC} = (a^{-1} - \tau_C\mu_C^{-1})\exp(a\tau_C/\mu_C),$$

$$x_O = \exp(\tau_O/\mu_O)[1 - \tau_O\mu_O^{-2}(\mu_O + a^{-1}\mu_C)],$$

$$x_C = a^{-1}\exp(\tau_O/\mu_O),$$

$$x_{OO} = \tau_O\mu_O^{-3}\exp(\tau_O/\mu_O)(2a^{-1}\mu_C + a^{-1}\tau_O\mu_C\mu_O^{-1} + \tau_O),$$

$$x_{CC} = 0,$$

$$x_{OC} = -a^{-1}\tau_O\mu_O^{-2}\exp(\tau_O/\mu_O),$$

$$y_O = \exp(\tau_O/\mu_O)(a^{-1}\mu_C - a^{-1}\tau_O\mu_O^{-1}\mu_C),$$

$$y_C = a^{-1}\mu_O\exp(\tau_O/\mu_O),$$

$$y_{OO} = a^{-1}\tau_O^2\mu_C\mu_O^{-3}\exp(\tau_O/\mu_O),$$

$$y_{CC} = 0$$

and

$$y_{OC} = (a^{-1} - a^{-1}\tau_C\mu_O^{-1})\exp(\tau_O/\mu_O).$$